Control of early-age cracking aimed at a test case for bacterial self-healing concrete

Y. Zondag

May 2021

TU Delft

Control of early-age cracking aimed at a test case for bacterial self-healing concrete

by

Y. Zondag

to obtain the degree of Master of Science
at the Delft University of Technology,
to be defended publicly on Thursday 27th of May 2021 at 4:00 PM.

Student number:	4624378	
Master programme:	Civil Engineering	
Thesis committee:	Prof. dr. ir. E. Schlangen,	TU Delft, chairman
	Dr. H.M. Jonkers,	TU Delft
	Dr. ir. M. Luković,	TU Delft
	Ir. W.J. van den Bos,	TU Delft / BAM
	Ir. W.H. de Brabander,	BAM

An electronic version of this thesis is available at `http://repository.tudelft.nl/`.

TU Delft

Preface

This thesis concludes my educational career at the Delft University of Technology, which I started in September 2016. During my Master I followed the track of Structural Engineering, specializing in concrete structures. Looking back, it has been a great experience becoming an engineer.

Besides my interest in structures, I have always been intrigued by concrete science. Therefore, I am grateful to be given the opportunity to investigate a case that involves both. This research also convinced me of the potential of bacterial self-healing concrete, which is very promising. I am thankful to carry this experience with me and will strive to promote bacterial self-healing technology in my professional career.

I am grateful to everyone who contributed to this thesis. First of all, I would like to thank Erik Schlangen, the chairman of my committee. Not only for the opportunity to examine such an intriguing subject, but also for his supervision and support. I also want to express my gratitude to Henk Jonkers for his constructive feedback and knowledge regarding bacterial self-healing concrete. Furthermore, I would like to thank Jeannette van den Bos, her motivation and help with the design of the concrete mixtures was very much appreciated. Finally, many thanks to Mladena Luković and Huibert de Brabander for their positive, yet critical feedback during the final stages of my research. Their advice on structural problems was crucial.

Special thanks also to Maiko van Leeuwen. Testing of the concrete mixtures would never have been possible without his practical advice and help in the laboratory. I really appreciated working together.

This preface would not be complete before I express my gratitude to my friends and family, in particular my parents. I will always be thankful for their support during my time at the TU Delft to become an engineer. Last, but not least, I want to thank my girlfriend, Floortje. Her loving care the past years kept my motivation high, especially in writing this thesis.

Youri Zondag
Nijmegen, May 2021

Abstract

Since 2006, the Delft University of Technology has been working on the development of bacterial self-healing concrete (BSHC). The self-healing ability of this concrete is based on a biological mechanism, in which mineral producing bacteria are added to repair cracks autonomously. This not only improves the durability of concrete structures, but could also reduce the need for crack-limiting reinforcement. So far, bacterial self-healing technology has been used in variety of applications, especially watertight structures, but always only as an additional safety measure. Hence, the full crack-sealing capacity, related to the reinforcement reduction potential, could not be proven. This will have to be resolved in a dedicated full-scale demonstrator project.

For this demonstrator project, a rectangular water reservoir has to be designed, which will essentially serve as a test case for the newly developed bacterial self-healing technology. This thesis aims to devise the concrete mixture and reinforcement layout for the side walls of this reservoir in such a way that imposed deformations induce a given degree of cracking at an early-age, which allows to demonstrate the crack-sealing capacity and reinforcement reduction potential of BSHC. Accordingly, this thesis roughly consists of two successive parts. The first part is related to the design and testing of the concrete mixture, which should provide an environment in which the bacteria can operate while not negatively affecting other concrete characteristics and also stimulating early-age cracking. A literature study has been performed in advance to support the design of the concrete mixture and to examine the respective influence of the mixture composition on factors that affect the cracking behaviour of concrete. The second part focuses on the cracking calculations, for which the test results of the first part constitute a considerable portion of the input. This comprises the determination of the probability of cracking, as well as the degree of cracking in relation to the reinforcement layout.

The design of a concrete mixture intended for the side walls of the reservoir led to four different mixtures, all of which have a cement content of 418 kg/m^3 (26% of CEM I 52.5 R and 74% CEM III/B 42.5 N), but vary in the addition of filler in the form of limestone powder and healing agent; a mixture of bacteria and calcium lactate encapsulated in PLA strings. The mixtures with healing agent, which represent BSHC, are meant for side wall A, whereas the mixtures without healing agent representing ordinary concrete can be used for side wall B, so it can serve as a reference. To investigate the effect of these additions, as well as to verify the designs and quantify the relevant physical and mechanical properties of the concrete mixtures, several tests were conducted. These revealed that the mixtures with filler exhibit a higher consistency, improved cohesiveness and more prosperous strength development compared to the mixtures without filler. Both the fresh properties and strength development were not affected by the addition of healing agent. Furthermore, it was found that the addition of filler causes autogenous shrinkage to increase by about 15%, whereas the addition of healing agent causes autogenous shrinkage to decrease by about 20%.

From the cracking calculations it is concluded that it is very likely that the early-age cracking of the side walls of the reservoir occurs as a consequence of imposed deformations. Cement hydration causes a large temperature rise, resulting in significant thermal shrinkage due to the subsequent temperature drop. The imposed deformations are restrained by the floor of the reservoir, as well as the foundation material underneath. This results in a maximum probability of cracking of 65% and 93% according to two different methods. In order to demonstrate the true crack-sealing capacity of BSHC, if is preferred to obtain various crack widths along the length of the side walls and the reinforcement layout must be configured to allow this to happen. Therefore, several methods that deal with the prediction of crack widths are implemented in this case. Based on the average of all prediction methods it is found that the following crack widths occur given the longitudinal reinforcement distribution in brackets: 0.09 (∅20–100), 0.20 (∅20–160), 0.31 (∅20–210) and 0.43 mm (∅20–250). However, it was also discovered that the mutual differences between the prediction methods are very large, in particular at lower reinforcement ratios. But then again, a reinforcement layout divided into multiple sections, consisting of the aforementioned longitudinal reinforcement distributions, offers the best chance of demonstrating self-healing ability.

Contents

Nomenclature

Abbreviations

ASR	Alkali-silica reaction
BSHC	Bacterial self-healing concrete
C_2S	Dicalcium silicate
C_3A	Tricalcium aluminite
C_3S	Tricalcium silicate
C_4AF	Tetracalcium aliminoferrite
CRM	Continuous restraining model
CSH	Calcium silicate hydrate
CTE	Coefficient of thermal expansion
FCS	Formative cracking stage
FD	Finite difference
GGBS	Ground granulated blastfurnace slag
HA	Healing agent
PDE	Partial differential equation
PLA	Polylactic acid
SCS	Stabilized cracking stage
TMM	Tensile member model
TU Delft	Delft University of Technology

Symbols

Latin letters

a_c	Thermal diffusivity of concrete
A_f	Cross-sectional area of floor
A_w	Cross-sectional area of wall
A_s	Cross-sectional area of reinforcement steel
A_c	Cross-sectional area of concrete
$A_{c,ef}$	Effective cross-sectional area of concrete in tension
$b_{c,ef}$	Effective width of concrete in tension
B_{ef}	Effective width of floor (i.e. part that provides restraint)
c	Concrete cover to longitudinal reinforcement
c_c	Specific heat of concrete
C	C-value of cement (i.e. temperature sensitivity)
C_c	Cement content of concrete
D_f	Thickness of floor
D_w	Thickness of wall
E_A	Apparent activation energy of cement
E_f	Elastic modulus of floor
E_w	Elastic modulus of wall
E_s	Elastic modulus of reinforcement steel
E_{cm}	Elastic (secant) modulus of concrete
f_c	Cylinder compressive strength of concrete (where f_{cm} and f_{ck} represent the mean and char-

	acteristic value, respectively)
$f_{c,cube}$	Cube compressive strength of concrete (where $f_{cm,cube}$ and $f_{ck,cube}$ represent the mean and characteristic value, respectively)
f_{ct}	Tensile strength of concrete (where f_{ctm} represents the mean value)
$f_{ct,ef}$	Effective tensile strength of concrete
f_y	Yield strength of reinforcement steel (where f_{yk} represents the characteristic value)
G	Thermal surface conductance (where G_1 includes formwork and G_2 excludes formwork)
$h_{c,ef}$	Effective height of concrete in tension
H	Height of wall
k	Coefficient that takes account of non-uniform self-equilibrating concrete stress distribution
k_1	Coefficient that takes account of cracking stress and bond strength ($= \sigma_{cr}/\tau_b$)
k_2	Coefficient that takes account of concrete cover
k_3	Coefficient that takes account of load duration
K_1	Coefficient for creep effects
K_2	Coefficient for sustained loading and weakest link effects
K_s	Compression modulus of foundation material
L	Length of wall
M	Maturity of concrete
M_w	Weighted maturity of concrete
p_{GGBS}	Share (by mass) of blastfurnace slag in cement
Q	Heat generated by cement hydration
Q_{ad}	Heat generated by cement hydration under adiabatic conditions
Q_{ult}	Ultimate heat generation by cement hydration
R	Degree of restraint
R_g	Universal gas constant
R^2	Relative error (i.e. square of deviation of fitted curve with respect to single measurement)
s	Reinforcement bar spacing
s_0	Transfer length
s_r	Crack spacing (where $s_{r,min}$, s_{rm} and $s_{r,max}$ represent the minimum, mean and maximum value, respectively)
T	Concrete temperature
T_{ad}	Concrete temperature under adiabatic conditions
T_{am}	Ambient temperature
T_{mix}	Mix temperature
T_{ref}	Reference temperature
t	Age of concrete
t_0	Age of concrete at application of stress increment
t_T	Equivalent age of concrete (i.e. corrected for thermal effects)
w	Crack width (where w_m and w_k represent the mean and characteristic value, respectively)
wcr	Water/cement ratio
x	Coordinate for length of wall (i.e. distance from center of wall)
y	Coordinate for height of wall (i.e. distance from joint between wall and floor)
z	Coordinate for depth of wall (i.e. distance from outer surface of wall)

Greek letters

α	Degree of hydration
α_{ad}	Degree of hydration under adiabatic conditions
α_{ult}	Ultimate degree of hydration
α_1	Ratio of mean to minimum crack spacing ($= s_{rm}/s_{r,min}$)
α_2	Ratio of maximum to mean crack spacing ($= s_{r,max}/s_{rm}$)
α_c	Coefficient of thermal expansion of concrete

α_e	Modular ratio of reinforcement steel to concrete ($= E_s/E_{cm}$)
ε_{ca}	Autogenous shrinkage strain (where ε_{cam} represents the mean value)
ε_{cr}	Cracking strain of concrete
ε_{ctu}	Tensile strain capacity of concrete
ε_{fdc}	Transition strain (i.e. imposed deformation at which crack pattern becomes fully developed)
ε_r	Restrained shrinkage strain
ε_s	Steel strain in cracks
$\varepsilon_{s,cr}$	Steel strain in cracks immediately after cracking
λ_c	Thermal conductivity of concrete
ν	Poisson's ratio of concrete
ρ	Reinforcement ratio ($= A_s/A_c$)
ρ_{ef}	Effective reinforcement ratio ($= A_s/A_{c,ef}$)
ρ_c	Specific mass of concrete
ϕ	Reinforcement bar diameter
ψ	Relaxation coefficient
σ_c	Concrete stress (where σ_{cm} represents the mean value)
σ_{cr}	Cracking stress of concrete
σ_s	Steel stress in cracks
$\sigma_{s,cr}$	Steel stress in cracks immediately after cracking
τ_b	Bond strength between reinforcement steel and concrete

1 Introduction

In this chapter, a general introduction into the background and state of the art of the current investigation into bacterial self-healing concrete is provided. This includes a brief description of the interaction between ordinary concrete and the newly developed bacterial self-healing technology. The problem statement and objective of this thesis, which can be derived from the research motivation, are provided hereafter. Finally, both the scope and outline of this thesis are presented.

1.1 Prologue

Concrete is one of the most commonly used construction materials in the world; an estimated 7.4 billion cubic meter is produced each year [1]. The popularity of concrete stems from it being relatively inexpensive and strong, and the ability to be cast in any shape. Concrete performs best under compression, but has limited capacity to withstand tension. In order to enhance the capability of concrete, this flaw is addressed by the addition of reinforcement steel into the areas of concrete where tension occurs. Once the concrete has hardened, a bond is formed between the reinforcement steel and concrete such that an interacting composite is established. This composite will also resist tension, since the reinforcement steel is equally strong in compression and tension. Although often not visible to the naked eye, the formation of (micro)cracks over the areas in tension is required to activate the reinforcement steel and thus facilitate the interaction between the reinforcement steel and concrete matrix. Besides external loads, cracking can also be initiated by imposed thermal and shrinkage deformations of the concrete matrix. These cracks can be controlled by adding crack-limiting reinforcement to a concrete structure, in addition to the structural reinforcement. If (excessive) cracking is not addressed, it will negatively affect a concrete structure's functionality, durability and aesthetics. Especially tightness is a cause for concern, since cracking can cause leakage.

The condition of the infrastructure is of major influence to society, both economical and socio-environmental. Preserving a structure's original condition comes at vast expense and often involves downtime of the structure. Replacing structures is generally even more disadvantageous, especially if the intended service life is not reached. The durability of structures is therefore of utmost importance. Durability can be defined as the ability of a structure to withstand deterioration processes to which it is expected to be exposed during its service life [2]. Degradation of concrete structures usually involves the infiltration of some harmful substance into the concrete. The durability of concrete is therefore primarily related to its permeability and the diffusion to liquids, gases or ions. Permeability is defined as the ease of flow of a liquid or gas through a porous medium. While larger cracks hamper both the structural integrity and durability of a concrete structure, also microcracks may result in durability problems by increasing its permeability [3]. Cracks provide a path for water (or moisture), ions, carbon dioxide and oxygen to penetrate into the concrete, causing deterioration. This could lead to one or more of the various degradation mechanisms of concrete, such as carbonation, (chloride induced) reinforcement corrosion, alkali-silica reaction, and attack by acids, salts or sulfates.

(a) Cause [4]. **(b)** Effect, source: Giatec Scientific Inc.

Figure 1.1: Degradation of concrete.

Maintenance is required to preserve a structure's performance, which may be affected by loss of functionality, durability or aesthetics. A lack of maintenance could even lead to collapse of a structure, with catastrophic consequences. In the past and present, maintenance is generally performed according to the repair concept, which distinguishes between regular and infrequent maintenance. In the repair concept, the design and preparation of structures is aimed at delaying the formation and increase of damage as a function of load and/or time. When the damage, like (excessive) cracking of concrete, is to such an extent that the structure's performance starts to suffer, man-made repairs are made. According to this concept, investing in frequent, small and relatively inexpensive repairs pays off; in the long-term, repair costs are much higher without regular maintenance (see Figure 1.2). Also, the downtime involved when big repairs are needed tends to be much longer than for smaller ones. However, frequent maintenance does not noticeably improve a structure's performance in the short-term, let alone the infrastructure as a whole, making it usually not very popular (i.e. it is often preferred to invest in new infrastructure).

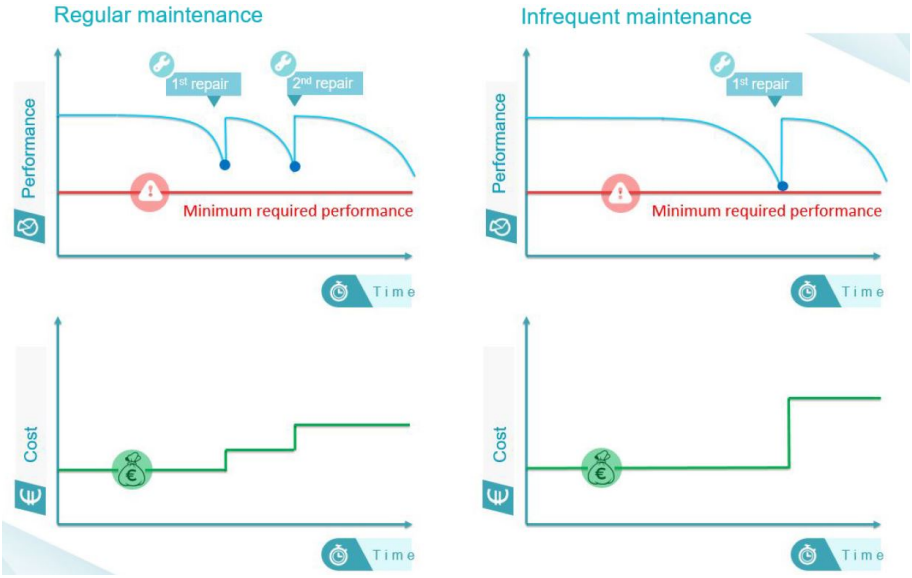

Figure 1.2: Repair concept by Van Breugel: cost and performance of structure versus elapsed time [4].

A welcome alternative to the repair concept is the more innovative self-healing concept. In the self-healing concept, materials are provided with an built-in capability to repair damage caused as a function of load and/or time. According to this concept, the formation of damage is allowed; the material itself is able to repair this damage and restore its performance autonomously. By introducing an autonomous self-healing mechanism into the material, the durability of the material could significantly be increased, likely resulting in a longer service life. Concrete in particular could benefit from this due to the regular occurrence of (micro)cracks, which can be regarded as minor damage that could reduce the durability of the structure. The requirement for maintenance could also be reduced, along with the associated costs [5, 6]. However, since the self-healing ability must be added to the material, the initial investment in the structure will be greater than required when implementing traditional material (see Figure 1.3).

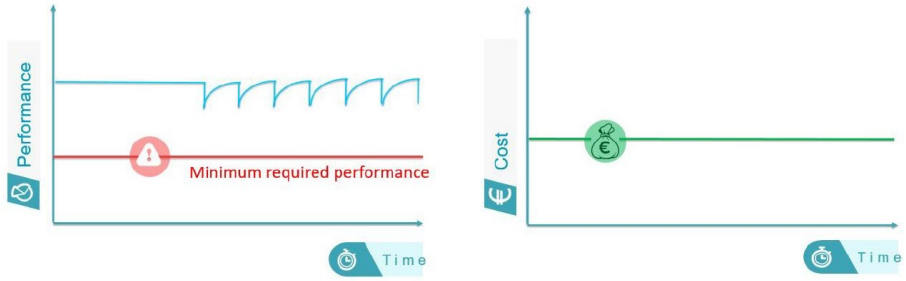

Figure 1.3: Self-healing concept by Van Breugel: cost and performance of structure versus elapsed time [4].

1.2 Self-healing concrete

Ordinary concrete already features a certain crack-sealing capacity, which originates from ongoing chemical, physical and mechanical processes. This capacity of concrete to fill up its cracks is referred to as autogenous self-healing. Autogenous self-healing can only occur in stable cracks up to 0.2 mm in width, if the flow rate through the crack is not too high and if the penetrating liquid is not aggressive [7]. The following autogenous self-healing mechanisms can be distinguished (see Figure 1.4):

- Continuous hydration: unhydrated cement particles on the crack's surface react and solidify once they come into contact with the penetrating water;
- Loose parts blocking the path: sedimentation of solid particles present in the fluid seeping through;
- Swelling of cement matrix: cement matrix swells due to the ingress of water;
- Carbonation: carbon dioxide present in the air, or diffused in the penetrating water, reacts with the calcium hydroxide to form limestone (see Equation 1.2).

The capacity of autogenous self-healing relates particularly to the clinker content and cement fineness [5, 6]. The higher the dosage and the coarser the cement particles, the higher the crack-sealing capacity of the concrete. However, these characteristics oppose the evolution of concrete that took place in the last decades. In order to create low CO_2 impact and rapid hardening concretes, the clinker content has been reduced and finer cements are applied. These types of concrete, typically high in slag and/or fly ash content, thus show less autogenous self-healing capacity. Going back to high clinker containing concretes is undesirable from an environmental point of view, low clinker containing concretes should therefore preferably also be provided with sufficient autonomous self-healing capacity. This desire once again emphasizes the demand for concrete with autonomous self-healing.

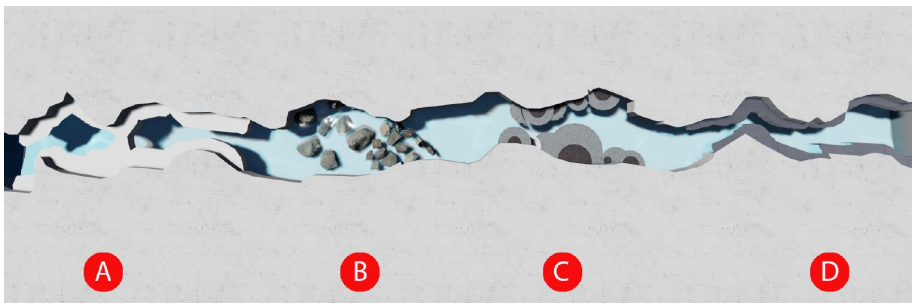

Figure 1.4: Schematic representation of autogenous self-healing mechanisms: carbonation (A), loose parts blocking the path (B), continuous hydration (C), and swelling of cement matrix (D) [4].

In 2006, the Delft University of Technology followed up on the self-healing concept, by starting with the development of construction materials that can repair their own damage, including concrete [1]. Under the supervision of Dr. H.M. Jonkers, a bacterial self-healing concrete has been developed. The self-healing ability of this concrete is based on a biological mechanism, in which mineral producing bacteria are added to repair cracks autonomously. The principle behind this autonomous self-healing mechanism is that the bacteria themselves act largely as a catalyst, and transform a precursor (calcium lactate) to a suitable filler material (limestone) [3, 6]. The bacteria are specifically selected to resist concrete matrix incorporation and, together with the precursor, will not negatively affect other concrete characteristics. Alkali-resistant bacteria of the Bacillus genus are embedded in the concrete in a dormant state, along with the calcium lactate. The bacteria and calcium lactate are encapsulated in PLA strings, in order to prevent interaction during mixing. Once the bacteria come in contact with water seeping through the crack, they germinate and start producing limestone out of the calcium lactate (see Equation 1.1) [3]. The product of this activity is carbon dioxide. This carbon dioxide reacts directly with the calcium hydroxide present on the crack's surface, forming additional limestone (see Equation 1.2). The limestone seals up the cracks, thereby reducing the permeability of the concrete and improving the tightness of the structure. Consequently, both the concrete matrix and the embedded reinforcement experience better protection against degradation processes.

$$\underset{\text{calcium lactate}}{Ca(C_3H_5O_2)_2} + \underset{\text{oxygen}}{7O_2} \xrightarrow{\text{bacteria}} \underset{\text{limestone}}{CaCO_3} + \underset{\text{water}}{5H_2O} + \underset{\text{carbon dioxide}}{5CO_2} \tag{1.1}$$

$$\underset{\text{carbon dioxide}}{CO_2} + \underset{\text{calcium hydroxide}}{Ca(OH)_2} \longrightarrow \underset{\text{limestone}}{CaCO_3} + \underset{\text{water}}{H_2O} \tag{1.2}$$

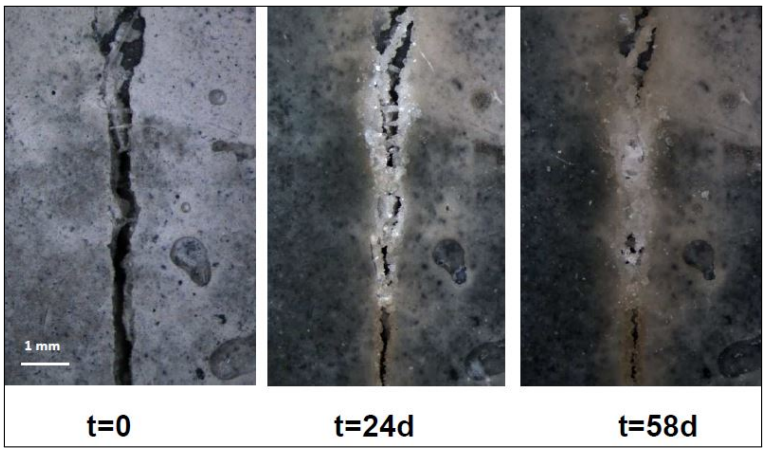

Figure 1.5: Autonomous self-healing of a 0.8 mm wide crack at a dosage of 15 kg/m^3 of HA for two months [5].

1.3 Research motivation

Laboratory studies have shown that the bacterial self-healing concrete (BSHC) is capable of sealing cracks up to 1.0 mm in width [5, 6]. This requires a dosage of 15 kilogram of healing agent (HA); a mixture of bacteria and calcium lactate encapsulated in PLA strings, per cubic meter of concrete mixture. A dosage of 5 kg/m^3 leads to a crack-sealing capacity of crack widths up to 0.4 mm. BSHC is particularly suitable for structures in wet environments, since contact with water activates the bacteria and initiates the production of the limestone that seals up the cracks. Furthermore, watertight structures could also benefit the most from the potential of BSHC, since they are commonly designed in such a way that only cracks up to 0.1 mm in width are allowed to occur. Such structures require a lot of crack-limiting reinforcement, which is both expensive and impractical (i.e. a fine reinforcement mesh hampers casting of the fresh concrete). In contrast, allowing larger crack widths would substantially reduce the amount of crack-limiting reinforcement required. Water tightness of these structures will have to be delivered by autonomous self-healing of concrete to which healing agent has been added. This will result in more economical structures with a smaller CO_2 footprint, as well as a better processability of the concrete mixture. The latter in turn enables faster construction and reduces the risk of air pockets forming that could potentially lead to a less durable structure.

Bacterial self-healing concrete has already been used in various watertight structures in the Netherlands, like a wastewater purification tank in Simpelveld and a extinguishing water storage tank in Rotterdam [5, 6]. In both applications, only parts of the structure were constructed from BSHC, in order to compare its behaviour with other parts from ordinary concrete (relying on the same mixture composition without HA). No negative effects of the addition of the healing agent to the concrete have been observed so far. Ongoing monitoring will have to determine the water tightness of the structures in the long-term. Since both structures are actually in use, they had to meet strict requirements regarding water tightness. It was therefore demanded that the amount of crack-limiting reinforcement applied in parts constructed from BSHC be the same as that applied in parts from ordinary concrete. Bacterial self-healing technology was merely used as an additional safety measure. The full crack-sealing capacity, related to the reinforcement reduction potential, can thus not be proven on the basis of these two applications. This will have to be resolved in a dedicated full-scale demonstrator project.

(a) Wastewater purification tank [6]. **(b)** Extinguishing water storage tank [6].

Figure 1.6: Applications of bacterial self-healing concrete in the Netherlands.

1.4 Problem statement

In order for the Delft University of Technology to demonstrate the full crack-sealing capacity of their innovation, a dedicated full-scale demonstrator project is needed. This may also further stimulate the introduction of the bacterial self-healing concrete to market. For this to be realized, the TU Delft is working together with contractor BAM and supplier Basilisk (TU Delft spin-of), which were also involved in the construction of the extinguishing water storage tank [1]. With this demonstrator project, they together strive to launch bacterial self-healing technology as a reliable crack management strategy that will replace the current crack prevention strategy; working towards the situation in which the addition of healing agent to concrete mixtures to form BSHC is widely accepted. This may require less crack-limiting reinforcement, which will not only not only save material (costs) and lower CO_2 footprint, but will also be more practical.

For this demonstrator project, a rectangular water reservoir has to be designed, which will essentially serve as a test case for the newly developed bacterial self-healing technology. Since this test only lasts a few months, the construction of this reservoir will be included in another ongoing project of BAM. After the test, the reservoir will be cut in L-shaped retaining wall pieces, which can be reused elsewhere in the project. The dimensions of the reservoir were predetermined considering both the aim of the test itself and the intention to reuse L-shaped retaining wall pieces cut from the reservoir. This led to the sketch design of the reservoir shown in Figure 1.7. Side wall A will be constructed from a concrete mixture to which healing agent is added, whereas side wall B will be from the same mixture without the addition of HA, so it can serve as a reference. This makes it possible to establish the crack-sealing capacity of BSHC (with autonomous self-healing) relative to that of ordinary concrete (with autogenous self-healing). However, the potential of BSHC can only be demonstrated if there are cracks present throughout the side walls of the reservoir that the bacteria can repair autonomously. Moreover, the cracking behaviour must meet three conditions. First, for practical and commercial reasons, the cracks need to be present at an early-age; just after construction of the reservoir, so that the crack-sealing capacity can be demonstrated quickly. Second, they have to be through-cracks, that is, cracks that run from the inner surface to the outer surface of the side walls. This allows water to flow through from the submerged inner surface, thereby activating the bacteria, while at the same time the cracks can be monitored from the accessible outer surface. Third, the cracks should preferably be initiated naturally through imposed thermal and shrinkage deformations, and controlled with crack-limiting reinforcement. This is preferable to the back-up plan that uses hydraulic jacks to artificially initiate and control cracking.

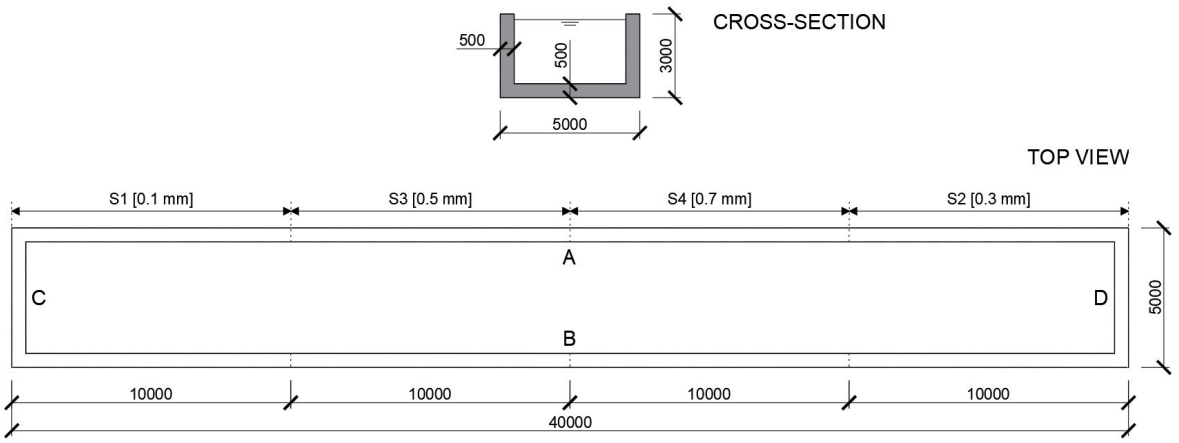

Figure 1.7: Sketch design of rectangular water reservoir and its sections, dimensions in mm.

Proposed crack pattern

To ensure that the true crack-sealing capacity of the bacterial self-healing technology is discovered, both side walls should exhibit the same degree of cracking. But instead of all cracks being the same width, it is preferred to obtain various crack widths along the length of the side walls. Hence, it was decided to divide the side walls of the reservoir in multiple sections of the same length, each different in desired crack width (see Figure 1.7). Preference is given to a crack width of 0.1 mm for the least cracked section, increasing (in three discrete increments) to a crack width of approximately 0.7 mm for the most cracked section. It must be emphasized that these crack widths only concern (through-)cracks resulting from imposed deformations and not any flexural cracks caused by external loads, such as the water load when the reservoir is filled. This is because flexural cracks cannot be through-cracks and as such are not suited to demonstrate the crack-sealing capacity of BSHC.

1.5 Objective

As outlined in the previous section, the overall aim is to demonstrate the crack-sealing capacity and reinforcement reduction potential of bacterial self-healing concrete. For this to be realized, a dedicated full-scale demonstrator project is set up by the TU Delft and BAM, in which the newly developed bacterial self-healing technology is given the opportunity to prove itself in the side walls of a rectangular water reservoir. This research focuses on the main challenge in the design of this reservoir, which is to devise the concrete mixture and reinforcement layout for the side walls in such a way that they reflect the desired cracking behaviour. The objective of this thesis can therefore be described as follows:

To establish a suitable concrete mixture and appropriate reinforcement layout for the side walls of a rectangular water reservoir using imposed deformations to obtain the proposed crack pattern at an early-age, so they can serve to demonstrate the crack-sealing capacity and reinforcement reduction potential of bacterial self-healing concrete.

Research questions

In support of this thesis, research questions are formulated that cover four parts of the objective:

- Which concrete mixture, that is compatible with the addition of healing agent and stimulates early-age cracking, is suitable for the side walls of the reservoir?
- What are the physical and mechanical properties of this concrete mixture relevant to its early-age cracking behaviour when hardened?
- What is the probability that early-age cracking of the side walls of the reservoir will occur as a consequence of imposed deformations?
- How can the longitudinal reinforcement of the side walls of the reservoir best be distributed in order to obtain the proposed crack pattern consisting of various crack widths?

1.6 Scope

This research bridges between the development and full-scale testing of bacterial self-healing concrete, as it aims to elaborate the test case itself. The development of the healing agent is not part of this thesis; the biological composition of the healing agent was a provided and fixed restriction. However, the design of the concrete mixture intended for the side walls, to which the healing agent will be added, is an important component of this research. The same holds for the determination of the physical and mechanical properties of this mixture related to its early-age cracking behaviour when hardened. Furthermore, the construction of the reservoir and the actual demonstration of the crack-sealing capacity of the bacterial self-healing technology, by monitoring the reservoir before and after it is filled, are not within the scope of this thesis. Nevertheless, it was desired that (where possible and required) the research also takes into account facets with regard to those components not included in the scope, such as construction practice and monitoring techniques. Although the author believes that more insight is to be gained from monitoring the occurring crack width and comparing it to the predicted crack width, back analysis of this data could not be included in this research, since it was unknown when the reservoir would be constructed.

As can be deduced from the objective, this research is not aimed at the complete design of the reservoir. The emphasis is on the elaboration of the most demanding design criterion; the desired cracking behaviour of the side walls. Other design criteria, such as durability, reusability and structural integrity of the reservoir, were taken into account (where possible and required), but are not elaborated. Figure 1.9 shows how and where this thesis fits in the design of the reservoir and the overall progress towards full-scale testing of BSHC. In terms of the reinforcement layout of the side walls, the entire focus of this research is on the crack-limiting reinforcement required to control the cracks resulting from imposed deformations. Because these are vertical cracks, as illustrated in Figure 1.8, they are controlled by the longitudinal reinforcement. The transverse reinforcement, which ensures the structural integrity of the reservoir and controls horizontal cracks such as any flexural cracks due to the water load (and soil load when reused as L-shaped retaining wall pieces), is not considered in this thesis. The same applies to the other elements of the reservoir, like the foundation, floor and end walls. However, possible interaction between the side walls and these elements is taken into account. Moreover, where necessary and conceivable, substantiated assumptions are made with regard to the design criteria and facets not included in the scope of this thesis. Having said that, the dimensions of the reservoir were a provided and fixed restriction, which also happened to limit the number of variables.

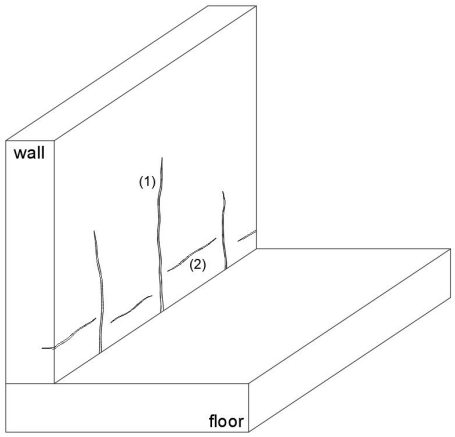

Figure 1.8: Schematic representation of (through-)cracks due to imposed deformations (2) and flexural cracks due to water load (1).

1.7 Outline

This thesis can roughly be divided into two successive parts. The first part is related to the design and testing of the concrete mixture intended for the side walls of the reservoir. This mixture must be compatible with the addition of healing agent and preferably shrink considerably to stimulate early-age cracking. Therefore, four different mixtures were investigated, varying in the addition of filler and healing agent. To investigate the effect of these additions, as well as to verify the designs and quantify the relevant physical and mechanical properties of the concrete mixtures, several tests were conducted. These tests consisted of determining the fresh properties, strength development and autogenous shrinkage, the latter two of which play a major role in the early-age cracking behaviour of hardened concrete. A literature study has been performed in advance to support the design of the concrete mixture and to examine the respective influence of the mixture composition on factors that affect the cracking behaviour of concrete. The first part is concluded with a detailed analysis of the test results (in relation to the test objectives).

The second part of this thesis is focused on the cracking calculations, for which the test results of the first part constitute a considerable portion of the input. The cracking calculations consist of identifying the probability and degree of cracking of the side walls of the reservoir. The probability of cracking is governed by magnitude of imposed deformations relative to the concrete strength, both of which are strongly influenced by the heat of hydration and the consequent temperature development and distribution within the side walls. These two topics were therefore addressed first, after which the strength development and imposed deformations, consisting of thermal deformations and autogenous shrinkage, have been quantified. The degree of cracking, the most notable attribute of which is the crack width, is a function of the reinforcement layout in conjunction with the concrete strength and imposed deformations. Accordingly, it has been examined how the longitudinal reinforcement of the side walls can best be distributed in order to obtain the proposed crack pattern. There are many different methods that deal with the prediction of crack widths, with little consensus in practice on which one is best. Hence, multiple of these methods were reviewed and compared with respect to their techniques and results from application in this case. In addition, two parameter studies have been performed to investigate the extent various aspects influence the probability and degree of cracking. Finally, the results from the cracking calculations and prediction of crack widths were analysed and processed, which led the appropriate reinforcement layout and recommendations regarding various aspects that contribute to a higher probability of cracking and the proposed crack pattern.

It must be pointed out that this research is not as linear as suggested above. Since the majority of this thesis is design based, it has a strong iterative (non-linear) character. Various 'loops' were required to obtain satisfactory results, in particular with regard to the cracking calculations. These cracking calculations were performed multiple times, each time increasing the level of complexity and degree of elaboration (i.e. more parameters are taken into account), and processing the knowledge acquired from previous loops. As a general rule, only the last loops, relating to the final results, are elaborated in this thesis. These loops are the most comprehensive and include the conditions and acquired knowledge on which the final results are based. However, exceptions have been made for the sake of completeness and/or the benefit of the reader.

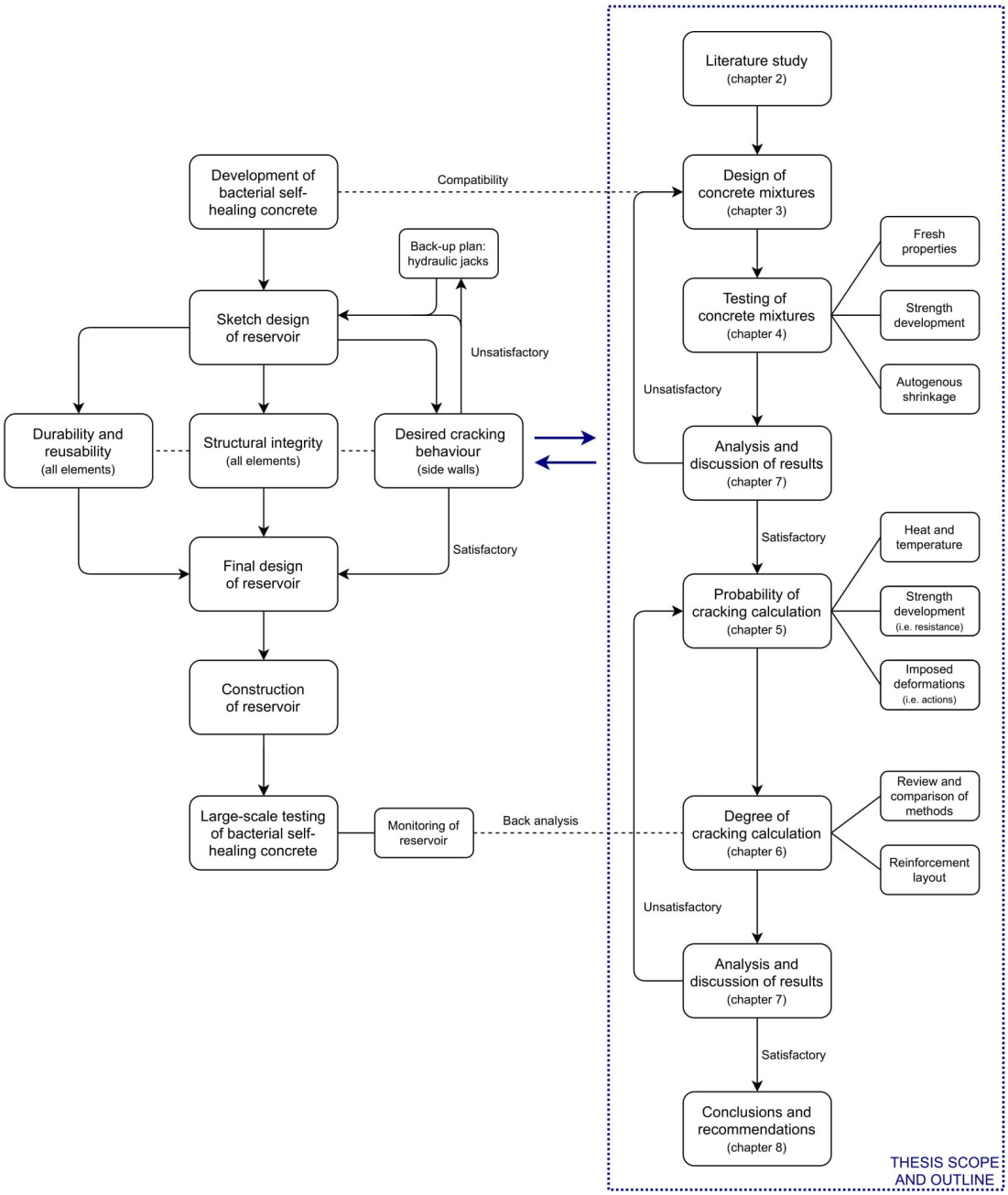

Figure 1.9: Overall progress towards full-scale testing of BSHC, including thesis scope and outline.

2 Literature study

The starting point of this research was to obtain a better understanding of concrete and its properties. Therefore, a literature study has been performed, focusing on the fundamentals of concrete and the factors influencing its characteristics. To facilitate the design of a concrete mixture for this thesis, the emphasis has been on the relation between the mixture composition and the concrete properties. This chapter presents an overview of the results of the literature study, bridging between concrete science and its application in practice.

2.1 Introduction

Concrete in its most basic form consists of roughly 6 parts of gravel, 4 parts of sand, 2 parts of cement and 1 part (by mass) of water. However, this is almost always deviated from, in order to obtain enhanced and/or specific properties. A change in mixture composition results in different concrete characteristics in the fresh and hardened state. Well-designed concrete has satisfactory properties in both the fresh and hardened state. In addition to the mixture composition, there are other factors influencing the concrete characteristics, of which the environmental conditions (e.g. wind, temperature and humidity) are one of the most influential. These influencing factors and their relative effects on the concrete properties are investigated in this literature study. With the aim of gaining a better understanding of the properties and their background that are relevant to this case, such as workability, strength development, heat of hydration and volume changes of normal and high-strength concretes. Special concretes (e.g. colloidal, fibre reinforced, very and ultra high-strength concrete) have not been considered, since they do not relate to this research. The same applies, albeit to a lesser extent, to the durability of concrete (in aggressive environments).

The following topics, each provided in individual sections, are highlighted in this literature study:

- Cement and hydration;
- Aggregates;
- Fresh concrete;
- Hardened concrete;
- Volume changes.

These topics have been investigated by examining various literature resources, in an attempt to bridge between concrete science and its application in the design of concrete mixtures and structures. Special attention has been paid to acquire sufficient knowledge necessary to design a concrete mixture for this thesis and the respective influence of the mixture composition on factors that affect the cracking behaviour of concrete. The literature resources therefore consist of (scientific) articles, reports and books, combined with (Dutch and European) standards and guidelines.

2.2 Cement and hydration

Cement is a finely ground, inorganic substance that initially forms a paste after mixing with water. This paste then hardens due to the chemical reaction between the cement and the added water. The product is an insoluble solid which preserves its strength and stability. Although the share of cement in concrete is relatively small, most properties are determined by it. A certain knowledge of cement is therefore imperative to make the right choices under the given circumstances.

2.2.1 Types and classification

The most used cements are Portland cement and cements derived thereof that contain other cementitious materials, such as blastfurnace slag, puzzolan and/or fly ash. The classification of cements is laid down in the NEN-EN 197-1 [8]. European cements are designated with CEM followed by the number of the cement type in Roman numerals (I to V) and a capital letter indicating the clinker content (A, B or C). Thereafter, another capital letter indicates which other cementitious materials the cement contains. An indication of the standard strength (32.5, 42.5 or 52.5) and early strength (S, N, or R) finalize the designation of European cements. An overview of the classification of cements by composition and strength according to the NEN-EN 197-1 is given in Figures 2.1 and 2.2, respectively. Summarizing the classification of cements with an example: CEM II/B-V 32.5R refers to a Portland-composite cement (type II) consisting of 65-79% clinker (B) and 21-35% of siliceous fly ash (V), with a standard strength of atleast 32.5 MPa and a high early strength (R).

Main types	Notation of the 27 products (types of common cement)		Composition (percentage by mass[a])										
			Main constituents										Minor additional constituents
			Clinker	Blast-furnace slag	Silica fume	Pozzolana		Fly ash		Burnt shale	Limestone		
						natural	natural calcined	siliceous	calca-reous				
			K	S	D[b]	P	Q	V	W	T	L	LL	
CEM I	Portland cement	CEM I	95-100	–	–	–	–	–	–	–	–	–	0-5
CEM II	Portland-slag cement	CEM II/A-S	80-94	6-20	–	–	–	–	–	–	–	–	0-5
		CEM II/B-S	65-79	21-35	–	–	–	–	–	–	–	–	0-5
	Portland-silica fume cement	CEM II/A-D	90-94	–	6-10	–	–	–	–	–	–	–	0-5
	Portland-pozzolana cement	CEM II/A-P	80-94	–	–	6-20	–	–	–	–	–	–	0-5
		CEM II/B-P	65-79	–	–	21-35	–	–	–	–	–	–	0-5
		CEM II/A-Q	80-94	–	–	–	6-20	–	–	–	–	–	0-5
		CEM II/B-Q	65-79	–	–	–	21-35	–	–	–	–	–	0-5
	Portland-fly ash cement	CEM II/A-V	80-94	–	–	–	–	6-20	–	–	–	–	0-5
		CEM II/B-V	65-79	–	–	–	–	21-35	–	–	–	–	0-5
		CEM II/A-W	80-94	–	–	–	–	–	6-20	–	–	–	0-5
		CEM II/B-W	65-79	–	–	–	–	–	21-35	–	–	–	0-5
	Portland-burnt shale cement	CEM II/A-T	80-94	–	–	–	–	–	–	6-20	–	–	0-5
		CEM II/B-T	65-79	–	–	–	–	–	–	21-35	–	–	0-5
	Portland-limestone cement	CEM II/A-L	80-94	–	–	–	–	–	–	–	6-20	–	0-5
		CEM II/B-L	65-79	–	–	–	–	–	–	–	21-35	–	0-5
		CEM II/A-LL	80-94	–	–	–	–	–	–	–	–	6-20	0-5
		CEM II/B-LL	65-79	–	–	–	–	–	–	–	–	21-35	0-5
	Portland-composite cement[c]	CEM II/A-M	80-88	<---------- 12-20 ---------->									0-5
		CEM II/B-M	65-79	<---------- 21-35 ---------->									
CEM III	Blast furnace cement	CEM III/A	35-64	36-65	–	–	–	–	–	–	–	–	0-5
		CEM III/B	20-34	66-80	–	–	–	–	–	–	–	–	0-5
		CEM III/C	5-19	81-95	–	–	–	–	–	–	–	–	0-5
CEM IV	Pozzolanic cement[c]	CEM IV/A	65-89	–	<---------- 11-35 ---------->					–	–	–	0-5
		CEM IV/B	45-64	–	<---------- 36-55 ---------->					–	–	–	0-5
CEM V	Composite cement[c]	CEM V/A	40-64	18-30	–	<-------- 18-30 -------->				–	–	–	0-5
		CEM V/B	20-38	31-49	–	<-------- 31-49 -------->				–	–	–	0-5

a The values in the table refer to the sum of the main and minor additional constituents.

b The proportion of silica fume is limited to 10 %.

c In Portland-composite cements CEM II/A-M and CEM II/B-M, in pozzolanic cements CEM IV/A and CEM IV/B and in composite cements CEM V/A and CEM V/B the main constituents other than clinker shall be declared by designation of the cement (for examples, see Clause 8).

Figure 2.1: Classification of cements by composition according to NEN-EN 197-1 [8].

Strength class	Compressive strength MPa				Initial setting time	Sound-ness (expan-sion)
	Early strength		Standard strength			
	2 days	7 days	28 days		min	mm
32,5 L[a]	-	≥ 12,0	≥ 32,5	≤ 52,5	≥ 75	≤ 10
32,5 N	-	≥ 16,0				
32,5 R	≥ 10,0	-				
42,5 L[a]	-	≥16,0	≥ 42,5	≤ 62,5	≥ 60	
42,5 N	≥ 10,0	-				
42,5 R	≥ 20,0	-				
52,5 L[a]	≥ 10,0	-	≥ 52,5	-	≥ 45	
52,5 N	≥ 20,0	-				
52,5 R	≥ 30,0	-				

a Strength class only defined for CEM III cements.

Figure 2.2: Classification of cements by strength according to NEN-EN 197-1 [8].

2.2.2 Chemical composition

The chemical composition of cement is highly dependent on manufacture, knowledge about the production process is therefore crucial. Although small differences between the various techniques exist, the production process of cement basically consists of the following steps [2, 9]:

1. The raw materials for the production of cement are dried, grounded and mixed in certain proportions to obtain a homogeneous meal. The most notable raw materials are limestone, clay and shale extracted from quarries, which mainly consist of lime (CaO), silica (SiO_2), alumina (Al_2O_3) and iron oxide (Fe_2O_3).
2. After preheating, the raw meal enters a large rotary kiln were the clinker formation takes place. Heated to temperatures up to 1450 °C, the raw meal sinters and fuses into balls known as clinker. The heating temperature and the ratio of raw materials dictate which clinker types are formed.
3. The clinker is then quickly cooled using cold air to a temperature of 150 °C to stop the ongoing clinker formation, after which the clinker is often temporarily stored until further manufacture.
4. Gypsum is added to the clinker, to prevent flash setting of the cement. Depending on the type of cement, blastfurnace slag, puzzolan, fly ash and/or other cementitious materials are added. Which cement type is obtained depends on the dosage of these cementitious materials.
5. This mixture of clinker, gypsum and other cementitious materials is then grounded into a powder known as cement. In a sieving installation, the cement grains are separated according to their fineness. The fineness determines certain properties of the cement, in particular the (early) strength classification.
6. Finally, the cement is stored in silos until bulk or packaged shipment to concrete plants and suppliers.

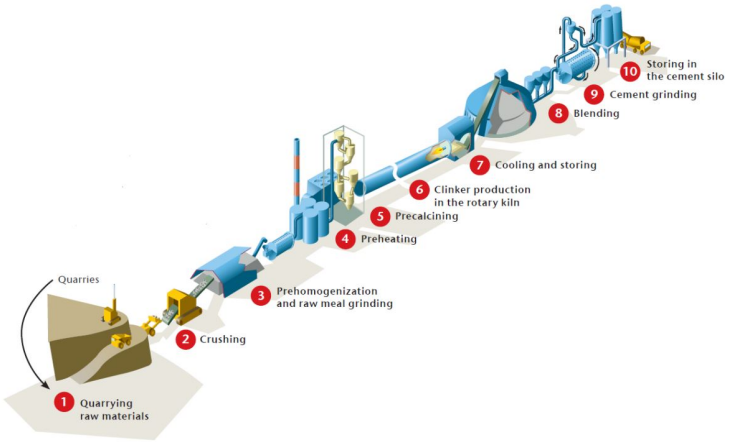

Figure 2.3: Schematic representation of cement manufacturing process, source: IEA.

Portland cement is the most common type of cement and consists, in addition of a small amount of gypsum, almost entirely out of clinker. As mentioned, the raw materials used in the manufacture of Portland cement consists mainly of lime (CaO), silica (SiO_2), alumina (Al_2O_3) and iron oxide (Fe_2O_3). These components interact with each other in the kiln to form a series of more complex compounds, referred to as clinker. Four clinker compounds are usually regarded as the major constituents of cement, these are listed in Table 2.1, together with their abbreviations [2, 10]. This abbreviated designation describes each oxide by one capital letter: $CaO = C$, $SiO_2 = S$, $Al_2O_3 = A$ and $Fe_2O_3 = F$. The calculation of the expected compound composition at a given ratio of raw materials is founded on work by Bogue [11]. Bogue's relations are presented in Equation 2.1, where the term in brackets represents the percentage of the given oxide in the total cement mass. From these relations it becomes clear how sensitive the compound composition is to changes in the dosage of raw materials. A decrease of SiO_2 from 21.5% to 19.8% and a simultaneous increase of CaO from 64.5% to 66.2% leads to an increase of C_3S from 50% to 70% and a decrease of C_2S from 25% to 4% [10]. Later it will appear, that changes in C_3S and C_2S will result in major differences in properties of the cement, especially with regard to the strength development and heat output. The characteristics of concrete can thus be altered by specific choices in the raw materials used for the production of cement.

$$\begin{aligned} C_3S &= 4.07\,(CaO) - 7.60\,(SiO_2) - 6.72\,(Al_2O_3) - 1.43\,(Fe_2O_3) - 2.85\,(SO_3) \\ C_2S &= 2.87\,(SiO_2) - 0.75\,(3\,CaO.SiO_2) \\ C_3A &= 2.65\,(Al_2O_3) - 1.69\,(Fe_2O_3) \\ C_4AF &= 3.04\,(Fe_2O_3) \end{aligned} \tag{2.1}$$

Name of compound	*Oxide designation*	*Abbreviation*	*Composition (% by mass)*
Tricalcium silicate	$3CaO.SiO_2$	C_3S	45-65
Dicalcium silicate	$2CaO.SiO_2$	C_2S	10-30
Tricalcium aluminate	$3CaO.Al_2O_3$	C_3A	5-15
Tetracalcium aliminoferrite	$4CaO.Al_2O_3.FeO_3$	C_4AF	5-12

Table 2.1: Designation and typical composition of clinker compounds in Portland cement, adapted from [2, 10].

Due to various events during the late twentieth century, such as a severe economic recession and an increase in environmental awareness, numerous cementitious materials were introduced to the Portland cements. These types of cement, which consist of more than 5% of cementitious materials other than clinker, are referred to as blended cements. The evolution of blended cements has been encouraged by environmental concerns about the manufacture of Portland cement (which entails high CO_2 emissions) and the way of disposal of industrial waste materials such as blastfurnace slag or fly ash. The cementitious materials consist largely of the same chemical components as Portland cement (see Table 2.2), albeit in different proportions and from other origins, and are therefore also hydraulic in nature [2, 10]. However, most of the cementitious materials used have latent hydraulic properties, that is, they may exhibit hydraulic activity only in the consequence of a chemical reaction with some other compounds such as the hydration products of Portland cement which co-exist in the blend. Cementitious materials which are largely chemically inert and more or less only have a physical effect on the properties of concrete are referred to as fillers and will be addressed later. Blastfurnace slag, often referred to as GGBS and by far the most used in the Netherlands alongside Portland cement, originates from the rapid cooling of slag (a by-product in the production of steel) with water, during which the liquid slag turns into solid, amorphous grains. After grinding, it can be processed into Portland-slag cement (type II) or blastfurnace cement (type III). The typical compound composition of these and other Portland-based cements can be obtained from Figure 2.1 combined with the data given in Table 2.2.

Component	*Composition (% by mass)*			
	Portland cement	*GGBS*	*Puzzolan*	*Fly ash*
CaO	60-67	35-48	2-10	2-10
SiO_2	17-25	28-38	48-71	45-65
Al_2O_3	3-8	6-17	16-22	20-35
Fe_2O_3	1-6	1-3	3-10	4-15

Table 2.2: Typical composition of components in various cementitious materials, adapted from [2, 10].

2.2.3 Hydration process

Hardening is a result of the hydration of cement, binding the aggregates together to form concrete. It should be emphasized that this hydration process is a exothermic chemical reaction and not a drying out process. In the presence of water, the silicates and aluminates listed in Table 2.1 form products of hydration which in time produce a firm and hard mass. In the hydration of cement, five distinct stages can be identified, during which various dissolution- and crystallization reactions take place (an indication of the duration of each phase is given between the parentheses):

- Stage 1: Pre-induction period (15 min);
- Stage 2: Induction, or dormant period (2 hours);
- Stage 3: Acceleration period (12 hours);
- Stage 4: Deceleration period (24 hours);
- Stage 5: Steady state (infinite).

The first reaction takes place immediately after mixing the cement with water. During this pre-induction period (stage 1), C_3A dissolves in the added water. This reaction is the most rapid of all and needs to be controlled to avoid flash setting, resulting in rapid stiffening of the paste and an early loss of workability. This is, as mentioned, achieved by the addition of gypsum to the cement. When a small amount of C_3A dissolves, it subsequently reacts with the gypsum which results in the formation of calcium trisulfoaluminate hydrate (see Equation 2.2), also known as trisulfate or ettringite [10, 12]. This ettringite is formed on the surface of the cement grains and the contact between the water and cement grains is obstructed. As a consequence, the rapid reaction of C_3A stops in a matter of minutes, the hydration process slows down and the dormant period

(stage 2) begins. Since the ettringite crystals are too small to bridge the space between the cement grains, no stiffness is developed and the initial consistency is maintained. The dormant period normally lasts one up to three hours and allows time for the concrete to be transported and processed. The speed of the chemical reactions can thus be altered by changing the gypsum content of the cement in the relation to that of C_3A. At a later time, during the deceleration period (stage 4), the ettringite becomes unstable and transforms into monosulfate (calcium monosulfoaluminate hydrate), by the consumption of C_3A and water (see Equation 2.3). Following the exhaustion of gypsum, the remaining C_3A reacts with water and carbon dioxide, a product of the hydration of C_3S and C_2S, to form tetracalcium aluminate hydrate (see Equation 2.4). Although beneficial in the manufacture of cement, it must be noted that the presence of C_3A is undesirable in the long-term, since it contributes little to the strength of the hydrated cement paste (except at early-age) and can make the concrete susceptible to sulfate attack [2].

$$\underset{\text{tricalcium aluminate}}{3CaO.Al_2O_3} + \underset{\text{water}}{26H_2O} + \underset{\text{gypsum}}{3CaSO_4.3H_2O} \longrightarrow \underset{\text{calcium trisulfoaluminate hydrate}}{3CaO.Al_2O_3.3CaSO_4.32H_2O} \tag{2.2}$$

$$\underset{\text{tricalcium aluminate}}{2(3CaO.Al_2O_3)} + \underset{\text{water}}{4H_2O} + \underset{\text{calcium trisulfoaluminate hydrate}}{3CaO.Al_2O_3.3CaSO_4.32H_2O} \longrightarrow \underset{\text{calcium monosulfoaluminate hydrate}}{3CaO.Al_2O_3.3CaSO_4.12H_2O} \tag{2.3}$$

$$\underset{\text{tricalcium aluminate}}{3CaO.Al_2O_3} + \underset{\text{water}}{12H_2O} + \underset{\text{calcium hydroxide}}{Ca(OH)_2} \longrightarrow \underset{\text{tetracalcium aluminate hydrate}}{3CaO.Al_2O_3.Ca(OH)_2.12H_2O} \tag{2.4}$$

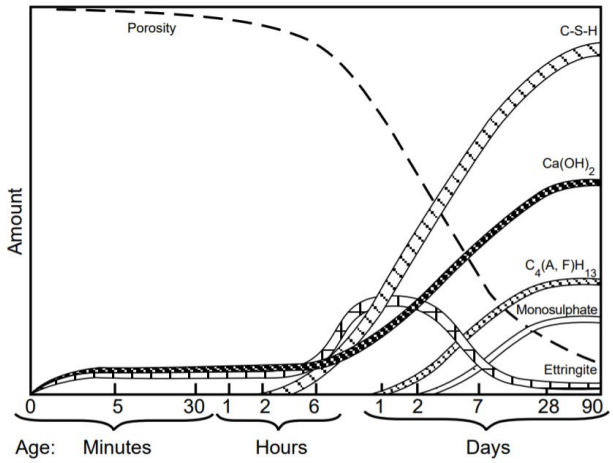

Figure 2.4: Schematic representation of hydration process of Portland cement; the formation of reaction products and reduction of porosity with time [12].

Due to the growth of the largest ettringite crystals at the expense of the smaller ones, water is eventually able to penetrate the cement grains and the surface layer of ettringite is broken down. This reflects the dawn of the acceleration period (stage 3) and the setting of the cement paste. As a result, C_3S dissolves and long fibre CSH crystals are produced (see Equation 2.6) [2, 10]. Another product of this activity is calcium hydroxide, which might partially react with the remaining C_3A (see Equation 2.4), if it is not already depleted by the tri- and monosulfate reactions. When sufficient gypsum is added to the cement (so proper retardation is ensured), most of the framework of the hydrated cement paste is established by calcium silicate hydrate (CSH), while, if C_3A where allowed to react first, a rather porous structure of calcium aluminate hydrate would form. The remaining clinker compounds would then hydrate within this porous framework and the strength of the cement paste would be adversely affected. Similar but slower than C_3A, C_4AF also reacts with the released calcium hydroxide to produce calcium aluminoferrite hydrate (see Equation 2.5), which, like the reaction products of C_3A, only regulates the hydration process and the durability of the hydrated cement paste.

$$\underset{\text{tetracalcium aliminoferrite}}{4CaO.Al_2O_3.Fe_2O_3} + \underset{\text{water}}{10H_2O} + \underset{\text{calcium hydroxide}}{2Ca(OH)_2} \longrightarrow \underset{\text{calcium aluminoferrite hydrate}}{6CaO.Al_2O_3.Fe_2O_3.12H_2O} \tag{2.5}$$

$$\underset{\text{tricalcium silicate}}{2(3CaO.SiO_2)} + \underset{\text{water}}{6H_2O} \longrightarrow \underset{\text{calcium hydroxide}}{3Ca(OH)_2} + \underset{\text{calcium silicate hydrate}}{3CaO.2SiO_2.3H_2O} \tag{2.6}$$

$$\underset{\text{dicalcium silicate}}{2(2CaO.SiO_2)} + \underset{\text{water}}{4H_2O} \longrightarrow \underset{\text{calcium hydroxide}}{Ca(OH)_2} + \underset{\text{calcium silicate hydrate}}{3CaO.2SiO_2.3H_2O} \tag{2.7}$$

The CSH crystals are responsible for the strength of the hardened cement paste. Its structure, which is studied in section 2.2.5, is also decisive in the drying shrinkage, creep and relaxation behaviour of concrete. C_2S also contributes to the production of calcium silicate hydrate (see Equation 2.7), albeit at a slower rate and a resulting in finer distribution than C_3S [2, 10]. These short fibre CSH crystals grow in the space left over between the long fibre C_3S-derived crystals. This takes place during the steady state (stage 5), during which the rate of hydration slows down and the diffusion through the pores of the products of hydration becomes the controlling factor (i.e. water needs to penetrate trough the surface layer of hydrated cement to reach the core of unhydrated cement). The rate of hydration thus decreases continuously, so even after a long time there remains an considerable amount of unhydrated cement. However, after approximately one year, the rate of hydration is of such a slow rate that the cement is assumed to be fully hydrated and therefore at full strength. At this age, the two silicates primarily responsible for the strength of hydrated cement paste, mass for mass, contribute almost equally to the ultimate strength, as can be seen from Figure 2.5. However, as an approximate rule, C_3S contributes most to the strength development during the first 4 weeks and C_2S affects the gain of strength thereafter [2]. Nevertheless, both these silicates are, as mentioned, much stronger than C_3A and C_4AF, which contribution to the strength development is almost negligible (except at early-age). From these philosophies it becomes clear, that both the early-age and ultimate strength of cement can be influenced by changing the proportion of clinker compounds, which is mainly determined by the ratio of raw materials and the heating temperature in the kiln.

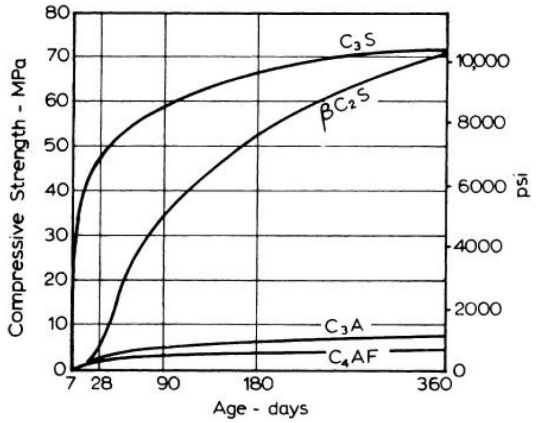

Figure 2.5: Strength development of pure clinker compounds in Portland cement [2].

It may be recalled that, because the hydration starts at the surface of the cement particles, it is the total surface area of cement that represents the material available for hydration. The rate of hydration thus depends on the fineness of the cement grains and, for a fast strength development, high fineness is required [2]. As can be seen from the relation between the concrete strength at different ages and the cement fineness, given in Figure 2.6, the ultimate strength is not affected by the fineness of the cement grains. In addition, an increase in fineness may improve the cohesiveness of a concrete mixture in the plastic state, but it also requires an increase in the amount of gypsum for proper retardation because more C_3A is available for early hydration.

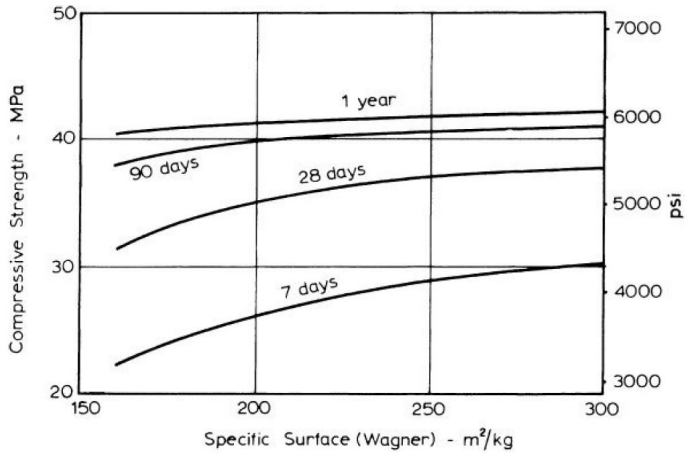

Figure 2.6: Relation between compressive strength at different ages and cement fineness [2].

The previous paragraphs described the hydration process of pure Portland cement. Nowadays, however, many blended cements are used, which in addition to clinker also contain other cementitious materials. Most of these cementitious materials, such as blastfurnace slag, puzzolan and fly ash, bind less water and are latent hydraulic, which means that they will only hydrate once activated. In case blastfurnace slag is blended with Portland cement, this activator is calcium hydroxide, that is mainly released by the reaction of C_3S [10]. Although the reaction products are essentially the same as with clinker, the hydration of blastfurnace slag is significantly slower, mainly due to a lower CaO content (see Table 2.2). Furthermore, less calcium hydroxide will be released, since it is incorporated in the CSH crystals formed due to the hydration of the slag. The characteristics of Portland cement blended with blastfurnace slag depend on the share of clinker in relation to that of the slag. The more blastfurnace slag is present, the more it will govern the properties and the hydration process of the cement. Up to a share of 35% of blastfurnace slag (type II), the character is more analogous to that of Portland cement, while cements with higher proportions (type III) will more strongly exhibit the properties of blastfurnace slag. The same principles hold for Portland cements blended with fly ash; the hydration of the fly ash is initiated by that of the clinker. Since fly ash contains hardly any CaO and it first needs to be broken down by high alkalinity pore water, the hydration proceeds even more slowly. As a rule of thumb it can be assumed that, under identical conditions and equal fineness, the time it takes for pure blastfurnace slag or fly ash to achieve the same degree of hydration is 3 or 7 times as long than that of Portland cement, respectively [10]. Therefore, to ensure extensive hydration of blastfurnace slag and even more in the case of fly ash, the cement paste must be kept moist for a long time or the cement grains should be ground more finely to guarantee faster hydration.

2.2.4 Heat of hydration

In common with many chemical reactions, the hydration of cement is exothermic. This means that energy in the form of heat is produced by the reaction of clinker and other cementitious materials with water. Since the thermal conductivity of concrete is comparatively low, it acts as an insulator, and hydration can result in a large temperature rise. Due to subsequent cooling of the concrete, thermal shrinkage occurs, which may result in cracking. From this it is clear then, that it is imperative to know the heat production of different cements in order to determine the most suitable cement for a given purpose. Although the hydration of cement is responsible for the temperature rise in young concrete, it is not the only factor of influence. In addition to the cement composition, fineness and dosage, there are other circumstances that affect the temperature development of young concrete, such as the physical and thermal properties of the concrete composite (mainly depending on the aggregates) and the temperature at which the hydration takes place (influenced by e.g. ambient and mix temperature, presence of insulation and artificial cooling or heating).

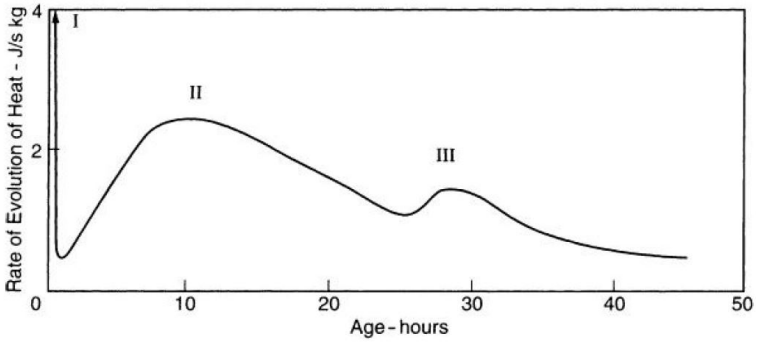

Figure 2.7: Heat development of Portland cement with water/cement ratio of 0.4 [2].

The heat of hydration is the quantity of heat, in joule per gram of unhydrated cement, evolved upon complete hydration at a given temperature. The heat of hydration is usually determined under adiabatic conditions, during which the produced heat cannot dissipate, thereby fueling the hydration of the cement. Typical ultimate heat of hydration of the clinker compounds of Portland cement are given in Table 2.3, in which the last column represents the proportion of heat of hydration of a clinker compound relative to a typically composed Portland cement (as calculated from data in Table 2.1). For practical purposes, it is not only the ultimate heat of hydration that matters but also the rate at which it develops, since heat produced over a longer period can be dissipated to a greater degree, resulting in a smaller temperature rise. In the heat development of Portland cement, which is presented in Figure 2.7, three peaks can be identified from the time when the dry cement first comes into contact with water [2, 10]. The first peak (I) is very high and corresponds to the rapid reactions of C_3A during the pre-induction period (stage 1). The duration of this peak is very short due to the formation of ettringite, which results in the dawn of the dormant period (stage 2). In the end, the surface layer of

ettringite is broken down and the rate of hydration increases again until it hits a second peak (II). During this acceleration period (stage 3), C_3S reacts with water to form CSH crystals and setting of the cement occurs. Following this peak, the deceleration period (stage 4) begins and the rate of hydration slows down over a long period. With most cements, there is a renewed increase in the rate of hydration up to a third and lower peak (III). This peak is corresponds to the renewed reaction of C_3A, following the depletion of gypsum. Finally, the steady state (stage 5) is reached, during which the diffusion through the pores becomes the controlling factor and the rate of hydration decreases even further. It can be deduced from the heat development that the stages in the heat production explicitly correspond to those of the hydration process of the cement. This means that the progress of the cement hydration, and indirectly also the strength development of the concrete, can be determined by measuring the produced heat.

Compound	*Heat of hydration*	
	Pure (J/g)	*Composed (% by heat)*
C_3S	502	55-71
C_2S	260	8-13
C_3A	867	14-22
C_4AF	419	7-11

Table 2.3: Typical heat of hydration of clinker compounds, pure and composed in Portland cement, adapted from [2, 10].

For a typical Portland cement, about 50% of the heat is evolved between 1 and 3 days, about 75% in 7 days, and 90% of the heat in 6 months [2]. However, the rate of heat development is sped up by an increased temperature at which the hydration takes place. There is little effect of the temperature on the ultimate heat of hydration. Both the early-age and ultimate heat of hydration depend on the chemical composition of the cement, and are approximately equal to the sum of the heat of hydration of the individual clinker compounds when hydrated separately. It follows that by reducing the dosage of the most rapidly hydrating compounds (C_3A and C_3S) the heat of hydration at an early-age can be reduced. A similar effect can be achieved through a decrease in cement fineness, which slows down hydration and thus heat production. Furthermore, also the richness (i.e. cement content) of the concrete mixture can be varied to control the heat development.

Typical heat of hydration (after 7 days) of various commonly used cement types in the Netherlands are given in Table 2.4. These Portland-based cements are distinguished by the addition of blastfurnace slag (GGBS) or fly ash. These cementitious materials hydrate, as discussed earlier, less rapid than clinker and bind less water, resulting in both lower early-age and ultimate heat of hydration. Since the hydration of these cementitious materials in blended cements must be activated by formation of calcium hydroxide due to reaction of the silicates present in Portland cement, little is known about the heat of hydration of these cementitious materials alone. However, in the case of pure blastfurnace slag, the typical ultimate heat of hydration is of the order of 350 J/g [10]. Blended cements which produce less than 270 J/g of heat in the first 7 days acquire an LH (low heat) designation in addition to their formal type description.

Type	*Composition (% by mass)*		*Heat of hydration (J/g)*
	Clinker	*GGBS & Fly ash*	
CEM I 52.5R	95-100		350
CEM II/B-V 32.5R	65-79	21-35	275
CEM III/A 52.5N	35-64	36-65	315
CEM III/B 42.5N	20-34	66-80	245

Table 2.4: Typical heat of hydration (after 7 days) of common cement types in the Netherlands, source: ENCI.

2.2.5 Structure and porosity

Many of the mechanical properties of hardened cement paste and concrete depend on the physical structure of the products of hydration and to a lesser extent on the chemical composition of the hydrated cement. Fresh cement paste is a plastic substance of cement particles in water but, after setting has occurred, its gross volume remains approximately constant [2, 10]. At any stage of hydration, in addition to some other minor components, the hardened cement paste mainly consist of CSH crystals from the hydration of the clinker compounds and other cementitious materials, collectively referred to as gel, of calcium hydroxide, unhydrated cement, and the residue of the water-filled spaces in the fresh paste. These voids are called capillary pores,

whereas the interstitial voids within the gel are referred to as gel pores. Calcium hydroxide is often present in these pore spaces and ensures a high alkalinity of the pore water. The ratio of the gel, formed by CSH crystals, to calcium hydroxide is roughly 7:2 [2]. In contrast to the gel, the contribution of calcium hydroxide to the strength of the cement paste is very small. The physical development of a hydrating cement paste is given in Figure 2.8, in which the black mass represents the unhydrated cement, the fine black grid the hydrated cement gel with gel pores, and the larger white cavities the capillary pores. From this it is clear that the porosity decreases during hydration and that the capillary pores are one or two orders of magnitude larger than the gel pores. The phases in the physical development should be interpreted as follows:

- Phase A: Immediately after mixing the cement; the unhydrated particles are dispersed in water, the cement paste is in a plastic state;
- Phase B: Two hours after mixing the cement; the hydration products start forming on the surface of the cement particles, setting of the cement paste occurs and the workability starts to decrease;
- Phase C: One day after mixing the cement; the products of hydration start to bridge the gaps between the cement particles, hardening of the cement paste occurs and the framework starts to form;
- Phase D: One week after mixing the cement; the products of hydration form a more dense mass, capillaries still exist which have not been filled with hydration products and the strength of the cement paste will be about 70% of the ultimate strength.

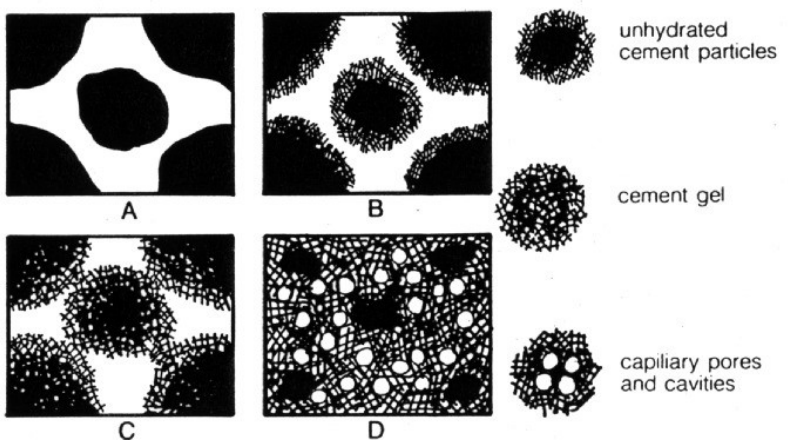

Figure 2.8: Schematic representation of the physical development a hydrating cement paste, source: Cortec Corp.

When zoomed in at the structure of the hydrated cement paste, as shown in Figure 2.9, it is clear that the CSH crystals occur in crumpled sheets between which interlayer water may be present. The actual source of the strength of the gel is not fully understood but it probably arises from two kinds of cohesive bonds [2, 10]. The first type being the chemical and interparticle bonds at the point where the CSH sheets are connected together. The second source of attraction is are the physical bonds between the surfaces of the CSH sheets, separated only by gel pores or interlayer water; this attraction is usually referred to as van der Waals' forces. The magnitude of these forces is inversely proportional distance between the two CSH sheets involved, as well as their surface area. The relative importance of the physical and chemical bonds is difficult to assess, but there is no doubt that they both contribute considerably to the strength of the hardened cement paste. It is also believed that the withdrawal of moisture from the gel pores, and the redistribution of CSH sheets forming the cement gel, are the main causes of the drying shrinkage, creep and relaxation behaviour of concrete.

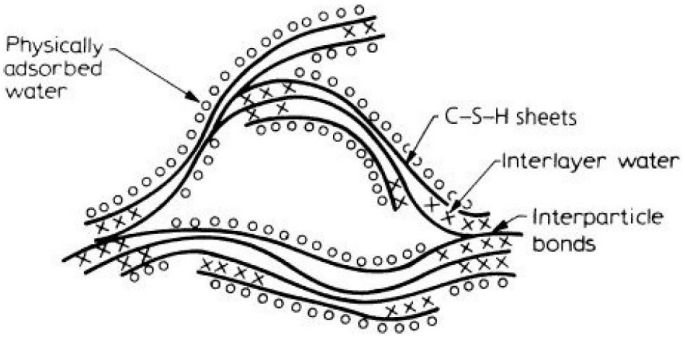

Figure 2.9: Schematic representation of the structure of CSH crystals [2].

During the hydration of cement a certain amount of water is chemically bonded to the clinker compounds and other cementitious materials. This so-called chemically bonded water forms a part of the gel particles and is not degradable (at temperatures up to 1000 °C). The transition to chemically bonded water is accompanied by about a 25% decrease in water volume, which is known as chemical shrinkage [10]. However, since the gross volume of the cement remains constant, pores must form internally. In addition to chemically bonded water, parts of the added water are also physically bonded. The voids in the hydrated cement paste occupied by this physically bonded water are considered to be the gel pores. The physically bonded water held at the surface of the gel particles is referred to as absorbed water, and the part which is held between the CSH sheets of the cement particles is called interlayer or zeolitic water [2]. Relative to the mass of cement is 25% chemically and 15% physically bonded water [10]. This means that, in theory, 40% water needs to be added to the cement to achieve complete hydration. For a water/cement ratio of 0.4, free water (held in the capillary pores beyond the surface forces of the gel particles) is no longer available at complete hydration, this phenomenon is known as self-desiccation and can be inferred from Figure 2.10. At lower water/cement ratios, unhydrated cement remains due to the lack of free water. The opposite holds for higher water/cement ratios; free water remains because the unhydrated cement is depleted. In practice, however, due to the progressively decreasing accessibility of unhydrated cement with ongoing hydration, complete hydration is almost never reached for any water/cement ratio. The ratio of the quantity of water that is actually bound at a given time to the maximum possible amount of water to be bound is called the degree of hydration. This is equivalent to the quantity of hydrated cement at a given time, divided by the available amount of cement. A higher ultimate degree of hydration is possible at a higher water/cement ratio. It can be deduced from this relationship that the water/cement ratio also affects heat of hydration, which is addressed in the previous section, as a larger quantity of water ultimately enables more cement to hydrate. With this in mind, the degree of hydration can also be established in virtue of the fact that the heat output is proportional to the amount of cement reacted.

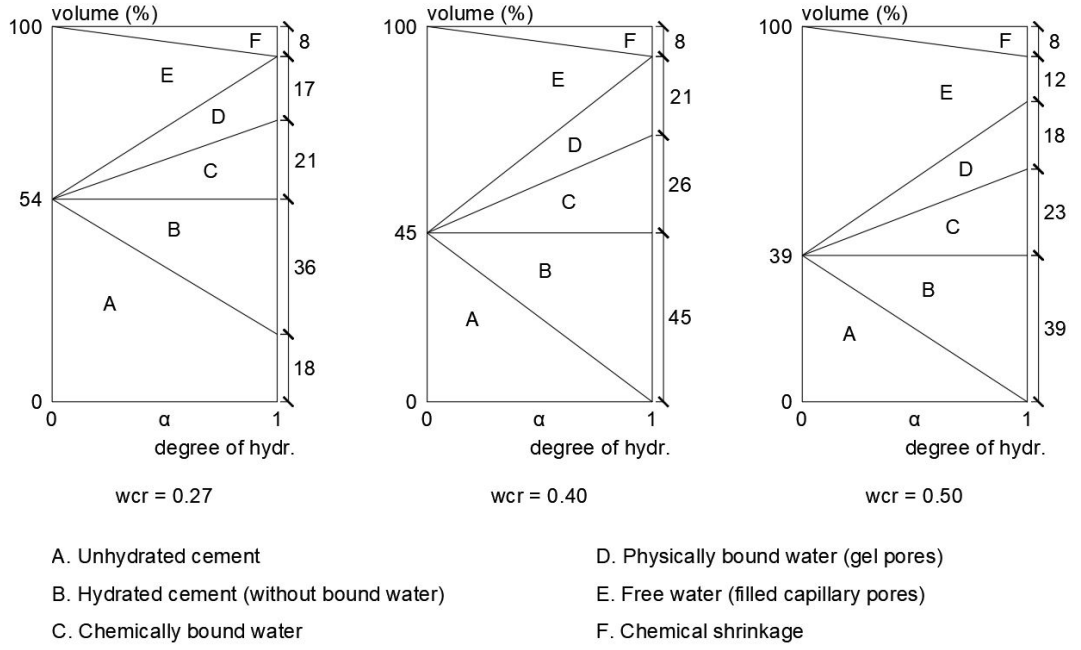

Figure 2.10: Schematic representation of hydration process for different water/cement ratios; development of component volumes as function of the degree of hydration, adapted from [10].

Porosity is defined as the total volume fraction of voids in a medium. The strength and durability of concrete is fundamentally dependent on the porosity and pore (size) distribution of the hydrated cement paste [2, 10]. Especially the capillary pores are of interest, since they are often largely responsible for the porosity. A higher porosity of the hydrated cement paste, thus a larger volume of capillary pores and entrapped air, has a an adversely effect on both the strength and durability of concrete. With regard to the durability, a higher porosity will most likely, but not necessarily, result in a higher permeability. This allows deleterious substances to penetrate the concrete more easily, which may lead to degradation. With regard to the concrete strength, the relation with the porosity p can be expressed by Equation 2.8, where c and n are coefficients that need not be constant. The exact form of this relation and the values of the coefficients are, however, uncertain. Furthermore, quantifying the porosity of a hydrated cement paste is difficult. Nevertheless, it is known that the cement paste exhibits a finer porosity and a lower total pore volume with decreasing water/cement ratio

and increasing degree of hydration. This means that the strength of concrete is affected, in addition to other influences, in the same way by these factors. Many empirical studies have confirmed this relationship between the degree of hydration, water/cement ratio and the strength development of concrete. Figure 2.11 illustrates the relation discovered by Fagerlund [13]. From this is it clear that after having reached a critical degree of hydration, the strength increases almost linearly with an increasing degree of hydration. This critical degree of hydration is a function of the water/cement ratio. This is expected since, after mixing the cement with water, the particles are further dispersed from each other in case of a higher water/cement ratio. Hence, the degree of hydration must be higher before the hydration products are able to bridge the gaps between the cement particles.

$$f_c = c \cdot (1-p)^n \tag{2.8}$$

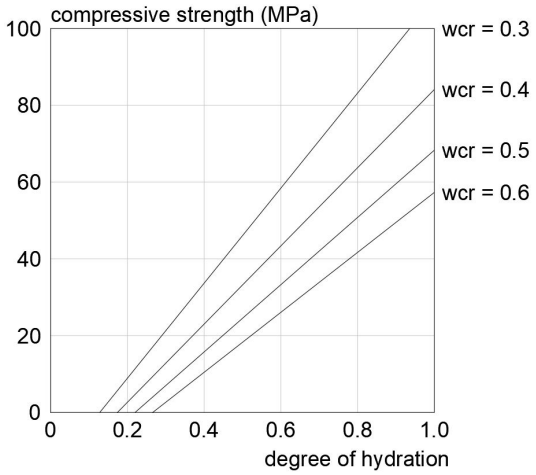

Figure 2.11: Relation between compressive strength and degree of hydration for different water/cement ratios, adapted from [13].

2.3 Aggregates

The hardened cement paste resulting from the hydration process between cement and water could achieve sufficient strength to enable it to function on its own. However, this is very expensive and it would suffer from high volume instability and a low durability. For these reasons, as much aggregates are introduced to the concrete mixture to allow the cement paste to function as the binder of the aggregates. Although not strictly true, aggregates can largely be viewed as chemically inert materials of which mainly the physical and thermal properties influence the performance of concrete. Because the aggregates take up approximately three-quarters of the volume of the concrete, it is clear that its characteristics are of considerable importance.

2.3.1 Types and classification

Aggregates can be classified according to various characteristics, the most common of which are particle size, specific weight and origin. The choice for type of aggregates, classified according to specific weight, depends to a large extent on the desired density of the concrete. With regard to the density, concrete is divided into three categories according to the NEN-EN 206, being [14]:

- Lightweight concrete: oven-dry specific weight below 2000 kg/m^3;
- Normalweight concrete: oven-dry specific weight between 2000 and 2600 kg/m^3;
- Heavyweight concrete: oven-dry specific weight above 2600 kg/m^3.

The classification of aggregates by their specific weight roughly corresponds to the above, with the exception that one speaks of heavyweight aggregates if their specific weight is at least 2800 kg/m^3.

When classifying aggregates by origin, a distinction can be made between natural, artificial and recycled aggregates. Artificial aggregates (e.g. expanded clay particles) are usually applied in lightweight concrete, but certain naturally occurring rocks such as pumice are also suitable. Lightweight concrete is often used as an insulation material and if there is a necessity to reduce the self-weight. Heavyweight concrete, mainly used in radiation shielding structures and counterweights, consists either of naturally occurring minerals such as barite, or synthetic compounds derived from various metals. Although light- and heavyweight concrete should be mentioned for the sake of completeness, the vast majority of structures are constructed from normalweight

concrete, which in most cases uses natural aggregates. However, encouraged by the desire for a circular economy, recycled masonry and concrete aggregates are also increasingly used. These aggregates are obtained from the selective crushing of debris from demolition works. Nevertheless, the following paragraph and upcoming sections will be limited to the further classification and properties of natural aggregates intended for normalweight concrete.

Many different types of natural aggregates exist, an overview of common aggregate types and their typical properties is presented in Table 2.5. These aggregates are composed of various minerals, such as quartz and feldspar. A further distinction between these aggregates can be made by looking at their respective origins and methods of extraction. Natural aggregates can be retrieved from inland or coastal deposits, which are often reduced to its present size by a weathering process (i.e. wind, water, or glacial erosion), or from the deliberate fragmentation of rocks extracted from quarries [2]. This distinction is reflected in the shape and texture of the aggregates. Crushed aggregates are rough and angular, while eroded aggregates are smooth and rounded. Although retrieval from inland or coastal deposits is preferred for its ease of extraction, the type of aggregates used mainly depends on geography, as not all types are widely available. In the Netherlands, aggregates like sand and gravel are primarily obtained from river deposits and largely consist of quartz and flint, respectively [15, 16].

Type	*Specific mass* (kg/m^3)	*Compressive strength* *(MPa)*	*Thermal expansion* $(\mu\varepsilon/K)$
Basalt	2700-3200	250-400	3-10
Diabase	2800-3100	140-300	3-10
Diorite	2800-3100	80-340	4-10
Dolomite	2800-2900	80-240	7-9
Flint	2400-2600	130-270	7-13
Gabbro	2700-3300	170-300	3-10
Gneiss	2600-3000	90-240	6-10
Granite	2600-3000	110-260	2-12
Limestone	2200-2800	90-240	2-12
Marble	2400-2700	50-240	2-16
Quartzite	2600-2700	120-420	7-13
Sandstone	2000-2700	40-240	4-14

Table 2.5: Typical properties of common natural aggregate types, adapted from [2, 10].

2.3.2 Shape, size and texture

Not so much the mineralogical composition of the aggregates, but the external characteristics are of influence to the properties of both fresh and hardened concrete, in particular the particle shape, size and surface texture. There is no doubt that the particle shape affects the workability of fresh concrete, but a suitable method measuring and describing shape is not yet available. Nevertheless, it is known that with rounded aggregate particles less water is required to obtain the same consistency as with angular aggregate particles [2, 10]. The likely reasons for this are that rounded particles have a smaller surface-area-to-volume ratio and are exposed to less inter-particle friction. Due to this lower water requirement, a higher strength is potentially possible. The same holds for the texture; a smooth particle surface demands less water compared to a rough one. From a workability point of view, naturally eroded aggregates are therefore preferable to crushed aggregates. Nevertheless, with angular particles a better bond can be achieved between the aggregates and the cement paste due to mechanical interlocking. This is reflected in a higher strength of concrete composed of crushed aggregates. However, this benefit is often lost due to a higher water requirement. It must be noted that, in addition to mechanical interlocking, the mineralogical composition of the aggregates also slightly affects the bonding with the cement paste. Although little is known about these phenomena, and relying on experience is still necessary to predict the bonding between aggregates and cement paste, chemical bonds may exist in case of limestone and siliceous aggregates.

(a) source: Grand Rapids Mulch. **(b)** source: American Landscape Supply Ltd.

Figure 2.12: Natural aggregates: crushed (a) and naturally eroded (b).

The aggregate particle size also directly affects the water requirement of concrete. For the same volume, smaller size particles have a larger surface area and thus require more water for lubrication, with a consequent reduction of the strength potential. As for the particle shape and texture, there is therefore also a clear desire regarding the size when only the workability of the fresh concrete is considered. However, other factors also play a role in the choice of aggregate particle size. First, the concrete cover to the formwork and fineness of present reinforcement must be kept in mind when choosing the size of the particles. The fresh concrete should be able to flow through the reinforcement, without the aggregates getting stuck or trapped in it, leading to segregation. This fact sets an upper limit to the particle size of the aggregates. Second, in order to obtain the best performing concrete in terms of strength and durability in relation to costs, voids between the aggregates should be avoided [2]. This can only be achieved if a range of particle sizes is applied, which increases the packing density of the concrete. A more densely packed concrete is more economical since less voids have to be filled by the more expensive cement paste, and it aids in minimizing the risk of segregation of the fresh concrete during processing. Therefore, in addition to the maximum particle size, also the particle size distribution of the aggregates is very important. More on the grading of aggregates and the particle size distribution in relation to the properties of fresh concrete will be addressed in the subsequent section.

It is clear that the strength of concrete cannot exceed that of a major part of the aggregates contained therein. As can be deduced from Table 2.5, natural aggregates are generally significantly stronger than hardened concrete. However, the concrete strength is usually not determined by the strength of the aggregates, since the hardened cement paste and its bond with the aggregates are weaker, they are decisive. The concrete strength is, for reasons discussed later, also considerably influenced by the difference between the elastic modulus of the hardened cement paste and that of the aggregates. Hence, it is important to get a sense of the stiffness of the aggregates. The elastic modulus of aggregates is rarely determined, but for the natural aggregates presented in Table 2.5 it is in the range of 20 to 100 GPa [10]. As is the case with the strength, the stiffness of the aggregates is greater than that of the hardened cement paste. Furthermore, the stiffness of the concrete is generally higher, the higher the elastic modulus of the aggregates embedded therein [2].

Finally, the presence of internal pores in aggregate particles must be mentioned. The porosity of aggregate, its permeability, and its absorption influence properties such as its specific mass, the bonding with the hardened cement paste, and the resistance of concrete to freezing and thawing. The pores in the aggregate vary in size, but are significantly larger than the gel pores in the cement paste [2]. For the natural aggregates given in Table 2.5, the porosity is in the order of 0.5% to 10% of their respective volume [10]. In addition to adsorption to the surface of the aggregates, water can be absorbed into its pores. When the pores are all full, they are said to be saturated. Normally, the aggregates are saturated at setting of the concrete [2]. This means that if the aggregates are added in a dry condition, water will be extracted from the fresh concrete to get the aggregates in a saturated condition, and this absorbed water is not present as free water any more. The absorption of water by aggregates may also result in some loss of workability. On the contrary, when saturated aggregates are added, no free water will dissipate due to absorption, but the dosage must take into account the increased specific mass of these aggregates. Furthermore, the degree of water adsorbed to the surface of the aggregates, referred to as moisture content, contributes to the content of free water and will occupy a volume in excess of that of the aggregate particles. In practice, the moisture content mainly depends on the way the aggregates are stored, since aggregates exposed to rain adsorb a substantial amount of water. It can thus be concluded, that the water content of the aggregates, which is the sum of the absorption and moisture content, should be accounted for in the concrete composition.

2.3.3 Grading

Grading is the operation of dividing aggregates into fractions, each consisting of particles of the same size. In practice, each fraction contains particles between specific limits, these being the openings of standard test sieves [2]. According to the NEN-EN 933-2, these standard test sieves must have square openings of the following sizes: 63, 31.5, 16, 8, 4, 2, 1, 0.5, 0.25, 0.125 and 0.063 mm [17]. One speaks of fine aggregates for particles that pass through the 4 mm sieve and of coarse aggregates for particles that are retained by the 4 mm sieve. The results of a sieve analysis, which is the passing of a representative sample of aggregates through a set of standard test sieves, are often expressed as the (cumulative) percentage by mass of aggregates retained by and/or passing through a sieve with given size. These results can be presented in tabular form or graphically in a so-called grading curve. The latter is extensively used since it makes it possible to see at a glance whether the grading of the aggregates conforms to that specified, or is too coarse or too fine, or deficient in a particular size. In addition, the results of a sieve analysis can also be represented by a single factor, referred to as the fineness modulus, and is defined as the sum of the cumulative percentages of aggregate residue held by specific sieves divided by 100. Although it is clear that one parameter, a weighted average, cannot be representative of a distribution, the fineness modulus does give an indication of the coarseness of the aggregates.

When looking at whether or not a particular grading of aggregates is suitable, it is important to know that no ideal grading curve exists, but a compromise should be aimed at. As mentioned earlier, the particle size distribution is primarily a trade-off between costs of cement paste and the workability of the fresh concrete. From a perspective of costs it is desirable to have the particle sizes evenly distributed (from maximum to minimum aggregate size) and let the aggregates occupy the largest relative volume possible, as the aggregates are cheaper than the cement paste. This results in the most densely packed concrete and allows the cement paste to act as the binder of the cement paste as much as conceivable. Nevertheless, this also means that, due to the large surface-area-to-volume ratio of the aggregates, a vast amount of water is needed for lubrication to obtain the desired consistency of the fresh concrete. The strength of the hardened concrete with given water/cement ratio is, in principle, not directly affected by the grading of the aggregates. However, as the strength is dependent on the water/cement ratio and the amount of water added is also related to the workability, the particle size distribution of the aggregates does have an indirect influence on the strength of the hardened cement paste. Besides the latter indirect influence, it can thus be stated that the desired grading of the aggregates is governed by the following factors, the latter two of which are addressed in more detail in subsequent sections [2]:

- The total surface area of the aggregates;
- The relative volume occupied by the aggregates;
- The workability of the fresh concrete;
- The tendency to segregation of the fresh concrete.

In general, there are few requirements with regard to the particle size distribution of aggregates in concrete and are also hardly included in standards such as the NEN-EN 206 [14]. Nevertheless, given the large influence on the workability and water requirement, it is broadly recommended to match the particle size distribution of the aggregates with proven gradings [18]. In this paragraph, the properties of some proven gradings and their respective differences with regard to workability and water requirement will be discussed. Three grading curves for a maximum aggregate size of 16 mm are shown in Figure 2.13. However, due to the presence of under- and oversized aggregates and because of possible variations within fractions, practical gradings are more likely to be in the vicinity of these curves than to follow them exactly. Therefore, it is preferable to consider grading zones, which are the areas between the curves. Grading zone I represents coarser gradings, whereas grading zone II represents finer gradings. Gradings in zone I are comparatively workable and are therefore suitable for concrete mixtures with a lower water/cement ratio or for rich mixtures [2]. However, with these gradings it is necessary to make sure no segregation takes place. In contrast, gradings in zone II will be more cohesive but less workable. If the same workability is to be obtained with gradings in zone I and II, the latter would require a considerably higher water content. This would result in a lower strength if both concretes have the same aggregate/cement ratio or, if the same strength is required, the concrete containing the finer aggregates would have to be noticeably richer. In the case of gradings lying in both zones, there is a danger of segregation when too many intermediate particles sizes are absent. A common measure to ensure that a concrete mixture is satisfactorily cohesive and workable, is to make sure that it contains sufficient fine material. According to the NEN 8005, fine material is defined as the summation of cement, fillers and aggregates passing trough the 0.25 mm sieve [19]. This partly explains why (since it is also for durability reasons), depending on the maximum aggregate size, a minimum amount of fine material in concrete is laid down in standards such as the NEN 8005.

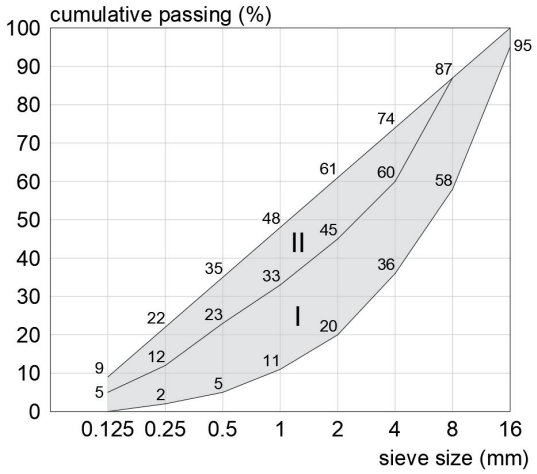

Figure 2.13: Grading curves and zones for maximum aggregate size of 16 mm, adapted from [18].

2.3.4 Fillers

Fillers are finely ground, inert or (latent) hydraulic substances, of about the same fineness as Portland cement, which can be added to the concrete to increase the amount of fine material. This has, due to the physical properties of fillers, a beneficial effect on certain properties such as the consistency and cohesiveness of fresh concrete, as well as the porosity and permeability of hardened concrete [2]. An increased amount of fine material results in a smaller proportion of voids to be filled by the cement paste (i.e. better packing density) and contributes to a finer porosity of the cement paste by refining the larger pores while more or less maintaining the total pore volume. The NEN-EN 206 distinguishes between inert (type I) and cementitious (type II) fillers [14]. Inert fillers such as limestone powder can best be considered as very fine aggregates since they have no binding function (i.e. no chemical reaction occurs with the added water). These fillers therefore only contribute to the packing density of concrete and may also act as additional nucleation sites for the hydration of the cement [2]. Cementitious fillers (e.g. fly ash, trass, silica fume and GGBS) do have a binding function due to their (latent) hydraulic character, provided that they are used in combination with a suitable cement type. These fillers thus not only affect the packing density of concrete, but also involve the reactivity of the cement paste during hydration, resulting in a higher strength potential. This should be taken into account by considering, under certain conditions, part of the cementitious filler as a binder in addition to the cement. In such cases one no longer speaks of a water/cement ratio but of a water/binder ratio. The binder content being the sum of the amount of cement and the quantity of cementitious fillers multiplied by a reduction factor depending on the type of cement, filler and the filler/cement ratio applied.

2.3.5 Alkali-silica reaction

Previously it was stated that aggregates are a largely chemically inert material. However, during the late twentieth century it became apparent that this is not strictly true. Certain chemical reactions between the aggregates and the hydrated cement paste may occur. The most common reaction is between the reactive silica of the aggregates and the alkalis in the cement, also known as alkali-silica reaction or ASR for short [2, 10]. When alkalis (e.g. Na_2O) present in cement come into contact with water, alkali-hydroxides are produced (see Equation 2.9). Subsequently, these alkali-hydroxides attack the siliceous minerals present in the aggregates (see Equation 2.10). As a result, an alkali-silicate gel is formed, either in pores of the aggregates or on the surface layer of the aggregate particles (where reactive silica is present). Because the gel consumes water, it has the consequent tendency to increase in volume. This results in internal pressures in the hydrated cement paste surrounding the aggregates, which may eventually lead to expansion, cracking and disruption of the concrete. However, the reaction proceeds very slowly and the degradation is often only visible after many years. Furthermore, harmful ASR can only occur if the following conditions are satisfied: [10]:

- The aggregates must be ASR-sensitive (i.e. they must consist of reactive silica);
- An adequate amount of alkalis must be present in the concrete;
- There must be sufficient moisture available in the concrete, permanently or regularly.

$$\underset{\text{alkali}}{Na_2O} + \underset{\text{water}}{H_2O} \longrightarrow \underset{\text{alkali-hydroxide}}{2NaOH} \tag{2.9}$$

$$\underset{\text{reactive silica}}{SiO_2.H_2O} + \underset{\text{alkali-hydroxide}}{2NaOH} \longrightarrow \underset{\text{alkali-silica gel}}{Na_2SiO_3.2H_2O} \tag{2.10}$$

Since ASR seriously affects the durability of concrete, it must be prevented in order to enhance its service life. This can be achieved by eliminating any of the above conditions that cause ASR. In the Netherlands, a guideline on the prevention of ASR has been drawn up, also known as CUR recommendation 89 [20]. It is generally accepted that the requirements of the NEN-EN 206 are met when following CUR recommendation 89. This guideline features preventative measures depending on the relative humidity and the presence of salts in the environment in which the concrete structure is located. From this it can be deduced that the use of a suitable cement (i.e. a cement that is low in alkalis) is the simplest way to avoid ASR. By applying blended cements to which adequate blastfurnace slag or fly ash has been added to obtain a low alkali content, it is predominantly possible to realize sufficient ASR-resistant concrete. When one cannot or does not want to adhere to the prescribed cements, aggregates must be used that have been demonstrated not to be ASR-sensitive. This can be demonstrated by carrying out one or more expansion tests, whose procedure is described in CUR recommendation 89. It must be pointed out that, since swelling cannot occur in case of an absence of moisture, harmful ASR does not appear in concrete structures located in a dry environment and less than 1 m thick. Therefore, no preventative measures need to be taken with regard to these structures, regardless of the concrete composition and the choice of aggregates.

2.4 Fresh concrete

Fresh concrete refers to concrete in the period between mixing and setting. During this period the concrete is in a plastic state and therefore workable, meaning it can be processed. The processing of concrete generally consists of the following successive activities: transport to construction site, pouring in formwork (i.e. casting), compaction, and smoothing or finishing. This section is devoted to the essential properties of fresh concrete, being consistency and cohesiveness, mainly affecting the extent to which these actions can be performed appropriately. Although the interest in these properties is only brief, it should be noted that the properties of hardened concrete, in particular the strength, are seriously affected by the degree of compaction and the care during handling. Finally, for the sake of completeness it must be mentioned that in the period between processing and setting the concrete is sometimes referred to as 'green'. The strength of fresh and green concrete has not been studied.

2.4.1 Workability and compaction

Workability and consistency are often confused with one another, but are fundamentally different. There are several descriptions of workability, which may also be referred to as processability, but it can best be defined as the ease with which fresh concrete can be processed without segregation [2]. As mentioned, one of the events in the processing of concrete is compaction. The definition of workability is therefore sometimes also described as the amount of work required to achieve full compaction. To understand this latter definition it is important to know what happens when concrete is being compacted. Compaction basically consists of removing entrapped air from the concrete, by ramming or vibration, until it has reached the closest configuration possible. Thus, work is needed to overcome the internal friction between the particles in concrete, as well as the surface friction between the concrete and the formwork or reinforcement. It should be noted that workability is not a inherent property of concrete as it also depends on the conditions (i.e. where and how the concrete is transported, poured, compacted, and finished or smoothed). For example, the workability of a concrete mixture that is workable enough for thick or massive concrete structures is not necessarily sufficient for thin, inaccessible or heavily reinforced structures. Simply put, fresh concrete of the same consistency may vary in workability. However, it goes without saying that the workability of concrete is largely determined by its consistency, which is examined in the next section.

In addition to fresh concrete, workability is also a crucial property as far as the hardened concrete is concerned because compaction must be possible with reasonable amount of work. The need for compaction becomes clear when looking at the relation between the strength and density (i.e. degree of compaction) of concrete, given in Figure 2.14. From this it can be deduced that the presence of voids greatly reduces the strength; 5% of voids can lower the strength by as much as 30%, and even 2% of voids can result in a strength drop of 10% [2]. These voids are either bubbles of entrapped air or capillary pores from which the free water has been removed. The volume of the latter depends mainly on the water/cement ratio of the concrete mixture. The entrapped air, which are essentially accidentally incorporated air bubbles one or two orders of magnitude larger than the capillaries, is more or less governed by the amount the fine material and can more easily be removed from a concrete mixture with a higher water content. It follows that there is an optimal water/cement ratio at which the sum of the entrapped air and the capillary pores is lowest and the most densely packed concrete can be obtained. However, this optimal water content may vary for different compaction techniques.

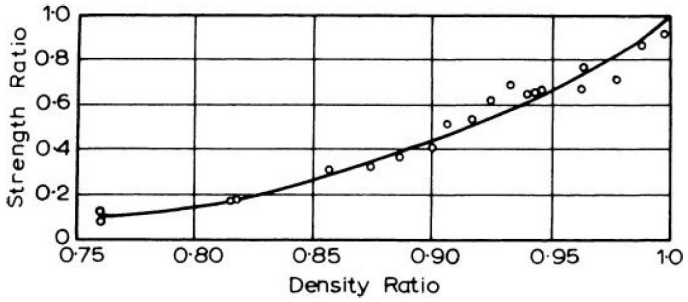

Figure 2.14: Relation between strength and density of concrete [2].

2.4.2 Consistency

Consistency is, in contrast to workability, purely a function of the concrete mixture and can best defined as the ease with which concrete will flow [2]. The flow behaviour of fresh concrete is complex, but it can reasonably be approximated by a Bingham plastic [21]. A Bingham plastic is a model for a viscoplastic material that behaves almost elastically as a solid until a critical stress is reached and it starts to flow like a fluid at a rate proportional to the excess of stress over the critical stress. In case of fresh concrete, it will start behaving like a fluid when the applied stress is sufficient to overcome the resistance to flow, which is primarily determined by inter-particle friction of the aggregates and drag between the aggregate and cement particles. This resistance is usually exceeded by means of vibration or brief imposed pressure imbalances (due to e.g. ramming, pumping or gravitational forces). Once the resistance is overcome, the flow rate develops more or less linearly with the applied stress, as is schematized in Figure 2.15.

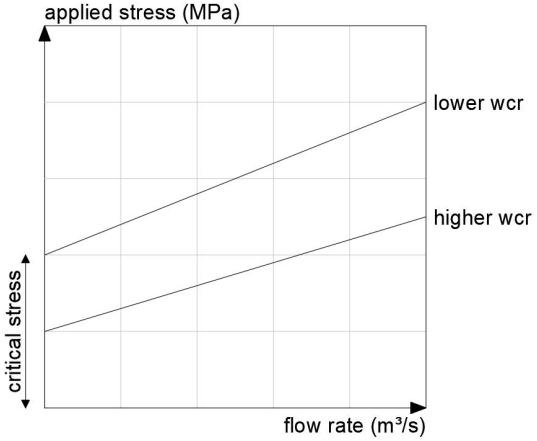

Figure 2.15: Schematic representation of flow behaviour of fresh concrete as a Bingham plastic, adapted from [21].

Multiple aspects determine the consistency and flow behaviour of fresh concrete, many of which have already been addressed to some extent in previous sections. The main factor is the water content of the concrete mixture. A higher water content will reduce the resistance to flow as the cement and aggregate particles are further dispersed from each other, meaning the fresh concrete starts to flow when a lower stress is applied (see Figure 2.15). It is convenient, though approximate, to assume that for given aggregate properties (i.e. shape, size and texture) and grading, the water content is independent of the aggregate/cement ratio or richness of the concrete mixture [2]. On the basis of this assumption, the water content can be approximated depending on the desired consistency, maximum aggregate size and grading. Table 2.6 gives approximate water requirements as a function of these parameters, in which the influence of the aggregate grading is represented by either a coarse (I) or fine (II) grading zone. From this it might be perceived that the higher the water content, the higher the consistency, the more workable the fresh concrete and therefore making it easier to compact. Although this reasoning is correct to a certain extent, it does not include the effect a higher water content has on the hydration of the cement paste. As explained in previous sections, a higher water/cement ratio results in a higher volume of capillary pores (i.e. a larger porosity), with as a consequence a lower strength. These opposing arguments therefore conflict in the choice with regard to the water content. The solution to this conflict is to realize a concrete mixture with the minimum consistency required to obtain full compaction, and thus achieve the lowest water content possible. It is also for this reason that water requirements for higher consistencies are not presented in Table 2.6. These should preferably be obtained with water-reducing admixtures, which are considered later, and not by the addition of more water [18].

Maximum aggregate size (mm)	*Water requirement (L/m^3)*					
	Earth moist		*Semi plastic*		*Plastic*	
	I	II	I	II	I	II
8	165	185	180	200	195	215
11.2	160	180	175	195	190	210
16	155	175	170	190	185	205
22.4	150	170	165	185	180	200
31.5	145	165	160	180	175	195

Table 2.6: Approximate water requirement for different consistencies (earth moist, semi plastic and plastic), grading zones and maximum aggregate sizes, adapted from [18].

The minimum consistency can vary significantly and depends mainly on various practical considerations relating to the processing activities of the fresh concrete and the type of structure. The following criteria are often the most important when choosing the minimum consistency:

- Method of pouring: a higher consistency is required if the fresh concrete is placed with a pump, but if it is deposited with a bucket, a lower consistency would be sufficient;
- Fineness of the reinforcement mesh: a fine reinforcement mesh demands a higher consistency, whereas a lower consistency is sufficient for a coarse reinforcement mesh;
- Dimensions of the structure: narrow columns, for example, requires a higher consistency than thick floors, which is satisfied with a lower consistency.

In practice, the consistency of fresh concrete is divided into classes. These consistency classes, according to the NEN-EN 206, are presented in Table 2.7 and coincide to the measurements of various consistency test methods [14]. It is for this reason that the consistency classes are designated by a capital letter indicating the test method followed by a number representing the measurement range corresponding to that particular consistency. There are a number of tests with which the consistency of fresh concrete can be measured, the most popular of which are also used for classification purposes, these being the degree of compactability test (C), slump test (S) and flow table test (F). The procedures of these and other consistency test methods will not be reviewed here, but can be looked up in the appropriate standards as they are fully prescribed, so that valid and reliable measurements are obtained with each test. Although Table 2.7 may give that impression, it is not by definition that, for example, a concrete mixture with a consistency equivalent to class S3 also complies with C3 and/or F3. It is for this reason that the NEN 8005 recommends a certain test method for a particular consistency range (the recommended test for a specific consistency is presented in bold) [19]. Nevertheless, it is generally assumed that, for a given concrete mixture, more or less the same consistency will be established regardless of the test method, provided that the test method is suitable in that consistency range (e.g. the consistency of a concrete mixture in class F5 cannot be determined by a degree of compactability test).

Consistency	*Classification*			*Test measurements*		
				Degree of compaction	*Slump size (mm)*	*Flow diameter (mm)*
Dry	**C0**			≥1.45		
Earth moist	**C1**	S1	F1	1.26-1.45	10-40	≤340
Semi plastic	C2	**S2**	F2	1.11-1.25	50-90	350-410
Plastic	C3	**S3**	F3	1.04-1.10	100-150	420-480
Very plastic	C4	S4	**F4**	≤1.03	160-210	490-550
Fluid		S5	**F5**		≥220	560-620
Very fluid			F6			≥630

Table 2.7: Consistency classes of fresh concrete according to NEN-EN 206, adapted from [18].

Finally, it should be mentioned that fresh concrete gains rigidity with time and that this is initiated almost immediately after mixing. However, this initial loss of consistency should not be confused with setting of the cement paste. It is simply that some water in the concrete mixture is absorbed by the aggregates (if not already saturated), some is lost by evaporation, and some is removed by the initial chemical reactions [2]. Nevertheless, fresh concrete will remain workable several hours after mixing. Once setting occurs (i.e. the transition from fresh to hardened concrete takes place), the consistency rapidly but gradually diminishes to

zero. The rate of consistency loss during this transition mainly depends on the rate of hydration and, to a lesser extent, of evaporation. The greater the rate of hydration, the faster the consistency loss. Correspondingly, as the hydration of the cement proceeds faster under higher temperatures, the consistency will decrease more quickly in warm environments. In addition to the temperature, the relative humidity is also of importance; in a dry environment the rate of moisture loss due to evaporation will be higher, which in turn contributes to an accelerated loss of consistency. The rate of consistency loss can therefore essentially also be managed with curing (i.e. control of moisture loss). However, as pouring and compaction come before curing, the consistency is often not so relevant any more (i.e. the consistency is allowed to decrease) when the fresh concrete is placed in its final position. Hence, in most cases, curing is not to delay the consistency loss, but to ensure sufficient saturation during hydration of the cement paste, a principle that will be explained later.

2.4.3 Cohesiveness

Another property describing the workability of fresh concrete is its cohesiveness, sometimes also referred to as stability, meaning the resistance of the concrete mixture to segregation during processing. Segregation is broadly defined as the separation of the constituents of a heterogeneous mixture so that their distribution is no longer uniform [2]. In the case of concrete, it is the differences in the sizes and specific mass of the cement and aggregate particles that are the main causes of segregation, but its extent can be controlled by an appropriate aggregate grading and by care in handling of the fresh concrete. A distinction can be made between two forms of segregation. The first one occurs in particularly dry mixtures, where the coarser aggregate particles tend to separate out of the mortar (i.e cement, water and fine aggregates). This can be dealt with by adding more water to the concrete mixture. The second form of segregation, occurring primarily in wet mixtures, is characterized by the separation of water or grout (i.e. water and cement) from the mixture. The cause for this generally lies in the excessive use of water, an incorrect dosage of water-reducing admixtures or a lack of fine aggregates. This latter form of segregation may lead to various related disadvantageous phenomena such as bleeding, plastic settlement and plastic shrinkage. Finally, it must mentioned that, in contrast to consistency, cohesiveness is difficult to measure quantitatively. However, segregation can easily be observed (visually) when handling the fresh concrete, and sometimes even immediately after mixing.

Bleeding is a form of segregation in which some of the water in the mixture is pushed upwards to the surface of the concrete, due to the inability of the large solid particles to hold the water when they settle downwards [2]. Some bleeding is normal, but excessive bleeding can be a problem and will not stop until the cement paste has stiffened enough to cease the sedimentation. Excessive bleeding may result in a weaker surface layer, an increase in water/cement ratio (i.e. a lower strength) near the surface, a reduced bond between the aggregate particles or reinforcement with the cement paste, and an increased permeability of the hardened concrete. The latter two of which occur when bleed water gets trapped under aggregate particles and/or reinforcement, leaving behind air pockets that can potentially reduce the durability of the hardened concrete by facilitating the ingress of deleterious substances. Furthermore, as a direct consequence of bleeding, plastic settlement could occur when the settlement of solid particles experiences local restraint due to the reinforcement. Where the other solid particles continue to settle compared to those which are prevented, cracks that reflect the reinforcement mesh may appear at the surface of the concrete as it is forced in tension. Although they both result in surface cracks, it must be noted that plastic settlement is fundamentally different from plastic shrinkage; another phenomenon related to bleeding that will be addressed later. Plastic settlement can be prevented by reducing the amount of bleeding that occurs, which in turn is controlled by the water content of the mixture, amount of fine material and cement fineness. The latter can be explained by the fact that more finely ground cement grains hydrate faster and because they are less susceptible to sedimentation.

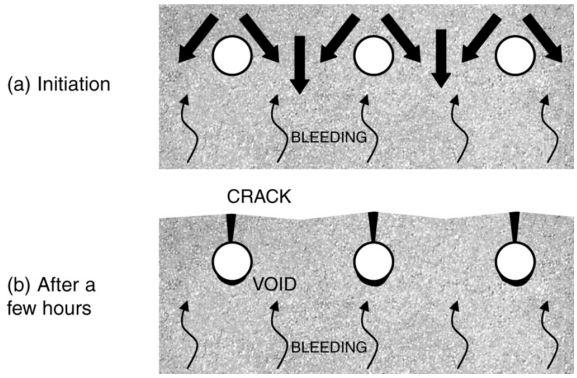

Figure 2.16: Schematic representation of the formation of plastic settlement cracks, source: Concrete Society.

2.4.4 Water-reducing admixtures

As their name implies, water-reducing admixtures can be added to reduce the water content of a concrete mixture. The purpose of this is to reduce the water/cement ratio while maintaining the desired consistency of the fresh concrete or, alternatively, to improve the consistency at a given water/cement ratio (see Figure 2.17). When it comes to water-reducing admixtures, a distinction can be made between so-called plasticizers and superplasticizers. Both plasticizers and superplasticizers are dispersants; substances that adhere to the cement particles causing them to (temporarily) repel each other. This results in an improved separation between the cement particles and, as they are no longer able to clump, an increased surface area of cement available for early hydration [2]. As a consequence, water can more easily circulate around the cement particles, reducing the resistance of the fresh concrete to flow (i.e. increasing the consistency). The main difference between plasticizers and superplasticizers is that plasticizers can reduce the need for water up to 15%, whereas superplasticizers can go as far as a water reduction of 30%. Furthermore, plasticizers are commonly produced from lignosulfates and superplasticizers mostly from sulfonated melamine- or naphthalene-formaldehyde condensates. However, in both cases the cement particles are given a negative charge, resulting in their dispersion through electrostatic repulsion. The main effect being an improved distribution of cement particles and possibly also enhanced hydration, while the structure of the hydrated cement paste remains the same. This also explains why the use of water-reducing admixtures, especially with superplasticizers, sometimes increases the concrete strength at a constant water/cement ratio. An increase of 10% after 1 day and 20% after 28 days has been recorded, but this behaviour has not been widely confirmed [2].

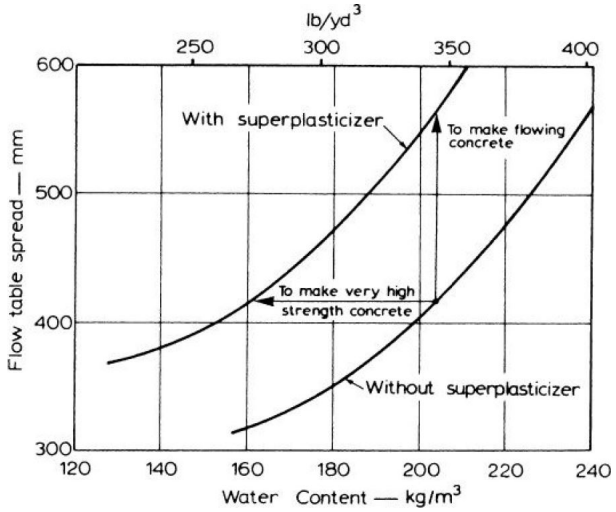

Figure 2.17: Relation between water content and consistency of fresh concrete with and without superplasticizer [2].

2.5 Hardened concrete

Hardened concrete refers to concrete in the period after setting. At the beginning of this period, the properties of hardened concrete develop rapidly. This development gradually diminishes, but the properties of hardened concrete continue to develop due to the ongoing hydration of the cement paste. In practice, however, concrete is considered to be fully hardened at the age of 28 days. The properties of hardened concrete are therefore traditionally characterized by a 28-day value, a decree that has been adopted here. The main focus in the sections below is on the strength of hardened concrete, which is commonly regarded as its most important property, albeit that durability may in fact be more important. Nevertheless, strength is always a vital property in construction and gives a indication of the concrete quality because it is directly related to the structure of the hydrated cement paste. The nature of the strength of concrete and its influencing factors have been examined, as well its elasticity and the strength and stiffness development in young concrete (i.e. between setting and the age of 28 days). Finally, the durability of hardened concrete is looked at, as the majority of problems with concrete are associated with poor durability rather than a lack of strength.

2.5.1 Nature of strength

When looking at the nature of the strength of concrete, its mechanical structure should be considered. Concrete is a composite material consisting of aggregate particles contained in the hardened cement paste, also called cement matrix. Because the aggregates are more rigid than the cement matrix, they attract the forces when the concrete is loaded [10]. In case of equal deformation of the aggregates and cement matrix, the stress in the aggregate particles will be n-times greater than the stress in the cement matrix (n being the modular ra-

tio of aggregates to cement matrix). A uniform external load therefore does not lead to a uniform distribution of the internal forces. Figure 2.18 displays the mechanical structure of concrete and the internal force transfer between the aggregate particles via the cement matrix under external tensile and compressive loading. When concrete is loaded, microcracks form in the cement matrix, originating from the interface between the aggregate particles and cement matrix. Where the microcracks are likely to arise relies on the type of loading. But their exact place of origin depends on the presence of flaws or discontinuities in the cement matrix, such as pores, poor bonding with aggregate particles and deviations in the cement gel structure. These flaws and discontinuities lead to high stress concentrations in very small regions of a specimen, resulting in microcracks, while the nominal stress in a specimen remains comparatively low [2]. As the flaws and discontinuities vary in size and number, the strength of concrete is thus also a problem of statistical probability, and the size of the specimen affects the nominal stress at which microcracking is observed (i.e. a larger size specimen exhibits a lower strength).

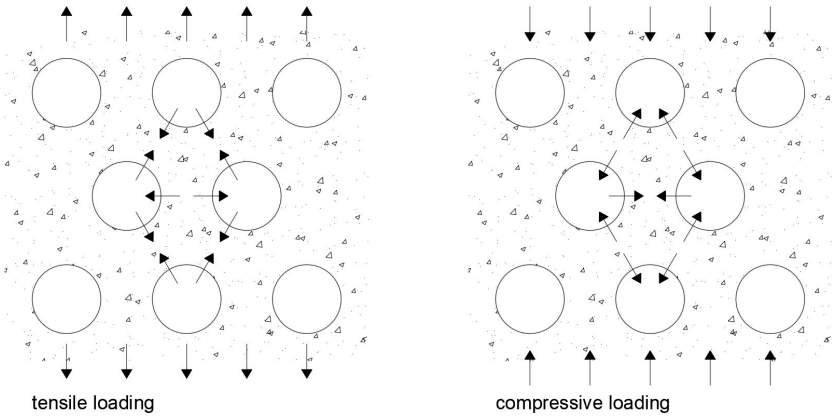

Figure 2.18: Schematic representation of internal force distribution between aggregate particles via cement matrix under external tensile and compressive loading, adapted from [10].

In case of tensile loading, the microcracks grow and possibly join under increasing load to form a substantial crack perpendicular to the load direction. Failure under tensile loading is a very local phenomenon, as a single crack causes the separation of a specimen, whereas normally no cracks appear in the other parts [10]. Unlike tension, failure under compression is a more complex and global phenomenon, caused by the formation of microcracks where splitting forces arise. These splitting forces occur perpendicular to the loading direction, meaning the microcracks form in the same direction as the load. If also a lateral compressive force is applied, microcracks will occur at a higher load, while a lateral tensile force results in microcracks at a lower load. After the occurrence of these microcracks under compressive loading, the internal force distribution changes. At the place were originally the compressive forces were acting, now also a splitting force emerges, as is illustrated in Figure 2.19. With increasing load a shear plane starts to form along which the cement matrix starts to shear. Eventually, a continuous crack pattern is formed as the microcracks connect and ultimately the aggregate particles with remnants of cement matrix disintegrate from the concrete.

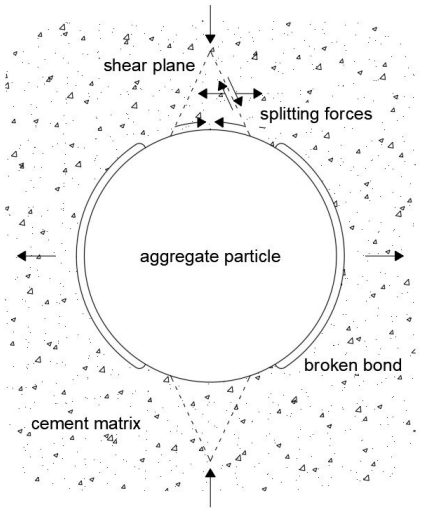

Figure 2.19: Schematic representation of force transfer around aggregate particle in compression, adapted from [10].

As mentioned in the previous paragraphs, lateral loading has a major influence on especially the compressive load at which concrete fails. The relation between the concrete strength and the applied biaxial stress, both of which can either be tension or compression, is given in Figure 2.20. From this it can be deduced that under biaxial compressive loading the concrete strength is approximately 25% higher than for uniaxial compressive loading. This also explains the difference in cylinder and cube compressive strength of concrete, since the former is the strength measured under uniaxial loading and the latter under triaxial loading, to which the theory of biaxial loading is even more applicable. Furthermore, it is clear that the tensile strength of concrete is less than 10% of its compressive strength. Therefore, the tensile strength is often ignored and reinforcement is installed to withstand all of the tensile stress. Because the compressive strength can be measured relatively easily and can be used to derive the tensile strength and other physical and mechanical properties of the concrete, it generally serves as a reference value. It is also for these reasons that strength classification of concrete and the following paragraph (and sections) are related to the compressive rather than tensile strength of hardened concrete. However, it must be noted that the aspects that influence the compressive strength usually have the same qualitative influence on the tensile strength.

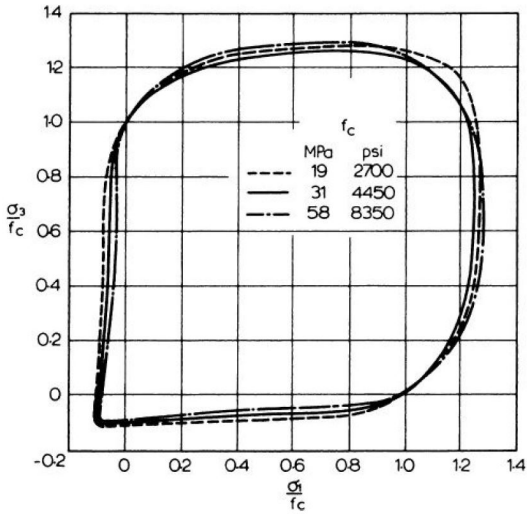

Figure 2.20: Relation between concrete strength and applied biaxial stress [2].

Based on the internal force transfer between and around the aggregate particles via the cement matrix, it is possible to qualitatively indicate which aspects play a role in the strength of hardened concrete [10]:

- The modular ratio of aggregates to cement matrix, which dictates the internal force distribution of the concrete composite;
- The (chemical) bonding between the cement matrix and aggregates, which depends on the mineralogical composition of the aggregates and the hydration of the cement paste;
- The tensile strength of the cement matrix, which is mainly determined by the water/cement ratio;
- The external characteristics (i.e. shape, size and texture) of the aggregates, which influence the shearing behaviour and its (mechanical) bonding with the cement matrix;
- The compressive and shear strength of the cement matrix, which affects the resistance to shearing;
- The volume of cement matrix in relation to that of the aggregates, which determines the magnitude of squeezing and possible deformation.

The influence of the concrete mixture on its strength in general is discussed in the subsequent section.

2.5.2 Influence on strength

As discussed earlier, the porosity and pore (size) distribution of the hydrated cement paste play a major role in the strength of concrete. The concrete strength is, among other less influential aspects, primarily related to the volume of the capillary pores and the entrapped air. The influence of the entrapped air and the basics of compaction have already been explained. At this stage only a fully compacted concrete will be considered, this is taken to mean a hardened concrete that was compacted, by ramming or vibration, such that it contains less than 1% of entrapped air. In case of a fully compacted concrete, its strength is inversely proportional to the capillary pore volume [2, 10]. Because the volume of capillaries is directly related to the water/cement ratio, the influence of the porosity and pore (size) distribution on the concrete strength can also be expressed by its relationship with the water/cement ratio. This relationship is also more convenient in practice, since quantifying the porosity of a hydrated cement paste is difficult. Equation 2.11, also known as the Abrams' law,

is the most basic expression of the relation between the water/cement ratio and the concrete strength, where a and b are empirical constants. The general form of this expression is shown graphically in Figure 2.21. This illustrates that at very low water/cement ratios the concrete becomes too difficult to compact due to its poor workability, resulting in a reduced strength. Water-reducing admixtures are therefore required to guarantee adequate workability for high-strength concretes. The Abrams' law is similar to Equation 2.12, referred to as the Féret's rule, relating the concrete strength to the volumes of cement, water and air, and a constant c. Since it includes the volume of air, the Féret's rule takes better account of the degree of compaction.

$$f_c = \frac{a}{b^{wcr}} \tag{2.11}$$

$$f_c = c \cdot \left(\frac{V_c}{V_c + V_w + V_a} \right)^2 \tag{2.12}$$

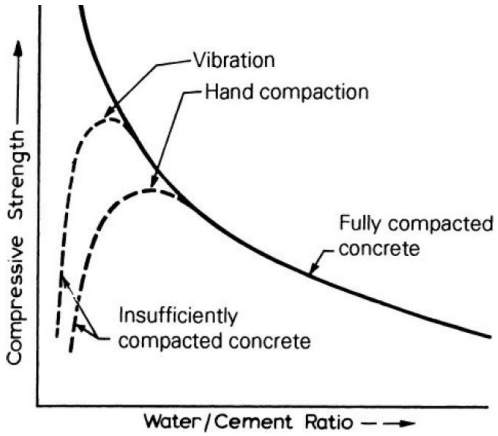

Figure 2.21: Relation between strength and water/cement ratio of concrete [2].

Figure 2.21 shows that the relation between the water/cement ratio and concrete strength is more or less hyperbolic. The exact shape of this hyperbola depends on the values of the constants, which in turn are mainly governed by the cement type. The type of cement can therefore also be considered as a property influencing the strength of concrete. For any cement type the actual relation between the water/cement ratio and concrete strength has to be determined experimentally. In practice, Equation 2.13 can be used to reasonably predict the concrete strength as a function of the water/cement ratio for Portland-based cements, where f_{cem} is the standard strength of the cement and a, b, and c are coefficients depending on the type of cement [18]. The values of these coefficients of various commonly used cement types in the Netherlands are given in Table 2.8, but are only valid in combination with universal aggregates (i.e. natural and normalweight aggregates).

$$f_{cm,cube} = a \cdot f_{cem} + \frac{b}{wcr} - c \tag{2.13}$$

Type	*a*	*b*	*c*
CEM I & CEM II/B-V	0.85	33	62
CEM III/A	0.80	25	45
CEM III/B	0.75	18	30

Table 2.8: Coefficients belonging to Equation 2.13 of common cement types in the Netherlands, adapted from [18].

Although the strength of concrete is mainly determined by the degree of compaction, water/cement ratio and cement type, it is not independent of other factors. Since the water required to achieve the desired workability relates to the water/cement ratio, the concrete strength also indirectly depends on the aspects that influence the water requirement such as the aggregate properties (i.e. shape, size and texture) and grading. The qualitative effects of these aspects on the concrete strength can be deduced from their respective impacts on the water requirement, which have already been considered and will therefore not be mentioned again. In addition, there are indications that the aggregate grading and the amount of fine material also directly affect the concrete strength, since these partly determine the packing density of the concrete and the pore

(size) distribution of the cement paste. For example, it seems that an increased amount of fine material may improve the concrete strength up to 30% at a constant water/cement ratio, as long as the workability can be controlled by water-reducing admixtures [22]. However, the knowledge about the quantitative effects of the aggregate grading and amount of fine material on the concrete strength is far less developed, especially because it is difficult to distinguish between their direct influence and that of other modifications made in parallel to ensure a constant water/cement ratio and workability. More is known about another factor not yet discussed; the aggregate/cement ratio. It has been found that, at a fixed water/cement ratio, a richer concrete mixture results in a lower strength [2, 10]. The most likely reason for this lies in the fact that the water content is higher for a richer mixture than a lean one. As a consequence, in a leaner mixture, the capillary pores (which have an adverse effect on the strength) form a smaller volume of the concrete. Furthermore, the aggregate particles will be more densely packed in case of leaner mixture. However, if the concrete mixture can no longer be compacted due to a lack of cement paste (i.e. too lean mixture), the entrapped air leads to a lower strength. Finally, examination of the influence of the aggregate content on concrete strength shows that when the aggregate volume is increased from zero to 20%, there is a gradual decrease in strength, but it increases from 40% to 80% [2]. The reasons for this behaviour are unknown, but it is roughly the same at any water/cement ratio.

2.5.3 Elasticity

In accordance with most materials, concrete will deform when loaded. Figure 2.22 presents the stress-strain relations of concrete and its two components, being hydrated cement paste and aggregates, when loaded individually. This shows that concrete initially behaves approximately elastically, meaning the stress is more or less proportional to the strain. The initial linear part of the stress-strain curve thus conforms to Hooke's law, and its slope is known as the modulus of elasticity or Young's modulus. Hereafter, the stress-strain relation becomes non-linear and the concrete behaves more plastically; a small stress increment is accompanied by a relatively large strain increase. It worth noting that the cement paste and aggregates, in contrast to the concrete composite, exhibit a near perfect linear stress-strain relation. The curvature in the stress-strain relation of concrete is mainly caused by the formation of microcracks at the interface between the aggregate particles and cement matrix [2, 10]. Up to a stress level of about 30% of the ultimate strength, these microcracks remain stable, after which they start to increase in length, width and number (i.e. slow crack propagation stage). When the stress increases beyond 70% of the ultimate strength, the microcracks bridge and a continuous crack pattern is formed (i.e. fast crack propagation stage) and the stress-strain curve bends over to a greater degree. Eventually, at the peak of the stress-strain curve, the ultimate strength is reached. The strain corresponding to the ultimate strength is generally in the order of 0.2% [10].

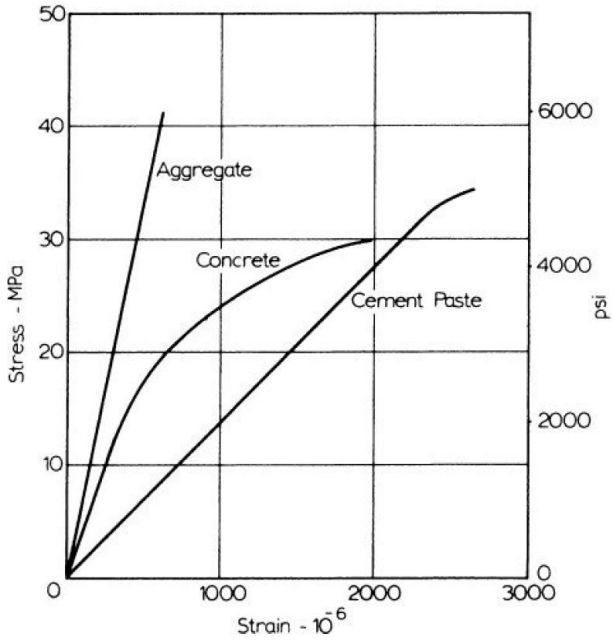

Figure 2.22: Stress-strain relationships for cement paste, aggregate and concrete [2].

What Figure 2.22 does not show is that, in case the stress-strain relationship is determined with a deformation-controlled test, the strain will continue to grow after the ultimate strength is reached, but accompanied by a decrease in stress. This descending part of the stress-strain curve represents the so-called strain softening of concrete. The shape of both the ascending and descending part of the stress-strain curve is determined by the concrete quality, which in turn depends on its mixture composition [2, 10]. In general, the lower the concrete strength, the greater the degree of curvature of the ascending part. A high-strength concrete is characterized by a steeper and longer linear part (and a sudden peak), thereby behaving more elastically due to the delayed formation of microcracks (i.e. it has a greater resistance to microcracking). However, a high-strength concrete therefore likewise behaves more brittle, all the more because its descending part of the stress-strain curve is comparatively steeper. The more gradual the descending part, the less ductile the behaviour, which is generally the case for low-strength concretes. In practice, an idealized, albeit more conservative, stress-strain relationship is often adopted in which strain softening is regularly neglected and/or the concrete is assumed to be perfectly plastic (i.e. the slope beyond the peak is equal to zero). These stress-strain relationships therefore consist of three vital characteristic properties, these being the elastic modulus, ultimate strength and the corresponding strain, of which the elastic modulus in particular requires some additional clarification.

For the definition of modulus of elasticity it is necessary to understand how concrete behaves under cyclic loading. Figure 2.23 illustrates the stress-strain relationship for concrete when its loaded and unloaded up to a stress well below the ultimate strength. This shows that some deformation remains after the concrete is unloaded; there is residual strain. Subsequent loading cycles take off where the previous ones ended rather than at the origin, but the curvature of the stress-strain relationship gradually reverses with increasing number of load cycles due to microcracking (i.e. the behaviour is less rigid with each cycle) [10]. Nevertheless, as can be seen from Figure 2.23, in the beginning the strain increases under an acting load. This effect is, in addition to the formation of microcracks, mainly caused by creep of the concrete. However, the differentiation between instantaneous and creep strain is difficult due to their dependence on the rate of loading. Hence, an arbitrary distinction is made; the deformation occurring during loading is considered elastic, and the subsequent increase is regarded as creep [2]. Accordingly, to disregard creep but to account for the effect of microcracking, the definition of the elastic modulus has been taken as that of the so-called secant modulus rather than the tangent modulus through the origin. Because the secant modulus reduces with an increase in stress, the stress at which it is determined is of great influence. For comparative purposes, this stress is generally fixed as 33% or 40% of the ultimate strength. Moreover, the elastic modulus is only determined after multiple load cycles to eliminate creep influences and settlement phenomena.

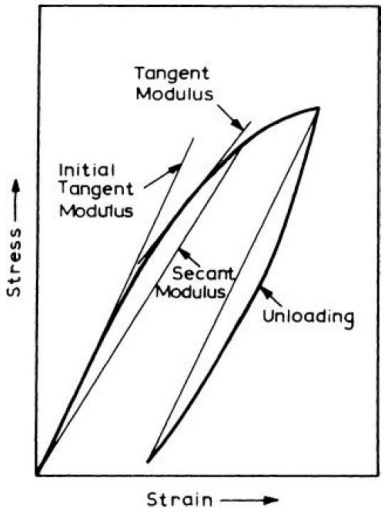

Figure 2.23: Schematic representation of stress-strain relationship of concrete under a single loading cycle [2].

Although the elastic modulus is related to the deformation behaviour of concrete, in practice it is generally derived from the concrete strength. It is clear that the elastic modulus, as previously mentioned, increases with an increase in concrete strength, but their precise relationship remains unknown. This can be explained by the fact that the stiffness of both the aggregates and cement matrix, as well as the volumetric proportion of aggregates in the concrete, together determine the elastic modulus of the concrete composite. All that can be said with certainty, is that the stiffness increment is progressively lower than the increase in concrete strength [2]. In most standardized relations, such as Equation 2.14, the elastic modulus is proportional to the strength

raised to power 0.5 or 0.3. Furthermore, the aspects that influence the strength (e.g. water/cement ratio, degree of compaction and aggregate/cement ratio) usually have the same qualitative influence on the elastic modulus. Finally, it should be mentioned that in case of uniaxial loading not only longitudinal strain takes place, but at the same time also transverse strain occurs, which is known as the Poisson effect. This transverse strain is of opposite nature and is ν-times greater than the longitudinal strain (ν being the Poisson's ratio). Although in practice assumed as constant, the Poisson's ratio of concrete may vary. However, for the majority of concretes with universal aggregates the Poisson's ratio will be in the range of 0.17 to 0.20 [2].

$$E_{cm} = 22 \cdot \left(\frac{f_{cm}}{10}\right)^{0.3} \tag{2.14}$$

2.5.4 Young concrete

An influence on the strength and stiffness of concrete not yet addressed is age. The strength and stiffness of hardened concrete develop with time due to the ongoing hydration of the cement paste. While this development is truly infinite, it is most relevant in young concrete, as in practice concrete is considered to be fully hardened at the age of 28 days. The rate of development relates to the cement type used. In essence, therefore, it is not so much the age that matters, but it is the degree of hydration that regulates the strength and stiffness development of hardened concrete. Nevertheless, in addition to the prevailing temperature, the degree of hydration largely depends on time. As stated earlier, the heat output is a measure for the degree of hydration. The greater the age of concrete and the higher the prevailing temperature during its existence, the greater the heat output relative to the maximum of the cement type used, the higher the ratio of the concrete strength at that time to the ultimate strength [10]. Accordingly, there is a distinct relation between the concrete strength on the one hand, and the time and temperature on the other. The same applies, in principle, to the stiffness and other physical and mechanical properties of concrete, but these can generally also be derived from the strength. However, as can be seen from Figure 2.24, the stiffness of concrete develops much faster than its strength. The elastic modulus is at approximately 90% of its ultimate value at the age of 3 days, whereas the strength requires roughly 7 days to reach 70% of its ultimate value.

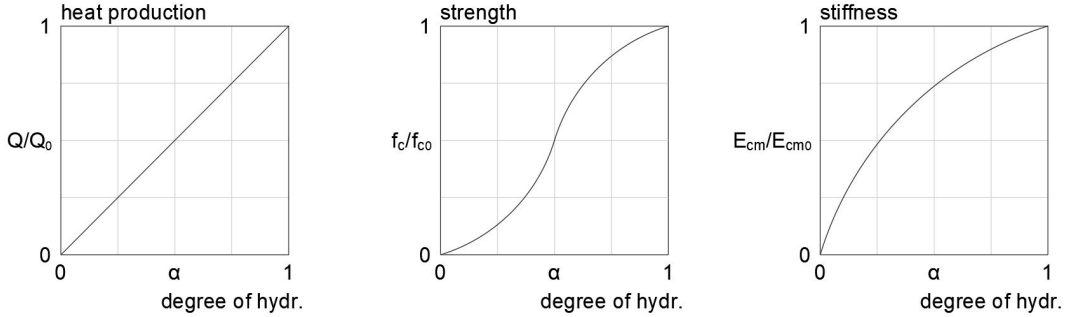

Figure 2.24: Schematic representation of development young concrete properties; relative heat production, strength and stiffness as function of the degree of hydration, adapted from [10].

The strength development of young concrete proceeds almost linearly with the logarithm of the maturity of concrete (see Figure 2.25). The maturity M as given by Equation 2.15 is defined as the summation of the products of hardening times and prevailing concrete temperature over established measurement intervals [2, 23]. The prevailing concrete temperature during hardening depends on the heat production due to hydration of the cement paste and the heat dissipation to the environment. On the other hand, the prevailing concrete temperature also affects the hydration of the cement paste; a higher temperature results in faster hydration, which in turn results in accelerated heat production. Therefore, in case of limited heat dissipation (e.g. massive concrete structures or in warm environments), the heat production fuels the hydration of the cement paste. As a consequence, such structures exhibit a faster development of the concrete strength. Higher prevailing concrete temperatures may therefore seem favourable. However, this interpretation ignores the fact that, due to subsequent cooling of the concrete, thermal shrinkage occurs, which may result in cracking. The fundamentals of thermal deformations will be looked at later, but in general it can be said that an accelerated strength development does not prevail over the occurrence of thermal shrinkage cracks, since these may negatively affect a concrete structure's functionality, durability and aesthetics.

$$M = \sum \left[T(\Delta t) - T_{ref} \right] \cdot \Delta t \tag{2.15}$$

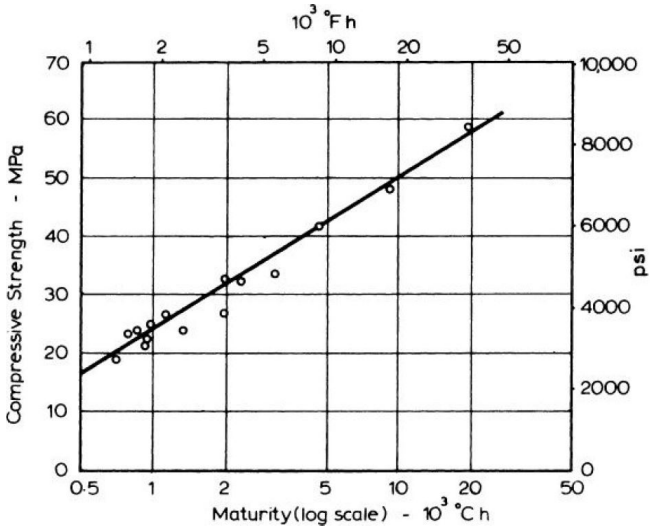

Figure 2.25: Relation between strength and maturity of concrete [2].

For the purpose of the determination of the maturity, the temperature is reckoned from a reference value T_{ref} of -10 °C. The reason for this is that below this temperature concrete does not appear to gain strength with time, while it does between the freezing point of water and -10 °C, albeit to a very limited extent [2, 23]. The logarithmic relation illustrated in Figure 2.25, referred to as the calibration curve, is described by Equation 2.16, where $f_c(M)$ is the concrete strength at maturity M. The coefficients A and B depend on the water/cement ratio of the concrete, since mixtures with a lower water/cement ratio gain strength more quickly than those with a higher water/cement ratio. This is because, as explained before, in the latter case the cement particles are further dispersed from each other, meaning it will take longer for the cement gel structure to form. In practice, as the strength is dictated by the water/cement ratio, the coefficients A and B are derived from the already known strength of concrete at given ages, hardened at a constant temperature, usually 20 °C. Furthermore, the early temperature also affects the strength-maturity relation. A high early temperature results in a lower strength at full maturity compared to when heating is delayed or absent. The ultimate strength of concrete hardened at 70 °C is about 70% of concrete hardened at 20 °C, but the ultimate strength is reached more quickly in case of high early temperatures [2]. Figure 2.26 displays the influence of the hardening temperature on the concrete strength at the age of 1 and 28 days.

$$f_c(M) = A + B \log_{10}(M \cdot 10^{-3}) \tag{2.16}$$

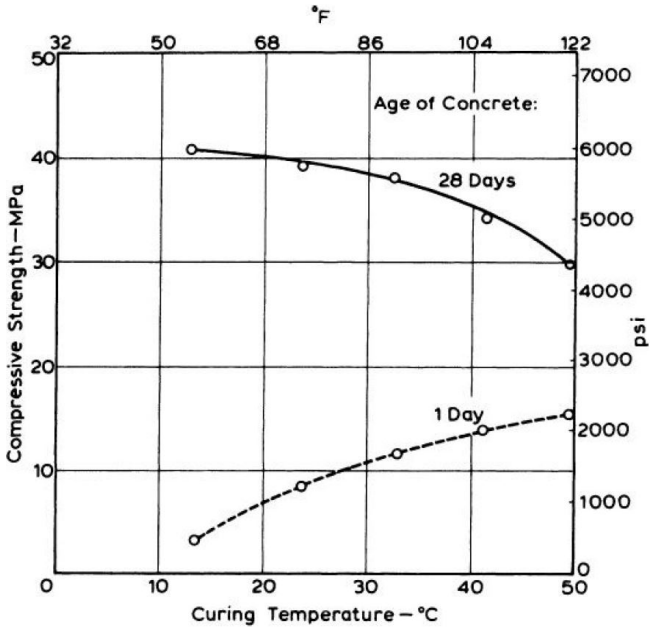

Figure 2.26: Relation between hardening temperature and concrete strength at the age of 1 and 28 days [2].

The fact that the original strength-maturity relation does not hold for any arbitrary concrete led to the concept of weighted maturity. This concept upholds the same calibration curve, but replaces the original maturity by a so-called weighted maturity that takes better account of the cement type. Equation 2.17 is one of the several expressions for the weighted maturity M_w and is known as the De Vree method, where $T(\Delta t)$ is the hardening temperature during time interval Δt and C is a value that reflects the temperature sensitivity of the cement type [18, 23]. The De Vree method is the prescribed weighted maturity concept in the Netherlands, described in its entirety in the NEN 5970 [24]. However, alternatives exist that also describe concrete strength as a function of the time and temperature. One common alternative, referred to as the equivalent age concept, converts the hardening time interval at any prevailing temperature to an equivalent hardening time interval at a reference temperature, usually 20 °C [2, 23]. Nevertheless, very much the same and appropriate strength-maturity relations can be obtained regardless of the concept, provided that the prevailing concrete temperatures during hardening are established correctly. The prevailing temperatures over time can either be measured on site or computed from the adiabatic heat production of the concrete mixture combined with the on site boundary conditions that regulate the heat dissipation to the environment.

$$M_w = \sum \frac{10 \cdot [C^{0.1T(\Delta t)-1.245} - C^{-2.245}]}{\ln C} \cdot \Delta t \tag{2.17}$$

2.5.5 Curing

For a prosperous development of properties in young concrete and to obtain good quality concrete in the long-term, concrete must remain saturated during hardening. This is achieved by curing; the name given to the procedures carried out after pouring with the aim of promoting the hydration of the cement paste. Curing consists of the control of temperature and of moisture movement from and into the concrete. The effect of the temperature on the hydration of the cement paste and on the development of properties in young concrete has already been considered extensively. The significance of the control of temperature during hardening can be inferred from what has been stated in previous sections and will not be elaborated here. The control of moisture from and into the concrete, however, does requires some additional clarification. With regard to the moisture level, the purpose of curing is to keep the concrete as saturated as possible until the originally water-filled spaces in the fresh cement paste have been filled enough by the products of hydration [2]. It is known that the hydration of the cement paste can only proceed at maximum rate when it is saturated and that it is greatly reduced when the relative humidity inside the capillary pores drops below 80%. From this it follows that for the hydration to continue, the relative humidity within the concrete has to be maintained at a minimum of 80%. In order to achieve this for concrete mixtures with relatively high water/cement ratios, it is sufficient to only prevent water loss from the concrete to the environment, as the rate of hydration of such a sealed specimen equals that of a saturated specimen. In case of concrete mixtures with comparably low water/cement ratios, the ingress of water into the concrete must be made possible, as water lost due to self-desiccation has to be replaced by water from the outside to ensure continuous hydration.

On the basis of the above, one can distinguish between curing in circumstances where only the loss of water needs to be prevented or circumstances where the ingress of water from the outside is required. It may be recalled that, in theory, a water/cement ratio of 0.4 could provide sufficient saturation to guarantee continuous hydration. In practice, however, a water/cement ratio of 0.5 better represents the dividing line [2]. These opposing circumstances each call for different curing methods. Wet curing can be applied in case the ingress of water is required, whereas membrane curing is suited if water loss needs to be prevented. In the event of wet curing, the surface of the concrete is kept in constant contact with water (as soon as is it no longer susceptible to damage). This can be accomplished by continuous spraying, flooding (ponding), or by covering the concrete with wet fabrics. Membrane curing relies on covering the surface of the concrete to obstruct evaporation without allowing water from the outside to enter. The techniques for this include overlapping with polyethylene sheeting or using spray-applied compounds that form a coating. With both methods, the duration of curing depends on the degree of evaporation, the rate of hydration, and requirements concerning the strength and durability of the concrete mixture. The degree of evaporation from the concrete surface is governed by the wind speed, solar radiation, the temperature and relative humidity of the surrounding air, and the temperature of the concrete itself. Finally, it must be added that the concrete remote from the surface is hardly subjected to moisture movement, which typically only affects an outer zone up to a depth of 50 mm, which usually represents all or most of the cover to the reinforcement. Thus, concrete in the inner zone is generally unaffected by curing, meaning curing is of minor importance to the overall strength of concrete structures unless they are very thin. However, the necessity for curing is emphasized by the fact that the permeability of the outer zone, through which deleterious substances penetrate the concrete, plays a major role in the protection of the concrete matrix and embedded reinforcement against degradation processes.

2.5.6 Durability and permeability

As mentioned in the introduction of this thesis, durability is the ability of a structure to withstand deterioration processes to which it is expected to be exposed during its service life. Which deterioration processes can be expected depends on the environment in which a structure is placed. In practice, concrete structures are classified according to their level of exposure based on the environment in which they serve. These so-called exposure classes are laid down in standards such as the NEN-EN 206 [14]. The various degradation mechanisms of concrete can be mechanical, chemical, or physical, the latter two of which in particular are considered in the classification according to the NEN-EN 206. Mechanical damage can be caused by impact, abrasion, erosion and/or cavitation, whereas chemical deterioration includes carbonation, (chloride induced) reinforcement corrosion, ASR, and attack by acids, salts or sulfates. Physical degradation generally stems from the effects of freezing and thawing or the exposure to high temperatures. Due to the wide variety of degradation mechanisms, it is difficult to attribute the durability of concrete to just a few factors. Furthermore, specific factors may influence the resistance against certain deterioration processes, while this may not be the case with others. However, one factor, being the permeability of concrete, nearly always plays a major role in its resistance against especially chemical and physical degradation mechanisms. It is for this reason, that the remainder of this section will be about the permeability of concrete and its influencing factors, rather than a explanation of all deterioration processes that may occur. The descriptions of these can be found in the appropriate literature [2, 10]. Nevertheless, it must be remembered that other measures can be taken to improve the durability of concrete besides trying to reduce its permeability. These measures mainly consist of adapting the concrete mixture to suit the kind of exposure. The resistance against attack by sulfates, for example, can be increased by using a cement with a low C_3A content. These cements can be recognized by an SR (sulfate resisting) designation in addition to their formal type description.

Since chemical or physical degradation usually involves the infiltration of some harmful substance into the concrete, the durability of concrete is primarily related to its permeability and diffusion to liquids, gases or ions. Permeability in general is defined as the ease of flow of a liquid or gas through a porous medium [2]. The permeability of concrete is determined by the nature of the porosity of the hardened cement paste (see Figure 2.27). It is the total volume of the pores, their relative sizes and their degree of connectivity that define the permeability of concrete. Only the capillary pores contribute to the permeability because, unlike the smaller gel pores, they are large enough for a liquid or gas to overcome the resistance to flow. However, these capillary pores must be continuous (i.e. connected to others), otherwise they do not contribute to the permeability. Entrapped air and pores within the aggregates may also be relevant to the permeability of concrete, but as the volume of entrapped air (after compaction) is generally much smaller than that of the capillaries and the aggregate pores are usually discontinuous, their respective contributions will be insignificant. In addition, (micro)cracking does seriously affect the permeability of concrete. Cracks provide a path for water (or moisture), ions, carbon dioxide and oxygen to penetrate into the concrete. While large cracks hamper especially the local tightness of a concrete structure, microcracks contribute to the overall porosity and may increase the pore connectivity, in both cases resulting in an increased permeability. Therefore, when trying to realize a durable concrete structure, crack management or prevention should not be disregarded.

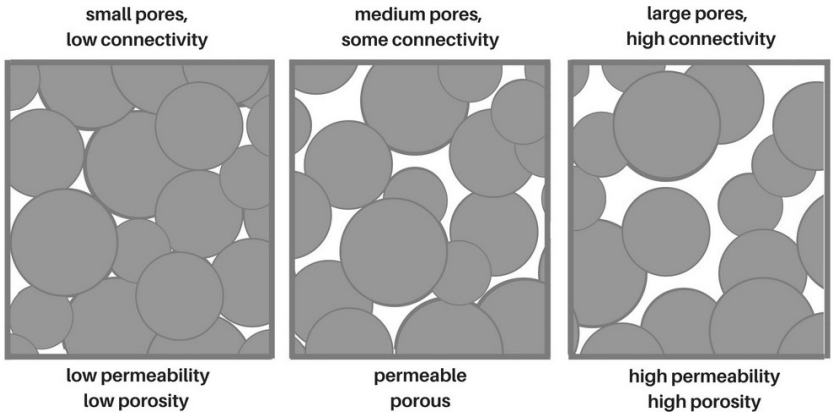

Figure 2.27: Schematic representation of permeability with respect to the nature of porosity, source: Cabot Oil & Gas.

Because the porosity of the cement paste is the governing influence on the permeability of concrete, the permeability mainly depends on the water/cement ratio and the degree of hydration [2, 10]. The permeability decreases as the hydration of the cement paste progresses. Table 2.9 presents the permeability at different ages for a cement paste with a water/cement ratio of 0.5. After approximately 28 days of hardening the porosity is

reduced to such an extent that the capillary pores lose a great deal of their connectivity, causing an accelerated decrease of permeability. A lower water/cement ratio will, for the same reasons as the strength, result in faster reduction of the permeability. For cement pastes hydrated to the same degree, the permeability is greater the higher the water/cement ratio. Figure 2.28 shows the permeability as a function of the water/cement ratio, in which 93% of the cement paste has hydrated. From this it can be seen that the slope of the curve drops considerably for water/cement ratios below about 0.6, at which the capillaries become discontinuous (i.e. the pore connectivity has decreased). This also explains why the NEN 8005, depending on the exposure class, has laid down maximum water/cement ratios from 0.70 to 0.45 for concrete structures placed in mild to aggressive environments, respectively [19]. The NEN 8005 also prescribes a minimum cement content depending on the exposure class. Although little information is available about the philosophy behind this measure, three arguments may be identified: guarantee of maximum water/cement ratio, need for sufficient fine material, and protection of reinforcement against (chloride induced) corrosion [25]. The amount of fine material is thus not only of interest with regard to the workability of fresh concrete, but since sufficient fine material leads to a better packing density and a finer porosity of the cement paste, it will be more difficult for deleterious substances to penetrate into the concrete, resulting in a better durability.

Age (days)	*Coefficient of permeability*
0	10^{-6}
1	10^{-9}
3	10^{-10}
7	10^{-12}
14	10^{-13}
28	10^{-14}
100	10^{-17}
240	10^{-19}

Table 2.9: Typical permeability at different ages for cement paste with water/cement ratio of 0.5, adapted from [10].

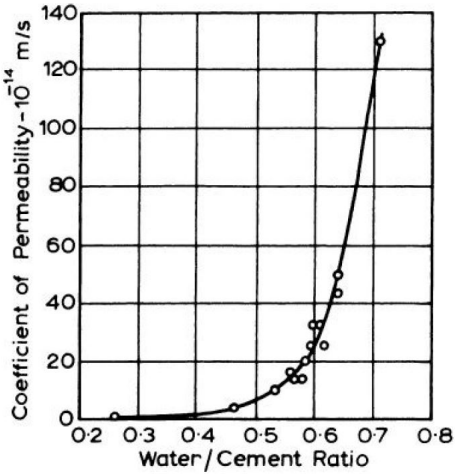

Figure 2.28: Relation between permeability and water/cement ratio of cement paste [2].

2.6 Volume changes

Volume change is the phenomenon of swelling or shrinkage of in particular hardened concrete as a result of chemical or physical reactions with its internal and external environment. These volume changes are characterized by the elongation or shortening of a specimen with increasing age, as they are time-dependent and caused by movement or loss of moisture rather than external loading. Swelling and shrinkage are not much of a problem if a concrete structure can freely elongate or shorten. However, if swelling and shrinkage are restrained, stress will arise in the concrete structure. This will, in the event of swelling, lead to compressive stress, whereas shrinkage will result in tensile stress. Since restraint can also occur within a concrete structure when, for example, the outer zone shrinks and the inner zone swells, differential stress may emerge. Because a tensile stress more easily exceeds the relatively low tensile strength of concrete, shrinkage frequently leads to

cracking. With swelling, on the other hand, the risk of damage is substantially smaller due to the comparably high compressive strength of concrete. This is why more attention has been paid in the past to the clarifications of shrinkage. It also for this reason that the upcoming sections are focused on various types of shrinkage rather than swelling. But the basics of shrinkage induced cracking in relation to the tensile strength of hardened concrete will be explained first. The section is finalized with the examination of creep and relaxation; other time-dependent phenomena related to volume changes of concrete.

2.6.1 Shrinkage induced cracking

Before elaborating on the different types of shrinkage, it is imperative to understand how shrinkage may induce cracking of hardened concrete. Especially since shrinkage does not necessarily lead to cracking. Whether it does depends, besides the magnitude of shrinkage, on the stiffness of the concrete at the time of shrinkage and the degree of restraint. In accordance with Hooke's law, it is impossible for stress to develop if the concrete has not yet stiffened. In addition, if a concrete structure can freely shorten in the direction along which shrinkage occurs, no stress will occur. Where stiffness is an inherent property of concrete, the degree of restraint is usually determined by the presence of adjacent structures acting as confinement (i.e. external restraint), but the degree of restraint can also be a function of the interior (i.e. internal restraint). The highest stress is normally, but not necessarily, obtained at total restraint and extensive development of the concrete stiffness. This increases the probability of shrinkage induced cracking, since the developed stress must exceed the tensile strength of concrete for cracking to occur.

The tensile strength is of particular importance when cracking is considered. From the nature of the strength of hardened concrete it can be deduced that the tensile and compressive strength are strongly related. Although their is no direct proportionality, the tensile strength increases as the compressive strength increases, albeit at a decreasing rate [2]. There are many empirical relations between the tensile and compressive strength, of which Equation 2.18 is one of those standardized. The differences between the various relations are not large. What is important, though, is that the tensile strength can be measured by fundamentally different tests (e.g. flexure, direct tension or splitting) that will not indicate the same strength values. Hence, the test method must be explicitly stated with the established relationship. The tensile strength of Equation 2.18 corresponds to the values obtained by direct tension. Since the tensile strength develops at about the same rate as the compressive strength, which in turn develops much slower than the stiffness, the probability of shrinkage induced cracking is often most significant in young concrete, all the more because many types of shrinkage occur during and as a result of the hydration of the cement paste.

$$f_{ctm} = 0.3 \cdot {f_{ck}}^{2/3} \tag{2.18}$$

2.6.2 Plastic shrinkage

Plastic shrinkage is an exception to the rule because it has its roots in fresh rather than hardened concrete. It is a special form of drying shrinkage related to bleeding; a form of fresh concrete segregation previously discussed, in which the water in the mixture is pushed upwards to the surface of the concrete. Depending on the environmental conditions (e.g. wind, temperature and humidity), this layer of bleed water at the surface may evaporate. This causes water menisci to develop in the capillary pores just below the concrete surface [26, 27]. When the rate of evaporation exceeds the rate of bleeding, the fluid pressure on the convex side of the meniscus will be less than on the concave side, that is, less than the pressure of the atmosphere. The subsequent lowering of the water meniscus, which is illustrated in Figure 2.30, increases the pressure on the pore walls and cement grains. The pore water pressure generated by capillary tension, occasionally referred to as suction, induces a volume reduction and is a function of the radius of curvature of the water meniscus. The concrete surface is forced in tension as the volume reduction is restrained by the concrete underneath. If the bleed water evaporates very rapidly, the concrete may still be in a plastic state, and cracks do not form at that time; but cracks will appear as soon as the fresh concrete starts to set because the tensile stress is likely to exceed the barely developed tensile strength. This is a common occurrence in concrete structures with large horizontal surfaces exposed to the atmosphere (e.g. floors and slabs) and can best be avoided by reducing the rate of evaporation from the surface by means of curing. The evaporation of bleed water can be prevented by keeping the concrete surface wet during hardening. Finally, it must be noted that the relation between bleeding and plastic shrinkage is complex; delayed setting, for example, allows for more bleeding and leads to increased plastic shrinkage [2]. On the other hand, more bleeding also hampers rapid desiccation of the concrete surface and this reduces the probability of shrinkage induced cracking. In practice, for reasons discussed before, it is cracking that matters most.

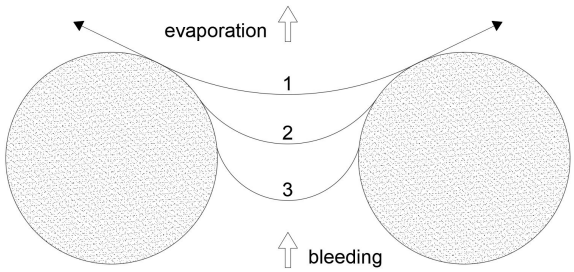

Figure 2.29: Schematic representation of suction between cement grains due to water meniscus, adapted from [26].

2.6.3 Chemical shrinkage

As mentioned earlier, the transition to chemically bonded water is accompanied by about a 25% decrease in water volume. The volume of the hydration products of the hardened cement paste is therefore smaller than the sum of the volumes of cement and water (see Figure 2.30) [26, 28]. This volume reduction, in cubic centimeter per gram of unhydrated cement, is defined as chemical shrinkage, sometimes also referred to as hardening shrinkage, and is proportional to the degree of hydration. For cement pastes hydrated to the same degree, the precise volume reduction depends on the composition of the cement and is approximately equal to the sum of the chemical shrinkage of the individual clinker compounds. Typical chemical shrinkage of the clinker compounds of Portland cement are given in Table 2.10, in which the last column represents the proportion of chemical shrinkage of a clinker compound relative to a typically composed Portland cement (as calculated from data in Table 2.1). Cements blended with other cementitious materials such as blastfurnace slag or fly ash exhibit a smaller chemical shrinkage than Portland cement, as they bind less water [28]. The water/cement ratio and cement fineness do not affect chemical shrinkage, but they will determine the rate of chemical shrinkage and the final volume reduction, since finer cements and higher water content ultimately allow more water to be chemically bonded (i.e. enable a greater degree of hydration) [26]. Chemical shrinkage does, in contrast to other types of shrinkage, hardly manifests as an external volume reduction, let alone the shortening of a specimen [27]. Instead, once the structure of hydration products starts to develop upon setting, pores are formed within the hardening cement paste as the rigid structure resists (further) chemical shrinkage. Chemical shrinkage can thus largely be considered a purely internal volume reduction. As a result, no tensile stress is introduced on macroscopic scale, meaning cracking cannot occur. Chemical shrinkage is thus less important in practice, but must be distinguished for the sake of completeness.

Compound	*Chemical shrinkage*	
	Pure (cm^3/g)	*Composed* (% by shrinkage)
C_3S	0.0532	38-56
C_2S	0.0400	9-13
C_3A	0.1113	13-19
C_4AF	0.1785	21-30

Table 2.10: Typical chemical shrinkage of clinker compounds, pure and composed in Portland cement, adapted from [26].

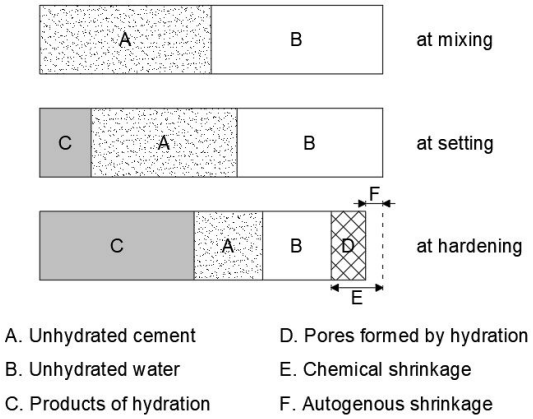

Figure 2.30: Schematic representation of chemical shrinkage; reduced volume of water and cement with increasing volume of hydration products and pores, adapted from [26, 28].

2.6.4 Autogenous shrinkage

Various definitions of autogenous shrinkage can be found in the literature, each with a somewhat different interpretation. Autogenous shrinkage is occasionally denoted as the volume reduction as a consequence of self-desiccation; the exhaustion of free water from capillary pores by ongoing hydration of the cement paste [2, 27]. Nevertheless, another generally accepted definition is the one denoted by Tazawa which describes autogenous shrinkage as the external, macroscopic volume reduction of the cement paste (from the beginning of setting) caused by hydration [26, 28]. Although these definitions may seem very different at first glance, they are in fact quite similar. The latter definition corresponds to Figure 2.30 and considers autogenous shrinkage as a portion of chemical shrinkage. It includes the external volume reduction of the cement paste in a plastic state, during which autogenous shrinkage equals chemical shrinkage. Correspondingly, the relation between chemical and autogenous shrinkage is presented in Figure 2.31. This shows that the majority of chemical shrinkage is converted into the formation of pores within the hydrated cement paste once the structure of hydration products gains rigidity upon setting. This is also the point (i.e. roughly 6 hours in) when autogenous shrinkage starts changing from being a function of chemical shrinkage to that of self-desiccation [26]. The autogenous shrinkage progressively diverges from the chemical shrinkage since the external volume reduction during hardening of the cement paste is decreasingly the result of chemical shrinkage. The further external volume reduction can be fully attributed to self-desiccation. It can thus be said that the former definition includes only part of Tazawa's definition of autogenous shrinkage, that is, the part of autogenous shrinkage due to self-desiccation. However, it must be noted that the majority of external volume reduction due to chemical shrinkage occurs at very early-age (i.e. within 1 day), of which even a considerable amount takes place in the plastic state, during which the cement paste has gained barely any rigidity. Therefore, the very early-age autogenous shrinkage will hardly result in the introduction of tensile stress on macroscopic scale and is thus less important in practice. It may also be for this reason that chemical shrinkage is sometimes left out of the definition of autogenous shrinkage or that it is measured from the beginning of setting, so that primarily the external volume reduction due to self-desiccation is assessed [28].

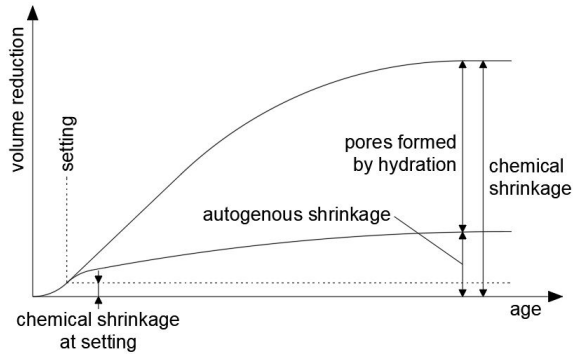

Figure 2.31: Schematic representation of relation between chemical and autogenous shrinkage, adapted from [26, 28].

Free water is consumed as the hydration of the cement paste progresses. This causes water menisci to develop in the capillary pores, resulting in a volume reduction of the products of hydration. The mechanism of autogenous shrinkage thus corresponds to that of plastic and drying shrinkage, with the exception that depletion of moisture is caused by self-desiccation of the internal environment rather than diffusion to the external environment. As can be deduced from Figure 2.30, the more the water meniscus is pulled inwards, the greater its curvature, the larger the suction. Autogenous shrinkage is therefore fundamentally dependent on the water/cement ratio of the cement paste [2, 26]. The influence of the water/cement ratio on autogenous shrinkage is twofold. First, self-desiccation occurs particularly in case of lower water/cement ratios because a lack of free water is more likely to lead to exhaustion. Second, a lower water/cement ratio will result in a finer porosity, which causes the meniscus to have a greater curvature. In addition, a higher fine content may also refine the larger pores towards a finer porosity [26]. Although autogenous shrinkage includes self-desiccation of the pores formed within the hardening cement paste as a consequence of chemical shrinkage since setting, there is no direct relation between the two. Nevertheless, the influencing factors of chemical shrinkage, which have been explained in the previous section, also affect autogenous shrinkage. Accordingly, analogous to chemical shrinkage, autogenous shrinkage is proportional to the degree of hydration [27].

Although autogenous shrinkage is essentially volumetric (i.e. three-dimensional), it is usually expressed as the linear (i.e. one-dimensional) change of a specimen, commonly referred to as strain, so that it can be considered alongside drying shrinkage. Because of its dependence on the water/cement ratio, autogenous shrinkage manifests itself mainly in high-strength concretes. For a cement paste with a water/ cement ratio of 0.4 the autogenous shrinkage will be about 700 $\mu\varepsilon$ [27]. However, in case of concrete this will only be about 120 $\mu\varepsilon$ due to the presence of rigid aggregates. A higher aggregate/cement ratio, that is, a larger relative volume of aggregates, leads to a decrease in autogenous shrinkage of concrete. The opposite applies to concretes with a lower aggregate/cement ratio. Finally, it must be mentioned that for low-strength concretes with a high water/cement ratio, autogenous shrinkage need not be distinguished from drying shrinkage, since the former is comparably small to the latter [2]. In such cases, it is sometimes assumed in practice that drying shrinkage includes autogenous shrinkage.

2.6.5 Drying shrinkage

When concrete is exposed to unsaturated air, moisture withdraws from the pores of the hardened cement paste over time, causing drying shrinkage. This lasts until the concrete has reached the so-called equilibrium moisture content. The volume of water lost is not equal to the volume reduction of drying concrete [2]. The loss of free water from the capillary pores, which takes place first, results in little shrinkage. Thereupon, as drying continues, absorbed water in the gel pores is lost, causing a shrinkage mechanism analogous to that of plastic and autogenous shrinkage (see Figure 2.30). The volume of this water loss does more or less correspond to the volume reduction of drying concrete. A part of the withdrawal of moisture is reversible; the concrete may swell afterwards when it is exposed to (near) saturated air. However, a large part of the shrinkage is irreversible. This can be explained by the redistribution of the CSH sheets forming the cement gel, which form new crystallized bonds [10]. Since moisture can only leave the concrete trough its surface, the loss of water with time relies on the size of the specimen, or more specifically its surface-area-to-volume ratio. Figure 2.33 presents the water lost over time for prismatic specimens drying from all surfaces. From this it can be deduced that drying shrinkage is, in contrast to other types of shrinkage, a slowly occurring phenomenon, as it takes a considerable time for a specimen to dry completely. Where autogenous shrinkage is a matter of days and weeks, drying shrinkage is a matter of months and years. However, drying shrinkage depends, in addition to the specimen size, also on the relative humidity of the air to which the concrete is exposed. Figure 2.32 shows that a lower relative humidity of the surrounding air results in both a greater ultimate value and an increased rate of drying shrinkage. These characteristics are affected in the same way by the air temperature, because an increased temperature ensures a lower equilibrium moisture content and aids in the diffusion of moisture towards the concrete surface.

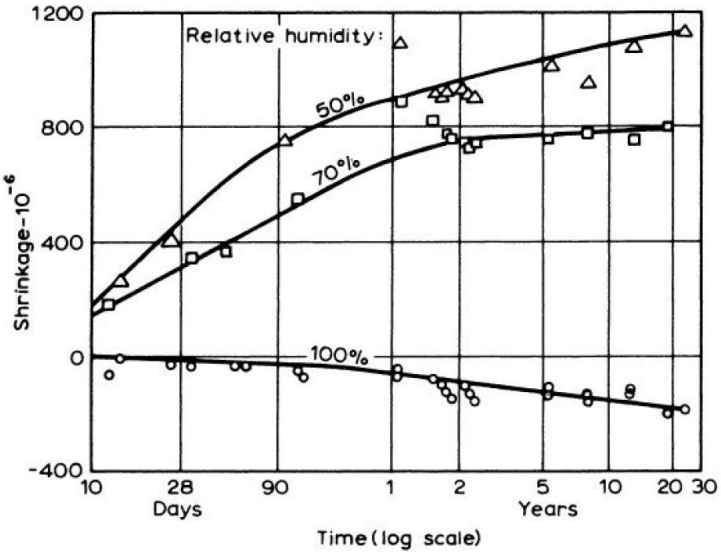

Figure 2.32: Relation between drying shrinkage of concrete over time and relative humidity of surrounding air [2].

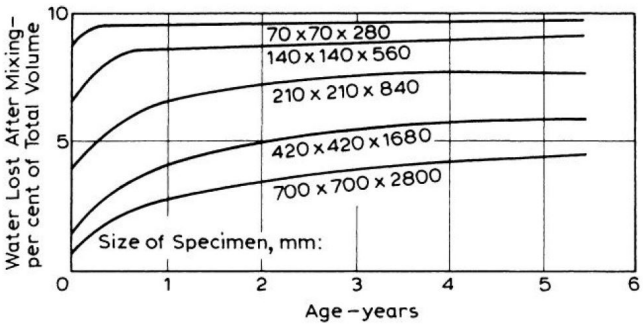

Figure 2.33: Relation between water lost from concrete over time and specimen size [2].

As far as shrinkage of the hardened cement paste is concerned, drying shrinkage is larger the higher the water/cement ratio [2, 10]. The influence of the water/cement ratio is again twofold. First, the water/cement ratio dictates the amount of free and absorbed water available for drying. Second, the rate at which moisture can diffuse through the pores of the cement paste towards the concrete surface depends on its permeability, which in turn is mainly dictated by the water/cement ratio. However, when concrete is considered, the aggregates also exert a major influence on the drying shrinkage since they provide resistance against volume reduction. Similar to autogenous shrinkage, a larger relative volume of aggregates, leads to a decrease in drying shrinkage of concrete. The combined influence of the cement content, that relates to the relative volume of aggregates, and the water/cement ratio on the drying shrinkage is given in Figure 2.34. In addition, the stiffness of the aggregates also plays a role since they dictate the delivered level of resistance. Nevertheless, for universal aggregates, the ratio of the drying shrinkage of concrete ε_c to that of cement paste ε_p as a function of the aggregate content a can be expressed by Equation 2.19, where n is a coefficient that typically has a value between 1.2 and 1.7 [2]. Finally, it must be mentioned that the effect of cement type and fineness on drying shrinkage of concrete is limited.

$$\frac{\varepsilon_c}{\varepsilon_p} = (1-a)^n \tag{2.19}$$

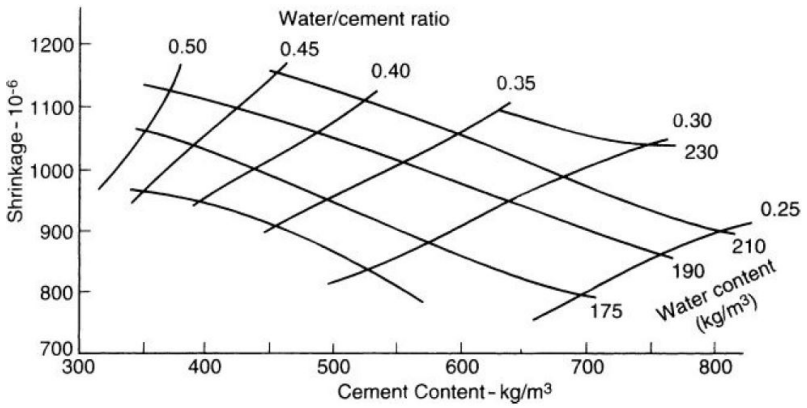

Figure 2.34: Relation between drying shrinkage after one year, water/cement ratio and cement content of concrete [2].

2.6.6 Thermal deformations

In accordance with most materials, concrete will expand when heated and contract when cooled, the latter is known as thermal shrinkage. Temperature change of concrete is generally caused by artificial processes, environmental conditions, cement hydration or a combination thereof. Hence, thermal shrinkage can occur early-age, but also later when the concrete is fully hardened. Although they may both result in cracking, thermal deformations of young concrete are of particular importance because the temperature change at this stage is not only responsible for the imposed deformation, but also influences the strength and stiffness development. How the temperature affects the strength and stiffness development was discussed earlier, this section is devoted to the characteristics of (young) concrete governing thermal deformations and diffusivity. One of those characteristics is the coefficient of thermal expansion (CTE), which is mainly a function of the aggregate content in the concrete mixture and the coefficient of the aggregate itself [2, 10]. The CTE represents the magnitude of volume reduction or increment with a change in prevailing concrete temperature. The expansion coefficients of common aggregate types are given in Table 2.5 and mainly depend on their silica

content, since more silicates equals a greater temperature sensitivity. The CTE of the aggregates is considerably lower than that of the cement paste, the values of which vary between 11 and 20 $\mu\varepsilon$/K. It is expected that this differential expansion between the aggregates and cement paste contributes to the reduction in ultimate strength of concrete when subjected to high early temperatures (see Figure 2.26). The variation in the CTE of cement paste is primarily due to its dependence on the moisture content, which is a consequence of the decrease in capillary tension with an increase in temperature. The CTE of the cement paste is greatest when it is partially saturated (i.e. at a relative humidity from 50% to 70%). Since the moisture content is changing significantly with the progress of hydration, the degree of hydration also affects the coefficient of the cement paste. However, because the aggregates take up approximately three-quarters of the volume of the concrete, the variation of the CTE of the concrete will be minor. Therefore, in practice, it is usually sufficient to assume a constant CTE (that is valid in a moderate temperature range), provided that the type of aggregates is accounted for.

In order to determine thermal deformations, it is necessary to obtain the prevailing temperatures within a concrete structure. However, concrete acts as an insulator due to its comparatively low thermal conductivity, which means the prevailing temperature is most likely not evenly distributed across the structure. That is to say, it takes time before the entire concrete structure has reached the same temperature as imposed by the source of heating or cooling. This is especially the case with massive concrete structures, where the large thickness further enhances this effect, or for young concrete, where cement hydration may result in a very large temperature rise. The time required for the concrete to adapt to an changing temperature depends on its thermal diffusivity, which represents the rate at which temperature changes within a medium can take place. The thermal diffusivity is a function of various characteristics of concrete, being the thermal conductivity, specific heat and mass. For all three characteristics it holds that, analogous to the coefficient of thermal expansion, they are mainly determined by the type of aggregates, the aggregate/cement ratio and the moisture content [2, 10]. Both the thermal conductivity and specific heat of concrete increase with an increase in moisture content. Contradictory observations regarding the influence of the degree of hydration on the thermal conductivity and specific heat of concrete can be found in literature. Nevertheless, it seems that the early-age values of thermal conductivity are usually slightly higher than those observed when the concrete is fully hardened, while the opposite is true for the specific heat [27]. As a result, the thermal diffusivity of concrete is not a constant. However, in practice, it is justified to adopt a constant value for the thermal diffusivity (that is valid in a moderate temperature range), since the variations will be minor too.

2.6.7 Creep and relaxation

Creep is the gradual increase in strain with time under a constant stress, while relaxation is the gradual decrease in stress under a constant strain. Relaxation is generally considered a favourable property of concrete, since it more or less relieves a structure of its load. Creep, on the other hand, usually has an adverse effect, because the deformation increase can be several times larger as the deformation on loading. Since this may seriously affect a concrete structure's functionality and safety, creep is of considerable importance. Creep and relaxation are two phenomena arising from a mechanism similar to that of drying shrinkage, that is, the withdrawal of moisture from the gel pores, and the redistribution of CSH sheets forming the cement gel. This mechanism and its influencing factors will be explained in more detail in the upcoming paragraphs from the perspective of creep.

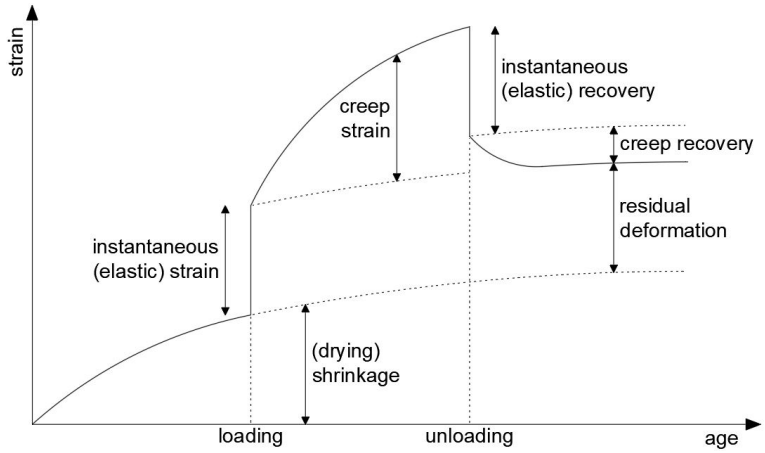

Figure 2.35: Schematic representation of deformation behaviour of concrete with time, adapted from [2].

Figure 2.35 displays the deformation behaviour of concrete with time, including instantaneous and creep strain as a consequence of loading, and drying shrinkage (denoted merely as shrinkage in this section). From this it can be seen that creep is a function of both time and loading. The differentiation between instantaneous and creep strain has been explained in section 2.5.3. Since the instantaneous strain depends on the rate of loading, it is not truly elastic as movement of free water between the capillary pores [10]. However, since short-time creep occurs very rapidly (i.e. within seconds of loading), it is considered to be elastic. Hence, long-time creep is more important in practice. With long-time creep, a distinction can be made between creep when no moisture movement takes place, known as basic creep, and additional creep caused by desiccation, referred to as drying creep [2]. A loaded and drying specimen will experience shrinkage, basic and drying creep, whereas a loaded specimen which has reached the equilibrium moisture content will only be subjected to basic creep. Although shrinkage and creep are not independent phenomena, it is convenient and close to correct to consider creep as a deformation in excess of shrinkage. The microscopic interpretation of long-time creep still remains up for discussion. However, it is thought that redistribution of the CSH sheets forming the cement gel is the main cause [10]. When the cement gel is loaded, the CSH sheets will not all be exposed to the same stress level. As a result, the crystallized bonds of the CSH sheets which endure the most stress may break, causing the CSH sheets to shift to another place where they form new bonds. The loss of water from the gel pores as a consequence of drying makes it easier for CSH sheets to form new bonds, thereby increasing the long-time creep. This mechanism also explains the difference between basic and drying creep, as well as why part of long-time creep is irreversible. The reversible part of long-time creep is most likely a consequence of elastic deformation of certain CSH sheets. These CSH sheets will shift back at unloading, where they will form new bonds until the stress has settled. Nevertheless, there will always be residual deformation after unloading, because this creep recovery is not complete.

Long-time creep, from now on simply referred to as creep, is affected more or less in the same way and by the same factors as shrinkage. Some of these factors are inherent properties of the concrete mixture, others depend on the environmental conditions. First of all, it should be mentioned that it is really the hardened cement paste that endures creep, the role of the aggregates in the concrete composite being that of resistance against volume reduction. Equation 2.20 relates the creep of concrete ε_c to that of the cement paste ε_p and the aggregate content a, where c is a coefficient depending on the modular ratio of concrete to aggregates [2, 10]. Furthermore, there is a direct proportionality between creep and the applied stress. However, there is an upper limit to this proportionality when microcracking becomes severe, typically at a stress in the range of 0.4 to 0.6 times the strength, after which a small stress increment is accompanied by a relatively large creep increase. Moreover, this proportionality does not hold at an early-age, likely because the CSH sheets are still in development (due to ongoing hydration) when the stress is applied, but information about this is scarce. Nevertheless, in the long-term and below the upper limit, which usually represents all or most of the stress occurring in structures, creep can be expressed as a linear function of the stress/strength ratio, as is shown in Figure 2.36. This is possible since creep is also inversely proportional to the strength of concrete at the time of loading. While this relationship is convenient in practice, it is not fundamental because it is, in essence, the water/cement ratio and degree of hydration that matter. A lower water/cement ratio and a greater degree of hydration, which corresponds to a higher strength, equals a smaller pore volume and a finer porosity of the cement paste at the time of loading. As a result, the diffusion of moisture through the pores of the cement paste is more difficult and there will be more bonds between CSH sheets (i.e. there is likely less redistribution), thereby reducing creep [10]. But since the water/cement ratio and degree of hydration impact mainly the strength, their influence on the creep of concrete can also be expressed by its relationship with the strength. In addition, cement type and fineness affect creep only in so far as they influence the strength of concrete at the time of loading [2].

$$\log\left(\frac{\varepsilon_c}{\varepsilon_p}\right) = c \cdot \log\left(\frac{1}{1-a}\right) \tag{2.20}$$

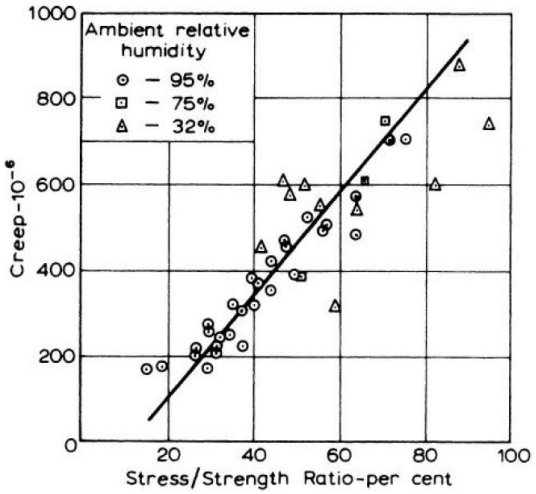

Figure 2.36: Relation between stress/strength ratio and creep of concrete [2].

The environmental condition mostly affecting creep is the relative humidity of the surrounding air. Figure 2.37 shows that creep of concrete is higher at a lower the relative humidity. Thus, the drying of a specimen while being loaded has an enhancing effect as it induces drying creep. A higher air temperature also stimulates drying creep since, for reasons discussed earlier, it plays a role in the drying behaviour of concrete. However, it must be noted that drying only continues until the specimen has reached the equilibrium moisture content. Because the loss of water with time depends on the surface-area-to-volume ratio of the specimen, its size also affects creep. An increased specimen size results in both a lesser ultimate value and a decreased rate of creep. The former is caused by the fact that when drying reaches the core of a specimen, it will have hydrated extensively and achieved a higher strength, leading to less creep [2]. On the basis of the foregoing, it can be inferred that a concrete structure which exhibits great shrinkage usually also shows great creep, and that shrinkage and creep occur in roughly the same period.

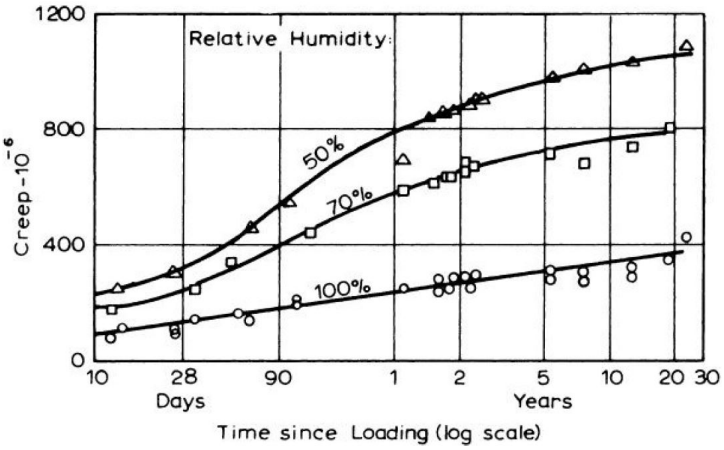

Figure 2.37: Relation between creep of concrete over time and relative humidity of surrounding air [2].

3

Concrete mixture design

Before the concrete mixture intended the side walls of the reservoir could be subjected to several tests to obtain its relevant physical and mechanical properties, it first had to be designed. Where the next chapter includes the testing itself, this chapter is devoted to the design of this mixture. Included are the design criteria and procedure, selection of ingredients and proportions, and an overview of the compositions of the various concrete mixtures that were eventually investigated.

3.1 Design criteria

The concrete mixture of the side walls of the reservoir is vital in the demonstration of the crack-sealing capacity of the bacterial self-healing technology. It not only forms the basis to which the healing agent is added, but also influences the early-age cracking behaviour trough its role in the strength development and being the incentive for imposed deformations. In addition, the concrete mixture affects its ability to be processed and the performance of the side walls in general during use and possible reuse. Hence, several considerations had to be taken into account in the design of the concrete mixture. These design criteria are highlighted separately in the upcoming paragraphs.

Compatibility

Side wall A will be constructed from BSHC, meaning healing agent is added to its concrete mixture. The concrete mixture must therefore be compatible with the addition of healing agent, that is, it should provide an environment in which the bacteria can operate while other concrete characteristics are not negatively affected. This seems to be mainly related to the chemical composition of the hydrated cement and alkalinity of the pore water. Therefore, to ensure a suitable environment for the bacteria, the cement type used in the composition must contain sufficient clinker. This can either be Portland cement or blended cements with a clinker content in excess of 50% [29]. Because the same mixture composition will be used for be used for side wall B (from ordinary concrete), it was decided to perform tests on the concrete mixture with and without the addition of healing agent. This makes it possible to verify the effects of the healing agent on the characteristics of the concrete; effects that are expected to be negligible (at the correct clinker content).

Realism

Even though healing agent can be added to a wide variety of concrete mixtures, only one mixture can be used in the demonstrator project. With the intention of demonstrating that the bacterial self-healing technology is capable of sealing cracks across the entire range of mixtures, it was decided to create a mixture that would be somewhere in the middle of this range. This means that the concrete mixture should be 'realistic'; composed of commonly used ingredients (in the Netherlands) in regular and economical proportions. Simply put, a mixture that more or less corresponds to the average of what is applied in practice (for normal to high-strength concretes). More specifically, this demands the use of universal aggregates, a popular cement type and a water/cement ratio in the range of 0.4 to 0.5. The former two requirements have also been devised to ensure that any concrete plant, which will eventually supply the concrete mixture when the reservoir is constructed, is likely to have these ingredients in stock. This is also an attempt to ensure that the mixture supplied by the concrete plant corresponds to the mixture that has been designed and tested as part of this thesis.

Workability

At the time of design of the concrete mixture, little was known about conditions which generally dictate the

desired workability, such as the method of pouring during construction of the reservoir and the fineness of the reinforcement mesh. Nevertheless, an assumption with regard to the desired workability had to be made since this considerably affects the mixture composition. Therefore, it was decided to apply a maximum aggregate size of 16 mm and to strive for a consistency equivalent to class F4 or F5 depending on the water/cement ratio (F4 if $wcr \geq 0.45$ or F5 if $wcr < 0.45$). This allows for compaction of the side walls with a vibration needle and the fresh concrete should be able to flow between a reinforcement mesh of up to approximately 50 mm without the aggregates getting stuck or trapped in it.

Incentive
This design criterion is the contrary of practice where shrinkage is usually despised, but in this case the concrete mixture should preferably shrink considerably to stimulate early-age cracking. Stimulation of early-age cracking of the side walls can primarily be accomplished by promoting thermal and autogenous shrinkage. However, due to other requirements relating especially to the cement type, it proved difficult to promote thermal shrinkage, as will become apparent in subsequent sections. As a result, the focus was mainly on the potential to increase autogenous shrinkage. In this regard, it was relevant to examine whether the concrete mixture would exhibit increased autogenous shrinkage if it had a higher fine content due to the addition of filler, which was expected because the cement paste is likely to have a finer porosity. Accordingly, it was decided to perform tests on the concrete mixture with and without the addition of filler. In addition, it had to be taken into account that richer mixtures generally manifest increased thermal and autogenous shrinkage.

Strength
At this point, it is appropriate to emphasize that there was no strict requirement regarding the strength as it could conflict with the other design criteria, in particular those related to the water/cement ratio, which were considered more important. Nevertheless, a relatively high strength potential of the concrete mixture is desired because, as will become apparent in later stages of this thesis, a higher strength allows for larger crack widths. Thus, a strength roughly corresponding to class C50/60 was targeted.

Comparability
So far, the concrete mixture has been regarded as one unique composition. However, due to variations in the addition of filler and healing, essentially four different mixtures can be identified, those being:

- Mix 1: no additions;
- Mix 2: addition of filler;
- Mix 3: addition of healing agent;
- Mix 4: addition of filler and healing agent.

Nevertheless, these concrete mixtures are quite similar, since it was decided to maintain the same cement paste. In other words, the cement type, water/cement ratio and richness are the same in all mixtures as the additions only replace some of the aggregates. This makes it possible to compare the effects of the additions on the characteristics of the concrete, because purely the differences due to the additions will be perceived.

3.2 Design procedure

The design procedure of the concrete mixtures involves seeking a compromise between the above criteria through the selection of ingredients and proportions. The selection of ingredients and proportions is elaborated in the next two sections and conforms to Dutch standards and guidelines. Many practical knowledge has been extracted from the 'Betonpocket'; a reference work which bundles Dutch regulations and data regarding concrete mixtures and its ingredients [18]. Where regulations determined the selection of ingredients and proportions, reference is made to the relevant standards. In the other cases, it is argued why certain ingredients and proportions were selected. Although the knowledge obtained through the literature study contributed significantly to the design of the concrete mixtures, it was not always sufficient. Certain aspects in the selection of proportions proved difficult to determine only on the basis of experience (acquired from literature). This was particularly the case with the dosage of superplasticizer in relation to the desired workability and water requirement, since its behaviour may be specific to a certain cement type and water/cement ratio. In this case, only trials could disclose whether the mixture composition is adequate, that is, the trial results match the design values. These trials consisted of determining the fresh properties of mix 1 (which contains no filler or healing agent), in common with the test procedure which is discussed in the subsequent chapter. Needless to say, the trial results are not part of the test results, because the trials relate to intermediate rather than final mixture compositions. Nevertheless, the trial results that contributed to the design of the concrete mixtures are included below in the selection of proportions.

3.3 Selection of ingredients

The concrete mixtures consist of cement, mixing water, aggregate and a water-reducing admixture and possibly also of filler and healing agent. These ingredients, with the exception of mixing water, are addressed separately. This includes the type of ingredient selected, their known and assumed properties, and associated reasoning. Since most ingredients are common in nowadays practice, much of their data is self-evident or easily traceable and is therefore not provided here.

3.3.1 Cement

For the binder, a blend of Portland and blastfurnace cement has been chosen, more specifically a combination of CEM I 52.5R and CEM III/B 42.5N. The choice for blastfurnace cement stems from it being by far the most used cement type in the Netherlands, in part because its manufacture entails less CO_2 emissions. Blastfurnace cement is the main ingredient in the blend, to which Portland cement has been added for two reasons. First, the addition of Portland cement ensures a greater heat output, thereby promoting thermal shrinkage. Second, Portland cement is required to achieve a clinker content in excess of 50% to ensure healing agent compatibility. However, this second reason conflicts with the prevention of ASR according to CUR recommendation 89, which prescribes a slag content of at least 50% in case of this blend [20]. As a result, the share of Portland cement in the blend is targeted as such that the clinker content approximately equals that of the slag (i.e. fifty-fifty). This is accomplished by proportioning the blend from 26% of CEM I 52.5R and 74% of CEM III/B 42.5N. Assuming a slag content of the latter of 70%, which may vary slightly (see Figure 2.1), the ratio will be about 48% clinker to 52% slag, disregarding other minor constituents in both cement types. The cement proportioning therefore contains a little margin with regard to the prevention of ASR. It must be noted that alternatives have been considered, in particular pure CEM III/A 52.5N. However, this binder was rejected since its clinker content may vary considerably, which would leave too much uncertainty about healing agent compatibility.

3.3.2 Aggregate

The aggregates can be divided into fine and coarse aggregate. For the fine aggregate, river sand 0/4 has been chosen, while the coarse aggregate are made up of river gravel 4/16. The choice for these natural aggregates stems from them being the most stocked at concrete plants in the Netherlands, mainly because they can be retrieved from river deposits in the vicinity. The aggregates, especially the coarse ones, are smooth and rounded due to erosion. Sieve analysis of the batches of fine and coarse aggregate used in testing of the concrete mixtures has not been performed. However, sieve analysis of other batches indicated the grading curves presented in Figure 3.1 and a fineness modulus of 3.10 and 6.63 of the fine and coarse aggregate, respectively. To facilitate the estimation of the water requirement, the ratio of fine to coarse aggregate is targeted as such the grading curve of the blend corresponds to grading zone I, the upper and lower limits of which are taken from Figure 2.13. This is accomplished by proportioning the blend from 45% of river sand 0/4 and 55% of river gravel 4/16, resulting in a fineness modulus of the blend of 5.04. Absorption of the fine aggregate is assumed to equal 0.4%, while 2.0% is taken into account for the coarse aggregate.

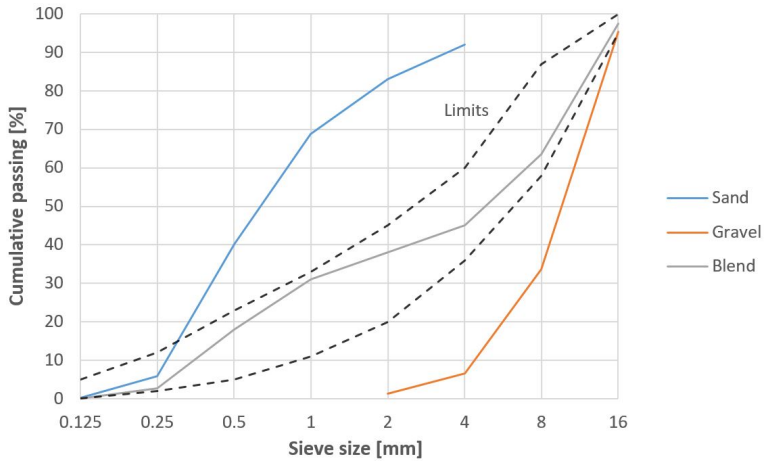

Figure 3.1: Grading curves of chosen aggregates, including grading zone limits.

3.3.3 Filler

To increase the fine content of two of the four concrete mixtures, it was decided to add limestone powder. Limestone powder is an inert (type I) filler, meaning it has no binding function and only contributes to the packing density of the concrete. The selection of limestone powder emanated from the fact that cementitious (type II) fillers such as fly ash, which do have a binding function, were rejected because they may disturb the chemical composition of the hydrated cement paste and the alkalinity of the pore water, which would leave too much uncertainty about healing agent compatibility. Another fact in favour of limestone powder is its availability (in the Netherlands), which is better than many other fillers. The dosage of limestone powder is aimed at increasing the amount of fine material by about 20%, which besides filler features cement and the aggregate passing trough the 0.25 mm sieve.

3.3.4 Admixture

A water-reducing admixture was required to obtain the desired workability. The intended consistency of the concrete mixtures required the addition of a superplasticizer. A lot of superplasticizers are available on the market, many of which would most likely also have been capable of fulfilling the necessary water reduction. The selection of the superplasticizer that has been used was therefore rather arbitrary.

Healing agent is basically also an admixture, which is added to two of the four concrete mixtures. In consultation with Dr. H.M. Jonkers it was decided to add 7.5 kg/m^3 of healing agent. The expected crack-sealing capacity at this dosage in combination with a clinker content of approximately 50% equals that of cracks up to 0.6 mm in width. The demonstrator project aims to prove this hypothesis in practice.

3.4 Selection of proportions

The selection of proportions has not been straightforward since it proved difficult to determine the dosage of superplasticizer in relation to the desired workability and water requirement. Trials with mix 1 have been carried out to overcome this problem, which allowed the concrete mixtures to be adjusted multiple times based on trial results. The evolution of the mixture compositions and the trial results are given in Table 3.1. Based merely on a rule of thumb concerning the selected superplasticizer and extrapolation of the approximate water requirements provided in Table 2.6 for grading zone I and a maximum aggregate size of 16 mm, it was the author's believe that the desired workability conformed to a water requirement of 180 L/m^3 and a superplasticizer dosage equal to 0.65% of the cement mass. However, during mixing it soon became apparent that the water requirement had been overestimated and less water was added in the process, that is, only 160 L/m^3. Nevertheless, this intermediate mixture composition was also rejected since segregation occurred immediately after mixing, the measured slump size of 210 mm was not in accordance with a consistency equivalent to class F5, and the measured air content of 0.4% was significantly lower than what had been assumed. The cause for the poor stability and inadequate air content was attributed to an overdose of superplasticizer. The superplasticizer dosage was therefore reduced to 0.40% of the cement mass, which was accompanied by an increased water requirement of 170 L/m^3. The latter also ensured that the water/cement ratio would again meet the design criteria. This final mixture composition was eventually accepted since the cohesiveness was found to be satisfactory, the measured slump size matched the design slump size of 240 mm, and the measured air content of 1.9% corresponded better to what had been assumed.

	Initial	*Intermediate*	*Final*
Water requirement (L/m^3)	180	160	170
Water/cement ratio	0.431	0.383	0.407
Superplasticizer (relative to cement mass)	0.65%	0.65%	0.40%
Strength potential acc. Equation 2.13 (MPa)	58	64	61
Slump size measurement (mm)		210	240
Stability judgement		Poor	Good
Air content measurement		0.4%	1.9%
Specific mass measurement (kg/m^3)		2404	2352

Table 3.1: Evolution of mixture compositions and trial results.

During the trials the richness of the mixture compositions presented in Table 3.1 remained equal, meaning the water/cement ratio only varied because the water requirement deviated. It may have been possible to further increase the richness of the concrete mixtures to promote thermal and autogenous shrinkage. However, it was decided to maintain a cement content of 418 kg/m^3 because more cement paste is uneconomical and therefore not regular in practice for mixtures with a similar water/cement ratio. The choice for a water/cement ratio in the lower regions of the permitted range of 0.4 to 0.5 was intentional as it increases autogenous shrinkage and provides a higher concrete strength. The strength potential of the concrete mixtures is estimated as a function of the water/cement ratio and cement type using Equation 2.13. Correspondingly, the design strength of the final mixture composition with a water/cement ratio of 0.407 equals 61 MPa.

3.5 Overview of concrete mixtures

Table 3.2 presents an overview of the concrete mixtures applied in testing. These mixtures have been designed in accordance with the selection of ingredients and proportions described above, making them suitable for the side walls of the reservoir. The water/cement ratio of all mixtures is 0.407, which corresponds to the water/cement ratio established based on trials with mix 1. As mentioned, the design strength and design slump size of the mixtures is 61 MPa and 240 mm, respectively. In addition, an air content of 1.5% has been assumed in the design of all concrete mixtures. Mixes 2 and 4 with filler have a fine content of 188 L/m^3, as opposed to a fine content of 158 L/m^3 for mixes 1 and 3 without filler. More data regarding the concrete mixtures can be found in Appendix A, which provides detailed compositions of each mixture.

Ingredient	*Proportion*[1] *(kg/m^3)*			
	Mix 1	*Mix 2*	*Mix 3*	*Mix 4*
CEM I 52.5R	109	109	109	109
CEM III/B 42.5N	309	309	309	309
Mixing water	170	170	170	170
River sand 0/4	797	761	790	754
River gravel 4/16	989	945	981	936
Limestone powder		84		84
Superplasticizer [30]	1.7	1.7	1.7	1.7
Healing agent [29]			7.5	7.5
Total	**2376**	**2378**	**2368**	**2370**

Table 3.2: Compositions of concrete mixtures applied in testing.

[1]Includes absorption of the aggregates.

4

Concrete mixture testing

The concrete mixtures have been subjected to several tests for different purposes, those being verification of their respective designs, quantification of relevant physical and mechanical properties and investigation into the effect of the addition of filler and healing agent on these properties. These test objectives are discussed in detail at the beginning of this chapter. This is followed by the test procedure, including a comprehensive description of the test setups. The chapter is finalized with the presentation of the test results.

4.1 Test objectives

The test objectives are decisive in the kind of tests that are to be conducted. Testing of the concrete mixtures serves multiple purposes related to the objective of this thesis, the most important of which are the following:

- Verification of the concrete mixtures with respect to their designs, that is, checking whether the design values and the assumptions made correspond to reality.
- Quantification of the physical and mechanical properties of the concrete mixtures relevant to their early-age cracking behaviour when hardened.
- Investigation of the effect of the addition of filler and healing agent on the relevant physical and mechanical but also the fresh properties of concrete, with special attention to the impact of an increased fine content on autogenous shrinkage of concrete.

Based on the above purposes it was decided to perform tests related to the fresh properties (i.e. consistency, cohesiveness, air content and specific mass), strength development and autogenous shrinkage of the concrete mixtures. The fresh properties have mainly been determined with the intention of verification of the design, these tests are therefore more practical in nature. The strength development, on the other hand, has been examined not only for verification purposes, but also because it plays a major role in the early-age cracking behaviour of hardened concrete. That is to say, the tensile strength at a given age affects both the probability and degree of cracking. Autogenous shrinkage of the mixtures is determined since it is of interest with respect to the probability of cracking and because there are indications from practice that specific concrete mixtures, such those with an increased fine content or high slag containing concretes, exhibit larger autogenous shrinkage than is prescribed by the standards, which generally only take into account the influence of the water/cement ratio. It must be noted that, besides strength development and autogenous shrinkage, there are other properties relevant to the early-age cracking behaviour of concrete, in particular creep, heat of hydration and thermal properties such as the CTE, the latter two of which govern thermal deformations. However, due to limited resources, it was simply not possible to determine all of these properties experimentally.

4.2 Test procedure

The concrete mixtures were prepared and tested in two stages. During both stages batches of 40 L of each mixture were prepared. Preparation was done with utmost care to ensure both batches of the same mixture were identical. Mixing, pouring and compaction of each batch was done identically. Furthermore, the ingredients of the concrete mixtures all came from the same batch. Verification of the fresh properties, pouring in the specimen moulds and compaction by means of a vibrating table all happened within half an hour from the start of mixing. The shapes and sizes of the specimens and their moulds complied to the NEN-EN 12390-1. Moreover, manufacture and curing of the specimens was done in line with the NEN-EN 12390-2. Accordingly, after pouring and compaction, the specimens were kept at room temperature and covered with polyethylene

sheeting to prevent early loss of water to the environment. Demoulding of the specimens took place one day later. The specimens for determination of autogenous shrinkage were all taken from second stage batches, while those with regard to the strength development emanated from both first and second stage batches. Likewise, the consistency and cohesiveness were checked of both first and second stage batches, whereas the air content and specific mass were only measured of first stage batches. The background and test setups, often laid down in standards, of each conducted test are described separately in continuation of this section.

4.2.1 Fresh properties

A sample of fresh concrete was taken in accordance with the NEN-EN 12350-1. Consistency was determined by means of a slump test as stated in the NEN-EN 12350-2. Simply put, the experimental protocol of a slump test consists of pouring and compacting (with a rod) three layers of fresh concrete in a hollow cone, than slowly removing the cone by carefully raising it in a vertical direction, allowing the fresh concrete to slump. The slump size is the difference between the height of the cone and the highest point of the slumped sample. Because a consistency equivalent to class F5 is targeted, the first stage batches were also subjected to a flow table test in line with the NEN-EN 12350-5. The experimental protocol of a flow table test comprises of a modified slump test performed on a flat plate hinged to a rigid base, the end of this plate is subsequently lifted and dropped 15 times over a height of 40 mm, allowing the fresh concrete to flow. The flow diameter is the average of the maximum dimension of the spread of the sample in two directions parallel to the plate edges.

(a) Mixing. **(b)** Flow table test.

Figure 4.1: Fresh concrete handling.

In contrast to consistency, cohesiveness is difficult to measure quantitatively. However, because cohesiveness is at least as essential as consistency, the tendency to segregation was continuously assessed (visually) when handling the fresh concrete. With this it is meant that the stability of the concrete mixtures was judged immediately after mixing when performing the slump and flow table tests, during which segregation manifests itself as a ring of water or grout extending beyond the slump or spread of the aggregate. Furthermore, inadequate cohesiveness could also easily be recognized if water or grout were to separate out and rise to the surface of the fresh concrete when it was left to rest in a wheelbarrow for several minutes. In the end, the stability of the concrete mixtures was judged either as 'poor' or 'good', that is, deficient or sufficient with regard to the desired workability, respectively.

The air content was measured according to the pressure gauge method prescribed by the NEN-EN 12350-7 using the air entrainment meter displayed in Figure 4.2. The procedure of this method features pouring and compacting (with a vibrating table) fresh concrete in a test container (10) of 8 L up to the rim, on top of which the so-called cover assembly is subsequently clamped airtight. Using a syringe, water is injected trough a valve (1) until water emerges from the other valve (2), indicating the test container is full. After all valves are closed, the air chamber (6) built into the cover assembly is pressurized using the air pump (3) until the needle on the pressure gauge (5) is on the initial pressure line. The main air valve (4) is then opened and the pressurized air is released into the test container, causing the needle on the pressure gauge to indicate the air content of the fresh concrete contained therein. Following the discovery of the air content, the cover assembly is removed and the test container is placed on a digital scale in order to determine the specific mass of the fresh concrete in compliance with the NEN-EN 12350-6.

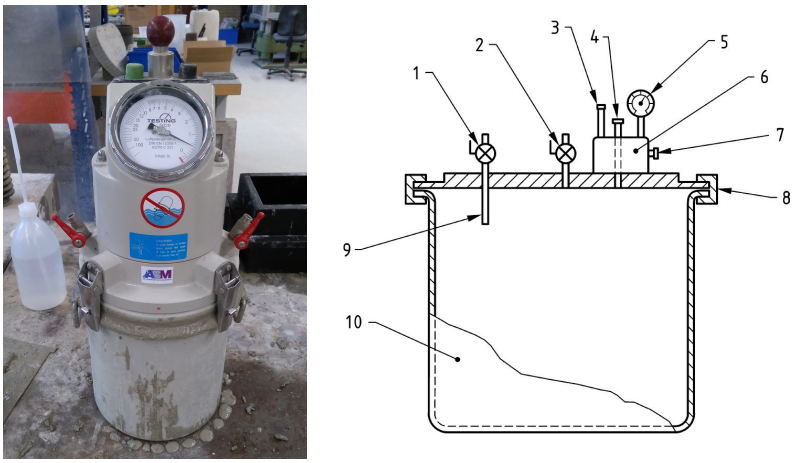

(a) In operation. **(b)** Components, source: NEN-EN 12350-7.

Figure 4.2: Air entrainment meter.

4.2.2 Strength development

The strength development of the concrete mixtures was determined on the basis of the compressive strength, which can be used to derive other physical and mechanical properties of the concrete. The specimens consisted of cubes with dimensions of 150x150x150 mm. A total of 32 cubes were made, being 8 per concrete mixture. The compressive strength of each mixture was determined in accordance with the NEN-EN 12390-3 at the ages of 1, 2, 3 (2x), 4, 7, 14 and 28 days in order to acquire the rate at which they gain strength and to verify their design strength. The pressure bench used for this complies with the NEN-EN 12390-4 and has a maximum relative error of 2%. The applied loading rate was 13.5 kN/s and the test was terminated once the applied load had dropped by 20%. The relationship between the cube compressive strength $f_{c,cube}(t)$ and the maximum applied load at failure $F(t)$ at age t is given by Equation 4.1, where A_{spec} is the cross-sectional area of the specimen (on which the applied load acts). After demoulding, the specimens pending their test were stored in a climatized room, where the temperature and relative humidity were kept constant at 20 °C and 100%, respectively. In addition, the specimens were examined post-testing to assess whether they failed satisfactorily and thus to assess the validity of the test results.

$$f_{c,cube}(t) = \frac{F(t)}{A_{spec}} \tag{4.1}$$

(a) In pressure bench. **(b)** Post-testing.

Figure 4.3: Specimen for strength development.

4.2.3 Autogenous shrinkage

Autogenous shrinkage was measured in compliance with the NEN-EN 12390-16 of prisms with dimensions of 400x100x100 mm. A total of 12 prisms were made, being 3 per concrete mixture. After demoulding, the specimens were taken to a climatized room, where the temperature and relative humidity were kept constant at 20 °C and 50%, respectively. There, the specimens were wrapped in a self-adhesive bitumen foil to prevent drying. Subsequently, analogue measuring devices were glued to the two opposite sides of the specimens. Incisions were made in the bitumen foil where the measuring devices were glued to the specimens, namely 100 mm from the end edges and 50 mm from the side edges of the specimen. The measuring devices thus recorded the shortening (or elongation) of the specimen over a gauge length of 200 mm, with an accuracy of 1 µm. The relationship between the autogenous shrinkage strain $\varepsilon_{ca}(t)$ and the recorded shortening $\Delta L(t)$ at age t is given by Equation 4.2, where L_{spec} is the gauge length of the specimen. In order to acquire the progress of the autogenous shrinkage, the measuring devices were frequently read (except during the weekend). The time between readings progressively increased as the recorded shortening decreased. In addition, when reading the measuring devices, one of three specimens of each concrete mixture was weighed to check for drying, which manifests as weight loss, and thus to assess the validity of the test results. The weight loss was determined using a digital scale with an accuracy of 0.1 gram.

$$\varepsilon_{ca}(t) = \frac{\Delta L(t)}{L_{spec}} \tag{4.2}$$

(a) Poured in steel mould.

(b) Wrapped in bitumen foil.

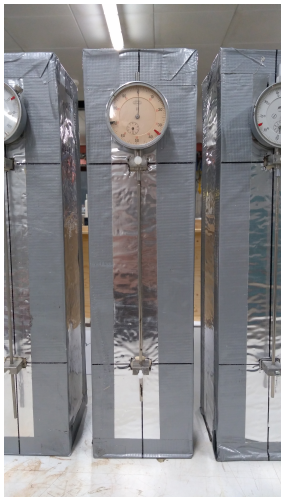

(c) Fitted with measuring devices.

Figure 4.4: Specimen for autogenous shrinkage.

4.3 Test results

This section presents the results of the conducted tests related to the fresh properties, strength development and autogenous shrinkage of the concrete mixtures. The test results are provided with a description where additional clarification is required. In addition, inconsistencies and uncertainties that were noted during testing are stated. It must be stressed that merely the observations and test results themselves are mentioned here, a detailed analysis of the test results (in relation to the test objectives) follows later on in this thesis.

4.3.1 Fresh properties

The measured fresh properties of each concrete mixture are presented in Table 4.1. This shows that mixes 1 and 3 are more or less comparable in terms of consistency and air content. The same seems to apply to mixes 2 and 4, albeit that they exhibit a greater consistency according to the flow table test and a slightly lower air content with respect to mixes 1 and 3. Although the stability of all mixtures was judged as good, a similar correlation was observed between the cohesiveness of mixes 1 and 3 on the one hand, and mixes 2 and 4 on the other. That is to say, mixes 2 and 4 demonstrated less tendency to segregation.

Measurement	*Mix 1*	*Mix 2*	*Mix 3*	*Mix 4*
	First stage batches			
Slump size (mm)	240	250	240	260
Flow diameter (mm)	610	680	620	700
Air content	1.9%	1.5%	2.0%	1.7%
Specific mass (kg/m^3)	2352	2377	2347	2365
	Second stage batches			
Slump size (mm)	240	230	230	250

Table 4.1: Fresh properties test results.

4.3.2 Strength development

Table 4.2 gives the measured compressive strengths of each concrete mixture at the ages of 1, 2, 3 (2x), 4, 7, 14 and 28 days. By plotting these test results in chronological order, Figure 4.5 is obtained, in which the two measurements at 3 days are averaged. This suggests that the strength development of mixes 2 and 4 is about equal. The same appears to hold for mixes 1 and 3, albeit that mix 1 seems to deviate from the observed trend after the age of 7 days. However, the measured strength development beyond 7 days involves much uncertainty because few specimens were tested after this age. Nevertheless, prior to 7 days, mixes 1 and 3 manifest an inferior strength development compared to mixes 2 and 4, more specifically a difference (on average over the first 7 days) of about 10%. Post-testing examination revealed that all specimens failed in line with satisfactory failures, that is, all four faces of the specimens showed similar damage, with little damage to the two other faces in contact with the pressure bench (i.e. the post-testing shape of the specimens was quite similar to that of an hourglass). In that respect, the test results are thus deemed valid.

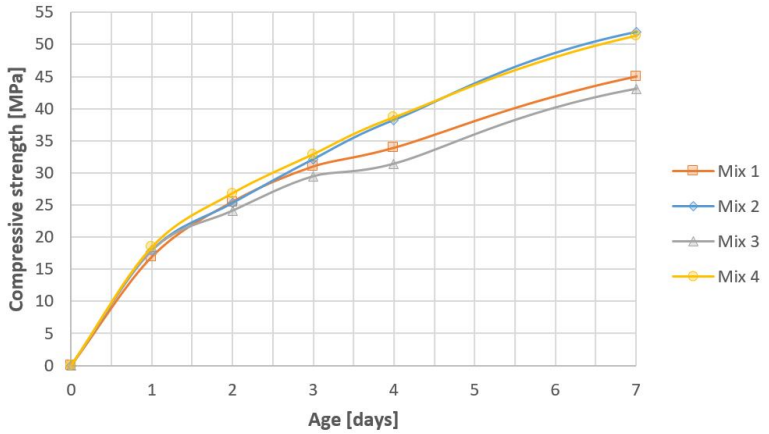

(a) One week.

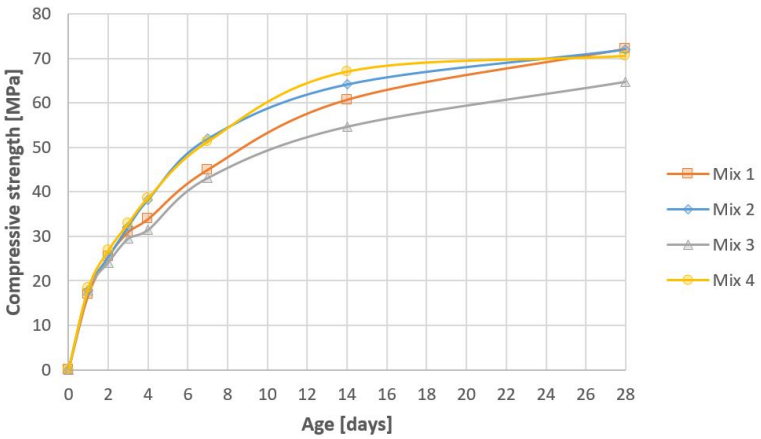

(b) Four weeks.

Figure 4.5: Strength development test results.

Age	*Compressive strength (MPa)*			
	Mix 1	*Mix 2*	*Mix 3*	*Mix 4*
	First stage batches			
3 days	32.9	32.8	31.4	34.8
7 days	45.0	52.0	43.1	51.3
14 days	60.8	64.2	54.6	67.1
28 days	72.2	72.0	64.7	70.6
	Second stage batches			
1 days	16.9	17.9	18.0	18.4
2 days	25.5	25.3	24.1	26.8
3 days	29.1	31.5	27.5	29.8
4 days	33.9	38.2	31.4	38.6

Table 4.2: Strength development test results.

To facilitate implementation of the test results in the cracking calculations, the strength development of each mixture is modelled. This is done by curve fitting; the process of constructing a curve that best fits a series of data. The shape of the fitted curves matches the strength development relation described in the NEN-EN 1992-1-1 and is expressed by Equation 4.3, where $f_{cm,cube}(t)$ is the mean cube compressive strength at age t [31]. Coefficient A corresponds to the mean cube compressive strength at 28 days and is determined individually for each concrete mixture using the method of least squares. Coefficient B is determined collectively for all mixtures using the method of least squares. It must be stressed that the measured compressive strengths at the ages of 14 and 28 days are not included in curve fitting. The reasoning for this is twofold. First, as will become apparent in later stages of this thesis, the strength development after the age of 7 days is less important to the early-age cracking behaviour. Second, as previously mentioned, the measured strength development beyond 7 days involves much uncertainty which may therefore also adversely affect the accuracy of the modelled strength development up to 7 days (when included in curve fitting). The modelled strength development is displayed in Figure 4.6 and the coefficients and relative errors belonging to these fitted curves are specified in Table 4.3. Between the strength development of mixes 1 and 3 on the one hand, and mixes 2 and 4 on the other, the fitted curves show, naturally, a similar correlation as the test results. The relative error R^2 mentioned here is the square of the deviation of the fitted curve with respect to a single measurement. As for the total R^2, the deviations of all measurements are summed, while the mean R^2 refers to the average of the deviations of all measurements.

$$f_{cm,cube}(t) = A \cdot \exp\left[B \cdot \left(1 - \left(\frac{28}{t}\right)^{0.5}\right)\right] \tag{4.3}$$

	Mix 1	*Mix 2*	*Mix 3*	*Mix 4*	*Average*
Coefficient A (MPa)	56	61	54	62	58
Coefficient B	0.29	0.29	0.29	0.29	0.29
Total R^2	0.021	0.032	0.058	0.036	0.034
Mean R^2	0.004	0.005	0.010	0.005	0.006

Table 4.3: Coefficients and relative errors belonging to the fitted curves of Equation 4.3.

The strength development of each mixture is also modelled as a function of the weighted maturity rather than age; an approach that is elaborated in the literature study. This is done by following the same process as above (i.e. curve fitting of the measured compressive strengths at the ages up to 7 days). For these calibration curves that represent the modelled strength development, however, reference is made to Appendix B.

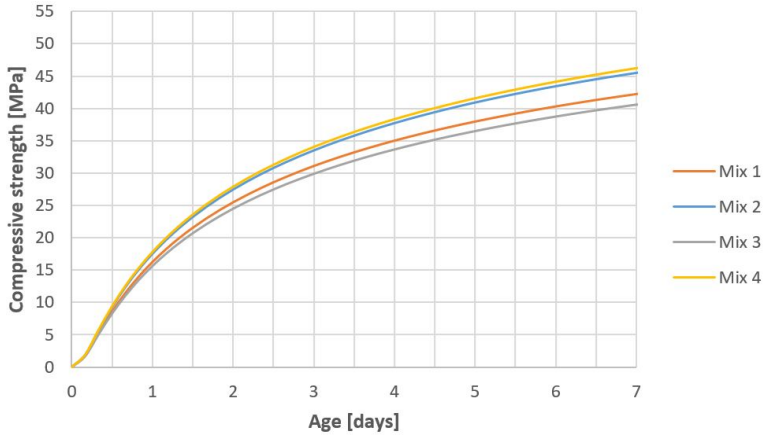

(a) One week.

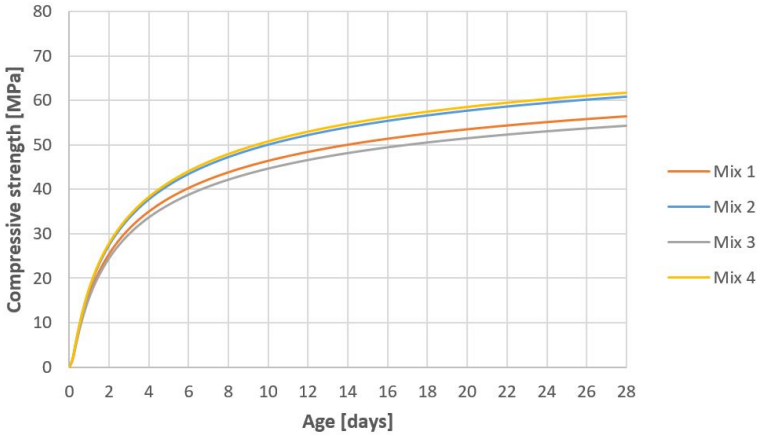

(b) Four weeks.

Figure 4.6: Strength development curve fitted.

4.3.3 Autogenous shrinkage

Autogenous shrinkage was measured for three months, the results of which are presented in Figure 4.7, in which each mixture is represented by the average of six measuring devices divided over three specimens, while Figure 4.8 illustrates the test results of each specimen (i.e. the average of two measuring devices). These indicate that mix 2 exhibits the most autogenous shrinkage, followed by mix 1 and then mix 4, with mix 3 demonstrating the least autogenous shrinkage. The difference (on average over three months) between mix 2 and 3 is about 35%, while mixes 1 and 4 only differ about 15% and 20% from mix 2, respectively. Furthermore, the autogenous shrinkage of mixes 1 and 3 appears to flatten more strongly, while the autogenous shrinkage of mixes 2 and 4 seems to progress more gradually. Weighing revealed that the specimens lost less than 1 gram of weight in the first 7 days, emphasizing that the bitumen foil prevented drying. In that respect, the test results are thus deemed valid. However, some inconsistencies were noted during testing, those being:

- One measuring device on S3.2 (i.e. specimen 2 of mix 3) suddenly started to record significant elongation halfway through the test.
- One measuring device on S3.3 initially did not record any shortening, but did so after it was reset three days into the test.
- One measuring device on S3.1 and one on S4.1 did not record any shortening at all, not even after these were reset.

The majority of these inconsistencies can likely be attributed to faulty measuring devices, since their recordings completely deviate from the observed trend. Therefore, the recordings of the faulty measuring devices on S3.1, S3.2 and S4.1 are not included in the test results. The recordings of the measuring device on S3.3 that was successfully reset are taken into account, assuming that the shortening in the three days before the reset equals that recorded by the other measuring device on the same specimen. Because less genuine recordings are available, it must be noted that the measured autogenous shrinkage of mix 3 in particular involves more uncertainty. Moreover, the substantial deviation of mix 3 from the observed trend should be questioned, but this will be addressed later on in the analysis.

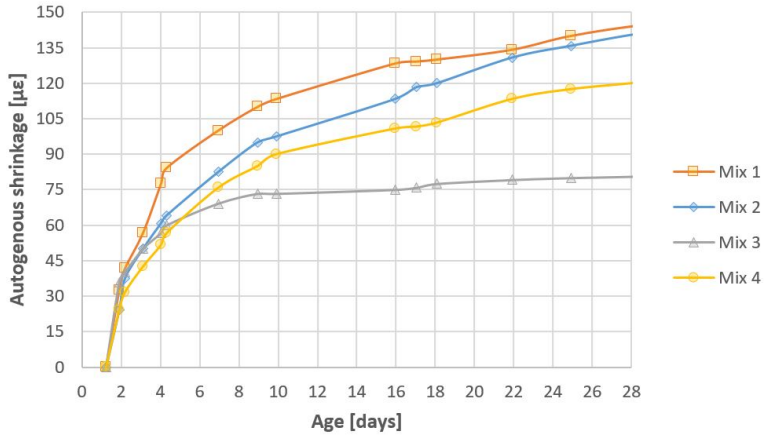

(a) One month.

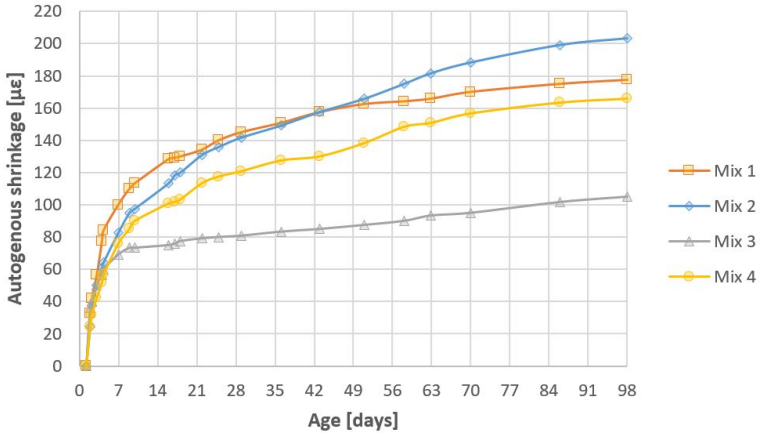

(b) Three months.

Figure 4.7: Autogenous shrinkage test results.

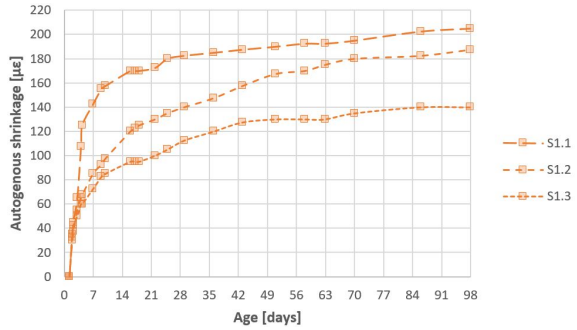

(a) Mix 1.

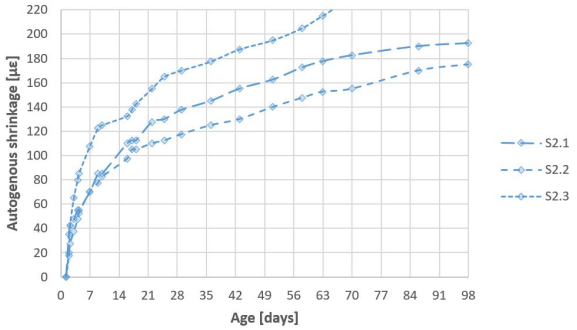

(b) Mix 2.

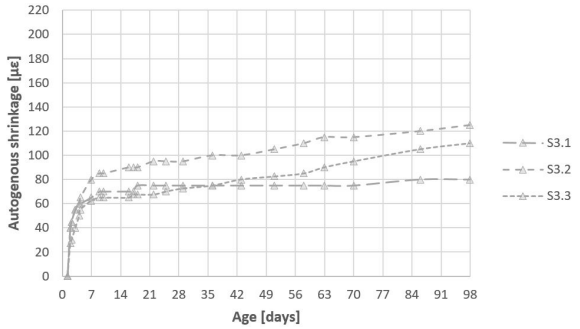

(c) Mix 3.

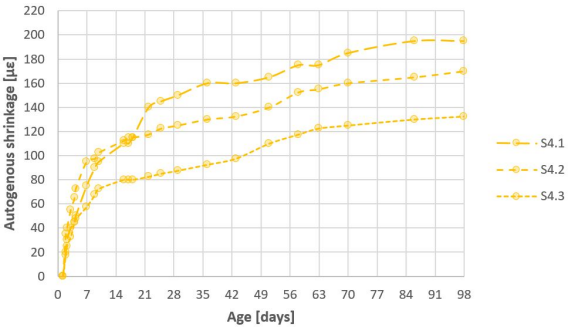

(d) Mix 4.

Figure 4.8: Autogenous shrinkage test results per specimen.

To facilitate implementation of the test results in the cracking calculations, the autogenous shrinkage of each mixture is modelled by curve fitting. The shape of the fitted curves matches the autogenous shrinkage relation described in the NEN-EN 1992-1-1 and is expressed by Equation 4.4, where $\varepsilon_{cam}(t)$ is the mean autogenous shrinkage strain at age t and t_1 the age reckoned from the beginning of measuring. It must be noted that this thus slightly differs from the NEN-EN 1992-1-1, which describes autogenous shrinkage strain proportional to t rather than t_1 [31]. Coefficient A corresponds to the mean ultimate autogenous shrinkage strain and is determined individually for each concrete mixture using the method of least squares. Coefficient B is determined collectively for all mixtures using the method of least squares. It is worth noting that the measured autogenous shrinkage at any age is included in curve fitting. Because the time between reading of the measuring devices progressively increased as the recorded shortening decreased, the accuracy of the modelled autogenous shrinkage is greater in the beginning. However, this is preferred because the autogenous shrinkage after the age of 7 days is less important to the early-age cracking behaviour. The modelled autogenous shrinkage is shown in Figure 4.9 and the coefficients and relative errors belonging to these fitted curves are stated in Table 4.4. Naturally, the fitted curves indicate the same sequence of mixtures as the test results, when it comes to the magnitude of autogenous shrinkage.

$$\varepsilon_{cam}(t) = A \cdot \left[1 - \exp\left(-B \cdot {t_1}^{0.5}\right)\right] \tag{4.4}$$

	Mix 1	*Mix 2*	*Mix 3*	*Mix 4*	*Average*
Coefficient A ($\mu\varepsilon$)	151	178	114	142	146
Coefficient B	0.22	0.22	0.22	0.22	0.22
Total R^2	20.469	8.614	7.980	12.335	12.349
Mean R^2	0.155	0.065	0.091	0.112	0.106

Table 4.4: Coefficients and relative errors belonging to the fitted curves of Equation 4.4.

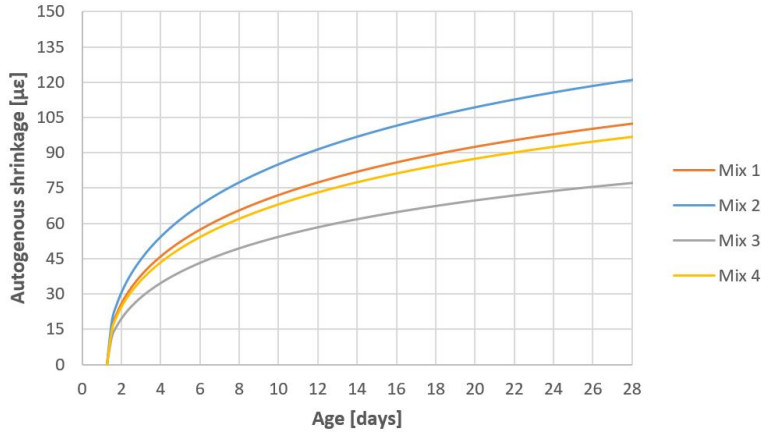

(a) One month.

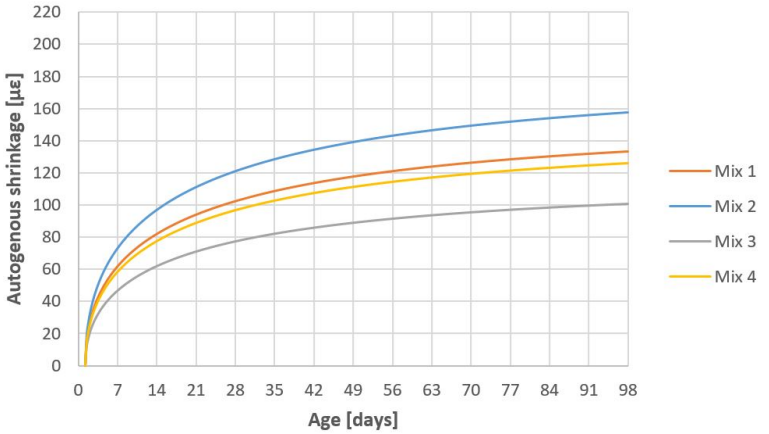

(b) Three months.

Figure 4.9: Autogenous shrinkage curve fitted.

5 Probability of cracking

For the demonstrator project to succeed, the imposed deformations must ensure that cracking of the side walls of the reservoir occurs at an early-age. Therefore, it is determined in advance how likely it is that the imposed deformations can actually cause this to happen. This chapter is dedicated to identifying the probability of cracking and to examine all aspects of influence, which include environmental conditions, structural dimensioning and construction practice, in addition to the aforementioned mixture composition.

5.1 Strategy

The probability that early-age cracking of the side walls of the reservoir occurs as a result of imposed deformations has been determined analytically. Two methods from literature have been consulted for this, varying in which quality they consider, namely stress or strain, and the way they account for relaxation. Their precise differences will be explained in the course of this chapter in light of application. Nevertheless, both methods demand that the strength development (i.e. resistance) and imposed deformations (i.e. actions) are to be quantified first. Although the test results provided in the previous chapter constitute a considerable portion of the input for this, the temperature development and distribution within the side walls also plays a major role in both. The temperature development and distribution is in turn strongly affected by the heat of hydration; one of the properties that, due to limited resources, was not determined experimentally and is therefore derived from literature. Hence, heat of hydration is addressed first in an individual section, followed by the temperature development and distribution. Subsequently, the strength development corrected for thermal effects and the imposed deformations including degree of restraint and relaxation are highlighted. Thereupon, the probability of cracking is determined, based on two different methods, in terms of the likelihood that the actions will exceed the resistance.

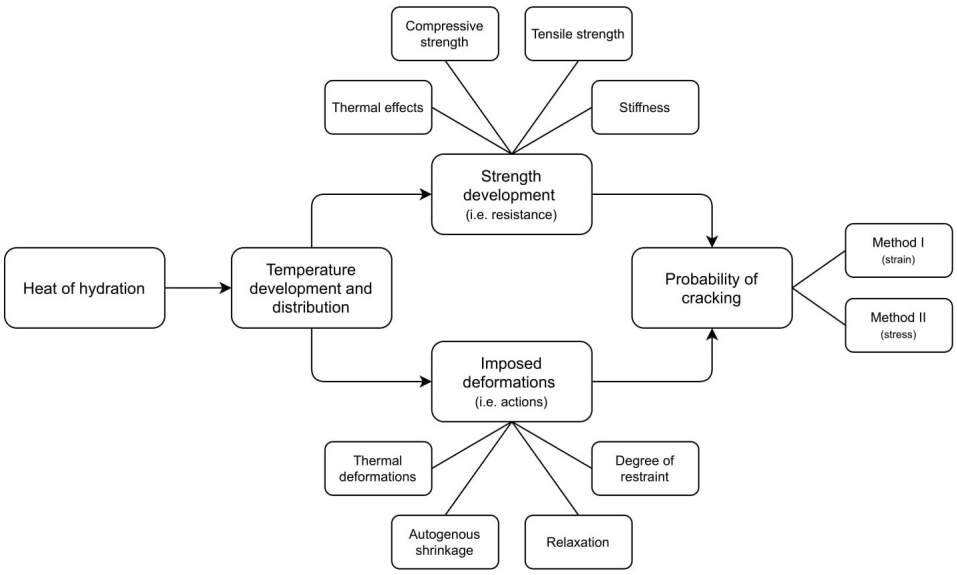

Figure 5.1: Strategy outline for determination of probability of cracking.

It must be emphasized that the probability of cracking is fundamentally different from the degree of cracking, which is treated in the next chapter. The probability of cracking relates to the likelihood that cracks arise (as a result of imposed deformations), whereas the degree of cracking refers to the width (and length) that the cracks will have when they emerge, as well as the number of cracks that occurs. From the perspective of this thesis, a high probability of cracking is desirable and the degree of cracking would be best if it matched the proposed crack pattern. Although the probability of cracking is a crucial attribute in itself, this chapter is also a prelude to the degree of cracking, because many aspects involving the probability of cracking, in particular the strength development corrected for thermal effects, also affect the degree of cracking.

5.2 Heat of hydration

The heat of hydration is modelled founded on work by Bamforth presented in the Ciria C660 [32]. This provides a model with reasonable accuracy for the adiabatic heat production of concretes consisting of a variety of combinations of Portland cement with fly ash or blastfurnace slag, which in turn is based on curve fitting trough data collected from a substantial test programme. Although this test programme did not include concrete mixtures to which healing agent was added, it is believed that the model is also applicable to these mixtures. This assumption has been made in virtue of the strength development test results given in the previous chapter. These indicate that there is hardly any difference in strength development, prior to 7 days, between mixes 1 and 3. This suggests that the heat of hydration of the mixtures with healing agent is likely to be similar, as the concrete strength at a certain maturity is proportional to the heat output so far. However, following the same reasoning, the model is likely to underestimate the heat of hydration of the mixtures with filler, given the fact that the test results demonstrate a superior strength development of mixes 2 and 4. If this is the case, the anticipated probability of cracking may not truly apply to these mixtures. But then again, it is likely to only be an underestimation, since a greater heat output increases the probability of cracking.

5.2.1 Adiabatic heat production

According to Bamforth, the shape of the adiabatic heat curve is best expressed by Equation 5.1, which consists of two components given equal weighting, being $Q_1(t)$ and $Q_2(t)$ [32]. Adding up these components gives the heat generated $Q_{ad}(t)$ at age t under adiabatic conditions. The ultimate heat generation Q_{ult} is stated in Equation 5.2, where Q_{41} refers to the heat generated at 41 hours. Needless to say, both depend on the type of cement used, or more specifically the share of fly ash or blastfurnace slag relative to Portland cement. However, since the binder of the concrete mixtures does not contain any fly ash, the expressions for concretes consisting of fly ash have been omitted. For pure Portland cement, Bamforth considers the heat generated at 41 hours to be 338 kJ/kg, allowing for an ultimate heat generation of 365 kJ/kg. In case the share of blastfurnace slag in cement p_{GGBS} is increased, the ultimate heat generation decreases, as well as the heat production rate (i.e. quotient Q_{41}/Q_{ult}). For the binder consisting of about 52% slag, the heat generated at 41 hours equals 259 kJ/kg and the ultimate heat generation corresponds to 340 kJ/kg.

$$\begin{aligned} Q_{ad}(t) &= Q_1(t) + Q_2(t) \\ Q_1(t) &= \frac{Q_{ult}}{2} \cdot \left[1 - \exp\left(-B \cdot t^C\right)\right] \\ Q_2(t) &= \frac{Q_{ult}}{2} \cdot \frac{t-A}{t-A+D} \end{aligned} \tag{5.1}$$

$$\begin{aligned} Q_{ult} &= \frac{Q_{41}}{0.003 \cdot {p_{GGBS}}^2 - 0.47 \cdot p_{GGBS} + 0.925} \\ Q_{41} &= 338 - 75 \cdot \left(\frac{p_{GGBS}}{1 - p_{GGBS}}\right)^{0.6} \end{aligned} \tag{5.2}$$

It should be pointed out that Equation 5.2 is a little different from the expression by Bamforth. A minor adjustment has been made to the expression for Q_{41} (i.e. the effect due to the share of slag is enhanced by increasing the multiplier in front of the parentheses from 60 to 75), as it is the author's believe that the model overestimates the adiabatic heat production of concretes containing a high share of blastfurnace slag when compared, for example, to the values of common cement types in the Netherlands provided in Table 2.4. This adjustment results in slightly lower values for Q_{ult}, which is preferable because it leads to a probability of cracking that is somewhat more conservative rather than overly optimistic. The other expressions, including those for the coefficients given in Equation 5.3, have not been altered.

$$
\begin{aligned}
A &= 3.5 + 1.25 \cdot p_{GGBS} \\
B &= 0.012 \\
C &= 1.6 - 0.72 \cdot p_{GGBS} - 0.003 \cdot {p_{GGBS}}^2 \\
D &= 6.2 + 8.48 \cdot p_{GGBS} - 0.04 \cdot {p_{GGBS}}^2
\end{aligned}
\tag{5.3}
$$

The model also corrects the adiabatic heat production to take account of the mix temperature T_{mix}. This is done by replacing the age t in Equation 5.1 for an equivalent age t_T expressed by Equation 5.4, known as the Rastrup function, where T_{ref} is a reference temperature of 20 °C [32]. It is recognized that the Rastrup function has its limitations in that it does not consider the temperature sensitivity of the cement type. Therefore, an alternative expression for the equivalent age has been applied, namely Equation 5.5, referred to in this thesis as the Arrhenius function, where R_g is the universal gas constant that equals 8.31 J/mol·K [23]. This expression takes into account the temperature sensitivity of the cement type by means of its apparent activation energy E_A and demands the mix and reference temperature to be stated in Kelvin. The activation energy applied in this case is addressed later on (see Table 5.1), but for now its worth mentioning that both expressions give the same results if the activation energy of the cement type corresponds to approximately 40 kJ/mol. All things considered, the model reveals the adiabatic heat curve displayed in Figure 5.2 for a concrete mixture analogous to mix 1 at a temperature of 16 °C. The philosophy behind this mix temperature, which stems from the environmental conditions, is discussed in the subsequent section.

$$
t_T = t \cdot 2^{\left(\frac{T_{mix} - T_{ref}}{12}\right)} \tag{5.4}
$$

$$
t_T = t \cdot \exp\left[\frac{E_A}{R_g} \cdot \left(\frac{1}{T_{ref}} - \frac{1}{T_{mix}}\right)\right] \tag{5.5}
$$

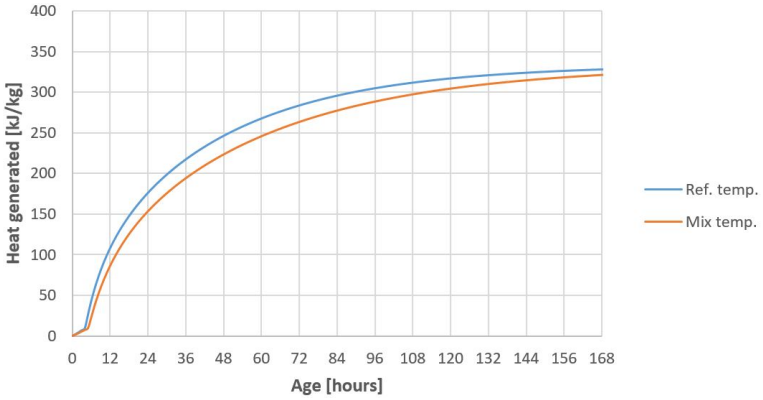

Figure 5.2: Adiabatic heat production at reference and mix temperature.

5.2.2 Adiabatic temperature rise

The heat generated $Q_{ad}(t)$ can be converted to a temperature rise $\Delta T_{ad}(t)$ by means of Equation 5.6, where c_c and ρ_c are the specific heat and mass (i.e. 2400 kg/m^3), respectively [27, 33]. Adding this up to the mix temperature gives the concrete temperature $T_{ad}(t)$ at age t under adiabatic conditions. At the cement content C_c of 418 kg/m^3, this results in the adiabatic temperature curve displayed in Figure 5.3. The applied specific heat of 1.01 kJ/kg·K corresponds to an early-age value, whose estimation is included in Appendix C.

$$
\begin{aligned}
T_{ad}(t) &= T_{mix} + \Delta T_{ad}(t) \\
\Delta T_{ad}(t) &= \frac{C_c \cdot Q_{ad}(t)}{\rho_c \cdot c_c}
\end{aligned}
\tag{5.6}
$$

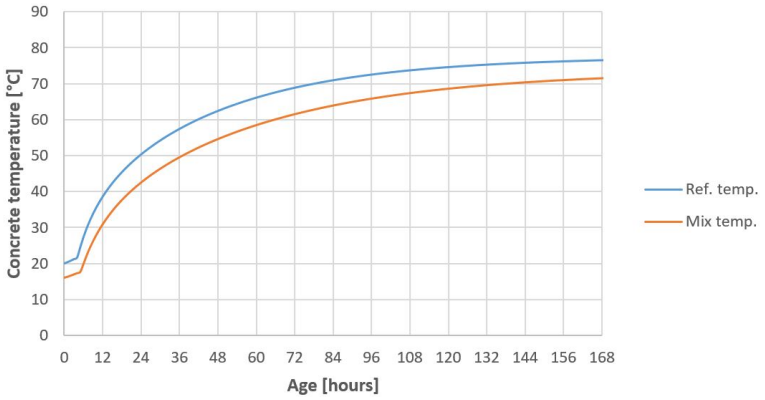

Figure 5.3: Adiabatic temperature rise at reference and mix temperature.

5.3 Temperature development and distribution

The temperature development and distribution within the side walls has been computed using the partial differential equation (PDE) of Fourier. Correspondingly, the three-dimensional heat transfer in a structure is described by Equation 5.7, where $T(t,x,y,z)$ is the concrete temperature at age t and at the coordinates x, y and z that indicate the position within the structure [27, 33]. The last component of the PDE denotes the source of heating, in this case the heat generated $Q(t,x,y,z)$ by cement hydration. The PDE can be solved with a numerical model, provided that the boundary conditions are known.

$$\frac{\partial T}{\partial t} = a_c \cdot \left[\frac{\partial^2 T}{\partial x^2} + \frac{\partial^2 T}{\partial y^2} + \frac{\partial^2 T}{\partial z^2} \right] + \frac{C_c}{\rho_c \cdot c_c} \cdot \frac{\mathrm{d}Q}{\mathrm{d}t} \tag{5.7}$$

For structures where the x and y dimensions are considerably larger than the z dimension (e.g. floors, slabs and walls), barely any heat is transferred along the x and y directions. In this event, the simplified PDE of Equation 5.8 is sufficient, since the heat transfer is approximately one-dimensional (i.e. only along the z direction). This also applies to the side walls of the reservoir, where heat is transferred primarily along the depth of the wall, except near the top and ends of the wall, as well as near the joint between the wall and the floor. Nevertheless, the simplified PDE provides reasonable accuracy for most of the wall. Moreover, solving this is less complex and demands less computing power, allowing the author to set up the numerical model himself, which in turn offers more flexibility with regard to the cracking calculations. Therefore, the simplified PDE has been used to compute the temperature development and distribution within the side walls.

$$\frac{\partial T}{\partial t} = a_c \cdot \frac{\partial^2 T}{\partial z^2} + \frac{C_c}{\rho_c \cdot c_c} \cdot \frac{\mathrm{d}Q}{\mathrm{d}t} \tag{5.8}$$

As mentioned in the literature study, heat production is significantly affected by the temperature at which hydration takes place. But then again, since the temperature itself depends on the produced heat, a distinct relation exists between the concrete temperature and the heat generated. The dependence of the rate of chemical reactions on the actual temperature can generally be described by the well-known Arrhenius equation. In view of this, the Arrhenius equation can also be used to express the relation between the heat production rate $\mathrm{d}Q/\mathrm{d}t$ and the corresponding heat production rate $\mathrm{d}Q_{ad}/\mathrm{d}t$ under adiabatic conditions at the same degree of hydration [27, 33]. Thus, an equivalent age t_{eq} can be identified that reflects the the same degree of hydration under adiabatic conditions, in the sense that $Q_{ad}(t_{eq}) = Q(t)$. However, as illustrated in Figure 5.4, the concrete temperatures $T_{ad}(t_{eq})$ and $T(t)$ are not equal due to the heat transfer that takes place. Having said that, the modified Arrhenius equation that describes the relation between the heat production rate and the corresponding one under adiabatic conditions, which has been established in the previous section, is specified by Equation 5.9.

$$\frac{\mathrm{d}Q}{\mathrm{d}t} = \exp\left[-\frac{E_A}{R_g} \cdot \frac{T_{ad}(t_{eq}) - T(t)}{T_{ad}(t_{eq}) \cdot T(t)} \right] \cdot \left. \frac{\mathrm{d}Q_{ad}}{\mathrm{d}t} \right|_{t=t_{eq}} \tag{5.9}$$

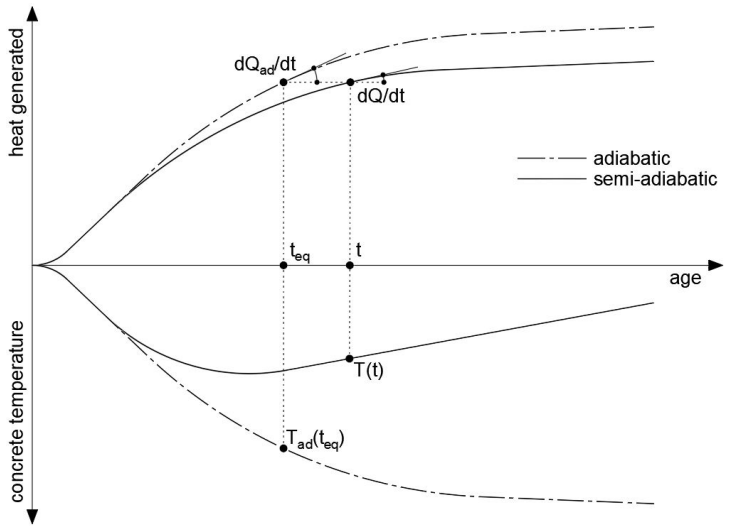

Figure 5.4: Schematic representation of adiabatic and semi-adiabatic heat production and temperature rise, adapted from [27, 33].

Another important component of the PDE is the thermal diffusivity a_c, which is defined by Equation 5.10. Although it truly depends on the degree of hydration, a constant value for the thermal diffusivity has been adopted in the computation of the temperature development and distribution within the side walls. To ensure reasonable accuracy, the thermal diffusivity of 0.0037 m^2/h corresponds to an early-age value. This follows from the applied thermal conductivity λ_c of 2.51 W/m·K, likewise an early-age value, whose estimation is given in Appendix C.

$$a_c = \frac{\lambda_c}{\rho_c \cdot c_c} \tag{5.10}$$

The remainder of this section is devoted to the boundary conditions that regulate the heat dissipation to the environment and the results of the numerical model, that is, the computed temperature development and distribution within the side walls. The numerical model itself based on the finite difference method, which comprises the solution to the PDE, is explained in Appendix D.

5.3.1 Boundary conditions

The boundary conditions consist of the ambient temperature, wind speed and formwork conditions, the latter two of which determine the thermal surface conductance (i.e. rate of heat dissipation). In terms of the environmental conditions, it is assumed that the reservoir will be constructed in late spring or early autumn, during which the mean minimum and maximum ambient temperature in the Netherlands coincide to 8 and 16 °C, respectively (source: KNMI, De Bilt). Hence, the mean ambient temperature and diurnal temperature variation match 12 and 8 °C, respectively. The temperature of the aggregates added to the concrete mixtures is likely to reflect the mean ambient temperature, as aggregates are generally stored outdoors. Because the aggregates occupy by far the largest relative volume of the mixtures and also contain the greatest specific heat, the mix temperature is taken as the temperature of the aggregates (i.e. mean ambient temperature) plus 4 °C for the energy generated by mixing. This results in the aforementioned mix temperature of 16 °C.

With regard to the formwork conditions, it is assumed that the reservoir is constructed using plywood with a thickness of 25 mm. For this type of formwork, the thermal surface conductance matches G_1 of Equation 5.11, where v_w is the mean wind speed [32]. Since the mean wind speed in the Netherlands in late spring and early autumn corresponds to approximately 3.5 m/s (source: KNMI, De Bilt), the initial thermal surface conductance equals 4.4 W/m^2·K. Once the formwork is removed, which is assumed to happen 24 hours after casting, the thermal surface conductance conforms to G_2 [32]. Correspondingly, the consequent thermal surface conductance equals 21.6 W/m^2·K. From this it is clear then, that formwork acts as a notable insulator, predominantly by shielding concrete from the wind. Nevertheless, because the boundary conditions allow a certain extent of heat dissipation to the environment, one speaks of semi-adiabatic conditions.

$$\begin{aligned} G_1 &= 3.7 + 0.2 \cdot v_w \\ G_2 &= 5.6 + 4.0 \cdot v_w \end{aligned} \tag{5.11}$$

5.3.2 Semi-adiabatic temperature rise

The results of the numerical model, in terms of the computed core and surface temperature development of the side walls, are shown in Figure 5.5. This illustrates that the peak core temperature corresponds to 34 °C, while the peak surface temperature is limited to 30 °C. The peak surface temperature is reached after 24 hours when the formwork is removed, while the peak core temperature occurs a little later at 26 hours. The continuation of the cracking calculations is founded on the computed mean temperature development of the side walls, which, in view of the parabolic nature of the non-uniform temperature distribution, coincides with the temperature development at a depth equal to one-third the wall thickness. This mean temperature development is displayed in Figure 5.6, which also contains the development of the differential temperature (i.e. the difference between core and surface temperature). This demonstrates that the peak mean temperature of 33 °C also takes place at the time of formwork removal. The temperature distribution along the depth of the side walls when the mean peak temperature occurs, as well as when the peak differential temperature of 10 °C arises (which occurs at the same time as the peak core temperature), is provided in Figure 5.7.

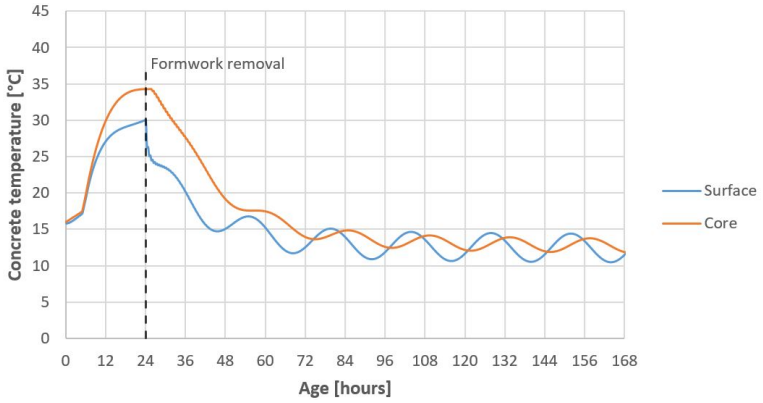

Figure 5.5: Core and surface temperature rise of side walls.

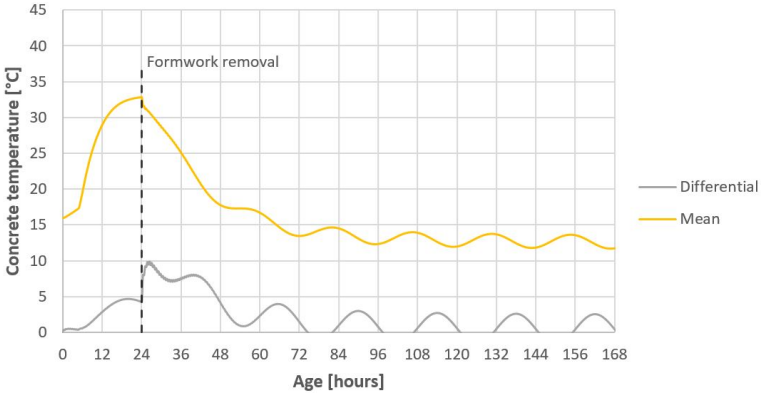

Figure 5.6: Mean and differential temperature rise of side walls.

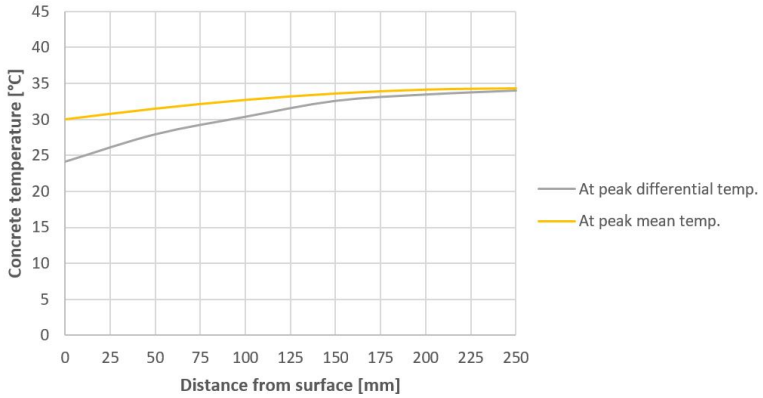

Figure 5.7: Temperature distribution at peak mean and differential temperature of side walls.

5.4 Strength development

The strength development for the cracking calculations is based on the average of the modelled strength development of all four concrete mixtures. Although the strength development was determined experimentally, it must be corrected for thermal effects. In other words, the temperature development as outlined in the preceding section does not match the reference temperature of 20 °C (i.e. storage temperature of specimens) to which the the strength development test results given in the previous chapter relate. To correct the strength development for thermal effects, two different concepts have been tried, namely the equivalent age concept according to the Arrhenius function and the weighted maturity concept known as the De Vree method. These two concepts were adopted because they are specific to a concrete mixture, that is, they take into account the cement type. Both concepts are highlighted separately in the following sections, whereupon the development of the stiffness and tensile strength have been derived from that of the compressive strength.

5.4.1 Equivalent age concept

This concept replaces the age t in the reference strength development of Equation 4.3 by an equivalent age t_T defined by Equation 5.12, where $T(\Delta t)$ is the concrete temperature during age increment Δt [23]. This results in the corrected strength development displayed in Figure 5.8. When compared to the reference strength development, it is clear that the large temperature rise significantly increases the concrete strength in the first few days, after which it starts to fall behind when the concrete temperature has taken on the ambient temperature. The apparent activation energy E_A has been estimated from the activation energies of the individual cement types and their relative proportions in the binder of the concrete mixtures. This estimation is presented in Table 5.1, in which the activation energies of the individual cement types have been collected from literature [23, 27].

$$t_T = \sum \exp\left[\frac{E_A}{R_g} \cdot \left(\frac{1}{T_{ref}} - \frac{1}{T(\Delta t)}\right)\right] \cdot \Delta t \tag{5.12}$$

Cement	*Proportion* (kg/m^3)	*Activation energy* ($kJ/mol{\cdot}K$)
CEM I 52.5R	109	33.5
CEM III/B 42.5N	309	43.5
Total	**418**	**40.9**

Table 5.1: Estimation of activation energy based on binder composition.

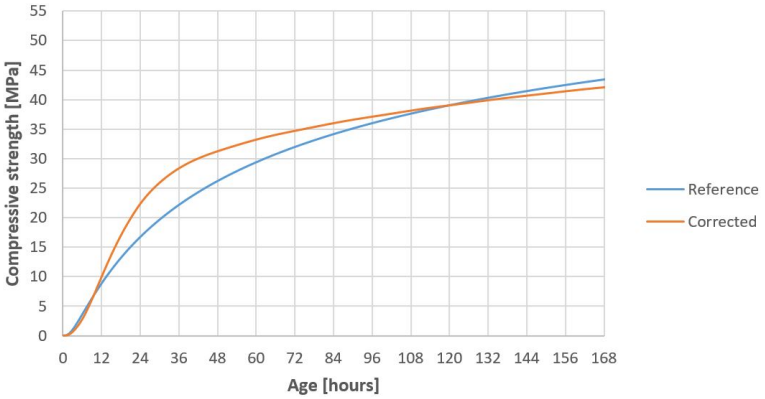

Figure 5.8: Strength development according to equivalent age concept.

5.4.2 Weighted maturity concept

This concept does not consider concrete strength as a function of age but of weighted maturity, which is defined by Equation 2.17. This requires the C-value, which has been estimated from the C-values of the individual cement types and their relative proportions in the binder of the concrete mixtures. This estimation is presented in Table 5.2, in which the C-values of the individual cement types have been collected from literature [18, 23]. The relation between the weighted maturity and concrete strength is described by the calibration curve of Equation B.1 in Appendix B. Consequently, both the reference and corrected strength development given in Figure 5.9 have been determined. When compared to the results of the equivalent age concept, it is clear that the differences between the concepts are insignificant. Hence, purely for arbitrary reasons, the continuation of the cracking calculations is founded on the strength development according to the equivalent age concept.

Cement	*Proportion* (kg/m^3)	*C-value*
CEM I 52.5R	109	1.20
CEM III/B 42.5N	309	1.55
Total	**418**	**1.46**

Table 5.2: Estimation of C-value based on binder composition.

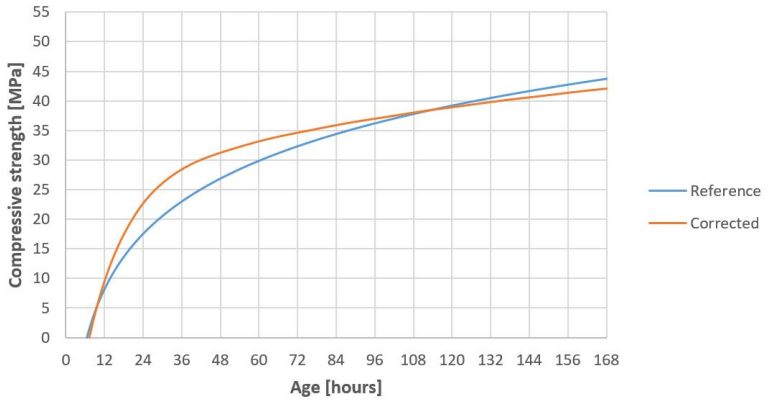

Figure 5.9: Strength development according to weighted maturity concept.

5.4.3 Stiffness and tensile strength

So far, the strength development has always been expressed through the compressive strength. However, because cracking is considered, the tensile strength is of particular importance. In addition, stiffness also plays a major role in the early-age cracking behaviour. Therefore, the development of the stiffness and tensile strength, which are provided in Figure 5.10, have been derived from the development of the compressive strength. The development of the stiffness is represented by Equation 5.13, where $E_{cm}(t)$ is the elastic modulus at age t, E_{cm} the elastic modulus at 28 days in line with Equation 2.14 and n a coefficient that equals 0.3. The development of the tensile strength is defined by Equation 5.14, where $f_{ctm}(t)$ is the mean tensile strength at age t and f_{ctm} the mean tensile strength at 28 days according to Equation 2.18. All four expressions emanate from the NEN-EN 1992-1-1, which also describes that $f_{cm} = f_{ck}+8$ and $f_{cm,cube} = f_{ck,cube}+8$ [31]. Furthermore, relying on Figure 2.20 and data given in the NEN-EN 1992-1-1, it has been assumed that $f_{ck,cube}/f_{ck} = 1.2$. Naturally, coefficient B and the mean cube compressive strength at 28 days, which corresponds to coefficient A, originate from the modelled strength development (see Table 4.3).

$$E_{cm}(t) = E_{cm} \cdot \left(\exp\left[B \cdot \left(1 - \left(\frac{28}{t_T} \right)^{0.5} \right) \right] \right)^n \tag{5.13}$$

$$f_{ctm}(t) = f_{ctm} \cdot \exp\left[B \cdot \left(1 - \left(\frac{28}{t_T} \right)^{0.5} \right) \right] \tag{5.14}$$

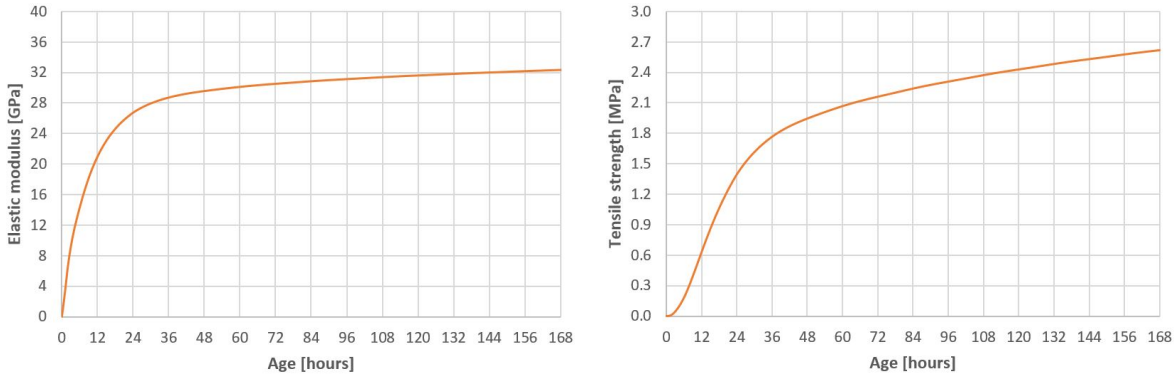

Figure 5.10: Development of stiffness and tensile strength.

5.5 Imposed deformations

Now that the strength development (i.e. resistance) has been quantified, it is the turn of the imposed deformations (i.e. actions). However, before going into detail on the imposed deformations, it is appropriate to describe the two methods with which the probability of cracking is determined, as they differ in which quality they consider, namely stress or strain, and the way they account for relaxation. The first method (I) is rather straightforward and comes from the Ciria C660 [32]. It compares the tensile strain capacity to the restrained shrinkage strain according to Equation 5.15, where $R(t)$ is the degree of restraint at age t. In doing so, it disregards very early-age thermal expansion due to the temperature rise, as relaxation is assumed to cause it to diminish to zero. Hence, only the temperature drop $\Delta T(t)$ that occurs after the peak temperature T_{max} is considered. Further relaxation of the restrained shrinkage strain $\varepsilon_r(t)$ is accounted for by means of the coefficient for creep effects K_1, which is a constant.

$$\begin{aligned} \varepsilon_r(t) &= K_1 \cdot R(t) \cdot [\alpha_c \cdot \Delta T(t) + \varepsilon_{cam}(t)] \\ \Delta T(t) &= T_{max} - T(t) \end{aligned} \tag{5.15}$$

The second method (II) is more complex, yet generally more accepted. It compares the effective tensile strength to the mean concrete stress which is determined in line with the superposition principle. This superposition principle is schematized in Figure 5.11, in which the gray area represents the mean concrete stress that remains after relaxation (i.e. after deduction of the white area). As follows from Equation 5.16, the mean concrete stress $\sigma_{cm}(t)$ at age t is found by summation of the stress increments $\Delta\sigma_{cm}(t,t_0)$, where t_0 denotes the age at application of the stress increment, that is, the middle of age increment Δt [27]. These stress increments are defined by the product of stiffness times degree of restraint and the change in imposed deformations over the established age increment. The relaxation coefficient $\psi(t,t_0)$ describes the reduction of concrete stress with age and is specific to a stress increment, as it depends on the age of application.

$$\begin{aligned} \sigma_{cm}(t) &= \sum \Delta\sigma_{cm}(t,t_0) \\ \Delta\sigma_{cm}(t,t_0) &= R(t_0) \cdot E_{cm}(t_0) \cdot \psi(t,t_0) \cdot [\Delta T(t_0) \cdot \alpha_c + \Delta\varepsilon_{cam}(t_0)] \end{aligned} \tag{5.16}$$

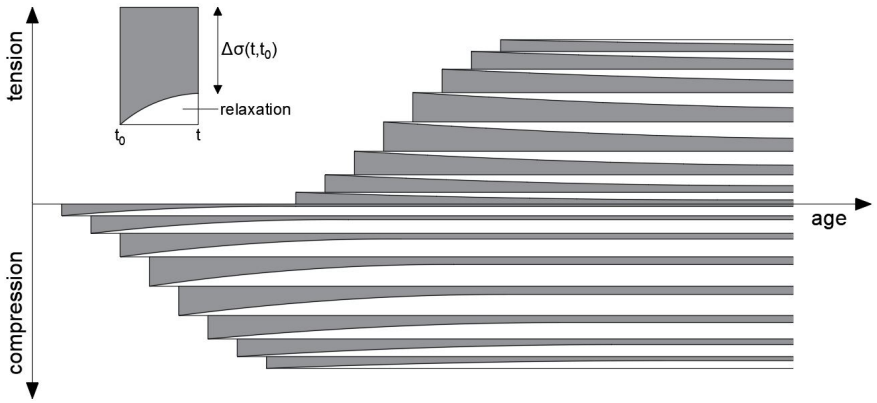

Figure 5.11: Schematic representation of superposition principle, adapted from [27].

As is evident from the method descriptions, the imposed deformations considered include thermal deformations and autogenous shrinkage, the latter being taken as the average of the modelled autogenous shrinkage of all four concrete mixtures. Drying shrinkage has been omitted because it occurs in the long-term. The thermal deformations are governed by the coefficient of thermal expansion α_c, which truly depends on the degree of hydration. However, in the absence of the expansion coefficients of the individual ingredients incorporated in the concrete mixtures or experimental determination of the CTE, a constant value has been adopted. The applied CTE of 11.4 $\mu\varepsilon$/K corresponds to the lower limit value according to the Ciria C660 for (saturated) concretes containing coarse aggregates out of flint [32]. By choosing the lower limit value it is tried to ensure reasonable accuracy while remaining somewhat conservative. Moreover, specifically this CTE has been adopted, because the gravel that is predominantly retrieved from river deposits in the Netherlands largely consists of flint [16].

5.5.1 Relaxation

The relaxation of concrete stress with regard to method II is modelled founded on work by Van Breugel, who provides an expression with reasonable accuracy for the relaxation coefficient $\psi(t, t_0)$ at an early-age, which is described by Equation 5.17, where coefficient n equals 0.3 [27, 34]. With the quotient $\alpha(t)/\alpha(t_0)$, the effect of the ongoing hydration between age t and application of the stress increment at age t_0 is taken into account. In this respect, the expression by Van Breugel differs from the one included in the NEN-EN 1992-1-1, which holds for relaxation in the long-term when there is a direct proportionality between relaxation and the applied stress. Figure 5.12 demonstrates the relaxation coefficients of various stress increments as a function of age. These have been established in virtue of the mean progress of hydration that is also shown, whose definition is consistent with that of the mean temperature development, namely the progress of hydration at a depth equal to one-third the wall thickness. The progress of hydration (i.e. degree of hydration) has been derived from the semi-adiabatic heat production, which emanates from the numerical model for heat transfer that is explained in Appendix D. Furthermore, coefficient d, which reflects the cement type ($d = 0.3$ for slow hardening, $d = 0.4$ for rapid hardening), has been taken equal to 0.35.

$$\psi(t, t_0) = \exp\left[1 - \frac{\alpha(t)}{\alpha(t_0)} - 1.34 \cdot wcr^{1.65} \cdot {t_0}^{-d} \cdot (t - t_0)^n \cdot \frac{\alpha(t)}{\alpha(t_0)}\right] \tag{5.17}$$

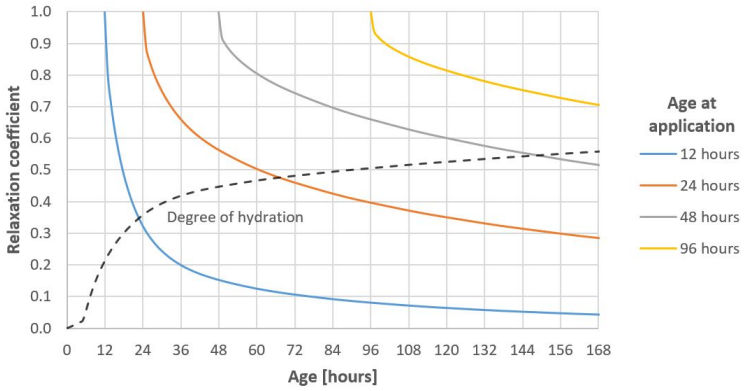

Figure 5.12: Relaxation coefficients of various stress increments.

Figure 5.12 reveals that relaxation causes the very early-age stress increments to diminish to almost zero. The assumption of method I therefore seems appropriate. Relaxation of later stress increments progressively decreases. Method I accounts for relaxation in this stage by means of a constant, the coefficient for creep effects K_1, which equals 0.65 [32]. Although the Ciria C660 does not explain this value, it appears to match the average of the relaxation coefficients for stress increments applied after the peak temperature.

5.5.2 Degree of restraint

An important attribute of both methods is the degree of restraint. The degree of restraint $R(t)$ is, as follows from Equation 5.18, defined as the ratio of the mean concrete stress $\sigma_{cm}(t)$ to the hypothetical stress $\sigma_{fix}(t)$ at total restraint, which is analogous to the ratio of the restrained shrinkage strain $\varepsilon_r(t)$ to the hypothetical strain $\varepsilon_{free}(t)$ at zero restraint. With regard to the early-age cracking behaviour, one can distinguish between internal and external restraint. External restraint occurs when the imposed deformations of a freshly placed structure are resisted by an adjacent previously placed structure acting as confinement. Internal restraint arises when one part of a freshly placed structure expands or contracts differentially to another part of the same structure.

This usually takes place during hydration when the core of a structure reaches a far greater temperature than its surface. However, the side walls of the reservoir are rather thin, resulting in a comparatively low differential temperature (see Figure 5.7). In this case, therefore, external restraint is governing and internal restraint has been neglected.

$$R(t) = \frac{\sigma_{cm}(t)}{\sigma_{fix}(t)} = \frac{\varepsilon_r(t)}{\varepsilon_{free}(t)} \tag{5.18}$$

The external restraint of the side walls is delivered by the floor of the reservoir on which the side walls are cast monolithically. The previously placed floor (already hardened) provides resistance against the imposed deformations of the freshly placed side walls in the manner illustrated in Figure 5.13. Since early-age cracking from this kind of restraint is a common occurrence, considerable research has been conducted into the computation of the degree of restraint in case of such a configuration. As a consequence, the degree of restraint can be computed by means of several methods, varying in complexity and accuracy. A suitable method for the purpose of this thesis has been identified in work by Nilsson [35]. The method suggested by Nilsson is comprehensive, allowing for reasonable accuracy, and offers flexibility with regard to the cracking calculations. The method in its entirety is not provided here, but its basics are described in the following paragraphs for the sake of understanding. The results of implementing the Nilsson method in this case are presented thereafter.

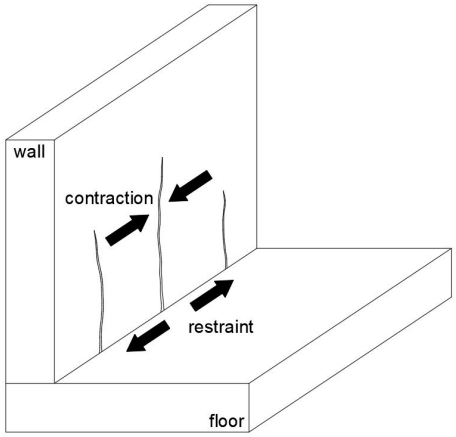

Figure 5.13: Schematic representation of restraint of wall due to adjacent floor.

Theoretical background

The essence of the Nilsson method is based on the assumption of linear strain distribution, which is equivalent to the principle that 'plane sections remain plane' [35]. Pursuant to this, the stress $\sigma(y)$ at height y of a wall shown in Figure 5.14, caused by the internal forces (i.e. axial force N and bending moment M) required to restore the wall to its original restrained position, can be determined according to Equation 5.19, where A_w and I_w are the area and second moment of inertia of the cross-section of the wall, respectively. The internal forces are defined by Equation 5.20, where R_T and R_R represent the external translational and rotational restraint against axial strain ε and curvature κ, respectively.

$$\sigma(y) = \frac{N}{A_w} + \frac{M}{I_w} \cdot (y - y_{cen}) \tag{5.19}$$

$$\begin{aligned} N &= R_T \cdot E_w \cdot A_w \cdot \varepsilon \\ M &= R_R \cdot E_w \cdot I_w \cdot \kappa \end{aligned} \tag{5.20}$$

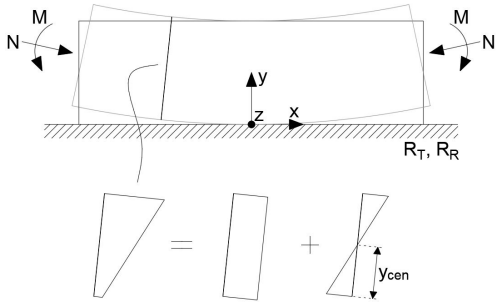

Figure 5.14: Schematic representation of determination of stress in wall caused by external restraint.

When the definition of the degree of restraint is considered in conjunction with the above theory, it is clear that the degree of restraint varies along the height of the wall as a function of the external restraint. This is reflected in Nilsson's expression for the degree of restraint, which is introduced in the next paragraph. It takes into account the external restraint imposed by the floor by including the floor in the transfer of the internal forces required to restore the wall to its original restrained position. In light of this, the stress along the height of the wall, and thus also the degree of restraint, depends on the dimensions and stiffness of the wall in relation to those of the floor. In addition to the external restraint imposed by the floor, Nilsson also considers the restraints imposed by the foundation material, which are referred to as boundary restraints. Since these restraints may vary along the length of the wall, so may the degree of restraint.

It must be pointed out that the principle of 'plane sections remain plane' is only valid for walls with a high slenderness. To overcome this, Nilsson defines so-called resilience factors at distinct heights of the wall depending on the slenderness, which correct the degree of restraint along the height of the wall to account for the non-linear strain distribution for walls with a low slenderness. Nilsson provides the resilience factors for the most common combination of boundary restraints and describes an approach to determine the resilience factors for other combinations using finite element analysis. However, the side walls of the reservoir are of such a high slenderness (i.e. $L/H = 16$), that the assumption of linear strain distribution is virtually valid. Accordingly, the resilience factors have been ignored. Note that in doing so, the Nilsson method is quite similar to the approach suggested by Van Breugel [27].

Applicable expression

Nilsson's expression (excluding resilience factors) for the degree of restraint of a wall located at the edge of a floor is denoted by Equation 5.21, which consists of three components [35]. The first component represents the restraint against axial strain, where $A_{trans}(t)$ is the area of the transformed cross-section and $R_{RT}(t,x)$ the translational boundary restraint due the foundation material. The second component represents the restraint against curvature around the z-axis, where $I_{trans,z}(t)$ and $R_{RR,z}(t,x)$ are the second moment of inertia of the transformed cross-section and the rotational boundary restraint for bending around the z-axis, respectively. The third component represents the restraint against curvature around the y-axis, where $I_{trans,y}(t)$ and $R_{RR,y}(t,x)$ are the second moment of inertia of the transformed cross-section and the rotational boundary restraint for bending around the y-axis, respectively. It is worth mentioning that the third component can be omitted when a wall is located in the middle of a floor, as the imposed deformations of the wall then do not induce curvature around the y-axis. For the definitions of the transformed cross-sectional properties, including the position of the centroid through $y_{cen}(t)$ and $z_{cen}(t)$ (see Figure 5.15), reference is made to Appendix E.

$$\begin{aligned} R(t,x,y) = 1 &- [1 - R_{RT}(t,x)] \cdot \frac{A_w}{A_{trans}(t)} \\ &- \left[1 - R_{RR,z}(t,x)\right] \cdot \frac{A_w \cdot (y_{cen}(t) - y) \cdot (y_{cen}(t) - \frac{H}{2})}{I_{trans,z}(t)} \\ &- \left[1 - R_{RR,y}(t,x)\right] \cdot \frac{A_w \cdot \left(z_{cen}(t) - \frac{B_{ef} - 2 \cdot D_w}{2}\right)^2}{I_{trans,y}(t)} \end{aligned} \tag{5.21}$$

The values of the structural parameters that have been applied in the computation of the degree of restraint of the side walls of the reservoir are given in Table 5.3 and stem from the sketch design in Figure 1.7. The effective width B_{ef} of the floor, being the part that provides restraint, has been assumed equal to the height H of the wall, which happens to correspond to half the width of the floor. As for the stiffness of the floor, it has been assumed that the floor complies with class C30/37 and that it is fully hardened once the wall is cast, meaning a constant value for its elastic modulus E_f has been adopted of 33 GPa. The stiffness of the wall, on the other hand, develops in line with Figure 5.10. Correspondingly, since the elastic modulus E_w of the wall is not a constant value, the transformed cross-sectional properties, boundary restraints and degree of restraint are age-dependent.

L (m)	B_{ef} (mm)	H (mm)	D_f (mm)	D_w (mm)	A_f (m^2)	A_w (m^2)	K_s (MPa)	E_f (GPa)	E_w (GPa)
40	2500	2500	500	500	1.25	1.25	40	33	$E_{cm}(t)$

Table 5.3: Values of structural parameters.

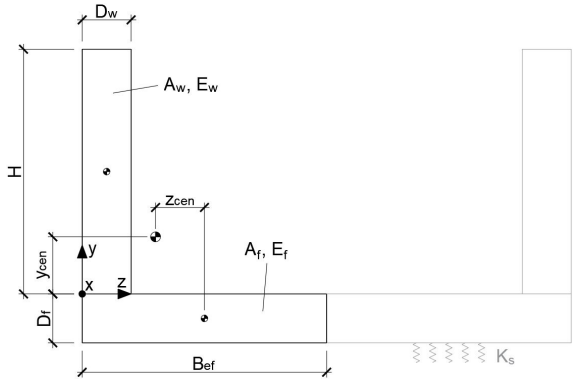

Figure 5.15: Designation of structural parameters.

In terms of the boundary restraints that have been applied in the computation of the degree of restraint, the recommendations by Nilsson, who extensively studied the influence of foundation material, have been adopted. Nilsson states that the translational boundary restraint is negligible in the event of a non-cohesive and low-friction foundation material (e.g. sand) [35]. As it is likely that such a foundation material will be used, the translational boundary restraint is set to zero (i.e. $R_{RT}(t,x) = 0$). While Nilsson argues that the same holds for the rotational boundary restraint for bending around the y-axis, a different mechanism occurs when it comes to the side walls of the reservoir. As demonstrated in Figure 5.16, the imposed deformations of one wall introduce a curvature around the y-axis opposite to the curvature caused by the imposed deformations of the other wall. These therefore counteract, meaning curvature is essentially restrained, provided that the side walls of the reservoir are cast (near) simultaneously. Assuming this construction practice will be adhered to, the rotational boundary restraint for bending around the y-axis is set to absolute (i.e. $R_{RR,y}(t,x) = 1$).

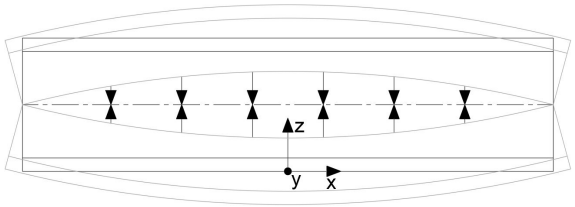

Figure 5.16: Schematic representation of rotational boundary restraint of side walls for bending around y-axis.

The rotational boundary restraint for bending around the z-axis is dictated by the stiffness of the foundation material, which is defined by its compression modulus K_s, and the length L of the wall. It can be determined, among other methods, from the well-known expressions for beams on elastic foundations. Further elaboration of this approach by Nilsson resulted in an expression for the rotational boundary restraint $R_{RR,z}(t,x)$ for bending around the z-axis at a distance x from the center of the wall, which is denoted by Equations F.1 and F.2 in Appendix F. Accordingly, the rotational boundary restraint increases with increasing stiffness of the foundation material or as the wall becomes longer. With respect to the foundation material that will support the reservoir, it has been assumed that the compression modulus equals 40 MPa, which corresponds to dense sand [35]. At $E_w/E_f = 0.93$, this results in the rotational boundary restraint distribution along the length of the side walls displayed in Figure 5.17, which illustrates that the center of the side walls experiences total restraint against curvature around the z-axis, while the end endures zero restraint.

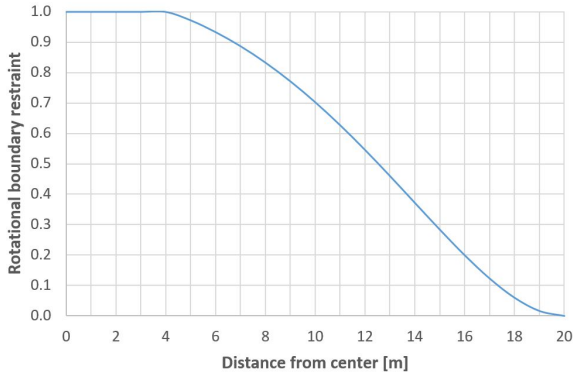

Figure 5.17: Distribution of rotational boundary restraint of side walls for bending around z-axis at $E_w/E_f = 0.93$.

Implementation results
Application of the Nilsson method revealed the distribution of the degree of restraint along the length and height of the side walls shown in Figure 5.18, which occurs 72 hours after casting when $E_w/E_f = 0.93$. This indicates that in the center the degree of restraint is equal over the height of the wall. This can be attributed to the considerable length of the side walls in combination with the notable stiffness of the foundation material, causing curvature in the center to be completely restrained. Towards the end of the side walls, however, the restraint against curvature decreases (see Figure 5.17), causing the degree of restraint to vary over the height. There, the greatest degree of restraint is found at the bottom and, following the principle of 'plane sections remain plane', reduces linearly towards the top.

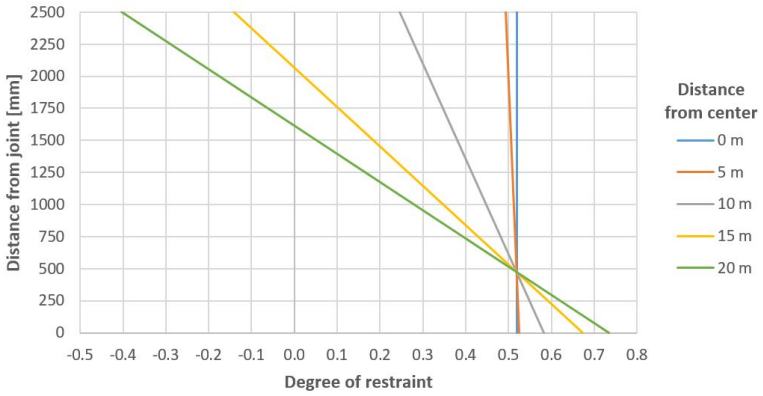

Figure 5.18: Distribution of degree of restraint of side walls at $E_w/E_f = 0.93$.

The continuation of the cracking calculations is founded on the degree of restraint 10 m from the center of the side walls and 500 mm above the joint between the wall and the floor, which at $E_w/E_f = 0.93$ matches 0.52. The development of the degree of restraint at the considered position is presented in Figure 5.19. This demonstrates that the degree of restraint is inversely proportional to the quotient E_w/E_f. However, as the stiffness of the wall develops relatively quickly, all the more because of the increased temperature at which hydration takes place, the degree of restraint remains virtually constant after 48 hours. It goes without saying that the degree of restraint at another position develops in a similar way. Furthermore, as the probability of cracking is proportional to the degree of restraint, the distribution of the degree of restraint also gives an impression of probability of cracking at another position, knowing the probability of cracking at the considered position. On this basis, it seems unlikely that near the end of the side walls, the cracks will reach the top. But this is something that will be discussed in more detail in the next chapter.

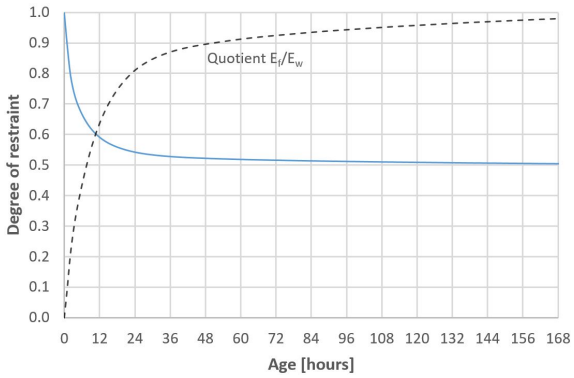

Figure 5.19: Development of degree of restraint of side walls.

5.6 Overall results

To determine whether early-age cracking of the side walls of the reservoir occurs, it has been examined whether and how much, based on two different methods, the actions will exceed the resistance. These methods have been explained in the preceding section in virtue of the description of the imposed deformations. Table 5.4 summarizes the two methods by presenting the quality they consider with respect to the imposed deformations (i.e. actions) and strength development (i.e. resistance). Following up on this, Figure 5.20 illustrates the development of restrained shrinkage strain versus tensile strain capacity and thus corresponds to method I, whereas Figure 5.21 presents the development of mean concrete stress versus effective tensile strength and

as such represents method II. This implies that, based on the assumptions and parameters established in the course of this chapter, early-age cracking of the side walls is likely to take place, as both methods anticipate that the actions will exceed the resistance. However, method II anticipates a larger surplus, while method I is more conservative. Note also that the mean concrete stress with respect to method II eventually starts to decrease, whereas the restrained shrinkage strain relating to method I continues to increase slightly. This latter difference can be attributed to the way both methods account for relaxation, namely by means of an age-dependent relaxation coefficient $\psi(t, t_0)$, as opposed to a constant coefficient for creep effects K_1, respectively.

	Actions	*Resistance*
Method I	Restrained shrinkage strain $\varepsilon_r(t)$ acc. Equation 5.15	Tensile strain capacity $\varepsilon_{ctu}(t)$ acc. Equation 5.22
Method II	Mean concrete stress $\sigma_{cm}(t)$ acc. Equation 5.16	Effective tensile strength $f_{ct,ef}(t)$ acc. Equation 5.23

Table 5.4: Methods for determination of probability of cracking.

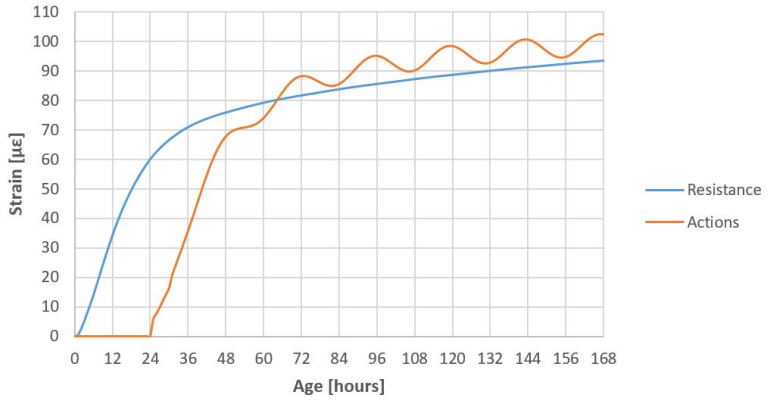

Figure 5.20: Development of tensile strain capacity versus restrained shrinkage strain (method I).

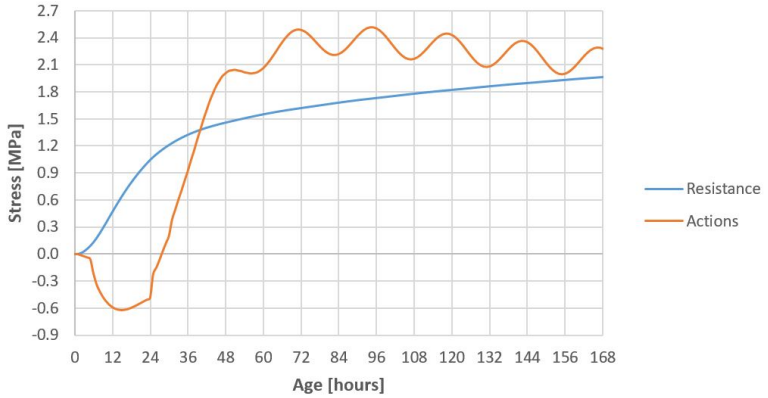

Figure 5.21: Development of effective tensile strength versus mean concrete stress (method II).

It should be pointed out that both methods account for the fact that early-age cracking due to imposed deformations generally does not occur at the mean tensile strength $f_{ctm}(t)$ but at a lower so-called effective tensile strength $f_{ct,ef}(t)$. This is done by means of the coefficient for weakest link and sustained loading effects K_2, whose name reveals the main causes of this phenomenon. That is to say, concrete maintained under a sustained tensile load exhibits a reduced tensile strength and cracks develop where the tensile strength is lowest. The values reported in literature for the ratio, at an early-age, of effective to mean tensile strength, range from 0.7 to 0.8 [27, 32]. In light of this, K_2 has been taken equal to 0.75.

$$\varepsilon_{ctu}(t) = \frac{K_2 \cdot f_{ctm}(t)}{K_1 \cdot E_{cm}(t)} \tag{5.22}$$

$$f_{ct,ef}(t) = K_2 \cdot f_{ctm}(t) \tag{5.23}$$

Although the above results seem promising, it should be borne in mind that the established parameters may deviate. This applies in particular to the environmental and mixture parameters, which are subject to both variability and uncertainty. One way this can be resolved is to perform Monte Carlo simulation; repeating the cracking calculations, each time based on a different parameter input. However, this demands huge computing power and thorough information of the variability and uncertainty of the established parameters, neither of which were available. Therefore, in order to determine the probability of cracking, it has instead been assumed that the actions and resistance of both methods are normally distributed with respective standard deviations equal to 20% of the computed values, which are considered to be the mean. This common simplification suggested by Van Breugel is schematized in Figure 5.22 and follows the definition that the probability of cracking is equivalent to the likelihood that the actions will exceed the resistance [27]. Consequently, with regard to the side walls of the reservoir, this results in the development of the probability of cracking displayed in Figure 5.23. This indicates that the maximum probability of cracking according to method II corresponds to 93% and arises after approximately 72 hours, while method I anticipates the maximum probability of cracking to be 65% after about 96 hours. These results again prove promising, but their true significance will be discussed in a detailed analysis later on in this thesis.

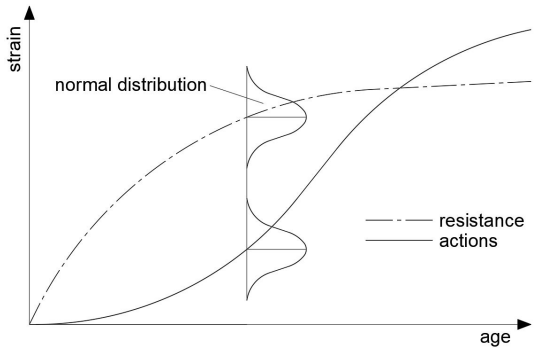

Figure 5.22: Schematic representation of actions and resistance being normally distributed.

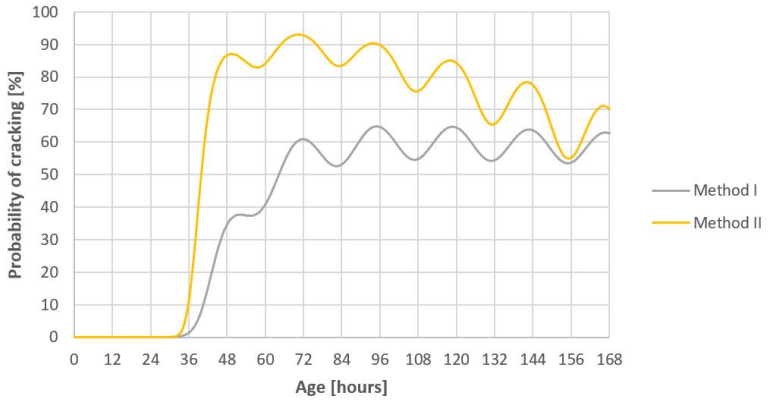

Figure 5.23: Development of probability of cracking of side walls.

5.6.1 Parameter study

Based on what has been presented in this thesis, it can be inferred that the probability of cracking depends on many aspects. Therefore, a parameter study has been performed in an effort to identify the extent of influence of these aspects and, in doing so, to determine the sensitivity of the probability of cracking to different parameter input. The procedure of the parameter study consists of repeating the cracking calculations as described in this chapter, each time changing just one parameter, while all other parameters remain the same. Accordingly, the parameter study is purely hypothetical, as certain parameters are actually related to others, meaning the change in one is accompanied by the change in others. This applies in particular to the mixture parameters, which are closely related. For the purpose of the parameter study, however, these relationships between the parameters have been disregarded (i.e. the parameters are 'uncoupled'). Nevertheless, even if only hypothetical, the parameter study offers exceptional insight into the extent various aspects influence the probability of cracking of the side walls of the reservoir. Moreover, it simulates the effect of accidental deviations in the mixture composition or environmental conditions and deliberate modifications in the structural dimensioning or construction practice.

The results of the parameter study are provided in Figure 5.24, in which each row corresponds to one of the parameters listed below, columns Y represent the parameters established in the course of this chapter (i.e. reference), and columns X and Z represent a change in the row-specific parameter. For example, increasing the mix temperature (7) from 16 to 18 °C, while all other parameters remain the same, leads to a maximum probability of cracking of 72% and 96% instead of 65% and 93% for method I and II, respectively. Because many of the results are self-evident and it is too much to go through them all, only crucial and remarkable results, some of which are reviewed later on in the analysis, are highlighted:

- A minor deviation in the share of blastfurnace slag in cement (1) appears to have a comparably large influence on the probability of cracking, as it significantly affects the temperature rise.
- In the previous chapter it had been found that the strength development (3) varies depending on the concrete mixture (see Table 4.3), here it seems that the probability of cracking is quite sensitive to this.
- The probability of cracking proves to be especially sensitive to the mutual difference between the mix temperature (7) and mean ambient temperature (10), that is, a substantially higher probability of cracking arises when this mutual difference increases.
- Although a smaller wall thickness (13) leads to an inferior temperature rise, the probability of cracking turns out to improve because the floor then provides relatively more restraint.

Parameter					Maximum probability of cracking						
PRM	Input			Unit	Method I			Method II			Unit
	X	Y	Z		X	Y	Z	X	Y	Z	
1	44	52	60	%	73		55	95		90	
2	398	418	438	kg/m³	61		68	92		94	
3	54	58	62	MPa	70		60	95		91	
4	0.70	0.75	0.80		73		56	96		90	
5	10.8	11.4	12.0	με/K	59		70	91		95	
6	126	146	166	με	62		68	92		94	
7	14	16	18	°C	56		72	88		96	
8	18	24	30	hours	65	65	64	89	93	94	%
9	3.7	4.4	5.1	W/m²·K	70		60	94		92	
10	10	12	14	°C	73		57	96		89	
11	6	8	10	°C	64		66	92		94	
12	3.0	3.5	4.0	m/s	63		66	92		94	
13	400	500	600	mm	72		57	96		87	
14	400	500	600	mm	54		72	89		95	
15	30	33	36	GPa	60		69	91		94	
16	20	40	60	MN/m²	64		65	93		93	

Figure 5.24: Results of parameter study on probability of cracking.

Mixture parameters

1. Share of blastfurnace slag in cement (p_{GGBS});
2. Cement content of concrete (C_c);
3. Coefficient *A* of modelled strength development (i.e. mean cube compressive strength at 28 days);
4. Coefficient for weakest link and sustained loading effects (K_2);
5. Coefficient of thermal expansion of concrete (α_c);
6. Coefficient *A* of modelled autogenous shrinkage (i.e. mean ultimate autogenous shrinkage strain);
7. Mix temperature (T_{mix});

Construction parameters

8. Age of concrete at formwork removal;
9. Thermal surface conductance including formwork (G_1);

Environmental parameters

10. Mean ambient temperature;
11. Mean ambient diurnal temperature variation;
12. Mean wind speed;

Structural parameters

13. Thickness of wall (D_w);
14. Thickness of floor (D_f);
15. Elastic modulus of floor (E_f);
16. Compression modulus of foundation material (K_s).

6 Degree of cracking

To demonstrate the crack-sealing capacity and reinforcement reduction potential of BSHC, it is desirable that the degree of cracking of the side walls of the reservoir coincides with the proposed crack pattern. This requires the reinforcement layout to be configured appropriately. Hence, in this chapter it is looked at how the longitudinal reinforcement can best be distributed in order to obtain the various crack widths, knowing from the previous chapter when the cracks are likely to emerge.

6.1 Strategy

Similar to the probability of cracking in the preceding chapter, the degree of cracking in relation to the reinforcement layout has been determined analytically. As mentioned in the beginning of this thesis, different methods exist that deal with the prediction of crack widths, with little consensus in practice on which one is best. This presents both a challenge as an opportunity in the sense that this thesis can provide some insight in the ongoing debate as to what would be the appropriate method. Therefore, after making an inventory, multiple of these methods described in literature have been implemented. This inventory is provided first in an individual section, which also includes a description of the fundamentals of the prediction methods. Subsequently, the results of applying each method in this case are reviewed and compared. These results consists of a set of graphs showing the relationship between the longitudinal reinforcement distribution and the predicted crack width per method, which are then used to establish the appropriate reinforcement layout for the side walls of the reservoir. Finally, it is attempted to define some other attributes of the degree of cracking that may be crucial to the demonstrator project, such as the number of cracks that are likely to emerge, as well as their length. It should be remembered that many aspects involving the degree of cracking, in particular the strength development corrected for thermal effects, have already been determined for the purpose of the probability of cracking. Hence, for clarification of these aspects, it is referred to the previous chapter.

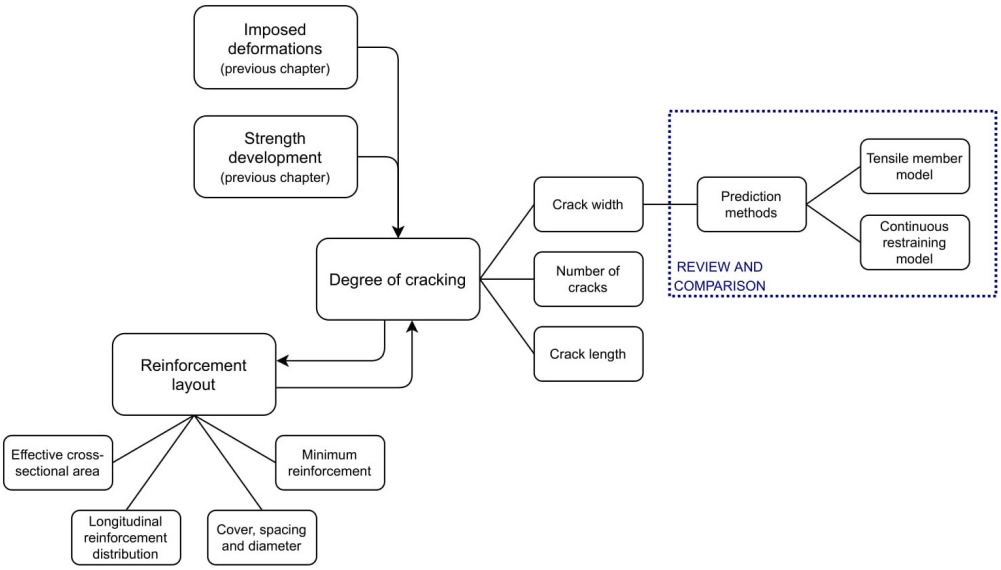

Figure 6.1: Strategy outline for determination of degree of cracking.

6.2 Inventory of prediction methods

Because of the numerous methods that deal with the prediction of crack widths and the fact that there is little consensus in practice on which one is best, a CROW[2] committee on 'crack width control of concrete structures' has been set up [36]. This CROW committee is tasked with seeking the best prediction method, which should become the standard in the Netherlands. At the time of writing this thesis, their research was still ongoing and no recommendations had yet been published. Nevertheless, it is worth mentioning that through unpublished reports (acquired from Ir. J.W. van den Bos), the author was aware of the preliminary findings of the CROW committee. A case in point being the survey conducted by the CROW committee which revealed the prediction methods commonly used in the Netherlands. This provided a starting point regarding the methods that should at least be included in this thesis. In addition, several other methods have been considered that enjoy popularity in other European countries. Altogether, Table 6.1 presents an overview of the prediction methods that have been reviewed and compared as part of this thesis, bearing in mind the following:

- The DIN 1045-1 is the German predecessor of the NEN-EN 1992-1-1 and, based on preliminary findings, is likely to form the basis of the method the CROW committee is going to recommend.
- The NEN-EN 1992-3 describes two methods, but it is referred here to the edge restraint approach, considering the end restraint approach is identical to Ciria C660 I.
- The ICE/0706/012 is a further development and combination of Ciria C660 I (i.e. end restraint approach) and Ciria C660 II (i.e. edge restraint approach), all of which are described by Bamforth.

Method	*TMM*	*CRM*
DIN 1045-1 [37]	X	
NEN-EN 1992-1-1 [31]	X	
NEN-EN 1992-3 [38]		X
Model Code 2010 [39]	X	
Van Breugel [27]	X	
Ciria C660 I [32]	X	
Ciria C660 II [32]		X
ICE/0706/012 [40]	X	X

Table 6.1: Inventory of prediction methods and their theoretical models.

A distinction can be made between prediction methods founded on the tensile member model (TMM) and those founded on the continuous restraining model (CRM). These designations refer only to the theoretical models upon which the methods are based and not necessarily to the kind of restraint to which they apply. The remainder of this section is dedicated to the clarification of both theoretical models for a better understanding of the background of the prediction methods. Furthermore, in doing so, certain attributes are described that explain the differences between the methods based on the same theoretical model. A comprehensive overview of the prediction methods can be found in Appendix G, which provides abstracts of each method.

6.2.1 Tensile member model

Most prediction methods are founded on the tensile member model, which consists of a single reinforcement bar surrounded by concrete subjected to a uniform tensile load. As illustrated in Figure 6.2, the response of the tensile member is linear elastic until the cracking force N_{cr} is reached and the first crack occurs where the tensile strength is lowest. Due to the formation of the crack, the axial stiffness of the tensile member decreases. This causes, in the event of an imposed deformation or deformation-controlled test, the axial force in the tensile member to drop below the cracking force. If the imposed deformation then continues to increase, the axial force increases again until a second crack occurs at the next weakest position along the tensile member. On further increase of the imposed deformation, the number of cracks grows. This gives the typical sawtooth in the load-deformation diagram and is referred to as the formative cracking stage (FCS). During the formative cracking stage, the axial force hardly increases, while the tensile member elongates considerably. For the sake of simplicity, however, it is assumed that the axial force remains constant throughout the formative cracking stage (i.e. the scatter in strength along the tensile member is neglected) and the sawtooth in the load-deformation diagram is portrayed by a straight line. Eventually, a situation is reached in which no new cracks can emerge; the crack pattern is then fully developed. This is also referred to as the stabilized cracking stage (SCS) and takes effect from the so-called transition strain ε_{fdc}.

[2]Dutch not-for-profit knowledge institute on the design, construction and management of infrastructure.

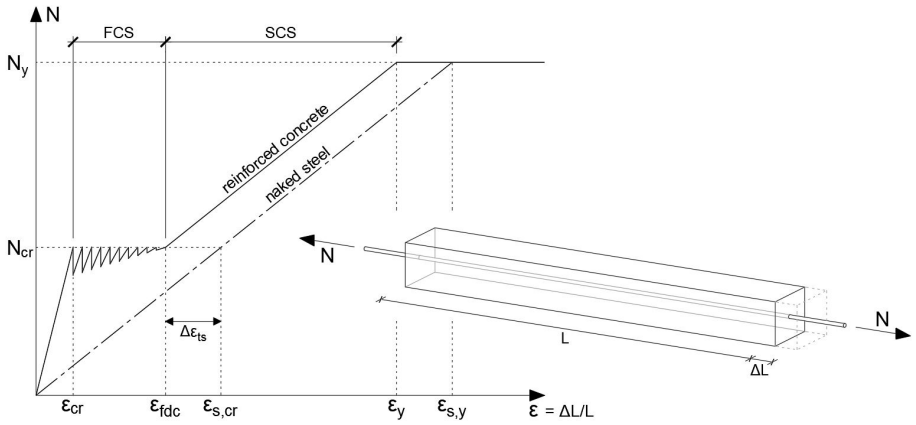

Figure 6.2: Schematic representation of load-deformation relationship of tensile member, adapted from [27].

In a crack, the axial force is entirely carried by the reinforcement steel, meaning the axial strain of concrete there equals zero. Next to a crack, the axial force is transferred from the reinforcement steel to the concrete by bonding, such that at the end of the transfer length, the axial strain of concrete matches that of the reinforcement steel. When the crack pattern is fully developed, the distances between the cracks, also known as the crack spacing, are all less than then twice the transfer length, indicating that there is no position along the tensile member left where the axial strain of concrete equals the cracking strain ε_{cr}. The crack width is equivalent to the integration of the strain difference between the reinforcement steel and concrete over the transfer length for the formative cracking stage (see Equation 6.1) or over the crack spacing for the stabilized cracking stage (see Equation 6.2). The way the strain difference and transfer length or crack spacing are determined differs per prediction method, but most of the methods founded on the tensile member model assume a constant bond-slip relationship, which translates into the linear strain distribution shown in Figure 6.3. Hence, the remainder of the description of the tensile member model is also from the perspective of a constant bond-slip relationship. The only method that deviates from this, namely Van Breugel, assumes the bond-slip relationship denoted by Equation 6.3, where δ is the slip displacement of the reinforcement bar relative to the concrete and τ_b the bond strength between the reinforcement steel and concrete [27]. While this is consistent with a non-linear strain distribution, the principles are the same.

$$w = 2 \cdot \int_0^{s_0} [\varepsilon_s(x) - \varepsilon_c(x)]\,\mathrm{d}x = 2 \cdot s_0 \cdot (\varepsilon_{sm} - \varepsilon_{cm}) \tag{6.1}$$

$$w = \int_0^{s_r} [\varepsilon_s(x) - \varepsilon_c(x)]\,\mathrm{d}x = s_r \cdot (\varepsilon_{sm} - \varepsilon_{cm}) \tag{6.2}$$

$$\tau_b = 0.38 \cdot f_{cm,cube} \cdot \delta^{0.18} \tag{6.3}$$

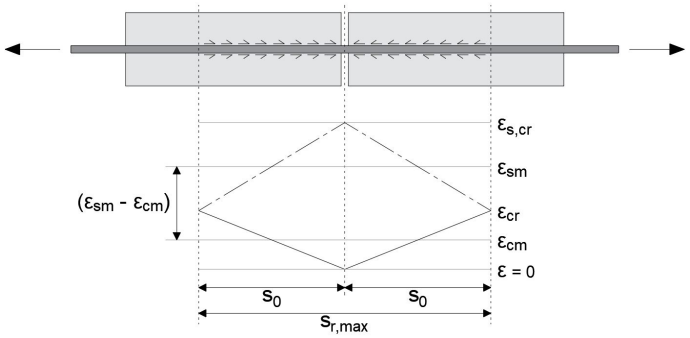

Figure 6.3: Schematic representation of strain distribution of tensile member in FCS.

Transfer length

The transfer length follows from the equilibrium given by Equation 6.4 between the bond force F_b and the axial force carried by the concrete between the cracks. Hence, at a constant bond-slip relationship, the transfer length s_0 is represented by Equation 6.5. The ratio of cracking stress to bond strength (i.e. σ_{cr}/τ_b) truly depends on the type of reinforcement used, degree of hydration and strength classification, the latter being consistent with indications that the bond strength is more closely related to the compressive rather than tensile strength of concrete [32]. Nevertheless, in most prediction methods it is considered a constant corresponding to deformed reinforcement bars and hardened, normal-strength concrete. Table 6.2 lists the ratio of cracking stress to bond strength maintained by each method. Note that because the ratio of cracking stress to bond strength is deemed a constant, it is generally replaced by coefficient k_1.

$$\varepsilon_{cr} \cdot E_{cm} \cdot A_{c,ef} = \pi \cdot \phi \cdot \int_0^{s_0} \tau_b(x)\,\mathrm{d}x \quad [= F_b] \tag{6.4}$$

$$s_0 = \frac{\sigma_{cr} \cdot \phi}{4 \cdot \tau_b \cdot \rho_{ef}} \tag{6.5}$$

Several methods also introduce the concrete cover in the expression for the transfer length, in the manner described by Equation 6.6. This measure is supported by empirical evidence and can be traced back to work by Beeby [41]. Beeby argues that the influence of the concrete cover can be explained by the fact that shear lag occurs (i.e. the concrete stress at the surface of the tensile member lags behind the concrete stress adjacent to the reinforcement bar), which is demonstrated in Figure 6.4. Accordingly, the distance between the crack and the undisturbed region is increased. The magnitude of this increase is reflected in coefficient k_2, which in turn thus relates to the extent of shear lag that is accounted for. However, this theory and the relative effect of the concrete cover are still under debate. It may also be for this reason that not all prediction methods embrace it. From Table 6.2 it can be inferred which methods include the concrete cover in the transfer length.

$$s_0 = k_2 \cdot c + 0.25 \cdot k_1 \cdot \frac{\phi}{\rho_{ef}} \tag{6.6}$$

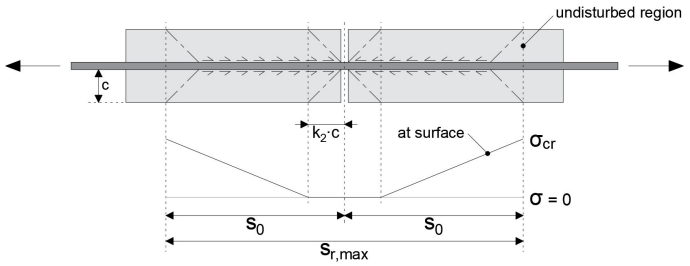

Figure 6.4: Schematic representation of concrete cover related shear lag in tensile member.

Method	k_1	k_2	α_1	α_1
DIN 1045-1 [37]	0.56		1.33	1.50
NEN-EN 1992-1-1 [31]	0.60	1.5	1.33	1.70
NEN-EN 1992-3 [38]	0.60	1.5	1.33	1.70
Model Code 2010 [39]	0.56	1.0	1.33	1.50
Van Breugel [27]	0.60[3]		1.50	1.50
Ciria C660 I [32]	0.60	1.5	1.33	1.70
Ciria C660 II [32]	0.60	1.5	1.33	1.70
ICE/0706/012 [40]	0.60	1.5	1.33	1.70

Table 6.2: Characteristics of prediction methods with regard to transfer length and crack spacing.

[3]For class C30/37 at a slip displacement of 1 μm.

Crack spacing
The crack spacing s_r is at least equal to the transfer length and, when the crack pattern is fully developed, not larger than twice the transfer length. However, where the minimum crack spacing is clear, the mean and maximum crack spacing are subject of discussion. Table 6.2 in conjunction with Equation 6.7 gives an impression of the mean and maximum crack spacing adhered to by each method. From this it can be deduced that some prediction methods actually maintain a maximum crack spacing that exceeds the theoretical upper limit of $2 \cdot s_0$. These methods reason that this is due to scatter in the cracking stress and bond strength along the tensile member, causing the transfer length to vary for each individual crack, which in turn results in a greater variety in distances between the cracks [27, 32].

$$\begin{aligned} s_{r,min} &= s_0 \\ s_{rm} &= \alpha_1 \cdot s_0 \\ s_{r,max} &= \alpha_1 \cdot \alpha_2 \cdot s_0 \end{aligned} \tag{6.7}$$

It must be stressed that the crack spacing mentioned here really only refers to the stabilized cracking stage. This is because, as displayed in Figure 6.5, the crack spacing is still variable in the formative cracking stage due to the emergence of new cracks. Nevertheless, the crack width in both the formative and stabilized cracking stage can be determined on the basis of the maximum crack spacing in the stabilized cracking stage, as it corresponds to the greatest distance over which the strain difference between the reinforcement steel and concrete can occur (see Figure 6.3). Consequently, a characteristic value of the crack width is obtained that has only a 5% probability of being exceeded. This approach is pursued by all prediction methods, except Van Breugel. The mean value of the crack width can determined in virtue of the mean crack spacing, or directly from $w_k/w_m = \alpha_2$. While the methods in question recognize that this only holds in the stabilized cracking stage, they do not disclose the ratio of characteristic to mean crack width in the formative cracking stage.

Van Breugel, on the other hand, makes a more explicit distinction between the formative and stabilized cracking stage. It determines the crack width in the formative cracking stage by means of the transfer length, whereas the mean crack spacing is adopted in the stabilized cracking stage, resulting in a mean value of the crack width in both cases. Moreover, as a result of scatter in the cracking stress and bond strength along the tensile member, Van Breugel states that $w_k/w_m = 1.3$ or $w_k/w_m = \alpha_2$, depending on whether it concerns the formative or stabilized cracking stage, respectively [27]. On this basis, in the absence of more thorough information, Equation 6.8 has been formulated, which is thought to be a reasonable description of the ratio of characteristic to mean crack width that fits all prediction methods. Accordingly, the ratio of characteristic to mean crack width has been made dependent on the number of cracks, which is proportional to the magnitude of the imposed deformation, to obtain a continuous rather than a discrete function that reflects the increasing difference between the mean and maximum crack spacing in the formative cracking stage (see Figure 6.5).

$$\frac{w_k}{w_m} = \begin{cases} 1.3 + \dfrac{\varepsilon - \varepsilon_{cr}}{\varepsilon_{fdc} - \varepsilon_{cr}} \cdot (\alpha_2 - 1.3) & \text{if } \varepsilon < \varepsilon_{fdc} \\ \alpha_2 & \text{if } \varepsilon \geq \varepsilon_{fdc} \end{cases} \tag{6.8}$$

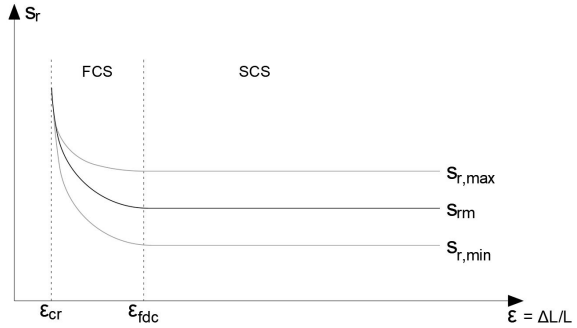

Figure 6.5: Schematic representation of crack spacing as function of axial strain of tensile member.

Crack width
As mentioned before, the crack width is defined as the integration of the strain difference between the reinforcement steel and concrete over the transfer length for the formative cracking stage (see Equation 6.1) or over the crack spacing for the stabilized cracking stage (see Equation 6.2). This is equivalent to the product of the weighted average of the strain difference between reinforcement steel and concrete, from now on simply referred to as the mean strain difference, and the transfer length or crack spacing. The mean strain difference truly depends on the distance over which it occurs, as shown in Figure 6.6. However, all prediction methods systematically establish the mean strain difference based on full use of the transfer length. In other words, the mean strain difference is not adjusted once the maximum crack spacing no longer applies due to the increasing number of cracks (i.e. as soon as 'overlap' occurs). In essence, therefore, only the characteristic crack width is really correct, whereas the mean crack width is an approximation. Note also that Equation 6.8 only applies because of this simplification.

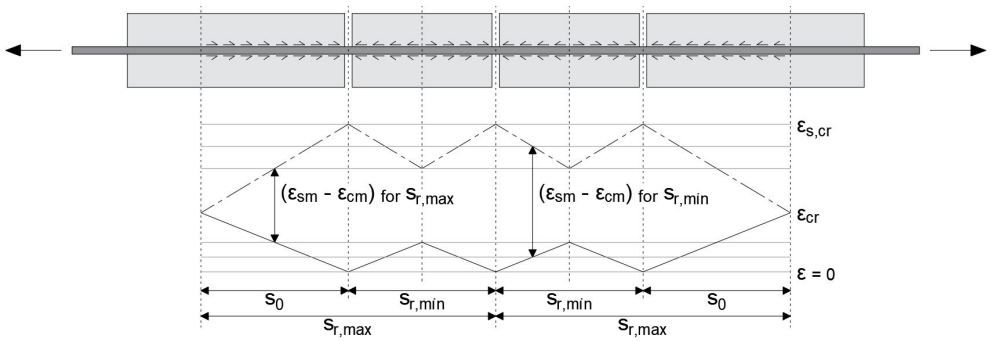

Figure 6.6: Schematic representation of strain difference for minimum and maximum crack spacing of tensile member.

The mean strain difference in the formative cracking stage can be derived from Figure 6.3. This is demonstrated in Equation 6.9, where $\varepsilon_{s,cr}$ is the steel strain in the cracks immediately after cracking. The same can be done for the stabilized cracking stage, but an increase in imposed deformation is then absorbed by the reinforcement steel and not by the formation of new cracks. Accordingly, the reinforcement steel experiences an additional strain, which is given by $\Delta\varepsilon_s = \varepsilon_s - \varepsilon_{s,cr}$, where ε_s is the steel strain in the cracks. Following up on this, Equation 6.10 represents the derivation of the mean strain difference in the stabilized cracking stage in accordance with Figure 6.7. It should be pointed out that the expression for the stabilized cracking stage is also applicable in the formative cracking stage when it is adopted that $\varepsilon_s = \varepsilon_{s,cr}$ (i.e. $\Delta\varepsilon_s = 0$).

$$\begin{aligned}(\varepsilon_{sm} - \varepsilon_{cm}) &= 0.5 \cdot (\varepsilon_{s,cr} - \varepsilon_{cr}) + \varepsilon_{cr} - 0.5 \cdot \varepsilon_{cr} \\ &= 0.5 \cdot \varepsilon_{s,cr}\end{aligned} \tag{6.9}$$

$$\begin{aligned}(\varepsilon_{sm} - \varepsilon_{cm}) &= 0.5 \cdot (\varepsilon_s - \Delta\varepsilon_s - \varepsilon_{cr}) + \varepsilon_{cr} + \Delta\varepsilon_s - 0.5 \cdot \varepsilon_{cr} \\ &= 0.5 \cdot (\varepsilon_s - \Delta\varepsilon_s) \\ &= \varepsilon_s - 0.5 \cdot \varepsilon_{s,cr}\end{aligned} \tag{6.10}$$

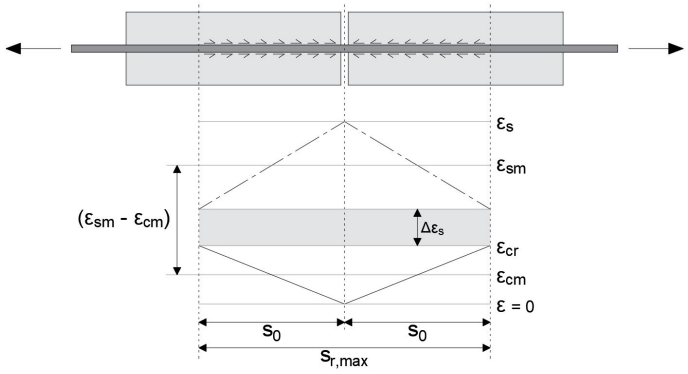

Figure 6.7: Schematic representation of strain distribution of tensile member in SCS.

The steel strain in the cracks immediately after cracking follows from the equilibrium denoted by Equation 6.11 between the cracking force N_{cr} and the axial force carried by the reinforcement steel in the cracks. Correspondingly, the expression for the mean strain difference can be rewritten into the form adopted by most prediction methods, namely Equation 6.12. It should be emphasized that the mean strain difference, and consequently also the crack width, remain constant during the formative cracking stage, as the axial force in the tensile member coincides with the cracking force, which implies that the steel stress in the cracks is also constant (i.e. $\sigma_s = \sigma_{s,cr}$). In the stabilized cracking stage, on the other hand, the increase of the steel stress in the cracks causes the mean strain difference and crack width to increase proportionally. This may continue until the yield strength of the reinforcement steel is reached.

$$\varepsilon_{s,cr} \cdot E_s \cdot A_s = \varepsilon_{cr} \cdot E_{cm} \cdot A_{c,ef} \cdot (1 + \alpha_e \cdot \rho_{ef}) \quad [= N_{cr}] \tag{6.11}$$

$$(\varepsilon_{sm} - \varepsilon_{cm}) = \frac{\sigma_s - 0.5 \cdot \dfrac{\sigma_{cr}}{\rho_{ef}} \cdot (1 + \alpha_e \cdot \rho_{ef})}{E_s} \tag{6.12}$$

It is worth mentioning that in the DIN 1045-1, NEN-EN 1992-1-1 and Model Code 2010 the multiplier 0.5 has been replaced by coefficient k_3, which is an empirical constant to assess the mean strain difference depending on the load duration ($k_3 = 0.4$ for long-term loading, $k_3 = 0.6$ for short-term loading). In doing so, these methods take into account that the assumption of a constant bond-slip relationship is not strictly true and that the linear strain distribution displayed in Figure 6.7 is actually somewhat more non-linear in nature. Moreover, the dependence on the load duration can be attributed to an increase in slip displacement between the reinforcement steel and concrete with time under a sustained tensile load. This phenomenon, sometimes referred to as bond creep, causes the transfer length or steel strain between the cracks to increase, depending on whether it concerns the formative or stabilized cracking stage, respectively [27]. In view of this, one can argue that bond creep only affects the mean strain difference in the stabilized cracking stage. However, because a greater transfer length has the same effect on the crack width as a higher steel strain between the cracks, it seems justified to also have the mean strain difference in the formative cracking stage dependent on the load duration.

Tension stiffening

As can be seen from the load-deformation diagram in Figure 6.2, the axial stiffness of the tensile member always exceeds that of the reinforcement steel alone. The contribution of the concrete between the cracks to the axial stiffness of the tensile member is known as tension stiffening. The tension stiffening strain represents the difference between the axial strain of the tensile member and that of the reinforcement steel alone, the latter being equivalent to the steel strain in the cracks. All prediction methods assume that the tension stiffening strain is constant once the crack pattern is fully developed, which translates into a linear relationship between the steel strain in the cracks on the one hand, and the mean strain difference and crack width on the other. In this event, the tension stiffening strain $\Delta\varepsilon_{ts}$ is defined by Equation 6.13, given that the axial strain of the tensile member in the stabilized cracking stage matches the mean strain difference. Hence, the transition strain ε_{fdc}, which represents the 'end' of the formative cracking stage, is specified by Equation 6.14.

$$\begin{aligned} \Delta\varepsilon_{ts} &= \varepsilon_s - (\varepsilon_{sm} - \varepsilon_{cm}) \\ &= \varepsilon_s - (\varepsilon_s - k_3 \cdot \varepsilon_{s,cr}) \\ &= k_3 \cdot \varepsilon_{s,cr} \end{aligned} \tag{6.13}$$

$$\begin{aligned} \varepsilon_{fdc} &= \varepsilon_{s,cr} - \Delta\varepsilon_{ts} \\ &= (1 - k_3) \cdot \varepsilon_{s,cr} \end{aligned} \tag{6.14}$$

6.2.2 Continuous restraining model

The continuous restraining model is in many ways similar to the tensile member model. It also consists of a single reinforcement bar surrounded by concrete subjected to a uniform tensile load. Now, however, there is an external restraint present along the tensile member, as illustrated in Figure 6.8. In addition, the continuous restraining model does not take into account that the axial force is transferred from the concrete to the reinforcement steel by bonding [40]. This means that the axial force is entirely carried by the concrete and that the mean strain difference is equivalent to the axial strain of the tensile member being restrained. Therefore, once the cracking strain is exceeded, the cracks all develop at the same time regardless of the degree of restraint, and the crack width is a linear function of the imposed deformation rather than the steel strain in the cracks. This difference between the tensile member model and continuous restraining model is indicated in Figure 6.9. The crack spacing, which multiplied by the mean strain difference gives the crack width, is determined in the same way as the tensile member model. This is remarkable to say the least, since the crack spacing emanates from the transfer length, while the methods founded on the continuous restraining model, namely the NEN-EN 1992-3 and Ciria C660 II, (partially) ignore the axial force transferred from the concrete to the reinforcement steel in their respective definitions of the mean strain difference.

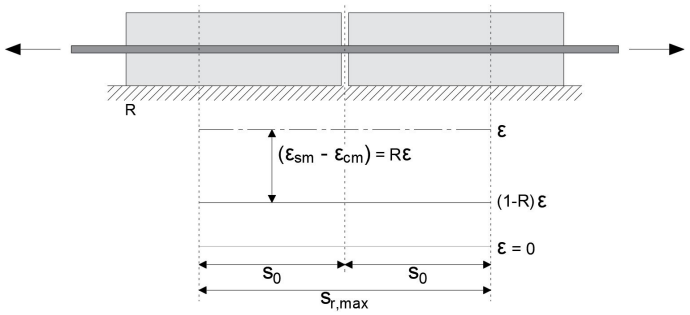

Figure 6.8: Schematic representation of strain distribution of tensile member according to continuous restraining model.

It is occasionally suggested that the continuous restraining model is flawed because it opposes the principle that the reinforcement steel takes over the axial force from the concrete when cracks occur, which is also the philosophy behind minimum reinforcement. Furthermore, Bamforth argues that the external restraint, like the reinforcement steel, tends to prevent cracks from reaching their potential width [40]. This led to the development of the ICE/0706/012 or ICE for short, which is a prediction method that essentially combines both theoretical models. The method considers two stages; the first stage considers the formation of the crack when the axial force is transferred from the concrete to the reinforcement steel by bonding. During the second stage the crack grows further as the imposed deformation allows the concrete to continue to contract relative to the reinforcement steel. The crack width is thought to be the summation of the first and second stage values of the crack width. The first stage crack width is determined on the basis of a revision of the tensile member model. The axial force in the tensile member is limited due to the external restraint. At total restraint (i.e. $R = 1$), all of the axial force is attracted by the external restraint, while none of the axial force is attracted at zero restraint (i.e. $R = 0$), the latter corresponding to the tensile member model in itself. As a result, the steel strain in the cracks is inversely proportional to the degree of restraint. Figure 6.9 reveals how this affects the crack width, namely that, in contrast to the continuous restraining model, the crack width becomes smaller as the degree of restraint increases. Moreover, the revision also takes account of strain relief in the undisturbed region. The second stage crack width is more or less assessed in line with the continuous restraining model, as it is proportional to the imposed deformation in excess of the cracking strain.

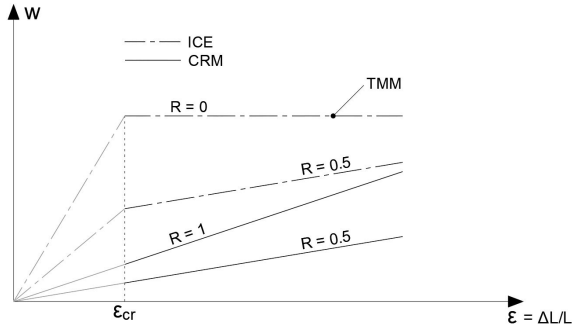

Figure 6.9: Schematic representation of crack width as function of axial strain of tensile member.

6.2.3 Effective cross-sectional area

An important attribute of both theoretical models is the determination of the dimensions of the tensile member and thus the effective cross-sectional area. The effective cross-sectional area represents the concrete surrounding the reinforcement bar that 'interacts' with the reinforcement steel, that is, the concrete whose axial force is transferred to the reinforcement steel once cracks occur. Depending on the dimensions of the structure, reinforcement layout and type of loading (i.e. bending or pure tension), the effective cross-sectional area $A_{c,ef}$ comprises the entire cross-sectional area A_c, or only part of it, whereupon one speaks of a hidden tensile member. Figure 6.10 shows that for a structure with a hidden tensile member, one can distinguish between primary and secondary cracks. The primary cracks run through the whole structure, while the secondary cracks are concentrated in the hidden tensile member, some of which tend to run towards (and join) the primary cracks [27]. Due to the secondary cracks, the imposed deformation is distributed over a larger number of cracks, resulting in a smaller crack width in the hidden tensile member compared to beyond the effective cross-sectional area. This applies in particular to massive concrete structures with reinforcement steel concentrated near the surface, but possibly also concerns walls that are rather thick. Other examples of structures with a hidden tensile member are beams and floors subjected to bending. However, only the effective cross-sectional area in case of pure tension is reviewed here, since this is also the type of loading to which the side walls of the reservoir are subjected (as a consequence of imposed deformations).

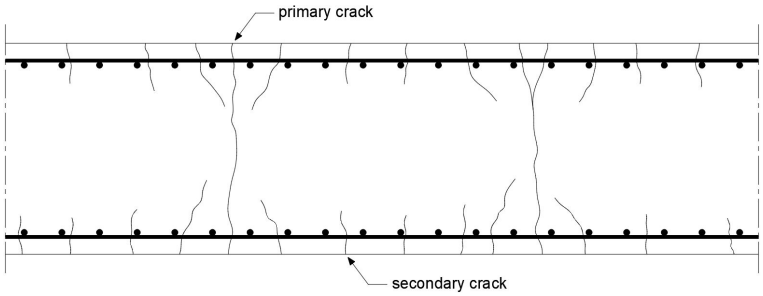

Figure 6.10: Schematic representation of primary and secondary cracks in structure with hidden tensile member.

Although the effective cross-sectional area can be derived from the transfer length of the secondary cracks, all prediction methods, except van Breugel, have generalized this approach such that it is merely a function of the concrete cover, bar diameter, bar spacing and thickness of the structure. Table 6.3 in conjunction with Figure 6.11 presents the definitions of the effective cross-sectional area reported by Van Breugel and the other methods. It is appropriate to highlight that for the prediction methods that do not specify the effective width $b_{c,ef}$, probably because the bar spacing rarely exceeds the actual upper limit, the description of the other methods has been adopted. Note also that by following Van Breugel's approach, which is schematized in Figure 6.12, the prediction of crack widths for massive concrete structures becomes an iterative process, as the effective height $h_{c,ef}$ depends on the transfer length, and vice versa.

	$h_{c,ef}$	$b_{c,ef}$
Van Breugel	The lesser of $D_w/2$ and $c + 2 \cdot \phi + 1.2 \cdot s_0$	The lesser of s and $15 \cdot \phi$
Other methods	The lesser of $D_w/2$ and $2.5 \cdot (c + \phi/2)$	The lesser of s and $5 \cdot (c + \phi/2)$

Table 6.3: Definitions of effective cross-sectional area for structures in pure tension.

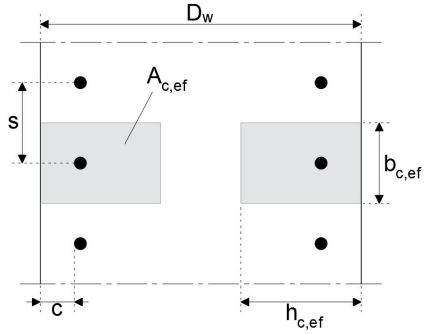

Figure 6.11: Schematic representation of effective cross-sectional area for structures in pure tension.

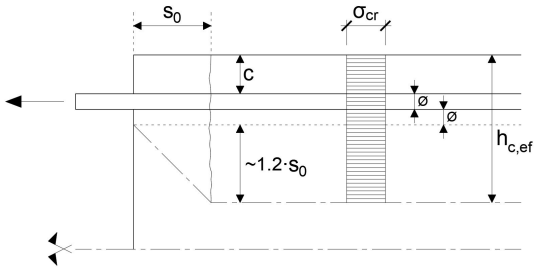

Figure 6.12: Schematic representation of effective cross-sectional area according to Van Breugel.

It is evident that for structures that involve a hidden tensile member, the transfer length and steel strain in the cracks are determined based on the effective cross-sectional area. From Equations 6.4 and 6.11 it can be deduced that as the effective cross-sectional area increases, both the transfer length and steel strain in the cracks decrease, which in turn means that the crack width becomes smaller. These relationships emphasize the large influence that the effective cross-sectional area has on the predicted crack width. Having said that, there are two prediction methods that assess the effective cross-sectional area differently, being the ICE/0706/012 and Ciria C660 I. While these methods also determine the transfer length based on the effective cross-sectional area $A_{c,ef}$, they take the entire cross-sectional area A_c into account when it comes to the determination of the steel strain in the cracks. It is not clear how the mechanism of primary and secondary cracks justifies a different basis for determining the steel strain in the cracks than for determining the transfer length. However, it is believed that the methods in question apply this measure to better fit empirical evidence [32]. In addition, in light of this measure, these methods introduce coefficient k, which allows for the effect of the non-uniform self-equilibrating concrete stress distribution that occurs due to the non-uniform temperature distribution during hydration. This phenomenon, which is shown in Figure 6.13, causes cracks to emerge at an average value of the concrete stress across the structure that is lower than the cracking stress σ_{cr}. Consequently, the equilibrium between the cracking force N_{cr} of the whole structure and the axial force carried by the reinforcement steel in the cracks is defined by Equation 6.15. Needless to say, the steel strain in the cracks immediately after cracking is generally greater when determined from this expression than when determined on the basis of the hidden tensile member (see Equation 6.11).

$$\varepsilon_{s,cr} \cdot E_s \cdot A_s = \varepsilon_{cr} \cdot E_{cm} \cdot A_c \cdot (k + \alpha_e \cdot \rho) \quad [= N_{cr}] \tag{6.15}$$

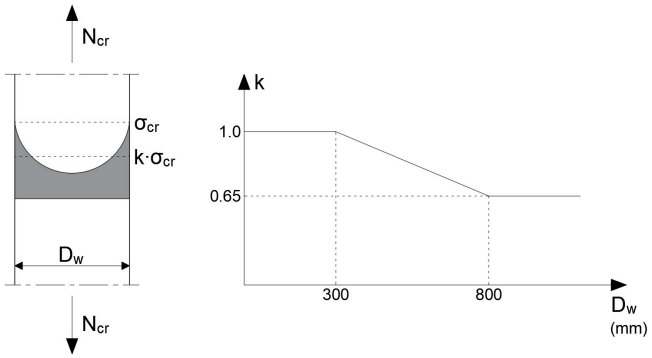

Figure 6.13: Schematic representation of non-uniform self-equilibrating concrete stress distribution, adapted from [32].

6.3 Implementation results

The prediction methods cannot be reviewed and compared by means of their theory alone. As set out in the preceding section and Appendix G, the prediction methods differ in several aspects, and only the sum of these aspects leads to a certain crack width. This makes it difficult to quantitatively compare the methods without implementing them. That is to say, it is not so much the techniques, but mainly the results of the methods in terms of the predicted crack width that has significance. Hence, the prediction methods have also been reviewed and compared with respect to their results when applied in the case of the side walls of the reservoir. These results have not only been used for comparative purposes, but also serve as a basis for deciding on the appropriate reinforcement layout. This means that the parameter input, which has been tailored to this case, is crucial. That is why the reference conditions are addressed before presenting the predicted crack width per method in relation to the longitudinal reinforcement distribution of the side walls of the reservoir.

6.3.1 Reference conditions

The reference conditions refer to the constraints and assumptions on which the prediction of crack widths is based. Clarification of these constraints and assumptions is imperative as together they govern the maximum crack width that can be achieved with regard to the side walls of the reservoir, and because they dictate the parameter input and as such also the results in general. Therefore, the reference conditions are highlighted separately in the upcoming paragraphs.

External loads

The fact that the demonstrator project requires cracking of the side walls of the reservoir to be the result of imposed deformations (so that through-cracks are obtained), does not necessarily mean that the effect of external loads can be neglected. The external loads, the most notable of which is the water load when the reservoir is filled, may affect the cracks that have emerged as a consequence of the imposed deformations, or even lead to flexural cracks themselves. However, the contribution of the water load is difficult to assess quantitatively. The reasoning for this is twofold. First, cracking due to the imposed deformations occurs at an early-age, while the water load only presents itself once the reservoir is put into use when the concrete strength and other properties have developed further. Second, as demonstrated in Figure 6.14, the imposed deformations act in-plane, whereas the water load acts out-of-plane. Nevertheless, due to the Poisson effect, the water load does not only introduce transverse stress, but also longitudinal stress, which 'adds' to the already present longitudinal stress caused by the imposed deformations. However, a relatively simple calculation, which is included in Appendix H, reveals that the water load induced stress (at the position where the maximum bending moment occurs) is only 5% of the imposed stress that arises 72 hours after casting, which can be inferred from Figure 5.21. In light of this, it seems justified to ignore the water load induced stress and consider only the imposed stress, and thus disregard the effect of external loads when it comes to the cracks due to imposed deformations.

It must be emphasized that this starting point only holds because of the significant thickness of the wall in relation to the water load, which leads to a very low transverse and longitudinal stress (i.e. the water load induced stress increases quadratically with decreasing wall thickness). Moreover, because the transverse stress is much lower than the tensile strength, it is unlikely that, in addition to the cracks resulting from imposed deformations, flexural cracks will develop (at the inner surface of the side walls). But then again, this only applies if the wall thickness is substantial.

One could also argue that the Poisson effect does not apply in this case, since (through-)cracks will already be present when the reservoir is put into use. This view is also supported by the NEN-EN 1992-1-1, which states that in such circumstances the Poisson's ratio is equal to zero [31]. This would mean that the transverse stress due to the water load is not converted into longitudinal stress, which in turn justifies ignoring the effect of external loads even more.

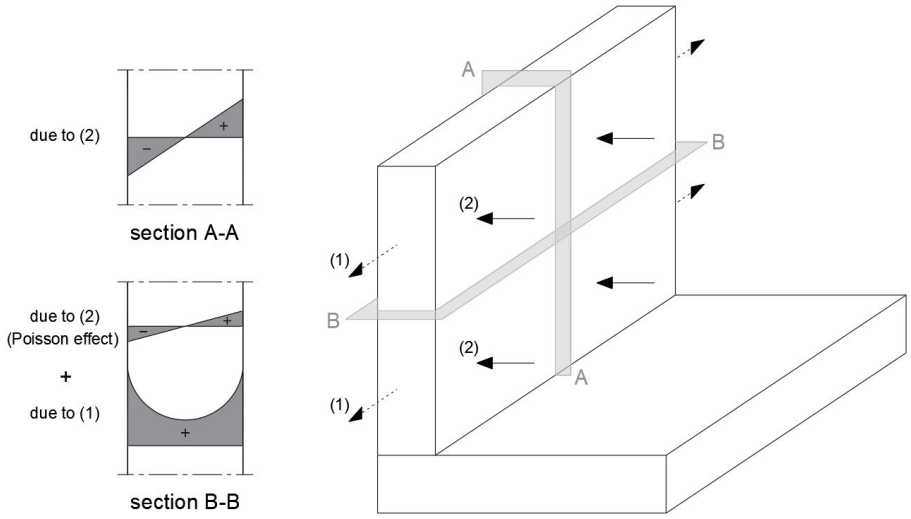

Figure 6.14: Schematic representation of transverse and longitudinal stress distribution due imposed deformations (1) and water load (2).

Age at cracking
Figure 5.23 in the previous chapter shows that cracking of the side walls of the reservoir is most likely to occur somewhere between 48 and 96 hours after casting. The age at cracking that has been adopted in the prediction of crack widths is therefore taken equal to 72 hours, which matches the time at which method II anticipates the maximum probability of cracking of 93%. The values of the material parameters corresponding to this age at cracking are given in Table 6.4, in which those regarding the concrete emanate from Figure 5.10 and those concerning the reinforcement steel represent grade B500. Note that because imposed deformations can be classified as sustained loading, the cracking stress σ_{cr} is not equal to the mean tensile strength f_{ctm}, but the effective tensile strength $f_{ct,ef}$ as denoted by Equation 5.23.

f_{yk} *(MPa)*	f_{ctm} *(MPa)*	$f_{ct,ef}$ *(MPa)*	σ_{cr} *(MPa)*	E_s *(GPa)*	E_{cm} *(GPa)*
500	2.16	1.62	1.62	200	30.5

Table 6.4: Values of material parameters.

Minimum reinforcement
The side walls of the reservoir should always be fitted with sufficient reinforcement steel such that when cracks emerge, the reinforcement steel will not yield. The minimum reinforcement ratio ρ_{min} is defined by Equation 6.16, which can be derived from Equation 6.15 when the steel stress in the cracks immediately after cracking is replaced by the yield strength of the reinforcement steel (i.e. $\sigma_{s,cr} = f_{yk}$). At the considered cracking stress of 1.62 MPa, this results in a minimum reinforcement ratio of 0.28%. Even though the first (and most) cracks appear at an early-age, it cannot be excluded that new cracks emerge in the long-term. Hence, a minimum reinforcement ratio of 0.48% has instead been maintained, which is based on the cracking stress at 28 days of 2.70 MPa. Bear in mind that the NEN-EN 1992-1-1 suggests a higher minimum reinforcement ratio, as it implies that the cracking stress is equivalent to the mean tensile strength rather than the lower effective tensile strength [31]. However, both Bamforth and, based on preliminary findings, the CROW committee recognize that this philosophy overestimates the crack width and minimum reinforcement ratio.

$$\rho_{min} = \frac{k \cdot \sigma_{cr}}{f_{yk} - \alpha_e \cdot \sigma_{cr}} \tag{6.16}$$

Reinforcement configuration
In terms of the reinforcement configuration of the side walls of the reservoir, it has been decided that the transverse reinforcement occupies the first layer and the longitudinal reinforcement the second layer (see Figure 6.15). This configuration allows for a greater concrete cover to the longitudinal reinforcement, which in turn tends to lead to a larger crack width. The concrete cover is taken equal to 50 mm, which is sufficient in most environments. Assuming that the bar diameter of the transverse reinforcement corresponds to 20 mm, the concrete cover c to the longitudinal reinforcement adds up to 70 mm.

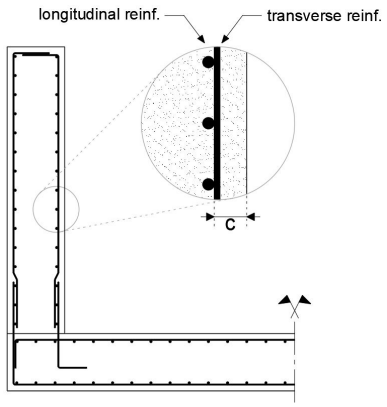

Figure 6.15: Reinforcement configuration[4] of side walls.

[4]Shown anchoring of reinforcement bars is for illustrative purposes only.

6.3.2 Comparison of prediction methods

The results in terms of the relationship between the longitudinal reinforcement distribution and the predicted crack width per method are presented in Figures 6.16 and 6.17, the former showing the mutual differences between the prediction methods at a bar diameter of 20 mm. Straightaway it is clear that the methods founded on the continuous restraining model are far more conservative, so to speak, than those founded on the tensile member model, in particular at lower reinforcement ratios. This can predominantly be attributed to the fact that the imposed deformations are still relatively small at an early-age and that, according to the continuous restraining model, the crack width increases linearly with the imposed deformation (see Figure 6.9). Hence, if the imposed deformations were greater, which is generally the case in the long-term when drying shrinkage sets in, less difference in predicted crack width would be observed between the two theoretical models. Especially because, according to the tensile member model, the crack width remains constant regardless of the magnitude of the imposed deformation, as long as the crack pattern is not fully developed. Instead, the crack width is a function of the steel strain in the cracks, which decreases as more reinforcement steel is applied. This explains why the methods founded on the tensile member model allow for a much larger crack width at lower reinforcement ratios than those founded on the continuous restraining model.

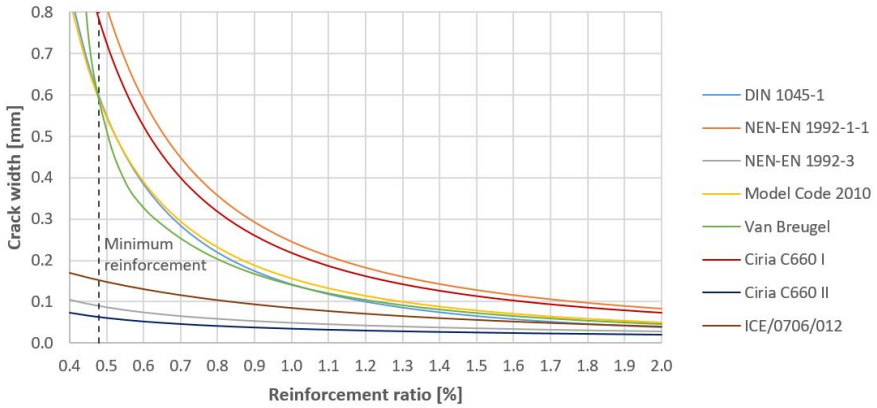

Figure 6.16: Relationship between longitudinal reinforcement distribution and predicted crack width per method for bar diameter of 20 mm.

The inventory of prediction methods has revealed that the methods founded on the tensile member model differ in the way they determine the strain difference and transfer length or crack spacing. This is reflected in the variety of results. However, the variations cannot be fully attributed to any of these aspects individually, since the prediction methods differ in several aspects, and only the sum of these aspects leads to a certain crack width. Likewise, the results cannot simply be generalized to other reference conditions, as some methods are more sensitive to a particular parameter input than others. Nevertheless, in general it can be said that the NEN-EN 1992-1-1 and Ciria C660 I allow for a larger crack width than the DIN 1045-1, Model Code 2010 and Van Breugel, which are more conservative. It also seems that whether or not the concrete cover is included in the transfer length plays a major role in these mutual differences. This is because this measure leads to a considerably greater crack spacing, which in turn results in a much larger crack width at the same strain difference.

The ICE/0706/012 is more conservative than the methods founded on the tensile member model, as expected, but allows for a larger crack width than the NEN-EN 1992-3 and Ciria C660 II. These results are based on the degree of restraint of 0.52 established in the previous chapter. If the degree of restraint were higher, less difference in predicted crack width would be observed between the methods founded on the continuous restraining model and the ICE/0706/012, as the latter follows the principle that the external restraint tends to prevent cracks from reaching their potential width.

At this point, it is appropriate to emphasize that the results presented in this section relate to the mean value of the crack width. The reason for this is that the longitudinal reinforcement distribution of the side walls of the reservoir should be configured such that various crack widths are obtained. From this perspective it makes more sense to show the mean crack width, and not the characteristic crack width which has only a 5% probability of being exceeded. Note that this deviates from practice where the aim is usually to ensure that a certain acceptable crack width is not exceeded and the amount of reinforcement steel thus relies on the characteristic value of the crack width.

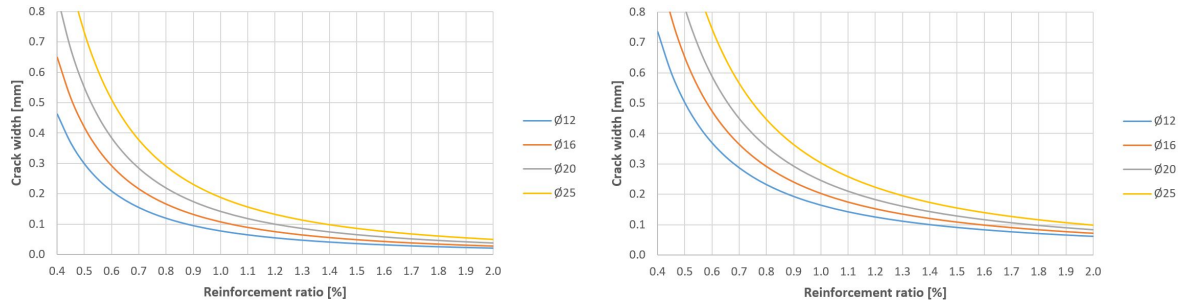

(a) DIN 1045-1.

(b) NEN-EN 1992-1-1.

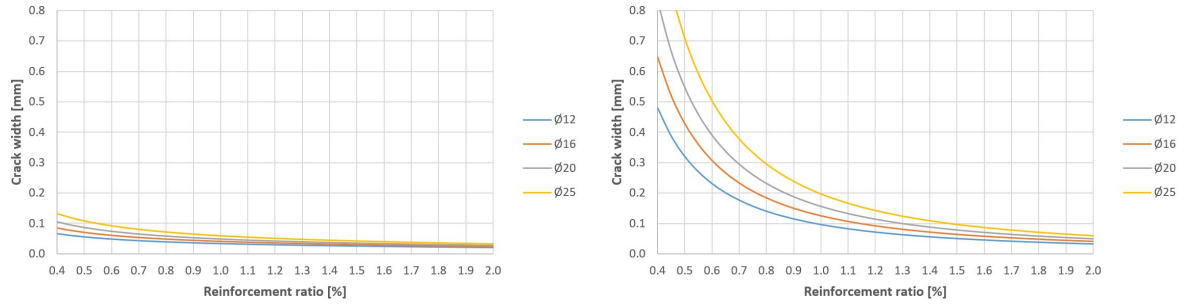

(c) NEN-EN 1992-3.

(d) Model Code 2010.

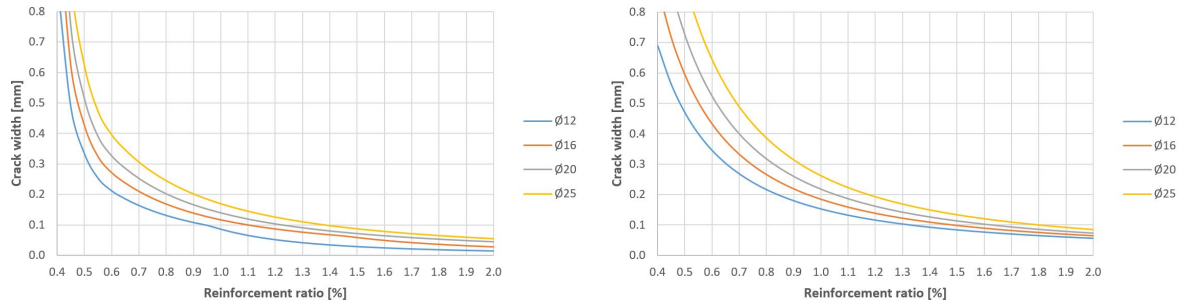

(e) Van Breugel.

(f) Ciria C660 I.

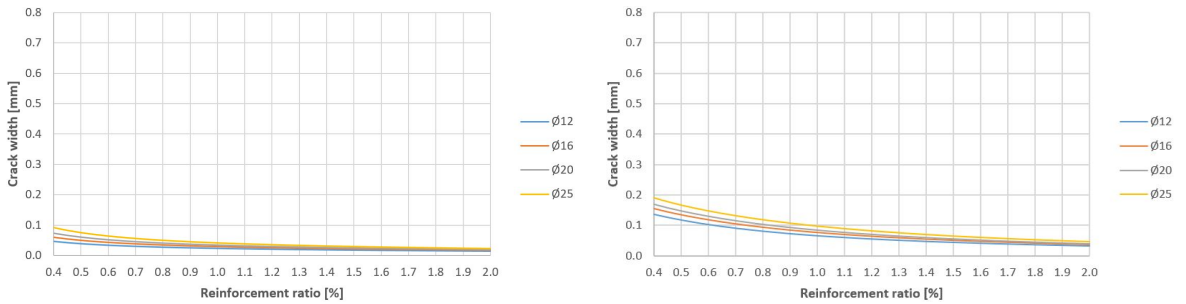

(g) Ciria C660 II.

(h) ICE/0706/012.

Figure 6.17: Relationship between longitudinal reinforcement distribution and predicted crack width per method.

The results indicate that the mutual differences between the prediction methods are very large, in particular at lower reinforcement ratios. This presents a challenge, as it raises the question which prediction methods should serve as a basis for deciding on the appropriate reinforcement layout. The literature studied is also inconclusive as to which prediction methods are best applicable in the case of the side walls of the reservoir. Some suggest that the methods founded on the continuous restraining model should be applied, as they were specifically developed with the kind of restraint illustrated in Figure 5.13 in mind. Others are in favour of the methods founded on the tensile member model, as they are based on decades of research and are better understood. Moreover, data comparing the occurring crack width to the predicted crack width in similar cases is scarce. Experimental research by Micallef indicates that the NEN-EN 1992-3 and Ciria C660 II are rather close to the occurring crack width [42]. On the contrary, the preliminary findings of the CROW committee includes data collected from practice demonstrating that the DIN 1045-1 and Van Breugel ensure reasonable accuracy. However, because these are contradictory observations, they do not provide much clarification.

All things considered, it has been decided to establish the appropriate reinforcement layout for the side walls of the reservoir based on the average of all prediction methods, which is presented in Figure 6.18. It is the author's believe that, in the absence of adequate information about which prediction methods are the most reliable, this is the most reasonable approach. This does not necessarily mean that the occurring crack width will indeed meet the average of all prediction methods. Hence, it is essential to also be aware of the minimum and maximum of all prediction methods (i.e. the predicted crack width in accordance with the most conservative method and the most optimistic method, respectively).

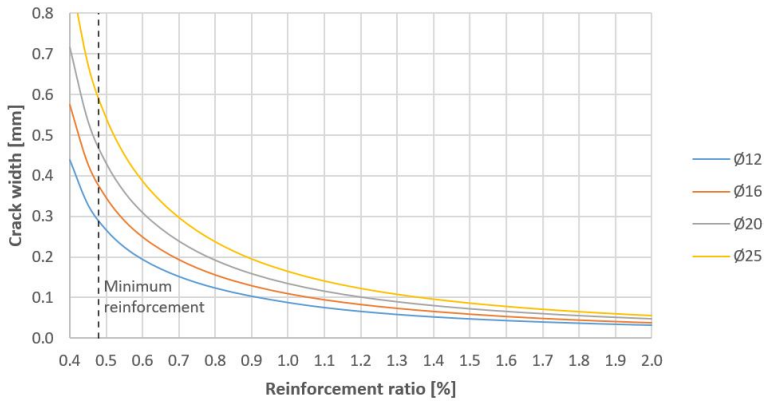

Figure 6.18: Relationship between longitudinal reinforcement distribution and predicted crack width.

6.3.3 Parameter study

Much like the probability of cracking, the degree of cracking depends on many aspects. Therefore, a parameter study has been performed in an effort to identify the extent of influence of these aspects, and in doing so, to determine the sensitivity of the predicted crack width to different parameter input. The procedure of the parameter study is the same as in the preceding chapter for the probability of cracking and will therefore not be described again. What is different, though, is that a few more parameters have been included, namely the age at cracking, concrete cover, bar spacing and bar diameter, the latter three of which are collectively referred to as the reinforcement parameters. The parameter study not only offers exceptional insight into the extent various aspects influence the degree of cracking of the side walls of the reservoir, but also demonstrates the differences between the methods in terms of how their prediction of crack widths is affected by changing just one parameter, while all others remain the same. Moreover, it simulates the effect of accidental deviations in the mixture composition or environmental conditions and deliberate modifications in the structural dimensioning, construction practice or reinforcement layout.

The results of the parameter study are provided in Figure 6.19, in which each row corresponds to one of the parameters listed below, columns Y represent the parameters established in course of this and the previous chapter (i.e. reference), and columns X and Z represent a change in the row-specific parameter. For example, increasing the wall thickness from 500 to 600 mm, while all other parameters remain the same, leads to a mean crack width of 0.21 and 0.26 mm instead of 0.20 and 0.19 mm for the DIN 1045-1 and Van Breugel, respectively. Note that a bar diameter of 20 mm and bar spacing of 150 mm have been taken as a reference. Because many of the results are self-evident and it is too much to go through them all, only crucial and remarkable results are highlighted:

- In general it can be said that the crack width is far less sensitive to the same deviations as the probability of cracking, regardless of which prediction method is adopted.
- A deviation in the strength development (3) only affects the crack width when it is determined by methods founded on the tensile member model, because it merely involves the steel stress in the cracks immediately after cracking.
- The methods founded on the tensile member model reveal that the crack width increases in case of a larger wall thickness (13), whereas the methods founded on the continuous restraining model disclose the complete opposite since the floor then provides relatively less restraint.
- The crack width, in particular when it is determined by methods founded on the continuous restraining model, proves to be especially sensitive to the age at cracking (17), that is, the crack width will be larger if the cracks occur later when the imposed deformations and other properties have developed further.
- All prediction methods, except van Breugel, indicate that reducing the concrete cover (18) leads to a substantially smaller crack width, as it results in either a lesser transfer length or a lower steel stress in the cracks due to the reduced effective cross-sectional area.

Parameter					Mean crack width												
PRM	Input			Unit	DIN 1045-1			NEN-EN 1992-1-1			NEN-EN 1992-3			Model Code 2010			Unit
	X	Y	Z		X	Y	Z	X	Y	Z	X	Y	Z	X	Y	Z	
1	44	52	60	%	0.20		0.19	0.34		0.32	0.06		0.05	0.22		0.21	
2	398	418	438	kg/m³	0.20		0.20	0.33		0.33	0.06		0.06	0.21		0.21	
3	54	58	62	MPa	0.19		0.21	0.31		0.35	0.06		0.06	0.20		0.22	
4	0.70	0.75	0.80		0.19		0.21	0.31		0.35	0.06		0.06	0.20		0.23	
5	10.8	11.4	12.0	με/K	0.20		0.20	0.33		0.33	0.05		0.06	0.21		0.21	
6	126	146	166	με	0.20		0.20	0.33		0.33	0.06		0.06	0.21		0.21	
7	14	16	18	°C	0.19		0.21	0.32		0.34	0.05		0.06	0.21		0.22	
8	18	24	30	hours	0.19		0.21	0.32		0.34	0.06		0.06	0.20		0.22	
9	3.7	4.4	5.1	W/m²·K	0.20		0.20	0.33		0.33	0.06		0.05	0.21		0.21	
10	10	12	14	°C	0.19	0.20	0.21	0.32	0.33	0.34	0.06	0.06	0.05	0.21	0.21	0.22	mm
11	6	8	10	°C	0.20		0.20	0.33		0.33	0.06		0.06	0.21		0.21	
12	3.0	3.5	4.0	m/s	0.20		0.20	0.33		0.33	0.06		0.06	0.21		0.21	
13	400	500	600	mm	0.19		0.21	0.31		0.35	0.06		0.05	0.20		0.22	
14	400	500	600	mm	0.20		0.20	0.33		0.33	0.05		0.06	0.21		0.21	
15	30	33	36	GPa	0.19		0.21	0.31		0.35	0.05		0.06	0.20		0.22	
16	20	40	60	MN/m²	0.20		0.20	0.33		0.33	0.06		0.06	0.21		0.21	
17	48	72	96	hours	0.18		0.21	0.30		0.35	0.04		0.06	0.19		0.23	
18	50	70	90	mm	0.11		0.31	0.19		0.52	0.04		0.07	0.12		0.33	
19	16	20	25	mm	0.36		0.11	0.58		0.19	0.07		0.05	0.38		0.12	
20	100	150	200	mm	0.09		0.35	0.17		0.54	0.04		0.07	0.10		0.36	

(a) Part one.

Parameter					Mean crack width												
PRM	Input			Unit	Van Breugel			Ciria C660 I			Ciria C660 II			ICE/0706/012			Unit
	X	Y	Z		X	Y	Z	X	Y	Z	X	Y	Z	X	Y	Z	
1	44	52	60	%	0.19		0.18	0.30		0.29	0.04		0.04	0.11		0.09	
2	398	418	438	kg/m³	0.19		0.19	0.29		0.29	0.04		0.04	0.10		0.10	
3	54	58	62	MPa	0.18		0.19	0.28		0.31	0.04		0.04	0.10		0.10	
4	0.70	0.75	0.80		0.17		0.21	0.27		0.31	0.04		0.04	0.10		0.10	
5	10.8	11.4	12.0	με/K	0.19		0.19	0.29		0.29	0.04		0.04	0.10		0.10	
6	126	146	166	με	0.19		0.19	0.29		0.29	0.04		0.04	0.10		0.10	
7	14	16	18	°C	0.18		0.19	0.29		0.30	0.04		0.04	0.09		0.11	
8	18	24	30	hours	0.18		0.19	0.28		0.30	0.04		0.04	0.10		0.10	
9	3.7	4.4	5.1	W/m²·K	0.19		0.19	0.30		0.29	0.04		0.04	0.10		0.10	
10	10	12	14	°C	0.18	0.19	0.19	0.28	0.29	0.30	0.04	0.04	0.04	0.10	0.10	0.10	mm
11	6	8	10	°C	0.19		0.19	0.29		0.29	0.04		0.04	0.10		0.10	
12	3.0	3.5	4.0	m/s	0.19		0.19	0.29		0.29	0.04		0.04	0.10		0.10	
13	400	500	600	mm	0.12		0.26	0.24		0.34	0.04		0.04	0.08		0.11	
14	400	500	600	mm	0.19		0.19	0.29		0.29	0.04		0.04	0.11		0.09	
15	30	33	36	GPa	0.12		0.26	0.24		0.34	0.04		0.04	0.10		0.10	
16	20	40	60	MN/m²	0.19		0.19	0.29		0.29	0.04		0.04	0.10		0.10	
17	48	72	96	hours	0.17		0.20	0.27		0.31	0.03		0.04	0.08		0.11	
18	50	70	90	mm	0.19		0.19	0.22		0.37	0.03		0.05	0.08		0.12	
19	16	20	25	mm	0.35		0.11	0.53		0.17	0.05		0.03	0.13		0.07	
20	100	150	200	mm	0.10		0.30	0.15		0.48	0.03		0.05	0.07		0.13	

(b) Part two.

Figure 6.19: Results of parameter study on degree of cracking.

Mixture parameters

1. Share of blastfurnace slag in cement (p_{GGBS});
2. Cement content of concrete (C_c);
3. Coefficient A of modelled strength development (i.e. mean cube compressive strength at 28 days);
4. Coefficient for weakest link and sustained loading effects (K_2);
5. Coefficient of thermal expansion of concrete (α_c);
6. Coefficient A of modelled autogenous shrinkage (i.e. mean ultimate autogenous shrinkage strain);
7. Mix temperature (T_{mix});

Construction parameters

8. Age of concrete at formwork removal;
9. Thermal surface conductance including formwork (G_1);

Environmental parameters

10. Mean ambient temperature;
11. Mean ambient diurnal temperature variation;
12. Mean wind speed;

Structural parameters

13. Thickness of wall (D_w);
14. Thickness of floor (D_f);
15. Elastic modulus of floor (E_f);
16. Compression modulus of foundation material (K_s);
17. Age at cracking;

Reinforcement parameters

18. Concrete cover to longitudinal reinforcement (c);
19. Reinforcement bar diameter (ϕ);
20. Reinforcement bar spacing (s).

6.4 Reinforcement layout

This section describes and substantiates the appropriate reinforcement layout for the side walls of the reservoir, which has been devised based on the average of all prediction methods. As mentioned in the problem statement, it is preferred to obtain various crack widths along the length of the side walls. Preference is given to a crack width of 0.10 mm for the least cracked section, increasing (in three discrete increments) to a crack width of approximately 0.70 mm for the most cracked section. This requires that the longitudinal reinforcement distribution varies per section. However, instead of varying both the bar diameter and bar spacing, it has been decided to maintain a bar diameter of 20 mm across all sections to limit the number of variables. The reason that specifically this bar diameter has been adopted stems from the desire to enhance the maximum crack width that can be achieved. That is to say, it has been found that when the minimum reinforcement ratio of 0.48% and the maximum bar spacing of 250 mm prescribed by the NEN-EN 1992-1-1 are adhered to, the maximum crack width that can be achieved is largest at a bar diameter of 20 mm.

The above insight led to the reinforcement layout provided in Table 6.5, in which the predicted crack width is given in accordance with the minimum, average and maximum of all prediction methods. For the predicted crack width per method it is referred to Appendix I, which provides more data regarding the prediction of crack widths. S4 reflects the maximum crack width that can be achieved since the maximum bar spacing is applied there. The desired crack width of 0.70 mm is unlikely to be reached as the average of all prediction methods indicates only a mean crack width of 0.43 mm (the most representative crack width is presented in bold). The bar spacing of S1 is tailored such that the average of all prediction methods indicates a mean crack width close to the desired crack width of 0.10 mm. Following up on this, S2 and S3 are configured so that the differences between the sections in terms of the predicted crack width are more or less the same.

	Desired crack width (mm)	*Longitudinal reinforcement*		*Predicted crack width (mm)*					
				Mean			*Characteristic*		
		Ratio	*Distribution*	*Min.*	*Ave.*	*Max.*	*Min.*	*Ave.*	*Max.*
S1	0.10	1.26%	∅20–100	0.03	**0.09**	0.17	0.04	0.13	0.23
S2	0.30	0.79%	∅20–160	0.04	**0.20**	0.37	0.06	0.26	0.49
S3	0.50	0.60%	∅20–210	0.05	**0.31**	0.59	0.07	0.41	0.78
S4	0.70	0.50%	∅20–250	0.06	**0.43**	0.81	0.08	0.56	1.06

Table 6.5: Reinforcement layout of side walls and prediction of crack widths.

6.4.1 Section arrangement

The sketch design in Figure 1.7 shows that all sections are equal in length. However, the author believes that it is better to adjust the section length depending on the number of cracks that are likely to emerge (so that the various crack widths are equally represented). In other words, instead of embracing the original section arrangement, resulting in a varying number of cracks per section, it makes more sense to adopt an alternative section arrangement such that roughly the same number of cracks occur per section. Table 6.6 presents both the original and alternative section arrangement, as well as the predicted number of cracks, which is equivalent to the product of the section length and restrained shrinkage strain (see Figure 5.20), divided by the mean crack width pursuant to the average of all prediction methods. It goes without saying that if the occurring crack width tends more towards the minimum or maximum of all prediction methods, the number of cracks will be higher or lower than stated here, respectively.

	Section length (m)	*Predicted number of cracks*
S1	10	9
S2	10	4
S3	10	3
S4	10	2

(a) Original.

	Section length (m)	*Predicted number of cracks*
S1	5	5
S2	8	3
S3	12	3
S4	15	3

(b) Alternative.

Table 6.6: Section arrangement of side walls and prediction of number of cracks.

6.4.2 Crack pattern

Figure 6.20 gives an impression of the crack pattern that is expected to occur in virtue of the reinforcement layout that is also shown. This has been drawn up on the basis the predicted number of cracks and the distribution of the degree of restraint along the length and height of the side walls shown in Figure 5.18. In the center of the side walls curvature is completely restrained (see Figure 5.17), allowing cracks to appear over the full height. Towards the end of the side walls the restraint against curvature decreases, making it unlikely that the cracks will reach the top. Hence, the cracks forming along S1 and S2 are likely to be shorter in length than those forming along S3 and S4. Besides being shorter in length, the cracks near the end of the side walls will probably also be inclined cracks instead of vertical cracks, since they develop perpendicular to the tensile stress trajectories [27]. Note that these tensile stress trajectories can be deduced from the distribution of the degree of restraint and are consistent with those found in literature.

It is worth mentioning that most cracks will probably be primary cracks, which means that indeed mainly through-cracks are obtained. This is evident from the fact that the prediction methods anticipate an effective cross-sectional area that comprises virtually the entire cross-sectional area (i.e. the effective height identified by Van Breugel or the other methods is exactly or almost equal to half the wall thickness, respectively). Simply put, despite that the reinforcement steel is concentrated near the surface, secondary cracks will hardly develop because the side walls of the reservoir are rather thin.

Not much can be said about the distances between the cracks, as they strongly depend on the occurring crack width and which prediction methods turn out to be the most reliable. The methods founded on the tensile member model report that the crack pattern is not fully developed, meaning the crack spacing is still variable and an increase in imposed deformation is accompanied by the formation of new cracks. In line with the methods founded on the continuous restraining model, however, the crack spacing is proportional to the number of cracks and an increase in imposed deformation results in a larger crack width. In addition, it is also conceivable that reality lies somewhere in the middle of these philosophies. Having said that, it is not to be expected that either the number of cracks or crack width will increase significantly right after the cracks have emerged at an early-age, because most of the imposed deformations will already have occurred before the age at cracking. In the long-term, however, this could well happen when drying shrinkage sets in, but this is not relevant to the demonstrator project as the test only lasts a few months.

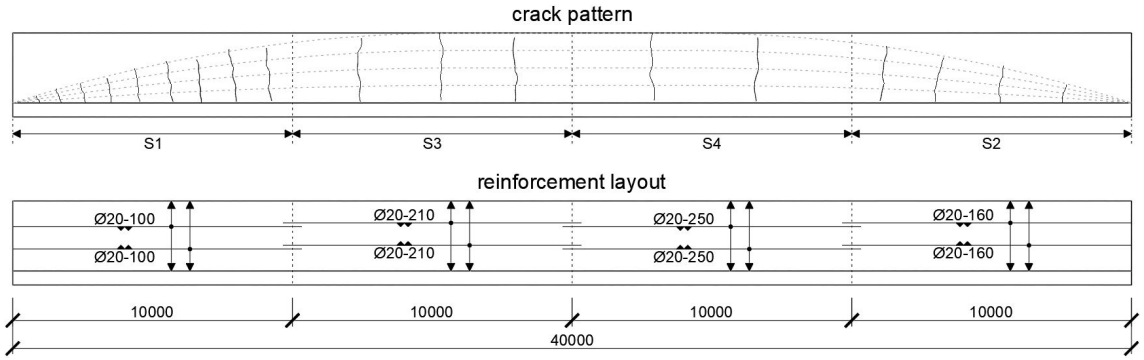

(a) Original section arrangement.

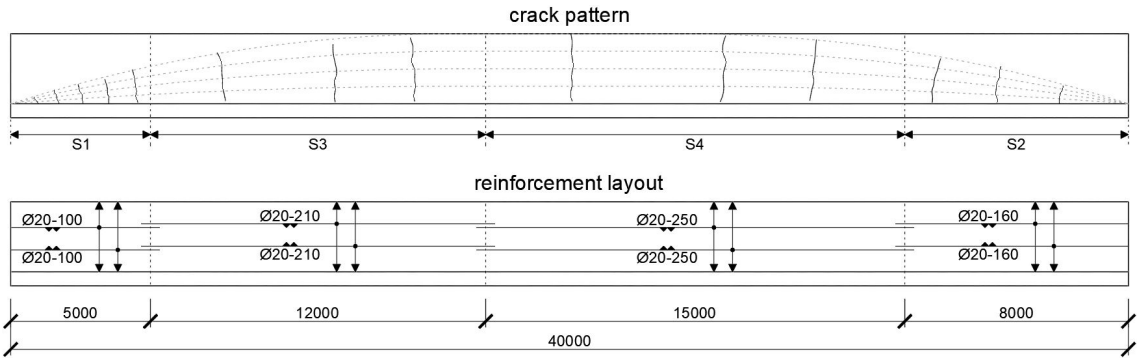

(b) Alternative section arrangement.

Figure 6.20: Crack pattern and reinforcement layout of side walls, dimensions in mm.

7 Analysis and discussion

In this chapter, the results presented throughout this thesis, as well as the way they were obtained, are critically analysed. First, the test results are interpreted and assessed for their reliability. In doing so, it is also reflected on the concrete mixtures and their respective designs. Second, the cracking calculations and prediction of crack widths are discussed, focusing on the consequence of the assumptions made on the accuracy and certainty of the determined probability and degree of cracking.

7.1 Concrete mixture and test results

The design of a concrete mixture intended for the side walls of the reservoir led to four different mixtures, varying in the filler and healing agent, all of which are suited due to the selection of ingredients and proportions based on predetermined design criteria. To fulfil the test objectives, several tests were conducted related to the fresh properties, strength development and autogenous shrinkage of these concrete mixtures. The observations and test results themselves were presented earlier in this thesis, this section is devoted to a detailed analysis of the test results (in relation to the test objectives).

7.1.1 Fresh properties

When it comes to the fresh properties of the concrete mixtures, a clear distinction has been observed between mixes 1 and 3 without filler and thus a fine content of 158 L/m^3 on the one hand, and mixes 2 and 4 with filler and as such a fine content of 188 L/m^3 on the other. While they are almost identical in terms of consistency according to the slump test, mixes 2 and 4 exhibit a higher consistency according to the flow table test and a slightly lower air content compared to mixes 1 and 3 (see Table 4.1). This lower air content also translates into a somewhat higher specific mass. Moreover, mixes 2 and 4 demonstrated less tendency to segregation (i.e. better cohesiveness). These test results are in accordance with the effects of an increased amount of fine material as reported in the literature study. What is more remarkable, though, is that with mixes 1 and 3 both the slump test and flow table test indicate a consistency equivalent to class F5, whereas with mixes 2 and 4 only the slump test indicates class F5, while the flow table test implies class F6. The most likely reason for this is that the slump test is not really suitable in this consistency range; the flow table test better demonstrates the true consistency. From this perspective, a lower dosage of superplasticizer for mixes 2 and 4 would have been better, as a consistency equivalent to class F5 was targeted. Nevertheless, despite this possible improvement, the fresh properties of all mixtures are quite consistent with their respective designs, emphasizing that the mixtures are more or less comparable in terms of processability. Finally, it is appropriate to highlight that, as expected, no significant effect of the addition of healing agent on the fresh properties has been observed.

7.1.2 Strength development

A similar correlation has been observed between the strength development of the concrete mixtures as with the fresh properties, that is, mixes 2 and 4 with filler manifest a superior strength development compared to mixes 1 and 3 without filler (see Figure 4.5). These test results are in accordance with more extensive research by Katz and Baum into the effects of a higher fine content [22]. At a similar increase in the amount of fine material, Katz and Baum report an increase in compressive strength (at the ages of 2, 7 and 28 days) of about 10%, which corresponds to the difference between the mixtures with and without filler in the form of limestone powder. The exact cause of this improved strength is still under debate, but it is generally attributed to a better packing density and a finer porosity of the cement paste, in combination with additional nucleation sites for the hydration of the cement [2, 22].

Even though these test results make sense, they can be questioned because the difference of 10% that was observed is merely based on the measured strength development in the first 7 days. Thereafter, mix 1 deviates from the observed trend. However, only a few specimens were tested after the age of 7 days. This was intentional as the strength development after this age is less important to the early-age cracking behaviour and because, due to limited resources, it was simply not possible to assess more specimens. As a result, the measured strength development beyond 7 days involves much uncertainty and should therefore only be interpreted as an indication. Having said that, given the results described in literature, it is to be expected that if more specimens were tested, mix 1 would continue to follow the observed trend. Furthermore, having tested just one specimen per mixture after 28 days also makes it difficult to truly verify the design strength of the concrete mixtures, which is expressed in a 28-day value. This normally requires at least three specimens per mixture. Nevertheless, the measured compressive strengths at the age of 28 days all well exceed the design strength (see Table 4.2), indicating that all mixtures are close to class C50/60, which was targeted.

As with the fresh properties, as expected, no significant effect of the addition of healing agent on the strength development has been observed. Note that this is particularly important because when the strength development of the mixtures with and without healing agent would differ, side wall A may exhibit a different cracking behaviour than side wall B, that is, both the probability and degree of cracking could vary. This would in turn make it difficult to compare the crack-sealing capacity of BSHC to that of ordinary concrete. But since this is not the case, it can be concluded that no improvement of the mixture composition is needed to compensate the strength development of the mixtures with and without healing agent.

7.1.3 Autogenous shrinkage

As for the autogenous shrinkage, the distinction that has been observed between the concrete mixtures is more complex than with the fresh properties and strength development. This is because not only filler seems to play a role, but also whether or not healing agent is added appears to influence the autogenous shrinkage of the mixtures. On the basis of the sequence of the mixtures with respect to the magnitude of autogenous shrinkage (see Figure 4.7), it can be inferred that the addition of filler causes an increase, while the addition of healing agent leads to a decrease in autogenous shrinkage. The former is consistent with the hypothesis that a higher fine content promotes autogenous shrinkage, because the cement paste is likely to have a finer porosity. Autogenous shrinkage of the mixtures with filler has been observed to be about 15% or 20% higher, depending on whether the difference between mixes 1 and 2 or mixes 3 and 4 is taken as a reference, respectively. At the same time, autogenous shrinkage of the mixtures with healing agent has been observed to be 20% or 25% lower, depending on whether the difference between mixes 2 and 4 or mixes 1 and 3 is taken as a reference, respectively. An explanation for the fact that healing agent reduces autogenous shrinkage has not been found.

Although the test results demonstrate a distinct effect of the addition filler and healing on autogenous shrinkage, the following inconsistencies and uncertainties should be borne in mind:

- The measured autogenous shrinkage of identical mixtures varies considerably from one specimen to another (see Figure 4.8). Some dispersion is normal, but at certain ages the range of the measurements of the same mixture is more than 15% of the mean, which is sometimes considered the upper limit of what is acceptable unless it can be justified. But then again, no explicit cause for the significant dispersion of the test results has been discovered.
- The measured autogenous shrinkage of mix 3 deviates substantially from the observed trend. A very likely reason for this is that, as mentioned earlier, less genuine recordings are available of mix 3 due to faulty measuring devices on two out of its three specimens. Therefore, as illustrated in Figure 7.1, the other measuring device on the same specimen does not record the actual shortening when it is not symmetrical (i.e. only the average of two measuring devices is truly reliable).
- The measured autogenous shrinkage is not corrected for drying, which manifests as weight loss. This is because, as no unsealed specimens were tested, the relationship between weight loss and drying shrinkage, which is specific to a concrete mixture, was unknown. Nevertheless, weighing revealed that the specimens lost less than 1 gram of weight in the first 7 days, indicating that drying plays a minor role in the test results.

It is recognized that these concerns reduce the reliability of the test results. Having said that, they still provide a comprehensive indication of the effect of the addition of filler and healing on autogenous shrinkage, even if the measured autogenous shrinkage of mix 3 is disregarded and only mixes 1, 2 and 4 are compared.

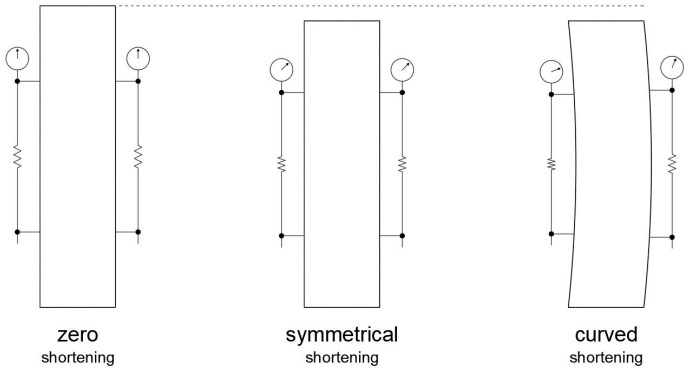

Figure 7.1: Schematic representation of various kinds of shortening of specimen.

The fact that the mixtures with healing agent exhibit less autogenous shrinkage may give the impression that the cracking behaviour of side wall A, which will be constructed from BSHC, could be different from that of side wall B (from ordinary concrete). While this is strictly true, it must be recalled that autogenous shrinkage is only responsible for about 15% of the imposed deformations (at the age at cracking); thermal shrinkage is far more significant in the case of the side walls of the reservoir. Accordingly, this is not really a cause for concern and no improvement of the mixture composition is needed to compensate the autogenous shrinkage of the mixtures with and without healing agent.

7.2 Cracking calculations

Both the probability and degree of cracking have been determined analytically. These cracking calculations were carried out according to a substantiated approach and, in doing so, certain assumptions have been made. In this section it is reflected on both the approach and assumptions, as well as their respective impacts on the results from the cracking calculations and prediction of crack widths, being the determined probability and degree of cracking. The different topics of this discussion are highlighted separately in the following paragraphs.

Heat of hydration and CTE

Due to limited resources, not all properties relevant to the early-age cracking behaviour of concrete could be determined experimentally and were therefore derived from literature. As a result, these properties, namely creep, heat of hydration and thermal properties such as the CTE, involve some uncertainty. This mainly concerns the heat of hydration and CTE, as these were found to most affect the probability of cracking. For the purpose of the cracking calculations, the heat of hydration was modelled founded on work by Bamforth. While this model for the adiabatic heat production provides reasonable accuracy, it only accounts for the type of cement used. If the model turns out to overestimate the heat of hydration, the temperature rise will be smaller, thereby reducing the probability of cracking. This is, in essence, the same as increasing the share of blastfurnace slag in cement, which results in a lower ultimate heat generation and heat production rate. The opposite holds in case the model underestimates the heat of hydration, or if there is less slag present. Such an underestimation is, for reasons discussed in section 5.2, also likely when the concrete mixture contains more fine material due to the addition of filler. But then again, this would only result in an even higher probability of cracking, which is desirable in this case.

As for the coefficient of thermal expansion, the probability of cracking may improve if the CTE is eventually found to be higher than the current value from literature. The surplus of the actions with respect to the resistance increases linearly with increasing CTE, since it only plays a role in the imposed deformations (i.e. actions). With the heat of hydration, this relationship is non-linear, as the consequent temperature development and distribution within the side walls also affects the strength development (i.e. resistance). While both the heat of hydration and CTE significantly affect the probability of cracking, their influence on the degree of cracking is minor. That is to say, deviations in these properties hardly affect the predicted crack width.

Temperature distribution

As discussed in section 5.3, the numerical model used to compute the temperature development and distribution within the side walls only considers one-dimensional heat transfer. While this is commonly believed to be an acceptable approach when the heat transfer primarily takes place along one direction, being the depth of the wall, it does somewhat compromise accuracy. This holds in particular near the end and top of the wall, as well as near the joint between the wall and the floor, where heat may also be transferred along either of

the two other directions (see Figure 7.2). Hence, the computed temperature development and distribution does not apply to those parts of the side walls of the reservoir. Nevertheless, the probability of cracking that is governing arises in the central part, where the highest temperature drop occurs and the relative error is insignificant, meaning this simplification is justified. Note that this also means that the predicted crack width is not likely to occur at the bottom, but at some distance above the joint between the wall and the floor. This is supported by Micallef, from whose experimental results it can also be inferred that heat dissipation to a concrete base is limited to a distance thereof equal to about the wall thickness, which in this case translates into approximately 500 mm above the joint between the wall and the floor [42].

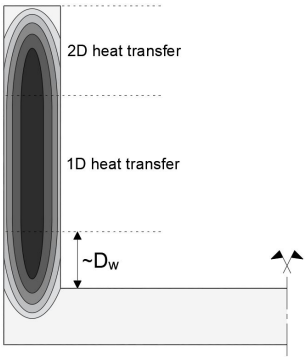

Figure 7.2: Schematic representation of two-dimensional temperature distribution (contour plot).

Degree of restraint

It should be remembered that for the purpose of the cracking calculations the degree of restraint 10 m from the center of the side walls and 500 mm above the joint between the wall and the floor has been taken as a reference. Hence, the anticipated probability of cracking essentially relates purely to the considered position. At another position the probability of cracking may deviate, because the degree of restraint varies along the height and length of the side walls. Table 7.1 presents the maximum probability of cracking depending on the degree of restraint, which in conjunction with Figure 5.18 gives an impression of the probability of cracking at another position. Having said that, the degree of restraint at the considered position is quite representative of the side walls of the reservoir as a whole, especially the lower regions (i.e. up to two-fifth the height of the wall). Therefore, the same holds for the anticipated probability of cracking.

Degree of restraint[5]	*Maximum probability of cracking*	
	Method I	*Method II*
0.2	0%	4%
0.3	7%	34%
0.4	30%	74%
0.5	61%	92%
0.6	81%	97%
0.7	92%	99%

Table 7.1: Maximum probability of cracking depending on degree of restraint.

The influence of the degree of restraint on the crack width is not as clear as its effect on the probability of cracking. This has to do with the fact that the prediction methods, whose fundamentals have been reviewed in detail in section 6.2, assess the degree of restraint differently. Only the methods founded on the continuous restraining model are influenced by the degree of restraint, as they consider the crack width to be linearly related to the imposed deformation being restrained. With the methods founded on the tensile member model, on the other hand, the crack width is a linear function of the steel strain in the cracks, which is not related to the degree of restraint unless the crack pattern is fully developed. Hence, which prediction methods turn out to be the most reliable, will reveal the true influence of the degree of restraint on the crack width. Having said that, it is recognized that the sum of the crack widths is proportional to the restrained shrinkage strain, which implies that the crack width becomes smaller when the degree of restraint decreases. Correspondingly, where the degree of restraint varies along the height of the wall, so does the crack width. Note that in this case, the predicted crack width refers to the largest crack width that appears over the full height.

[5] At $E_w/E_f = 0.93$, as in 72 hours after casting.

Strength development
The last point to be discussed is the fact that the cracking calculations are based on the average of the modelled strength development of all four concrete mixtures. This solution has been adopted because it is uncertain which mixtures will ultimately be preferred. If mixes 1 and 3 are used, whose strength development is inferior to the average of all four concrete mixtures, the probability of cracking will be higher. The opposite applies when mixes 2 and 4 are embraced, whose strength development is superior to the average of all four concrete mixtures. This may give the impression that the mixtures without filler are preferable to the mixtures with filler. However, the contrary is desirable from the perspective of the degree of cracking, as a higher strength (at the age at cracking) allows for larger crack widths. But then again, this is only supported by the methods founded on the tensile member model, as the methods founded on the continuous restraining model do not consider the steel stress in the cracks immediately after cracking.

7.3 Reinforcement layout

It is recognized that the reinforcement layout described in section 6.4 does not result in the various crack widths included in the proposed crack pattern. The minimum reinforcement limits the maximum crack width that can be achieved. A desired crack width of 0.70 mm can only be reached if the reinforcement steel is allowed to yield or, alternatively, if somehow no longitudinal reinforcement is applied at all (so that the crack spacing is proportional to the height of the wall). However, this is not suggested because the cracks are then essentially no longer controlled, that is, the imposed deformation is not distributed over multiple cracks. Moreover, in view of the intention to reuse L-shaped retaining wall pieces cut from the reservoir, it should be questioned whether it is desirable, let alone permitted, to ignore the minimum reinforcement.

Even though the various crack widths included in the proposed crack pattern are not exactly met, the crack widths are still sufficient to demonstrate the crack-sealing capacity and reinforcement reduction potential of BSHC. On the basis of the prediction of crack widths in relation to the reinforcement layout of the side walls, it is possible to derive the reinforcement reduction potential as a function of the crack-sealing capacity. This is shown in Figure 7.3, in which the reinforcement reduction potential, with respect to the crack-sealing capacity, is reckoned from the amount of reinforcement steel required to ensure that only crack widths up to 0.10 mm arise. From this it can be deduced that, for example, to save 60 kg/m^3 of longitudinal reinforcement with a bar diameter of 20 mm, the bacterial self-healing concrete should be capable of sealing cracks up to 0.18 mm in width. While this appears promising, the following should be kept in mind:

- The reinforcement reduction potential relates purely to the crack-limiting reinforcement, like the longitudinal reinforcement in the case of the side walls of the reservoir. Structural reinforcement installed to withstand tensile stress can never be omitted, regardless of the crack-sealing capacity.
- Accordingly, this relationship between the crack-sealing capacity and the reinforcement reduction potential cannot simply be generalized; it only holds in this case. Also, it does not apply to the transverse reinforcement required to ensure structural integrity of the reservoir.
- This relationship is based on the prediction of crack widths as outlined in this thesis, which means that its correctness is dependent on the reliability of the prediction methods. If the occurring crack width turns out to be smaller than the predicted crack width, the reinforcement reduction potential in relation to the crack-sealing capacity is less than suggested here.
- The full crack-sealing capacity does not occur immediately; it takes time before cracks are closed completely. Hence, when choosing BSHC and reducing the amount of crack-limiting reinforcement, it should always be assessed whether the presence of cracks for a short period after their occurrence is acceptable.

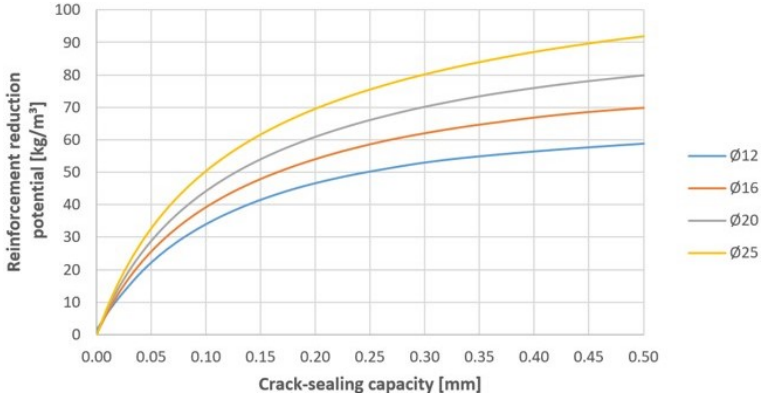

Figure 7.3: Relationship between crack-sealing capacity and reinforcement reduction potential.

8

Conclusions and recommendations

In this final chapter, the conclusions and recommendations of this research are summarized. The conclusions relate to the objective of this thesis itself, but also to the results that were obtained in the process. The conclusions are followed by the presentation of the recommendations, distinguishing between recommendations as to what can be done to increase the chance that the demonstrator project becomes a success, and recommendations for future research in general.

8.1 Conclusions

Based on the first part of this thesis, related to the design and testing of the concrete mixtures intended for the side walls, the following conclusions have been drawn:

- The four different mixtures are all suitable for the side walls of the reservoir. For side wall A that will be constructed from BSHC either mix 3 or 4 can be used, while for side wall B (from ordinary concrete) either mix 1 or 2 is applicable. To meet the design criteria, all concrete mixtures have a cement content of 418 kg/m^3 (26% of CEM I 52.5 R and 74% of CEM III/B 42.5 N) and a water cement-ratio of 0.407. The combination of Portland and blastfurnace cement ensures healing agent compatibility and sufficient heat output, and at the same time satisfies the requirements regarding the prevention of ASR.

- At the same dosage of superplasticizer equal to 0.40% of the cement mass, mixes 2 and 4 with filler (i.e. in which limestone powder replaces some of the aggregates to increase the fine content by about 20%) exhibit a higher consistency and improved cohesiveness compared to the mixes 1 and 3 without filler. The fresh properties were not affected by the addition of healing agent.

- The mixtures with filler demonstrate a more prosperous strength development compared to the mixtures without filler, that is, the compressive strength at any age is increased by about 10%. The strength development was not affected by the addition of healing agent. The average of all mixtures in terms of compressive strength at the ages of 1, 3 and 7 days corresponds to 18, 31 and 48 MPa, respectively.

- The addition of filler causes autogenous shrinkage to increase by about 15%, whereas the addition of healing agent causes autogenous shrinkage to decrease by about 20%. The average of all mixtures in terms of autogenous shrinkage at the ages of 3, 7 and 28 days corresponds to 50, 92 and 124 $\mu\varepsilon$, respectively. Accordingly, the autogenous shrinkage of these mixtures is approximately 1.5 to 2.5 times larger than prescribed by the NEN-EN 1992-1-1.

Based on the second part of this thesis, related to the cracking calculations and prediction of crack widths in relation to the reinforcement layout of the side walls, the following conclusions have been drawn:

- Cement hydration causes a large temperature rise, resulting in an accelerated strength development in the first few days, as well as significant thermal shrinkage due to the subsequent temperature drop. In the case of the side walls of the reservoir, thermal shrinkage is responsible for about 85% of the imposed deformations at an early-age, with autogenous shrinkage accounting for the difference. The imposed deformations are restrained by the floor of the reservoir, as well as the foundation material underneath. The degree of restraint varies along the height and length of the side walls, but overall matches 0.52.

- The maximum probability of cracking according to method I, which compares the tensile strain capacity to the restrained shrinkage strain, corresponds to 65% and arises after approximately 96 hours. Method II, which compares the mean concrete stress to the effective tensile strength, anticipates the maximum probability of cracking to be 93% after about 72 hours. Hence, it is very likely that early-age cracking of the side walls of the reservoir occurs as a consequence of imposed deformations.

- The longitudinal reinforcement of the side walls of the reservoir can best be distributed in the manner reported in Table 8.1. This reinforcement layout does not result in the various crack widths included in the proposed crack pattern. The occurrence of larger crack widths is prevented by minimum reinforcement. S4 reflects the maximum crack width that can be achieved as it is closest to the minimum reinforcement ratio of 0.48%. The longitudinal reinforcement distributions of S1, S2 and S3 ensure that the differences between the sections in terms of crack width are approximately equal.

	Longitudinal reinforcement		*Predicted crack width (mm)*	
	Ratio	*Distribution*	*Mean*	*Charact.*
S1	1.26%	∅20–100	0.09	0.13
S2	0.79%	∅20–160	0.20	0.26
S3	0.60%	∅20–210	0.31	0.41
S4	0.50%	∅20–250	0.43	0.56

Table 8.1: Abstract of reinforcement layout of side walls and prediction of crack widths.

- The predicted crack width in Table 8.1 is based on a concrete cover to the longitudinal reinforcement of 70 mm and relates to the average of all prediction methods. The mutual differences between the prediction methods are very large, in particular at lower reinforcement ratios. The methods founded on the continuous restraining model are far more conservative, so to speak, than those founded on the tensile member model. This makes it particularly difficult to assess the occurring crack width in advance.

- The probability of cracking is very sensitive to changes in the mixture composition, environmental conditions, structural dimensioning and construction practice. The same applies to the crack width, albeit to a lesser extent and depending on the prediction method. Therefore, it is imperative that the demonstrator project roughly fulfils the circumstances set out in this thesis on which the anticipated probability of cracking is based, such as the use of plywood formwork that is removed 24 hours after casting.

8.2 Recommendations

The knowledge acquired from the cracking calculations and prediction of crack widths has been converted into recommendations for the demonstrator project, in terms of various aspects that contribute to a higher probability of cracking and the proposed crack pattern. In addition, considerations are given on future research for which this thesis may form a starting point.

8.2.1 Demonstrator project

- It is recommended to take active measures to further increase the probability that early-age cracking of the side walls of the reservoir occurs as a result of imposed deformations. For example, maximizing the time between casting the floor of the reservoir and the side walls, preheating the ingredients of the concrete mixture to increase the mix temperature, applying formwork with high insulation capacity, and casting when the highest ambient temperature occurs.

- Apply the same quality concrete for the floor of the reservoir as for the side walls to decrease the quotient E_w/E_f, which in turn increases the degree of restraint and therefore the probability of cracking. In addition, it is advisable to reduce the restraint against curvature around the z-axis as much as possible to allow cracks to appear over the full height. This can be accomplished by choosing rigid foundation material such as dense sand, gravel or a combination thereof.

- Rather than the original section arrangement in which all sections are equally long, it is recommended to adopt an alternative section arrangement in which the section length is adjusted so that the number of cracks that is likely to emerge is evenly distributed across all sections. More specifically, a section length of 5, 8, 12 and 15 m for S1, S2, S3 and S4, respectively.

- A greater concrete cover to the longitudinal reinforcement tends to lead to a larger crack width. Hence, it is advisable to let the transverse reinforcement occupy the first layer and the longitudinal reinforcement the second layer. Moreover, a concrete cover that well exceeds the minimum value prescribed for durability reasons is desirable.

- Although both the mixtures with and without filler are suitable for the side walls of the reservoir, it is recommended to use the mixtures with filler as they are likely to reflect a higher concrete strength when cracks occur, thereby allowing for larger crack widths. Furthermore, they exhibit increased autogenous shrinkage and greater heat output, albeit the latter is merely a theory and has not been proven. However, in doing so, it should be looked at to improve the dosage of superplasticizer such that the desired workability is obtained (i.e. the current consistency of these mixtures does not meet class F5).

8.2.2 Future research

- This thesis has revealed that the mutual differences between the prediction methods are very large. Therefore, a lot of insight is to be gained from monitoring the occurring crack width and comparing it to the predicted crack width. Back analysis of this data will reveal which prediction method best assessed the occurring crack width and may contribute to the ongoing debate as to what would be the appropriate method. This should be resolved after the reservoir has been constructed.

- All prediction methods suggest that reducing the concrete cover leads to a smaller crack width, but by how much varies significantly. Moreover, in much of the literature studied, the true influence of the concrete cover on the crack width is questioned, especially in cases similar to the side walls of the reservoir. An investigation into the effect of the concrete cover could provide the necessary clarification.

- The test results indicate that healing agent reduces autogenous shrinkage of concrete. However, the empirical evidence for this is 'thin' due to, among other reasons, faulty measuring devices. Accordingly, future research is needed to verify and explain this phenomenon.

Bibliography

[1] T. Verheijen, Cobouw, 'Nieuwe trend: scheuren managen met zelfhelend beton', 28 March 2018. URL: https://www.cobouw.nl/bouwbreed/nieuws/2018/03/nieuwe-trend-scheuren-managen-met-zelfhelend-beton-101259446_ga=2.97450780.2098496156.1587464465-1541767990.1587464465.

[2] A.M. Neville, *Properties of Concrete*, 5th ed. Harlow, United Kingdom: Pearson Education Limited, 2011. ISBN: 9780273755807.

[3] H.M. Jonkers, 'Bacteria-based self-healing concrete', *HERON*, vol. 56, no. 1/2, 2011. URL: https://repository.tudelft.nl/islandora/object/uuid%3A8326f8b3-a290-4bc5-941d-c2577740fb96.

[4] M. Megalla, 'Bacteria based self-healing concrete', MSc. thesis, Faculty of Civil Engineering and Geosciences, Delft University of Technology, 2017. URL: https://repository.tudelft.nl/islandora/object/uuid%3A90b616df-d43c-475e-8963-394869461807?collection=education.

[5] H.M. Jonkers and R.M. Mors, 'Bacteria-Based Self-Healing Concrete: Towards Standardization', *Research and Development in Material Science (RDMS)*, vol. 10, no. 2, 2019. DOI: 10.31031/RDMS.2019.10.000732.

[6] H.M. Jonkers, 'Zelfherstellend beton, nuttig of noodzaak? Eerste praktijkprojecten van start', *Betoniek*, vol. 2, 2018. URL: https://www.betoniek.nl/zelfherstellend-beton-nuttig-of-noodzaak.

[7] C.R. Braam, K. Van Breugel, J. Niemantsverdriet, C. Van Veen and J.C. Walraven, 'Design and proportioning of liquid retaining structures', *Translation of original Dutch book (2001): Ontwerpen en dimensioneren van vloeistofkerende constructies*, n.d.

[8] *Cement - Deel 1: Samenstelling, specificaties en conformiteitscriteria voor gewone cementsoorten*, NEN-EN 197-1, Nederlands Normalisatie Instituut, Delft, The Netherlands, 2011.

[9] ENCI, 'Productieproces cement', Online video, 7 February 2017. URL: https://www.youtube.com/watch?time_continue=158&v=Q27gG5GGbsA&feature=emb_title.

[10] H.W. Reinhardt, *Beton als constructiemateriaal: eigenschappen en duurzaamheid*. Delft, The Netherlands: Delftse Universitaire Pers, 1985. ISBN: 9789062751655.

[11] R.H. Bogue, *The chemistry of Portland cement*, 2nd ed. New York, United States: Reinhold Publishing Corporation, 1955.

[12] Portland Cement Association, 'Concrete Information: Ettringite Formation and the Performance of Concrete', *PCA R&D Serial*, no. 2166, 2001. URL: https://www.cement.org/docs/default-source/fc_concrete_technology/is417-ettringite-formation-and-the-performance-of-concrete.pdf?sfvrsn=412%26sfvrsn=412

[13] G. Fagerlund, 'Relations between the strength and degree of hydration and porosity of cement paste, cement mortar, and concrete', *Proceedings of seminar on hydration of cement (Copenhagen, Denmark)*, 1987.

[14] *Beton - Specificatie, eigenschappen, vervaardiging en conformiteit*, NEN-EN 206, Nederlands Normalisatie Instituut, Delft, The Netherlands, 2016.

[15] M. Janssens, Geologie van Nederland, 'Zand', n.d. URL: https://https://www.geologievannederland.nl/ondergrond/afzettingen-en-delfstoffen/zand.

[16] M. Janssens, Geologie van Nederland, 'Grind', n.d. URL: https://www.geologievannederland.nl/ondergrond/afzettingen-en-delfstoffen/grind.

[17] *Beproevingsmethoden voor geometrische eigenschappen van toeslagmaterialen - Deel 2: Bepaling van de korrelgrootteverdeling - Controlezeven, nominale afmetingen van de openingen*, NEN-EN 933-2, Nederlands Normalisatie Instituut, Delft, The Netherlands, 1996.

[18] ENCI, Mebin and Sagrex, *Betonpocket 2016*, 7th ed. 's-Hertogenbosch, The Netherlands, 2015.

[19] *Nederlandse invulling van NEN-EN 206: Beton - Specificatie, eigenschappen, vervaardiging en conformiteit*, NEN 8005, Nederlands Normalisatie Instituut, Delft, The Netherlands, 2017.

[20] *Maatregelen ter verkoming van betonschade door alkali-silica reactie (ASR)*, CUR-Aanbeveling 89, CROW, Ede, The Netherlands, 2017.

[21] G.H. Tattersall and P.F.G. Banfill, *The rheology of fresh concrete*. London, United Kindom: Pitman Books Limited, 1983. ISBN: 9780273085584.

[22] A. Katz and H. Baum, 'Effect of High Levels of Fines Content on Concrete Properties', *ACI Materials Journal*, vol. 103, no. 6, 2006. URL: https://www.researchgate.net/publication/285641228_Effect_of_high_levels_of_fines_content_on_concrete_properties.

[23] M. Soutsos, F. Kanavaris and A. Hatzitheodorou, 'Critical analysis of strength estimates from maturity functions', *Case Studies in Construction Materials*, vol. 9, 2018. DOI: 10.1016/j.cscm.2018.e00183.

[24] *Bepaling van de druksterkte-ontwikkeling van jong beton op basis van de gewogen rijpheid*, NEN 5970, Nederlands Normalisatie Instituut, Delft, The Netherlands, 2001.

[25] R. Wasserman, A. Katz and A. Bentur, 'Minimum cement content requirements: a must or a myth?', *Materials and Structures*, vol. 42, 2009. DOI: 10.1617/s11527-008-9436-0.

[26] E.E. Holt, *Early age autogenous shrinkage of concrete*, VTT Publication 446. Espoo, Finland: Technical Research Centre of Finland (VTT), 2001. ISBN: 9789513858704.

[27] K. Van Breugel, C.R. Braam, C. van der Veen and J.C. Walraven, 'Concrete Structures under Imposed Thermal and Shrinkage Deformations - Theory and Practice', *Translation of the original book (1994): Betonconstructies onder Temperatuur- en Krimpvervormingen*, 2016.

[28] E. Tazawa, *Autogenous Shrinkage of Concrete*. London, United Kingdom: E & FN Spon, 1999. ISBN: 9780419238904.

[29] Basilisk, *Product Data Sheet: Basilisk Healing Agent*, 17 January 2019. URL: https://www.basiliskconcrete.com/wp-content/uploads/2019/12/20190117_HA_PDS_Product-Data-Sheet.pdf

[30] Cugla, *Product Information Brochure: CUGLA LR-9800 con.30% SPL*, 11 November 2018. URL: https://www.cugla.nl/upload/Hulpstoffen/Superplastificeerders/LR/PIB%20LR-9800%20SPL%20-%2020180711.pdf

[31] *Eurocode 2: Ontwerp en berekening van betonconstructies - Deel 1-1: Algemene rekenregels voor gebouwen*, NEN-EN 1992-1-1, Nederlands Normalisatie Instituut, Delft, The Netherlands, 2011.

[32] P.B. Bamforth, *Early-age thermal crack control in concrete*, Ciria C660. London, United Kingdom: CIRIA, 2007. ISBN: 9780861076602.

[33] E. Martinelli, E.A.B. Koenders and A. Caggiano, 'A numerical recipe for modelling hydration and heat flow in hardening concrete', *Cement & Concrete Composites*, vol. 40, 2013. URL: https://www.sciencedirect.com/science/article/pii/S0958946513000516.

[34] K. Van Breugel, 'Relaxation of young concrete', *Research report by Delft University of Technology*, 1980.

[35] M. Nilsson, 'Restraint factors and partial coefficients for crack risk analyses of early age concrete structures', PhD. thesis, Department of Civil and Mining Engineering, Luleå University of Technology, 2003. URL: https://www.semanticscholar.org/paper/Restraint-factors-and-partial-coefficients-for-risk-Nilsson/e1e80366e6f3a0c4c18ad9c4b2e92356653ce10d.

[36] M. Dijk, 'Berekenen scheurvorming in de praktijk', *Cement*, vol. 7, 2017. URL: https://www.cementonline.nl/berekenen-scheurvorming-in-de-praktijk.

[37] S. Röhling, *Zwangspannungen infolge Hydratationswärme*. Düsseldorf, Germany: Verlag Bau + Technik, 2009. ISBN: 9783764005009.

[38] *Eurocode 2: Ontwerp en berekening van betonconstructies - Deel 3: Constructies voor keren en opslaan van stoffen*, NEN-EN 1992-3, Nederlands Normalisatie Instituut, Delft, The Netherlands, 2006.

[39] J. Walraven et al., *Model Code for Concrete Structures 2010*. Lausanne, Switzerland: Fédération internationale du béton (FIB), 2013. ISBN: 9783433030615.

[40] P.B. Bamforth, S. Denton and J. Shave, 'The development of a revised unified approach for the design of reinforcement to control cracking in concrete resulting from restrained contraction', *Technical report of ICE research project 0706*, 2010.

[41] A.W. Beeby, 'The prediction of crack widths in hardened concrete', *The Structural Engineer*, vol. 57A, no. 1, 1979. URL: https://www.scribd.com/doc/275718621/A-W-Beeby-The-Prediction-of-Crack-Widths-in-Hardened-Concrete

[42] M. Micallef, 'Crack control in base-restrained reinforced concrete walls', PhD. thesis, Department of Civil and Environmental Engineering, Imperial College London, 2015. URL: https://spiral.imperial.ac.uk/handle/10044/1/55245.

A

Compositions of concrete mixtures

A.1 Mix 1

General					
Total volume	1000	L	Aggregate content (dry)	1764	kg
Design strength	61	MPa	Sand (relative to aggregates)	45	%
Design slump size	240	mm	Maximum grain size	16.0	mm
Water-binder ratio	0.407		Fineness modulus	5.04	
Water-cement ratio	0.407		Air content	15	L
Cement content	418	kg	Filler content	0	L
Water requirement	170	kg	Admixture content	1.6	L
Absorbed water	23	L	Fine content	158	L
Adsorbed water	0	L	Chloride content (estimate)	0.51	kg
Mixing water	170	L	Alkali content (estimate)	3.52	kg

	Dry mass	Dosage mass	Dosage volume	Fine volume	Share (V/V)
	kg	kg	L	L	
Cement	**418**	**418**	**140**	**140**	**14.0%**
CEM I 52.5R	109	109	35	35	3.5%
CEM III/B 42.5N - LH/SR	309	309	105	105	10.5%
Aggregate	**1764**	**1786**	**673**	**18**	**67.3%**
River sand 0/4	794	797	302	18	30.2%
River gravel 4/16	970	989	372	0	37.2%
Admixture	**1.7**	**1.7**	**1.6**	**0.0**	**0.16%**
CUGLA LR-9800 con.30% SPL	1.7	1.7	1.6	0.0	0.16%
Mixing water	**170**	**170**	**170**	**0**	**17.0%**
Tap water	170	170	170	0	17.0%
Air	0	0	15	0	1.5%
Total	**2354**	**2376**	**1000**	**158**	**100%**

Figure A.1: Detailed composition of concrete mix 1.

A.2 Mix 2

General

Total volume	1000	L	Aggregate content (dry)	1684	kg
Design strength	61	MPa	Sand (relative to aggregates)	45	%
Design slump size	240	mm	Maximum grain size	16.0	mm
Water-binder ratio	0.407		Fineness modulus	5.04	
Water-cement ratio	0.407		Air content	15	L
Cement content	418	kg	Filler content	31	L
Water requirement	170	kg	Admixture content	1.6	L
Absorbed water	22	L	Fine content	188	L
Adsorbed water	0	L	Chloride content (estimate)	0.51	kg
Mixing water	170	L	Alkali content (estimate)	3.55	kg

	Dry mass	Dosage mass	Dosage volume	Fine volume	Share (V/V)
	kg	kg	L	L	
Cement	**418**	**418**	**140**	**140**	**14.0%**
CEM I 52.5R	109	109	35	35	3.5%
CEM III/B 42.5N - LH/SR	309	309	105	105	10.5%
Aggregate	**1684**	**1705**	**643**	**17**	**64.3%**
River sand 0/4	758	761	288	17	28.8%
River gravel 4/16	926	945	355	0	35.5%
Filler	**84**	**84**	**31**	**31**	**3.1%**
Limestone powder	84	84	31	31	3.1%
Admixture	**1.7**	**1.7**	**1.6**	**0.0**	**0.16%**
CUGLA LR-9800 con.30% SPL	1.7	1.7	1.6	0.0	0.16%
Mixing water	**170**	**170**	**170**	**0**	**17.0%**
Tap water	170	170	170	0	17.0%
Air	0	0	15	0	1.5%
Total	**2357**	**2378**	**1000**	**188**	**100%**

Figure A.2: Detailed composition of concrete mix 2.

A.3 Mix 3

General

Total volume	1000	L	Aggregate content (dry)	1748	kg
Design strength	61	MPa	Sand (relative to aggregates)	45	%
Design slump size	240	mm	Maximum grain size	16.0	mm
Water-binder ratio	0.407		Fineness modulus	5.04	
Water-cement ratio	0.407		Air content	15	L
Cement content	418	kg	Filler content	0	L
Water requirement	170	kg	Admixture content	7.6	L
Absorbed water	22	L	Fine content	158	L
Adsorbed water	0	L	Chloride content (estimate)	0.51	kg
Mixing water	170	L	Alkali content (estimate)	3.52	kg

	Dry mass	Dosage mass	Dosage volume	Fine volume	Share (V/V)
	kg	kg	L	L	
Cement	**418**	**418**	**140**	**140**	**14.0%**
CEM I 52.5R	109	109	35	35	3.5%
CEM III/B 42.5N - LH/SR	309	309	105	105	10.5%
Aggregate	**1748**	**1770**	**667**	**18**	**66.7%**
River sand 0/4	787	790	299	18	29.9%
River gravel 4/16	961	981	368	0	36.8%
Admixture	**9.2**	**9.2**	**7.6**	**0.0**	**0.76%**
CUGLA LR-9800 con.30% SPL	1.7	1.7	1.6	0.0	0.16%
Basilisk Healing Agent	7.5	7.5	6.0	0.0	0.60%
Mixing water	**170**	**170**	**170**	**0**	**17.0%**
Tap water	170	170	170	0	17.0%
Air	0	0	15	0	1.5%
Total	**2345**	**2368**	**1000**	**158**	**100%**

Figure A.3: Detailed composition of concrete mix 3.

A.4 Mix 4

General

Total volume	1000 L	Aggregate content (dry)	1668 kg
Design strength	61 MPa	Sand (relative to aggregates)	45 %
Design slump size	240 mm	Maximum grain size	16.0 mm
Water-binder ratio	0.407	Fineness modulus	5.04
Water-cement ratio	0.407	Air content	15 L
Cement content	418 kg	Filler content	31 L
Water requirement	170 kg	Admixture content	7.6 L
Absorbed water	21 L	Fine content	188 L
Adsorbed water	0 L	Chloride content (estimate)	0.51 kg
Mixing water	170 L	Alkali content (estimate)	3.54 kg

	Dry mass	Dosage mass	Dosage volume	Fine volume	Share (V/V)
	kg	kg	L	L	
Cement	**418**	**418**	**140**	**140**	**14.0%**
CEM I 52.5R	109	109	35	35	3.5%
CEM III/B 42.5N - LH/SR	309	309	105	105	10.5%
Aggregate	**1668**	**1689**	**637**	**17**	**63.7%**
River sand 0/4	751	754	285	17	28.5%
River gravel 4/16	917	936	351	0	35.1%
Filler	**84**	**84**	**31**	**31**	**3.1%**
Limestone powder	84	84	31	31	3.1%
Admixture	**9.2**	**9.2**	**7.6**	**0.0**	**0.76%**
CUGLA LR-9800 con.30% SPL	1.7	1.7	1.6	0.0	0.16%
Basilisk Healing Agent	7.5	7.5	6.0	0.0	0.60%
Mixing water	**170**	**170**	**170**	**0**	**17.0%**
Tap water	170	170	170	0	17.0%
Air	0	0	15	0	1.5%
Total	**2349**	**2370**	**1000**	**188**	**100%**

Figure A.4: Detailed composition of concrete mix 4.

B

Strength-maturity calibration curves

The calibration curves are described by Equation B.1, where $f_{cm,cube}(M_w)$ is the mean cube compressive strength at weighted maturity M_w in °Ch. For the purpose of curve fitting, the weighted maturity according to Equation 2.17 is determined on the basis of the reference temperature of 20 °C (i.e. storage temperature of specimens) and the C-value given in Table 5.2. Coefficient A is determined individually for each concrete mixture using the method of least squares, whereas coefficient B is determined collectively for all mixtures using the same method. As explained earlier, the measured compressive strengths at the ages of 14 and 28 days are not included in curve fitting. As a result, the calibration curves are shown in Figure B.1 and the corresponding coefficients and relative errors are specified in Table B.1.

$$f_{cm,cube}(M_w) = A + B \log_{10}(M_w \cdot 10^{-3}) \tag{B.1}$$

	Mix 1	*Mix 2*	*Mix 3*	*Mix 4*	*Average*
Coefficient A (MPa)	24	26	23	26	25
Coefficient B	31	31	31	31	31
Total R^2	0.018	0.043	0.057	0.037	0.039
Mean R^2	0.003	0.007	0.009	0.006	0.006

Table B.1: Coefficients and relative errors belonging to calibration curves of Equation B.1.

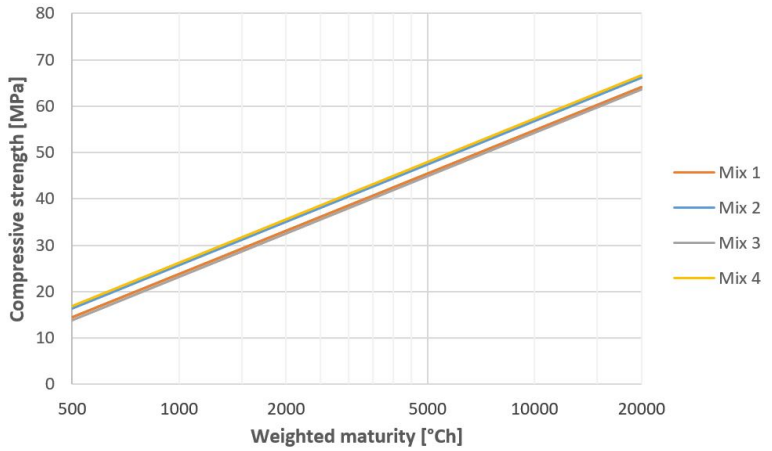

Figure B.1: Strengh-maturity calibration curves.

C

Estimation of thermal properties

The thermal properties applied in the cracking calculations have been estimated from the thermal properties of the individual ingredients (except superplasticizer) and their relative proportions in mix 1, following the techniques described in the Ciria C660 [32]. The thermal properties have been established at a degree of hydration α equal to 0.35, which is reached at an early-age (i.e. after about 24 hours according to Figure 5.12) and is roughly the average value during the period of the large temperature rise and subsequent cooling. Because the precise thermal properties of the individual ingredients incorporated in the concrete mixtures are not known, approximate values for cement, water and aggregates have been extracted from literature [10, 32]. The values for the aggregates are thereby taken as the average of quartz (sand) and flint (gravel), because these are predominantly retrieved from river deposits in the Netherlands [15, 16].

Thermal conductivity

The estimation of the thermal conductivity is divided into the determination of the initial thermal conductivity λ_{ci} (i.e. at zero hydration) provided in Table C.1, which is then converted to the thermal conductivity λ_c at the appropriate degree of hydration. The latter is done by means of Equation C.1, which is stated in the Ciria C660, where α_{ult} is the ultimate degree of hydration of 0.85 that can be expected according to Equation D.8 based on the water/cement ratio and cement type of the concrete mixtures. Consequently, the early-age value of the thermal conductivity corresponds to 2.51 W/m·K.

Ingredient	*Proportion* (L/m^3)	*Thermal conductivity* $(W/m{\cdot}K)$
Cement	140	1.85
Water	170	0.60
Aggregates	637	3.85
Total	**983**	**3.00**

Table C.1: Estimation of initial thermal conductivity based on mixture composition.

$$\lambda_c = \frac{\lambda_{ci}}{1.33 - 0.33 \cdot (\alpha/\alpha_{ult})} \tag{C.1}$$

Specific heat

In the estimation of the specific heat c_c given in Table C.2, the appropriate degree of hydration has already been taken into account by distinguishing between free and bound water and their respective differences in specific heat. This indicates an early-age value of the specific heat of 1.01 kJ/kg·K.

Ingredient	*Proportion* (kg/m^3)	*Specific heat* $(kJ/kg{\cdot}K)$
Cement	418	0.87
Water - free	110	4.18
Water - bound	60	2.22
Aggregates	1786	0.80
Total	**2376**	**1.01**

Table C.2: Estimation of specific heat based on mixture composition.

D

Numerical model for heat transfer

The numerical model set up for the computation of the temperature development and distribution within the side walls is based on the finite difference (FD) method. In this way, the simplified PDE of Equation 5.8 has been converted into FD expressions in each node of an age-space mesh that is displayed in Figure D.1. The space domain (denoted by n) divides the wall into spaces with a thickness Δz equal to one-tenth the wall thickness. If then the age increment Δt of the age domain (denoted by i) satisfies Equation D.1 (to obtain a stable solution to the PDE), the concrete temperature $T_{n,i+1}$ at the $(n, i+1)$-node can be computed according to Equation D.2 [27, 33]. The surface concrete temperature can be computed by including the boundary conditions in the FD expression, which results in Equation D.3, where $T_{am,i}$ and G_i are the ambient temperature and thermal surface conductance at age t_i, respectively. Because the boundary conditions are symmetrical, the numerical model only considers half the wall thickness, meaning the core concrete temperature can be computed according to Equation D.4. Naturally, the initial conditions include $T_{n,0} = T_{mix}$ for every n.

$$\Delta t = \frac{0.5 \cdot \Delta x^2}{a_c} \tag{D.1}$$

$$T_{n,i+1} = \frac{T_{n+1,i} + T_{n-1,i}}{2} + \frac{C_c \cdot \Delta Q_{n,i}}{\rho_c \cdot c_c} \tag{D.2}$$

$$T_{0,i+1} = T_{am,i} + \frac{a_c \cdot \left(T_{1,i} + T_{am,i}\right)}{a_c + G_i \cdot \Delta z} + \frac{C_c \cdot \Delta Q_{0,i}}{\rho_c \cdot c_c} \tag{D.3}$$

$$T_{5,i+1} = T_{4,i} + \frac{C_c \cdot \Delta Q_{5,i}}{\rho_c \cdot c_c} \tag{D.4}$$

The heat increment $\Delta Q_{n,i}$ over age increment Δt_i can be computed for every n through Equation D.5, which conforms to the FD scheme presented in Figure D.1, where $\Delta Q_{ad,eq,n,i}$ is the heat increment under adiabatic conditions at the equivalent age that reflects the corresponding degree of hydration [27, 33]. Likewise, $\Delta T_{ad,eq,n,i}$ represents the concrete temperature under adiabatic conditions at equivalent age $t_{eq,n,i}$, whose definition is based on the degree of hydration $\alpha_{n,i}$ evolved at the (n, i)-node. This degree of hydration has been assessed by means of Equation D.6, where the heat generated $Q_{n,i}$ is found by summation of the preceding heat increments. The equivalent age can then be obtained by searching for the identical degree of hydration $\alpha_{ad,eq,n,i}$ under adiabatic conditions, which complies with Equation D.7. Since in practice, for reasons discussed in the literature study, complete hydration does not occur, the definition of the degree of hydration includes the ultimate degree of hydration α_{ult} of 0.85 that can be expected based on the water/cement ratio and cement type of the concrete mixtures. To establish the ultimate degree of hydration, the relationship reported in the Ciria C660 has been applied, which is given in Equation D.8 [32].

$$\Delta Q_{n,i} = \Delta Q_{ad,eq,n,i} \cdot \exp\left[-\frac{E_A}{R_g} \cdot \frac{T_{ad,eq,n,i} - T_{n,i}}{T_{ad,eq,n,i} \cdot T_{n,i}}\right] \tag{D.5}$$

$$\begin{aligned} \alpha_{n,i} &= \alpha_{ult} \cdot \frac{Q_{n,i}}{Q_{ult}} \\ Q_{n,i} &= \sum \Delta Q_{n,i} \end{aligned} \tag{D.6}$$

$$\alpha_{ad,eq,n,i} = \alpha_{ult} \cdot \frac{Q_{ad,eq,n,i}}{Q_{ult}} \tag{D.7}$$

$$\alpha_{ult} = \frac{1.031 \cdot wcr}{0.194 + wcr} + 0.3 \cdot p_{GGBS} \tag{D.8}$$

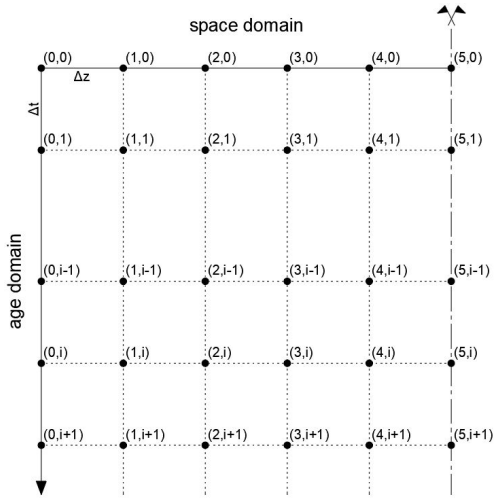

(a) FD age-space mesh.

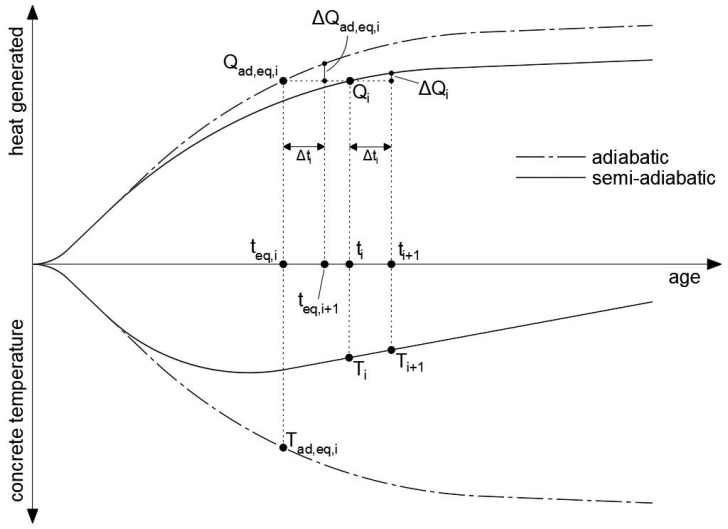

(b) FD scheme.

Figure D.1: Schematic representation of numerical model for heat transfer.

E

Transformed cross-sectional properties

The definitions of the transformed cross-sectional properties required for Nilsson's expression for the degree of restraint of a wall located on the edge of a floor (i.e. Equation 5.21) are provided below [35]. The reader is referred to Figure 5.15 for the designation of the structural parameters.

$$y_{cen} = \frac{\frac{H}{2} - \frac{D_f}{2} \cdot \frac{E_f}{E_w} \cdot \frac{A_f}{A_w}}{1 + \frac{E_f}{E_w} \cdot \frac{A_f}{A_w}} \tag{E.1}$$

$$z_{cen} = \frac{\frac{B_{ef} - D_w}{2}}{1 + \frac{E_f}{E_w} \cdot \frac{A_f}{A_w}} \tag{E.2}$$

$$A_{trans} = A_w + \frac{E_f}{E_w} \cdot A_f \tag{E.3}$$

$$I_{trans,y} = A_w \cdot \left[\frac{{D_w}^2}{12} + \left(z_{cen} - \frac{B_{ef} - D_w}{2} \right)^2 + \frac{E_f}{E_w} \cdot \frac{A_f}{A_w} \cdot \left(\frac{{B_{ef}}^2}{12} + {z_{cen}}^2 \right) \right] \tag{E.4}$$

$$I_{trans,z} = A_w \cdot \left[\frac{H^2}{12} + \left(y_{cen} - \frac{H}{2} \right)^2 + \frac{E_f}{E_w} \cdot \frac{A_f}{A_w} \cdot \left(\frac{{D_f}^2}{12} + \left(y_{cen} + \frac{D_w}{2} \right)^2 \right) \right] \tag{E.5}$$

F

Rotational boundary restraint

Nilsson identified Equation F.1 from the well-known expressions for beams on elastic foundations as the expression for the rotational boundary restraint $R_{RR,z}(x)$ for bending around the z-axis at a distance x from the center of the wall, where L_e is the so-called elastic length according to Equation F.2 and:

- $I_{trans,z}$ is the second moment of inertia of the transformed cross-section for bending around z-axis;
- K_s is the compression modulus of the foundation material;
- sf is a shape factor for the area of the floor in contact with the foundation material, which in turn depends on the quotient B_{ef}/L [35].

$$
\begin{aligned}
R_{RR,z}(x) &= \begin{cases} \overline{R}_{RR,z}(x) & \text{if } L/L_e < 4.73 \\ 1 & \text{if } L/L_e \geq 4.73 \end{cases} \\
\overline{R}_{RR,z}(x) &= 1 - \frac{2}{\sin\left(\frac{L}{L_e}\right) + \sinh\left(\frac{L}{L_e}\right)} \\
&\quad \cdot \left(\left[\cos\left(\frac{L}{2L_e}\right) \cdot \sinh\left(\frac{L}{2L_e}\right) + \sin\left(\frac{L}{2L_e}\right) \cdot \cosh\left(\frac{L}{2L_e}\right) \right] \cdot \cos\left(\frac{x}{L_e}\right) \cdot \cosh\left(\frac{x}{L_e}\right) \right. \\
&\quad \left. - \left[\cos\left(\frac{L}{2L_e}\right) \cdot \sinh\left(\frac{L}{2L_e}\right) - \sin\left(\frac{L}{2L_e}\right) \cdot \cosh\left(\frac{L}{2L_e}\right) \right] \cdot \sin\left(\frac{x}{L_e}\right) \cdot \sinh\left(\frac{x}{L_e}\right) \right)
\end{aligned}
\tag{F.1}
$$

$$
L_e = \left(\frac{2 \cdot E_w \cdot I_{trans,z} \cdot sf}{K_s} \right)^{1/4} \tag{F.2}
$$

G

Abstracts of prediction methods

G.1 DIN 1045-1

Source: [37]
Year: 2008
Origin: Germany
Type: Standard
Theory: Tensile member model

Effective cross-sectional area

$$h_{c,ef} = \min \begin{cases} \frac{D_w}{2} \\ 2.5 \cdot (c + \frac{\phi}{2}) \end{cases} \qquad b_{c,ef} = \min \begin{cases} s \\ 5 \cdot (c + \frac{\phi}{2}) \end{cases} \tag{G.1}$$

Transfer length

$$s_0 = 0.25 \cdot k_1 \cdot \frac{\phi}{\rho_{ef}} \leq 0.25 \cdot k_1 \cdot \frac{\sigma_s \cdot \phi}{\sigma_{cr}} \tag{G.2}$$

where: $k_1 = 0.56$

Crack spacing

$$\begin{aligned} s_{r,min} &= s_0 \\ s_{rm} &= \alpha_1 \cdot s_0 \\ s_{r,max} &= \alpha_1 \cdot \alpha_2 \cdot s_0 \end{aligned} \tag{G.3}$$

where: $\alpha_1 = 1.33$
$\alpha_2 = 1.50$

Crack width

$$w_k = s_{r,max} \cdot (\varepsilon_{sm} - \varepsilon_{cm}) \tag{G.4}$$

$$(\varepsilon_{sm} - \varepsilon_{cm}) = \frac{\sigma_s - k_3 \cdot \frac{\sigma_{cr}}{\rho_{ef}} \cdot (1 + \alpha_e \cdot \rho_{ef})}{E_s} \geq 0.6 \cdot \frac{\sigma_s}{E_s} \tag{G.5}$$

where: $k_3 = \begin{cases} 0.4 & \text{for long-term loading} \\ 0.6 & \text{for short-term loading} \end{cases}$

G.2 NEN-EN 1992-1-1

Source: [31]
Year: 2011
Origin: Europe
Type: Standard
Theory: Tensile member model

Effective cross-sectional area

$$h_{c,ef} = \min \begin{cases} \frac{D_w}{2} \\ 2.5 \cdot (c + \frac{\phi}{2}) \end{cases} \qquad b_{c,ef} = \min \begin{cases} s \\ 5 \cdot (c + \frac{\phi}{2}) \end{cases} \tag{G.6}$$

Transfer length

$$s_0 = k_2 \cdot c + 0.25 \cdot k_1 \cdot \frac{\phi}{\rho_{ef}} \tag{G.7}$$

where: $k_1 = 0.60$
$k_2 = 1.5$

Crack spacing

$$\begin{aligned} s_{r,min} &= s_0 \\ s_{rm} &= \alpha_1 \cdot s_0 \\ s_{r,max} &= \alpha_1 \cdot \alpha_2 \cdot s_0 \end{aligned} \tag{G.8}$$

where: $\alpha_1 = 1.33$
$\alpha_2 = 1.70$

Crack width

$$w_k = s_{r,max} \cdot (\varepsilon_{sm} - \varepsilon_{cm}) \tag{G.9}$$

$$(\varepsilon_{sm} - \varepsilon_{cm}) = \frac{\sigma_s - k_3 \cdot \frac{\sigma_{cr}}{\rho_{ef}} \cdot (1 + \alpha_e \cdot \rho_{ef})}{E_s} \geq 0.6 \cdot \frac{\sigma_s}{E_s} \tag{G.10}$$

where: $k_3 = \begin{cases} 0.4 & \text{for long-term loading} \\ 0.6 & \text{for short-term loading} \end{cases}$

G.3 NEN-EN 1992-3

Source: [38]
Year: 2006
Origin: Europe
Type: Standard
Theory: Continuous restraining model

Effective cross-sectional area

$$h_{c,ef} = \min \begin{cases} \frac{D_w}{2} \\ 2.5 \cdot (c + \frac{\phi}{2}) \end{cases} \qquad b_{c,ef} = \min \begin{cases} s \\ 5 \cdot (c + \frac{\phi}{2}) \end{cases} \tag{G.11}$$

Transfer length

$$s_0 = k_2 \cdot c + 0.25 \cdot k_1 \cdot \frac{\phi}{\rho_{ef}} \tag{G.12}$$

where: $k_1 = 0.60$
$k_2 = 1.5$

Crack spacing

$$\begin{aligned} s_{r,min} &= s_0 \\ s_{rm} &= \alpha_1 \cdot s_0 \\ s_{r,max} &= \alpha_1 \cdot \alpha_2 \cdot s_0 \end{aligned} \tag{G.13}$$

where: $\alpha_1 = 1.33$
$\alpha_2 = 1.70$

Crack width

$$w_k = s_{r,max} \cdot (\varepsilon_{sm} - \varepsilon_{cm}) \tag{G.14}$$

$$(\varepsilon_{sm} - \varepsilon_{cm}) = \varepsilon_r \tag{G.15}$$

G.4 Model Code 2010

Source: [39]
Year: 2013
Origin: Europe
Type: Guideline
Theory: Tensile member model

Effective cross-sectional area

$$h_{c,ef} = \min \begin{cases} \frac{D_w}{2} \\ 2.5 \cdot (c + \frac{\phi}{2}) \end{cases} \qquad b_{c,ef} = \min \begin{cases} s \\ 5 \cdot (c + \frac{\phi}{2}) \end{cases} \tag{G.16}$$

Transfer length

$$s_0 = k_2 \cdot c + 0.25 \cdot k_1 \cdot \frac{\phi}{\rho_{ef}} \tag{G.17}$$

	Formative cracking stage	Stabilized cracking stage
Short-term loading	$k_1 = 0.56$ $k_2 = 1.0$	$k_1 = 0.56$ $k_2 = 1.0$
Long-term loading	$k_1 = 0.74$ $k_2 = 1.0$	$k_1 = 0.56$ $k_2 = 1.0$

Crack spacing

$$\begin{aligned} s_{r,min} &= s_0 \\ s_{rm} &= \alpha_1 \cdot s_0 \\ s_{r,max} &= \alpha_1 \cdot \alpha_2 \cdot s_0 \end{aligned} \tag{G.18}$$

where: $\alpha_1 = 1.33$
$\alpha_2 = 1.50$

Crack width

$$w_k = s_{r,max} \cdot (\varepsilon_{sm} - \varepsilon_{cm}) \tag{G.19}$$

$$(\varepsilon_{sm} - \varepsilon_{cm}) = \frac{\sigma_s - k_3 \cdot \frac{\sigma_{cr}}{\rho_{ef}} \cdot (1 + \alpha_e \cdot \rho_{ef})}{E_s} - k_4 \cdot \varepsilon_r \tag{G.20}$$

	Formative cracking stage	Stabilized cracking stage
Short-term loading	$k_3 = 0.6$ $k_4 = 0$	$k_3 = 0.6$ $k_4 = 0$
Long-term loading	$k_3 = 0.6$ $k_4 = 0$	$k_3 = 0.4$ $k_4 = 1$

G.5 Van Breugel

Source: [27]
Year: 1996
Origin: The Netherlands
Type: Guideline
Theory: Tensile member model

Effective cross-sectional area

$$h_{c,ef} = \min \begin{cases} \frac{D_w}{2} \\ c + 2 \cdot \phi + 1.2 \cdot s_0 \end{cases} \qquad b_{c,ef} = \min \begin{cases} s \\ 15 \cdot \phi \end{cases} \tag{G.21}$$

Transfer length

$$s_0 = 1.2 \cdot w_{mo} \cdot \frac{E_s}{\sigma_{s,cr}} \tag{G.22}$$

Crack spacing

$$\begin{aligned} s_{r,min} &= s_0 \\ s_{rm} &= \alpha_1 \cdot s_0 \\ s_{r,max} &= \alpha_1 \cdot \alpha_2 \cdot s_0 \end{aligned} \tag{G.23}$$

where: $\alpha_1 = 1.50$
$\alpha_2 = 1.50$

Crack width

$$w_{mo} = 2 \cdot \left(\frac{0.4 \cdot \phi}{f_{cm,cube} \cdot E_s} \cdot \sigma_{s,cr} \cdot (\sigma_{s,cr} - \alpha_e \cdot \sigma_{cr}) \right)^{0.85} \tag{G.24}$$

$$w_{mv} = \frac{s_{rm}}{E_s} \cdot (\sigma_s - 0.5 \cdot \sigma_{s,cr}) \tag{G.25}$$

$$w_m = \begin{cases} k_5 \cdot w_{mo} & \text{if } \varepsilon_r < \varepsilon_{fdc} \\ k_5 \cdot w_{mv} & \text{if } \varepsilon_r \geq \varepsilon_{fdc} \end{cases} \tag{G.26}$$

where: $\sigma_{s,cr} = \frac{\sigma_{cr}}{\rho_{ef}} \cdot (1 + \alpha_e \cdot \rho_{ef})$

$k_5 = \begin{cases} 1.3 & \text{if } \sigma_s \leq 295 \text{ MPa} \\ \frac{1}{1 - 9 \cdot {\sigma_s}^3 \cdot 10^{-9}} & \text{if } \sigma_s > 295 \text{ MPa} \end{cases}$

$\varepsilon_{fdc} = (60 + 2.4 \cdot \sigma_{s,cr}) \cdot 10^{-6}$

G.6 Ciria C660 I

Source: [32]
Year: 2007
Origin: United Kingdom
Type: Guideline
Theory: Tensile member model

Effective cross-sectional area

$$h_{c,ef} = \min \begin{cases} \frac{D_w}{2} \\ 2.5 \cdot (c + \frac{\phi}{2}) \end{cases} \qquad b_{c,ef} = \min \begin{cases} s \\ 5 \cdot (c + \frac{\phi}{2}) \end{cases} \tag{G.27}$$

Transfer length

$$s_0 = k_2 \cdot c + 0.25 \cdot k_1 \cdot \frac{\phi}{\rho_{ef}} \tag{G.28}$$

where: $k_1 = 0.60$
$k_2 = 1.5$

Crack spacing

$$\begin{aligned} s_{r,min} &= s_0 \\ s_{rm} &= \alpha_1 \cdot s_0 \\ s_{r,max} &= \alpha_1 \cdot \alpha_2 \cdot s_0 \end{aligned} \tag{G.29}$$

where: $\alpha_1 = 1.33$
$\alpha_2 = 1.70$

Crack width

$$w_k = s_{r,max} \cdot (\varepsilon_{sm} - \varepsilon_{cm}) \tag{G.30}$$

$$(\varepsilon_{sm} - \varepsilon_{cm}) = \frac{0.5 \cdot \frac{\sigma_{cr}}{\rho} \cdot (k + \alpha_e \cdot \rho)}{E_s} \tag{G.31}$$

where: $k = \begin{cases} 1.0 & \text{if } D_w \leq 300 \text{ mm} \\ 1.0 - 0.7 \cdot 10^{-3} \cdot (D_w - 300) & \text{if } 300 < D_w < 800 \text{ mm} \\ 0.65 & \text{if } D_w \geq 800 \text{ mm} \end{cases}$

G.7 Ciria C660 II

Source: [32]
Year: 2007
Origin: United Kingdom
Type: Guideline
Theory: Continuous restraining model

Effective cross-sectional area

$$h_{c,ef} = \min \begin{cases} \frac{D_w}{2} \\ 2.5 \cdot (c + \frac{\phi}{2}) \end{cases} \qquad b_{c,ef} = \min \begin{cases} s \\ 5 \cdot (c + \frac{\phi}{2}) \end{cases} \tag{G.32}$$

Transfer length

$$s_0 = k_2 \cdot c + 0.25 \cdot k_1 \cdot \frac{\phi}{\rho_{ef}} \tag{G.33}$$

where: $k_1 = 0.60$
$k_2 = 1.5$

Crack spacing

$$\begin{aligned} s_{r,min} &= s_0 \\ s_{rm} &= \alpha_1 \cdot s_0 \\ s_{r,max} &= \alpha_1 \cdot \alpha_2 \cdot s_0 \end{aligned} \tag{G.34}$$

where: $\alpha_1 = 1.33$
$\alpha_2 = 1.70$

Crack width

$$w_k = s_{r,max} \cdot (\varepsilon_{sm} - \varepsilon_{cm}) \tag{G.35}$$

$$(\varepsilon_{sm} - \varepsilon_{cm}) = \varepsilon_r - 0.5 \cdot \alpha_e \cdot \frac{\sigma_{cr}}{E_s} \tag{G.36}$$

G.8 ICE/0706/012

Source: [40]
Year: 2010
Origin: United Kingdom
Type: Guideline
Theory: Combination of tensile member model and continuous restraining model

Effective cross-sectional area

$$h_{c,ef} = \min \begin{cases} \frac{D_w}{2} \\ 2.5 \cdot (c + \frac{\phi}{2}) \end{cases} \qquad b_{c,ef} = \min \begin{cases} s \\ 5 \cdot (c + \frac{\phi}{2}) \end{cases} \tag{G.37}$$

Transfer length

$$s_0 = k_2 \cdot c + 0.25 \cdot k_1 \cdot \frac{\phi}{\rho_{ef}} \tag{G.38}$$

where: $k_1 = 0.60$
$k_2 = 1.5$

Crack spacing

$$\begin{aligned} s_{r,min} &= s_0 \\ s_{rm} &= \alpha_1 \cdot s_0 \\ s_{r,max} &= \alpha_1 \cdot \alpha_2 \cdot s_0 \end{aligned} \tag{G.39}$$

where: $\alpha_1 = 1.33$
$\alpha_2 = 1.70$

Crack width

$$w_{k1} = \frac{0.5 \cdot s_{r,max} \cdot \frac{\sigma_{cr}}{E_s} \cdot \alpha_e \cdot (1-R) \cdot B}{1 - \frac{s_{r,max} \cdot R}{k_6 \cdot H} \cdot \left(1 - 0.5 \cdot \left(B + \frac{1}{1-R}\right)\right)} \tag{G.40}$$

$$w_{k2} = \frac{s_{r,max}}{R} \cdot (1 - 0.5 \cdot R) \cdot \left(\varepsilon_r - \alpha_e \cdot \frac{\sigma_{cr}}{E_s}\right) \tag{G.41}$$

$$w_k = w_{k1} + w_{k2} \tag{G.42}$$

where: $B = \frac{k}{\alpha_e \cdot \rho} + 1$

$$k = \begin{cases} 1.0 & \text{if } D_w \leq 300 \text{ mm} \\ 1.0 - 0.7 \cdot 10^{-3} \cdot (D_w - 300) & \text{if } 300 < D_w < 800 \text{ mm} \\ 0.65 & \text{if } D_w \geq 800 \text{ mm} \end{cases}$$

$k_6 = 1.5$

H

Calculation of water load induced stress

By means of a relatively simple calculation, which is schematized in Figure H.1, it has been attempted to assess the impact of the water load (when the reservoir is filled) on the cracks that have emerged as a consequence of the imposed deformations. Taking into account a Poisson's ratio ν of 0.20, the water load induced stress (at the position where the maximum bending moment occurs) has been established as follows:

- Maximum water load q of 25 kN/m^2;
- Maximum bending moment M of 26 kNm/m;
- Transversal stress σ_y at outer fibre of 0.62 MPa;
- Longitudinal stress σ_x at outer fibre of 0.12 MPa.

This reveals that the water load induced stress is virtually negligible compared to the imposed stress that arises 72 hours after cracking, which can be inferred from Figure 5.21. Note also that both the transversal and longitudinal stress do not exceed the tensile strength.

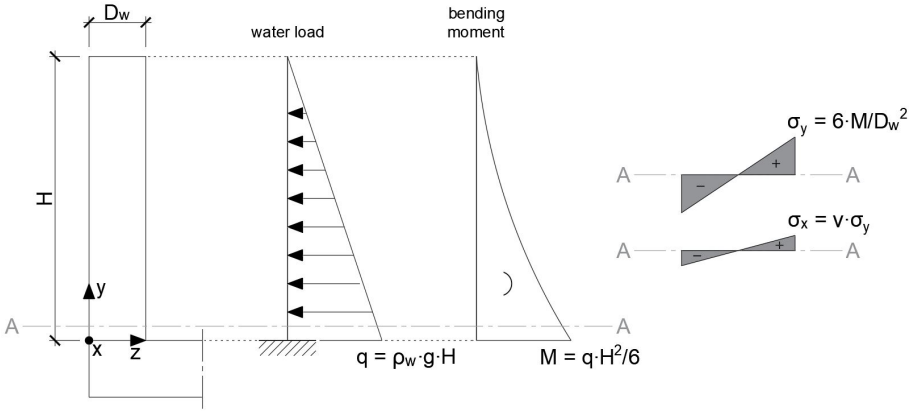

Figure H.1: Schematic representation of calculation of water load induced stress.

I

Prediction of crack widths

Method	*Theory*	$h_{c,ef}$ (mm)	s_0 (mm)	$s_{r,max}$ (mm)	$(\varepsilon_{sm}-\varepsilon_{cm})$ (με)	w_m (mm)	w_k (mm)
DIN 1045-1 [37]	TMM	200	177	354	341	0.09	0.12
NEN-EN 1992-1-1 [31]	TMM	200	296	671	341	0.17	0.23
NEN-EN 1992-3 [38]	CRM	200	296	671	90	0.04	0.06
Model Code 2010 [39]	TMM	200	306	612	277	0.10	0.14
Van Breugel [27]	TMM	250	166	373	341	0.10	0.13
Ciria C660 I [32]	TMM	200	296	671	303	0.15	0.20
Ciria C660 II [32]	CRM	200	296	671	64	0.03	0.04
ICE/0706/012 [40]	TMM/CRM	200	296	671	150	0.07	0.10
Average						**0.09**	**0.13**
Average TMM methods						**0.12**	**0.16**
Average CRM methods						**0.04**	**0.05**

Table I.1: Detailed prediction of crack widths for S1: ∅20–100 (1.26%).

Method	*Theory*	$h_{c,ef}$ (mm)	s_0 (mm)	$s_{r,max}$ (mm)	$(\varepsilon_{sm}-\varepsilon_{cm})$ (με)	w_m (mm)	w_k (mm)
DIN 1045-1 [37]	TMM	200	283	566	526	0.23	0.30
NEN-EN 1992-1-1 [31]	TMM	200	411	931	526	0.37	0.49
NEN-EN 1992-3 [38]	CRM	200	411	931	90	0.06	0.08
Model Code 2010 [39]	TMM	200	447	895	351	0.24	0.31
Van Breugel [27]	TMM	250	231	520	527	0.21	0.27
Ciria C660 I [32]	TMM	200	411	931	469	0.33	0.44
Ciria C660 II [32]	CRM	200	411	931	64	0.04	0.06
ICE/0706/012 [40]	TMM/CRM	200	411	931	160	0.11	0.15
Average						**0.13**	**0.20**
Average TMM methods						**0.27**	**0.36**
Average CRM methods						**0.05**	**0.07**

Table I.2: Detailed prediction of crack widths for S2: ∅20–160 (0.79%).

Method	*Theory*	$h_{c,ef}$ (mm)	s_0 (mm)	$s_{r,max}$ (mm)	$(\varepsilon_{sm}-\varepsilon_{cm})$ (με)	w_m (mm)	w_k (mm)
DIN 1045-1 [37]	TMM	200	371	743	681	0.39	0.51
NEN-EN 1992-1-1 [31]	TMM	200	506	1147	681	0.59	0.78
NEN-EN 1992-3 [38]	CRM	200	506	1147	90	0.08	0.10
Model Code 2010 [39]	TMM	200	565	1130	454	0.39	0.51
Van Breugel [27]	TMM	250	280	631	682	0.33	0.43
Ciria C660 I [32]	TMM	200	506	1147	608	0.53	0.70
Ciria C660 II [32]	CRM	200	506	1147	64	0.05	0.07
ICE/0706/012 [40]	TMM/CRM	200	506	1147	158	0.13	0.18
Average						**0.31**	**0.41**
Average TMM methods						**0.44**	**0.59**
Average CRM methods						**0.06**	**0.09**

Table I.3: Detailed prediction of crack widths for S3: ∅20–210 (0.60%).

Method	*Theory*	$h_{c,ef}$ (mm)	s_0 (mm)	$s_{r,max}$ (mm)	$(\varepsilon_{sm}-\varepsilon_{cm})$ (με)	w_m (mm)	w_k (mm)
DIN 1045-1 [37]	TMM	200	442	884	804	0.54	0.71
NEN-EN 1992-1-1 [31]	TMM	200	582	1320	804	0.80	1.06
NEN-EN 1992-3 [38]	CRM	200	582	1320	90	0.09	0.12
Model Code 2010 [39]	TMM	200	659	1319	536	0.54	0.71
Van Breugel [27]	TMM	250	364	819	806	0.50	0.66
Ciria C660 I [32]	TMM	200	582	1320	718	0.72	0.95
Ciria C660 II [32]	CRM	200	582	1320	64	0.06	0.08
ICE/0706/012 [40]	TMM/CRM	200	582	1320	154	0.15	0.20
Average						**0.43**	**0.56**
Average TMM methods						**0.62**	**0.82**
Average CRM methods						**0.08**	**0.10**

Table I.4: Detailed prediction of crack widths for S4: ∅20–250 (0.50%).